PLEASE NOTE:

In all cases this material has been filmed in the best possible way from the available copy. Problems encountered with this document have been identified here with a check mark ✓.

1. Glossy photographs _____
2. Colored illustrations _____
3. Photographs with dark background _____
4. Illustrations are poor copy _____
5. Print shows through as there is text on both sides of page _____
6. Indistinct, broken or small print on several pages 149 throughout 152
7. Tightly bound copy with print lost in spine _____
8. Computer printout pages with indistinct print _____
9. Page(s) _____ lacking when material received, and not available from school or author _____
10. Page(s) _____ seem to be missing in numbering only as text follows _____
11. Poor carbon copy ✓
12. Not original copy, several pages with blurred type _____
13. Appendix pages are poor copy _____
14. Original copy with light type _____
15. Curling and wrinkled pages _____
16. Other _____

University Microfilms International

300 N. ZEEB RD., ANN ARBOR, MI 48106 (313) 761-4700

A MICROSCOPIC FRACTURE STUDY IN THE TWO DIMENSIONAL TRIANGULAR LATTICE

BY

ADEL GOHAR

A dissertation submitted to the Graduate Faculty in Physics in partial fulfilment of the requirements for the degree of Doctor of Philosophy, The City University of New York.

1979

This manuscript has been read and accepted for the Graduate Faculty in Physics in satisfaction of the dissertation requirement for the degree of Doctor of Philosophy.

1/30/79
date

Arthur Kaskin
Chairman of Examining Committee

1/30/79
date

Frank Martino (RC)
Executive Officer

G. Dienes

A. C. Damask

B. Kramer

R. Harrison

Supervisory Committee

The City University of New York

ACKNOWLEDGMENTS

I would like to take this opportunity to thank Prof. A. Paskin for his constant encouragment and advice. Thanks are also due to Prof. G. J. Dienes for many useful discussions.

TABLE OF CONTENTS

LIST OF TABLES

NOTE ON FIGURES

This thesis contains 183 figures. It would be rather impractial to list all of them here. A discription of the contents of the figures is given on page 171 (fig. captions). Most of the figures are given in a separate section (pp 177-277). However some of the figures which are closely connected with the text are given when they are introduced.

NOTE ON TABLES

In all tables ℓ is the crack half-length in bonds, σ is the load, β the damping parameter, ε the total strain. In (3-1), (3-2), (3-3) the value of ℓ is 9. σ up, σ right, σ left, σ down are the maximum stresses on the different central rows near the tip. In 3-12(a) $\sigma_f^{(1)}$ is the critical Griffith stress for E = 79.6 & $\sigma_f^{(2)}$ is the critical Griffith stress for E = 81.13. σ_{PRE}^{MD} is the critical stress by molecular dynamics in preloading. F is the maximum stress concentration in all tables. The superscript (MD = molecular dynamics), (C = continuum), (ER = Eringen) in all tables. In (3-15) σ_{local}(MAX) is the maximum value of the stresses near the tip. In (3-16)W is given in units of ℓ. To convert between ℓ in bonds and ℓ in units of α the relation ℓ (in α) = (2 ℓ(in bonds) + 1)/4 is used. Thus ℓ = 9, 19, 39 bonds gives ℓ = 4.75, 9.75, & 19.75 α respectively.

Introduction

In this thesis a microscopic study of fracture will be carried out. The study will be performed on a two dimensional triangular lattice consisting of atoms interacting via a L-J potential. The case of uniaxial fixed loads with a crack perpendicular to the axis of tension will be investigated.

The goal of the present study will be to compare the behaviour of this atomic simulation to the assumption & predictions of the different continuum theories and of other atomistic studies. An attempt will be made to understand the reasons for differences between continuum predictions and atomistic results in terms of the assumptions which go into the continuum theories. In particular, a critical study of the assumptions which go into the Mott and Griffith theories will be conducted. These assumptions will be tested on the present computer simulation. In order to do such a test the time evolution of the different parts of the energy of the system will be monitored (i.e. surface, strain, kinetic, and load energies). The degree to which these assumptions are satisfied will throw some light on the value of such energy fracture criteria as the Griffith one.

Stress fracture criteria will also be studied. In order to do that the stress(force) profiles around the crack tip and along different directions of interest in the lattice

will be computed and compared with those obtained by the Eringen non-local continuum theory. The Rice-Thomson continuum theory provides a criterion for predicting the brittleness or ductility of a material. The predictions of this theory will be compared to the behaviour of the present model. The creation and annihilation of dislocations at crack tips, and the occurrence of tip blunting will be investigated as a function of the loading parameter and crack lengths.

Dynamical continuum theories predict some interesting effects for cracks moving with appreciable velocities. Among these effects such theories predict the occurrence of bifurcation, bending, and surface roughening for cracks which are accelerated through a velocity $0.6C_s$ (C_s = shear wave velocity). Simulations will be attempted for high enough stresses and long enough cracks to see whether such effects will occur in this lattice, and to examine the stress profiles around the tip before the occurrence of these effects.

Earlier atomistic simulations have reported the occurrence of supersonic crack velocities. In the present study some of the idealizations and restrictions in these previous simulations will be removed in order to see whether the supersonic velocities were a result of the idealizations or whether they represent the true behaviour of a highly stressed atomic lattice. Continuum theories predict an upper limit of C_s on the crack velocity.

Previous atomistic calculations performed by Thomson et al on one and two dimensional solids have predicted the occurrence of the so-called lattice trapping of cracks in solids. Subsequently other workers (Ashurst & Hoover) have obtained appreciable trapping in their atomistic calculations. This phenomenon will be investigated.

Chapter 1 will summarize the basic results and predictions of continuum mechanics, and will give an account of the lattice trapping models of Thomson et al.

In chapter 2 the importance of atomistic models of fracture processes will be indicated. The previous attempts of Weiner - Pear, Ashurst - Hoover, and Kanninen et al will be given in some detail. The specific restrictions and idealizations used in these models and how they affect the results will be outlined. The motivations for performing the present computer simulation will then be given.

In chapter 3 the results will be given and discussed. Section 3A will review the parts of molecular dynamics which are pertinent to the present calculation. In 3B the details of the present calculation will be given. In 3C the mechanical properties of this lattice are outlined. 3D will be an introduction to the results of the present simulation. The results of these simulations will be given in 3E. The remaining sections of this chapter will discuss the data and suggest simple models for analysing the different runs.

Chapter One

I A CRACKS AS STRESS CONCENTRATORS

The study of cracks in solids is of great importance since such cracks act as stress concentrators and therefore reduce the mechanical strength of the material appreciably. The role of cracks as stress concentrators has been well established by numerous tests performed on solids under laboratary conditions and by a large number of structural failures of ships, planes, and pressure vessels. (For examples, see Rolfe and Barsom 1978, and Hahn 1976). These structural failures have been satisfactorily explained on the basis of the catastrophic propagation of prexisting microcracks.

If an accurate formula for the stress concentration factor $\mathcal{F}$ of a crack(defined below) were available, then one could combine this with an atomistic estimation of the ideal strength of the solid to obtain the mechanical strength of the cracked sample. However accurate values of $\mathcal{F}$ are not available for a general crack problem, although a huge amount of serious mathematical effort has been devoted to the problem. The lack of accurate values of $\mathcal{F}$ is due to the mathematical difficulty of the problem. This is because the problem does not fall under the general boundary value type which could be solved by the methods of classical elastostatics. Here the boundary values of vanishing stress are given on the crack wall which is not known until the

final solution is obtained. As an elastostatic problem the crack problem is thus unsolvable. The unsolvability results from trying to treat the problem as a static one. Ideally one should attack it as an initial value one. One introduces a cut in the material and studies the motion of the parts of the continuum adjacent to the cut under the action of the unbalanced stresses which have resulted from the cutting process. One looks for a final equilibrium position and shape of the crack walls such that the normal stresses on them would vanish. The final deformation state is then combined with the appropriate constitutive equation to give the stress state and consequently the stress concentration factor.

The mathematics required to carry out the above steps is not available. Instead one has to resort to some idealized model of a crack. Griffith (1920) for example pictured the crack as an elliptic hole shrunk to zero thickness. Westergaard (1939) pictured a crack as a thin mathematical slit (no material removed). The difference between the two is more mathematical than physical.

The Griffith picture of a crack will be discussed here briefly. In this picture the Inglis solutions (1913) for the stress fields of an elliptic hole are used. The case of interest in this thesis is the so called mode I in which the loading is uniaxial, with the major axis being perpendicular

to the axis of tension. For an ellipse of semi-major axis a, and semi-minor axis b, the stress concentration factor F, is defined as the ratio of the maximum stress on the rim of the elliptic hole to the applied load σ. Following a standard (but tedious) stress analysis the maximum is found to occur at the tip and to be given by

$$F = \sigma_{yy}(l, 0)/\sigma = 1 + 2l/b = 1 + 2\sqrt{l/\rho} \quad (1)$$

where ρ is the radius of curvature of the ellipse at the tip, and σ_{yy} is the stress in the y direction.
Figure 1(a) shows the mode 1 loading configuration of uniaxial tension, Figure 1(b) shows the variation of the tensile fields as a function of $x' = x - l$.

For the zero thickness limit it is clear that the fields are singular at the tip. This type of singularity is common to many continuum treatments of the crack problem. A natural way to remove this unphysical singularity will be discussed in a later section. The general form of the Inglis displacement field is

$$u_\alpha = \sigma l \, f_\alpha(\xi, \eta, \nu) \quad (2)$$

where $\alpha = x, y$, E is Young's modulus, f_α is a dimensionless function of the elliptic coordinates ξ, η and ν is Poisson's ratio. u_x, and u_y are given here since they are

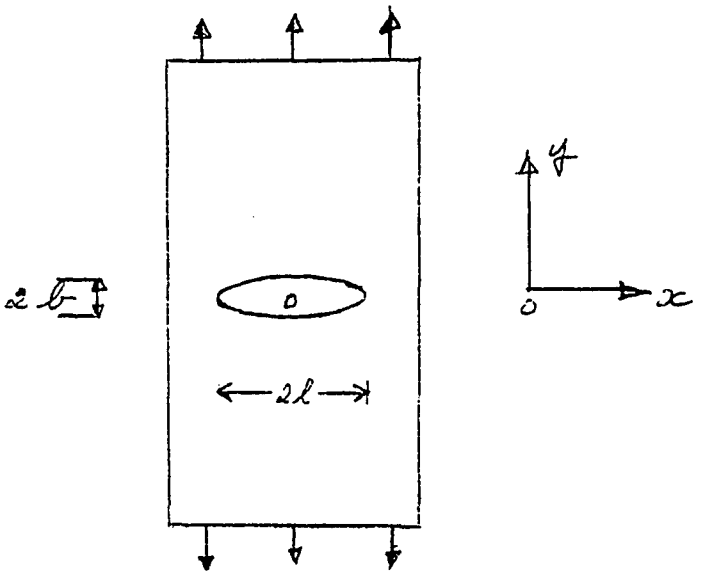

(a)

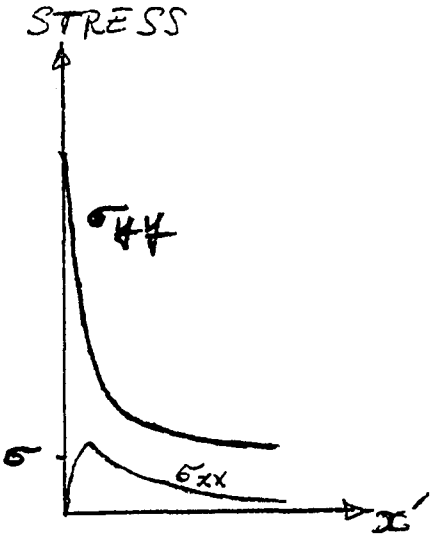

$l = 3b$

$x' = x - l$

(b)

FIG. 1-1

going to be used when the Mott theory is introduced.

Near the tip the stress fields have a $\frac{1}{\sqrt{r}}$ dependence, where r is the distance from the tip to the observation point. The stress fields are proportional to σ, (the applied load) but their θ, and l dependence differ from treatment to treatment.

I B THE GRIFFITH APPROACH TO THE CRACK PROBLEM

The Griffith approach is based on the fact that as a crack extends, energy is released from the loads and the strain field to the crack tip. At the same time energy is consumed in creating additional crack surfaces. If the rate of energy supply to the tip (with respect to crack length) is greater than the rate of energy consumption in the surface creation then the crack extends, otherwise it closes.

It should be mentioned that the strain energy behaves in different ways as the crack extends depending on the type of loading. Under fixed strain it decreases, and under fixed stress it increases. Thus,

$$\left(\frac{\partial U_E}{\partial l}\right)_\varepsilon < 0 \quad \& \quad \left(\frac{\partial U_E}{\partial l}\right)_\sigma > 0$$

where U_E is the strain energy due to the crack of half-length l.

Concentrating on the case of plane stress one can write an expression for the internal energy of the system which consists of the solid plus the loads,

$$U = U_E + U_L + U_S + U_k \qquad (1)$$

where U_L is the potential energy of the loads, U_S the surface energy, and U_k the kinetic energy. Griffith considered the variation in internal energy dU as the crack varies its half-length by (δl).

$$dU = dU_E + dU_L + dU_S + dU_k \qquad (2)$$

If the temperature of the system is small then $dF = dU$, where F is the free energy. Also $(dU_L = -dW_L)$ where dW_L is the additional infinitesimal work done by the loads on the solid during the variation $2(\delta l)$ of crack length. Thus,

$$dF = -dW_L + dU_E + dU_S \qquad (3)$$

Griffith used the Inglis result for the strain energy content of a plate containing a thin elliptic hole of length $2l$,

$$U_E = \pi \sigma^2 l^2 / E \qquad (4)$$

(4) is the result of integrating the energy density $\sum_{\alpha\beta} \sigma_{\alpha\beta}^2 / 2E$ for the stresses presented in 1A over the area of the body.

Griffith also used the result that,

$$dW_L = 2\,dU_E \tag{5}$$

This result is based on the assumption that a linear relation holds between stress and strain. For the surface energy U_S, Griffith used,

$$U_S = 4\gamma l \tag{6}$$

Where γ is the surface energy per unit length. Thus from the above he could write

$$dU = d\left(4\gamma l - \frac{\pi}{E}\sigma^2 l^2\right) \tag{7}$$

Griffith used the thermodynamic principle (based on the second law) which states that a system will move in such a way so as to try minimize its free energy F. Thus for any thermodynamically preferable motion

$$dF \leq 0 \tag{8}$$

Where the equality sign will hold only when the system arrives to an equilibrium (minimum F) if such an equilibrium exists for the system. The condition that

$dF < 0$ could be

achieved in two ways

(a) $\left(\frac{\partial F}{\partial l}\right) > 0$ & $\delta l < 0$ Healing or closure

<u>OR</u>

(b) $\left(\frac{\partial F}{\partial l}\right) \begin{matrix} > \\ \downarrow \\ < \end{matrix} 0$ & $\delta l > 0$ Extension or propagation

The cases (a) & (b) together define a critical Griffith half-length l_g for a given stress σ . A crack of half-length $l < l_g$ will try to minimize its free energy by healing (if it is left free to do so). A crack of length $l > l_g$ will minimize F by propagating. The critical half-length will be defined by

$$l_g = 2E\gamma / \pi\sigma^2 \qquad (9)$$

It should be emphasized that a crack of half-length l_g under a stress σ will not be in equilibrium but in a highly unstable state because

$$(\partial^2 F / \partial l^2)_{l=l_g} > 0$$ i.e. F has a maximum rather than a minimum.

Equation (9) could also be used to get a critical stress for a crack of given half-length l . This gives

$$\sigma_g = \sqrt{2E\gamma/\pi l} \qquad (10)$$

Griffith tested his criterion (10) by introducing cracks of known length in bulbs made of very brittle glass. He burst these bulbs (cylindrical and spherical) by exerting an internal pressure via an inserted fluid. Using Poisson ratio one could get the tangential stress. Also for small cracks the radius of curvature is relatively large and the curvature is small so that a crack on the bulb is in an environment close to the plane situation used in the derivation. Griffith found a linear relation between σ_g & $(1/\sqrt{l})$

which agrees with his prediction. The constant of proportionality agreed with his predictions to within 10%. Despite this discrepancy the theory was considered quite a trimmph. This is because it explained the large difference between the experimentally measured strength for crack free samples, which is about 10^8 psi for this glass and the observed strengths for cracked glasses of about 10^3 psi. Thus the criterion established the fact that cracks were responsible for the drastic reduction of strengths of solids. However, subsequent work reduced the value of the theory as a quantitative tool for predicting mechanical strengths. Schand (1959,1961) has shown that values of γ calculated from (10) are much higher than the measured surface energy by independent methods. This was done for soda glass. This clearly indicates that the fracture is accompanied by plastic deformation at the tip even in brittle materials. The Griffith criterion could by remedied by considering γ to be a fracture energy γ_F which includes both the thermodynamic surface energy and the plastic work per unit length of crack.

$$\gamma_F = \gamma_{Thermo} + \gamma_{Plastic} \qquad (11)$$

For very brittle solids the main contribution to γ_F is from γ_{THERMO} . For soda glass Schand (1961) has shown that γ_F could be as large as $50\,\gamma_{THERMO}$. For metals for example plastic work is 10^3 times the thermodynamic surface energy(Goodier & Feld 1963). The importance of including

plastic work has also been dictated by the repeated observation of plastically deformed regions around the tips of cracks by x-ray and photoelastic methods.

I C THE MOTT THEORY

Mott (1948) extended the Griffith approach to include kinetic effects. Going through the same steps as in the Griffith approach but including the kinetic term gives

$$dU = d\left(-\frac{\pi}{E}\sigma^2 l^2 + 4\gamma l\right) + dU_k \qquad (1)$$

since $dU = 0$ this leads to

$$d\,U_k = d\left(\frac{\pi\sigma^2 l^2}{E} - 4\gamma l\right) \qquad (2)$$

Eliminating γ from (2) by using the Griffith condition at $l = l_g$ gives

$$dU_k = d\left[\frac{\pi}{E}\sigma^2 (l^2 - 2 l l_g)\right]$$

Integrating this equation with the assumption that $U_k = 0$ at $l = l_g$ gives

$$U_k = \frac{\pi\sigma^2 l^2}{E}\left(1 - \frac{l_g}{l}\right)^2 \qquad (3)$$

On the other hand the kinetic energy of a two dimensional continuum containing a crack is given by

$$U_k = \frac{1}{2}\rho v_c^2 \iint_R \left[\left(\frac{\partial u_x}{\partial l}\right)^2 + \left(\frac{\partial u_y}{\partial l}\right)^2\right] dx\,dy \qquad (4)$$

Where u_x, u_y are the components of the displacement field,

v_c is the velocity of the crack, and R is the region of influence of the propagating crack. To evaluate (4) Mott made two assumptions. The first one is that the fields of the moving crack are very close to the static ones. The second is that R extends over the whole solid. Recalling the form of the displacement fields in the static situations one can write

$$u_x = (\sigma l/E)\, f(\nu, \xi, \eta)$$

$$u_y = (\sigma l/E)\, g(\nu, \xi, \eta) \qquad (5)$$

Where ξ, η are elliptic coordinates and ν is Poisson's ratio. From (5) it is clear that f, g are dimensionless. Using (5) in (4) one obtains

$$u_k = \tfrac{1}{2}\rho v_c^2 \frac{\sigma^2}{E^2} \iint \left[f^2(\nu, \xi, \eta) + g^2(\nu, \xi, \eta)\right] dx\,dy$$

$$= \frac{1}{2}\rho v_c^2 \frac{\sigma^2}{E^2} \iint h(\nu, \xi, \eta)\, dx\, dy$$

Since h will also be dimensionless, the integral in the above equation will have the dimensions of an area. Mott assumed the integral to be proportional to l^2

$$u_k = \tfrac{1}{2} k \rho v_c^2 \sigma^2 l^2 / E^2 \qquad (6)$$

Where k is a numerical constant. Equating (3) and (6) Mott obtained

$$v_c = v_T (1 - l_g/l) \qquad (7)$$

where $v_T = \sqrt{\frac{2\pi E}{k\rho}} = \sqrt{\frac{2\pi}{k}}\, c_L$, c_L = long. sound vel.

(7) implies that the crack will have a terminal velocity v_T, which is independent of the applied stress and depends only the elastic properties of the material and on the constant k which should be the same for all isotropic-elastic solids (same γ). During the initial part of the motion however, v_c will depend on the applied σ through l_g, since

$$l_g = 2E\gamma/\pi\sigma^2$$

It could be shown that the Mott theory implies that the time required for the crack to reach some multiple of its original length is inversly proportional to σ^2. This will be left to the discussion chapter (3) of this thesis. In the Mott picture the applied σ is just infinitesimally above σ_g, or equivalently l is infinitesimally above l_g so that initially $v_c = 0$, $U_k = 0$. This is a rather special situation. In general a solid is subjected to a stress σ and a crack of length l_0 is introduced, where

$$l_0 = m l_g$$

For propagation m is some number greater than one and according to (3) & (7) the initial values of U_k & v_c will not be zero.

Roberts and Wells (1955) have evaluated the Mott constant k. To do this they removed the Mott assumption

which states that $\mathcal{R}$ extends over the whole solid. Instead they argued that the disturbance due to the propagating crack cannot move with a speed larger than c_L . Hence in a time t the disturbance travels a distance $c_L t = \mathcal{R}$ and the crack moves a distance $v_c t = (l - l_0)$, hence

$$\mathcal{R} = l\sqrt{\frac{k}{2\pi}} \qquad \text{(neglecting } l_0\text{)}$$

They used a circular region of radius $\mathcal{R}$. This converts the expression for k into an integral equation

$$k = \iint h(\nu, \xi, \eta)\, d\nu\, d\psi$$

$$k = \int_0^{2\pi} \int_0^{l\sqrt{\frac{k}{2\pi}}} H(r,\theta)\, r\, dr\, d\theta$$

They solved this equation numerically to obtain,

$$\sqrt{\frac{k}{2\pi}} \approx 0.38$$

This is in close agreement with the observations of Schardin & Struth (1954) on glasses. Other experiments carried out by Akita & Ikeda (1959) on polycrystalline steel indicate a dependence of the terminal velocity on applied stress. The discrepancy in behavior is not well understood.

In most materials however, other dynamic effects take place before a terminal velocity is reached. The most common effects are the occurence of bifurcation and bending.

Finally it should be mentioned that the Mott theory

makes some very interesting predictions in the case of fixed strain. When the crack starts propagating the macroscopic compliance of the sample goes up. The effective stress at the outer surfaces drops. This means that the applied stress which was above critical initially will be below critical after the length $2l_o$ of the crack increases. It is found that u_k and v_c will have other zeros beside the initial one. Thus Mott predicts the occurence of crack arrest. This has been observed by Carlsson (1963) and Van Elst (1964).

I D LATTICE TRAPPING

In this section the ideas behind the so called lattice trapping of cracks will be outlined. The work of Thomson and co-workers (1971, 1973) will be presented. A critical evaluation of their model and why it should imply the absence of trapping in real solids will be postponed to chapter (3) after presentation of the molecular dynamic results.

The above authors have predicted that a crack in a crystalline solid would be stable over a range of stresses of the order of magnitude of the critical Griffith stress σ_g. This idea is in contradiction with the continuum Griffith approach. According to Griffith there exists a unique stress σ_g (for a certain crack length) below which the crack would heal (or close), and above which it would propagate (or extend). The Thomson etal treatments imply that there are two

critical stresses, σ_- below which the crack closes, and σ_+ above which it extends. Furthermore their results indicate that

$$\sigma_+ - \sigma_- \approx \sigma_q \qquad (1)$$

The authors of the lattice trapping papers believe that this effect is a consequence of the discretness of the lattice. They have treated a one dimensional model (1971) and later a two dimensional one(1973). In the two dimensional case they have discussed the wedge problem, that is the case in which the forces are applied directly to the walls of the crack. They have also worked out the classical mode I crack problem (the uniaxial tension case of Griffith), in which the stresses are applied to the external surfaces and transmitted via the crystal to the crack. The details of the solutions in the different cases are a little different but the main features are the same. Two types of calculations were done, an energy calculation and a force calculation.

In the energy calculation a form was assumed for the bond energy across the crack. For the n-th bond

$$E(n) = \frac{1}{2} E_b \left[1 - \frac{2}{\pi} \tan^{-1}\left(\frac{n}{2}\right) \right] \qquad (2)$$

Where it is assumed that initially the critical bond is at $n = 0$ so that its energy $E(0) = \frac{1}{2} E_b$. The justification of this particular form is that it allows an analytic evaluation of the required sums, besides it satisfies the

asymptotic forms

$$E(-\infty) = E_b \quad , \quad E(+\infty) = 0$$

Of ccurse the energies here correspond to a reference energy in which an unstreched bond has zero energy and two completely separated atoms have an energy E_b.

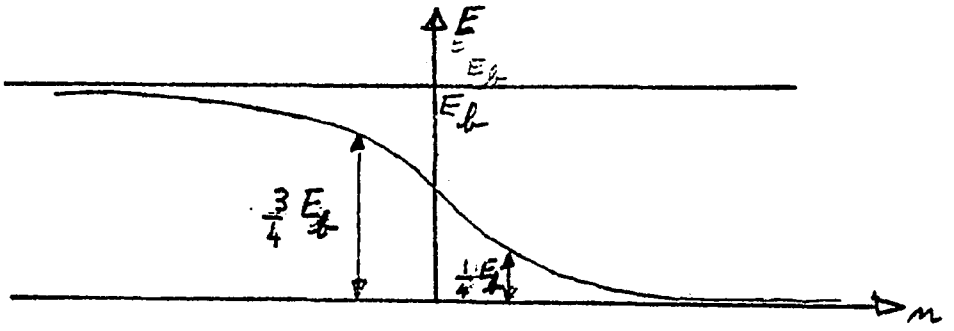

FIG. 1-2

The surface energy is $\sum_{-\infty}^{\infty} E(n)$, when the tip is at x the surface energy is $\sum_{-\infty}^{\infty} E(n-x)$. Both these sums diverge for an infinite crystal. However the quantity of interest is

$$S(x) = \sum_{-\infty}^{\infty} \left\{ E(n-x) - E(n) \right\}, \quad 0 \leq x \leq 1 \qquad (3)$$

$S(x)$ is a measure of the varition of the energy as the crack moves, and hence the force to move the crack is $-dS/dx$ Thomson etal evaluated the above sum. They defined σ_+ & σ_- as the maximum and minimum of $-dS/dx$ respectively. The ratio of σ_+/σ_- differs slightly from the one to the two dimensional case.

$$\left.\begin{aligned} \sigma_+/\sigma_- &= 1 + 4e^{-2\pi\eta}, \quad 2\pi\eta > 1 \longrightarrow (1D) \\ \sigma_+/\sigma_- &= \coth(\pi\eta) \longrightarrow (2D) \quad \text{for large crack} \end{aligned}\right\} (4)$$

The important point to note about these two relations is that they predict negligible trapping for large η. A value of $\eta = 0.2$ in the I-D case gives $\sigma_+/\sigma_- = 2.1$. The parameter η is the width of the crack tip. In other words the number of bonds across the central line which are extented appreciably is proportional to η . To see this one solves the energy equation for n to get

$$n = \eta \cot\left[\pi\left(\frac{E}{E_b}\right)\right] \qquad (5)$$

If for example one defines the tip as that region which contains bonds that are extended so that their strain energy is $E_b/4$ or more, then for an atom to be in the tip it should have $n \leq \eta$. If η is chosen as 0.2 for example(in order to give $\sigma_+/\sigma_- = 2.1$) then the tip would contain only the bond for which $n = 0$ i.e. the critical bond only. Thus the Thomson etal surface energy formulation gives appreciable trapping only in the case in which the region of appreciable bond extension is shrunk to a singular point. Thus in this picture all the bonds to the right of the tip are almost unstretched and those to the left are almost broken.

In the force calculation linear springs with a cutoff at an extension of δ were used. In the one dimensional case, forces resisting the bending of the lateral springs were also included. In the two dimensional case the x & y motions

were decoupled ($\nu = 0$). The position of the tip is at bond number ($N+1$). σ_+ is defined as that stress which would make the entension of that bond equal to δ . σ_- is defined as that stress which will make the bond at N have an extension δ . Once the bond at N has an extension δ ,the broken bond will heal and the crack will start closing.

It should be mentioned that Ashurst & Hoover (1976) have observed lattice trapping in their atomistic computer simulation. They reported a trapping parameter $\sigma_+ / \sigma_- = 3.7$.

I E THE CRACK TIP SINGULARITY & THE ERINGEN THEORY

In a previous section it was mentioned that a very thin crack gives rise to a stress field which diverges at the origin (tip). The nature of the tip singularity could be understood in several ways. The most direct way is to remember that the singularity in the fields resulted because of the assumption of an infinitely thin crack. On an atomic scale a crack could not have a zero thickness (or equivalently a tip with a zero radius of curvature). The tip is thus never infinitely sharp in a real material. One could thus get rid of the singularities in the fields and in the stress concentration by discarding the mathematical idealization of a thin crack. While this is the logical way to view the problem, there is no quantitative way to evaluate the curvature in a precise and unique manner for a small

number of atoms lying at a crack tip. This would enable us to combine the continuum results with the assumption of an atomic nonsharp tip.

There were numerous rather artificial attempts made in the last few years to remove the singularity without throwing away the other continuum results. Barenblatt (1962) and Dugdale (1960) introduced compressive stress fields which were also singular at the tip. These fields were chosen in such a way as to cancel the original singularity. Barenblatt for example determined this additional field by requiring that the tip closes in the form of a cusp and that the boundary conditions be satisfied at the cusp surface. While such attempts do indeed remove the singularity, the physical justification for the additional compressive fields acting only around the tip is by no means clear. The details of such theories will thus be left out.

Recently Eringen and co-workers have been reformulating continuum mechanicas so as to include the effects of nonlocality in space and time in the formulations of the problem (see Eringen 1977 a for a complete reference list) The phenomena covered include wave dispersion, dislocation problems, and fracture mechanics. Nonlocal linear elasticity manages to remove the crack tip singularity in a natural way. The basic features of this theory will thus be outlined below.

THE PHYSICAL ORIGIN OF NON-LOCAL THEORIES

In any classical field theory there are global conservation laws

$$\int_{V-S} q\, dV + \int_{S} G\, da = 0 \qquad (1)$$

Where V is some arbitary volume and S is a discontinuity surface sweeping that volume, q and G will depend on the particular field under consideration. (For example see Eringen 77a) Such global conservation laws are common to both local and non-local theories. To obtain a local theory one makes the assumption that the above law applies to any arbitary volume no matter how small. This then implies that

$$q = 0 \qquad \& \qquad G = 0 \qquad (2)$$

To obtain the non-local theories one realizes that (1) does not necessarily apply to arbitarily small volumes. Thus (2) does not become a necessary condition. However in order to retain the global conservation (1) we equate q, G to the so called residuals $\hat{q}, \hat{G}$ to get

$$q = \hat{q} \quad , \quad G = \hat{G} \qquad (3)$$

(1) & (3) thus yield

$$\int_{V-S} \hat{q}\, dV + \int_{S} \hat{G}\, da = 0 \qquad (4)$$

The residuals $\hat{q}, \hat{G}$ measure the effect of all other

points of the body on the observation point. These should add up to zero for a given system. For example if a body contains no discontinous surfaces S' then (4) becomes

$$\int_V \hat{q}\, dV = 0$$

if one takes the example $\hat{q} = \hat{f}$ where $\hat{f}$ is the force due to all parts of the body on the observation point then (4) states that the sum of all interactions between the particles of the body add up to zero. In this case the result is trivial and follows from equality of action and reaction. For other physical quantities the above equations place non-trivial restrictions on the allowable forms for residuals. The main goal of non-local continuum mechanics is to determine the forms of the residuals after the specification of the appropriate global conservations. This process will in general yield field equations (3) which are different from the local ones.

NON-LOCAL LINEAR ELASTICITY

In the local linear elasticity the stress at a certain point is proportional to the strain at that point. In the non-local case the stress at a point depends on the strains at other points in the medium.

$$t_{kl} = \int_{V-S'} \left[\lambda'(|\underline{x}'-\underline{x}|)\, \varepsilon'_{rr}(\underline{x}')\, \delta_{kk} + 2\mu'(|\underline{x}'-\underline{x}|)\, \varepsilon'_{kl}(\underline{x}') \right] dv(\underline{x}') \qquad (5)$$

Where $\lambda'(|x'-x|)$, $\mu'(|x'-x|)$ are the non-local elastic moduli. In the limit in which λ', μ' become Dirac Delta functions of $(|x'-x|)$ then (5) becomes the linear Hooks law of classical elasticity. The second major difference between non-local and local theories is that the Stokes-Navier field equations get replaced by a general field equations which depend on λ', μ'. These generalized field equations tend to the Navier-Stokes equations as λ', μ' approach Dirac delta functions. When λ', μ' vanish everywhere except around a discrete set of points, then (5) corresponds to a lattice dynamic representation of the solid.

The first advantage of non-local over local elasticity is that it predicts wave dispersion. By fitting the dispersion relations to the expression obtained from non-local elasticity one could find λ', μ' for any particular solid. For example, Eringen (1977) fitted the non-local results to the dispersion relations obtained from a one-dimensional harmonic lattice of lattice parameter a, and obtained

$$\lambda'(|x-x'|) = \lambda\,\alpha(|x-x'|)$$

$$\mu'(|x-x'|) = \lambda\,\alpha(|x-x'|) \qquad (6a)$$

where $\alpha(|x-x'|) = \frac{1}{a}\left(1 - \frac{|x-x'|}{a}\right)$, $\frac{|x-x'|}{a} \leq 1$

$= 0$, $\frac{|x-x'|}{a} > 1$

This form is by no means unique and the same fit could be obtained by

$$\alpha(|\underline{x}'-\underline{x}|) = \alpha_0 \, e^{-\left[\frac{k^2}{a^2}(\underline{x}'-\underline{x})\cdot(\underline{x}'-\underline{x})\right]} \tag{6b}$$

for $k = 1.65$. The main point is that λ', μ' are decaying functions of $(|\underline{x}'-\underline{x}|)$ and go to δ- functions as $a \to 0$.

Eringen used the first form (6a) above in his treatment of the crack problem. In his treatment a local stress field σ is defined as

$$\sigma_{kl}(\underline{x}') = \sigma'_{kl} = \lambda \, \varepsilon'_{rr}(\underline{x}')\,\delta_{kl} + 2\mu\,\varepsilon'_{kl}(\underline{x}') \tag{7}$$

In terms of the local σ's the stress t_{kl} is given by

$$t_{kl} = \int_V \alpha(|\underline{x}'-\underline{x}|)\,\sigma_{kl}(\underline{x}')\,dv(\underline{x}') \tag{8}$$

With the residual equations (3) equation (8) gives

$$\int_V \alpha(|\underline{x}'-\underline{x}|)\,\sigma_{kl,l'}(\underline{x}')\,dv(\underline{x}') - \int_{\partial V} \alpha(|\underline{x}'-\underline{x}|)\,\sigma_{kl}(\underline{x}')\,dv(\underline{x}') = 0$$

For a large (macroscopic) body this gives,

$$\int_V \alpha(|x'-x|)\,\sigma_{kl,k'}(x')\,dv(x') = 0 \qquad (9)$$

If α is continuous and of bounded support then (9) implies

$$\sigma_{kl,k} = 0 \qquad (10)$$

(10) is only the fundamental equation of elastostatics for any well posed boundary value problem. The solution of this equation has been given in general form by Sneddon (1951)

$$u(x,y) = \frac{1}{\sqrt{2\pi}} \int_{-\infty}^{\infty} \frac{i}{k} \left[|k| A(k) + (|k|y - \frac{\lambda+3\mu}{\lambda+\mu} B(k) \right] \times e^{(-|k|y - ikx)}\, dy \qquad (11)$$

$$v(x,y) = \frac{1}{\sqrt{2\pi}} \int_{-\infty}^{\infty} \left[A(k) + y B(k) \right] e^{(-|k|y - ikx)}\, dk$$

u , v are used to obtain the stresses through (7) & (8) and through the definition of ε_{ij} when this is done and when these stresses t_{kl} are used with the boundary conditions a set of integral equations for $A(k)$ and $B(k)$ is obtained. Eringen et al 77 has solved this set numerically. Once $A(k)$ & $B(k)$ are determined, the stress field follows automatically from (11). Eringen carried out the solution for the conditions

$$\begin{aligned} t_{yx} &= 0 \quad , y=0 \\ t_{yy} &= -t_0 \quad , y=0 \quad , |x| < l \\ v &= 0 \quad , y=0 \quad , |x| > l \end{aligned} \qquad (12)$$

After obtaining the solution to this crack problem one could obtain the solution to the Griffith problem by superimposing a uniform tensile stress field all over space.

The results of the Eringen calculation are summarised in the relation

$$P = \frac{t_{\psi\psi}(l, 0)}{t_0} = C(\nu)\sqrt{\frac{2l}{a}} \qquad (13)$$

where P is the stress concentration at the tip, and $C(\nu)$ is a material constant which depends very weakly on Poisson's rario ν .

Whereas (13) removes the infinite stress concentration of local elasticity the exact form will depend on the choice of $\alpha(|x'-x|)$. The modulus (λ', μ') functions appear ex-

of $\alpha(|x'-x|)$. the integral equations for $A(k)$, $B(k)$ and are most likely to affect the dependence of P on l and the value of $C(\nu)$.

The stress distribution curves obtained by Eringen are given below (Fig. 1-3). They will be compared with the ones obtained by molecular dynamics later in the thesis.

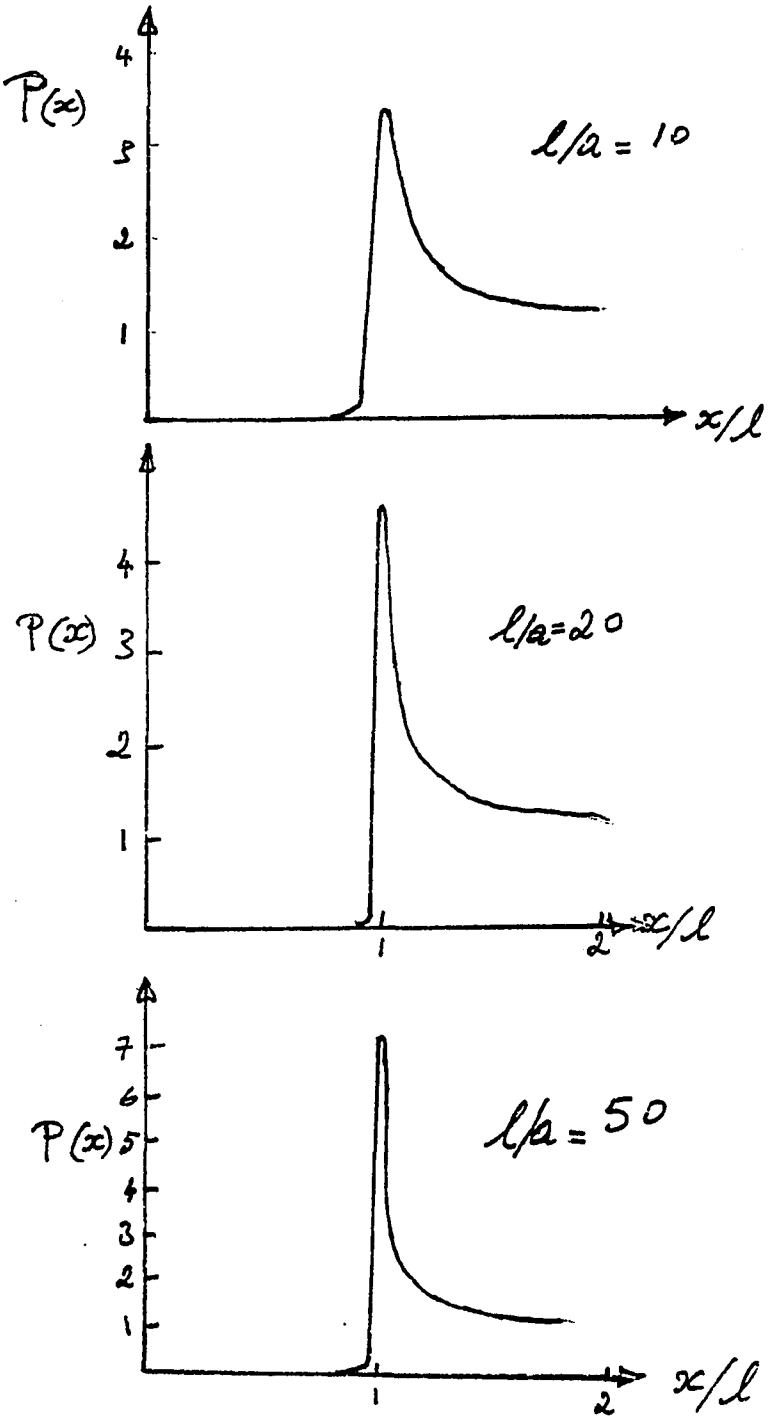

ERINGEN STRESS PROFILES

FIG. 1-3

I F BRITTLNESS AND DUCTILITY OF CRYSTALS

In this section the question of whether a solid will fracture in a brittle or in a ductile fashion will be addressed. For most crystals an amount of plastic deformation is always present around the tip. Still, one could classify a certain fracture as brittle or ductile. In a brittle fracture the atomically sharp appearance of the crack is maintained throughout the process. In a ductile fracture the crack loses the initial sharp appearance, the tip becomes blunted, and the solid fractures through shear (slip) motions having a large component perpendicular to the crack line. Between these two extremes lie a large number of solids exhibiting an intermediate behaviour.

It has been realized that a solid will be brittle or ductile depending on the ratio of tensile strength to the shear strength of the solid, or on the relative ease of bond rupture and atomic slip or glide. Kelly, Tyson,and Cottrell (1967) studied the problem and postulated a criterion for ductility. According to these authors, tip blunting will occur and a shear instability will result if the maximum shear stress in the tip region exceeds the theoretical shear strength of the solid. Rice and Thomson (1974) have shown that the Kelly - Tyson - Cottrell criterion cannot be sufficient. This is because the shear stress fields aroung the tip are highly localized. The fact that these fields

exceed a maximum at one point of the shear plane (shear line in 2D) does not guarantee that the slipping (or gliding) condition will be satisfied on all points of the shear plane. Thus the picture of tip blunting via uniform shear motions had to be abandoned. Rice and Thomson reasoned that the matching of the highly sheared medium near the tip with the non-sheared medium at greater distances, defines a dislocation. They have worked out a criterion for brittleness versus ductility. In order to do that, the general interaction between a crack tip and a dislocation was found. This interaction is attractive for small distances (from tip to disl) and repulsive at larger distances. If a dislocation is present at a distance greater than the critical distance r_c then it will be driven away to infinity. If it is at a distance less than r_c it will be attracted to the tip and get annihilated. The situation of interest is not that of an already existing dislocation but of one which is created at the tip. In the Rice-Thomson theory one considers the dislocation just after its creation. A comparison is made between the core cutoff r_0 and the critical radius r_c . If $r_c > r_0$ then the newly created dislocation will find itself in the attractive part of the interaction and will not be free to leave the tip. Thus for solids satisfying this condition, tip blunting will not occur and brittle behaviour will result. This will continue to be the case until sufficient energy is supplied to the dislocation to overcome the attractive barrier and cause a brittle-ductility transition.

Actually, even when such energy is made available to the tip region (e.g. by thermal fluctuations) the solid might still prefer to use it in bond tearing rather than for slip processes. This means that substances satisfying the condition $\tau_c > \tau_0$ will be very good candidates for brittle behaviour.

On the other hand $\tau_c \sim \tau_0$ or $\tau_c < \tau_0$ will give rise to ductile behaviour. The continuum analysis is not quantitatively valid for this situation but it still reveals the behaviour of the system. In this case the newly created dislocation finds itself in the repulsive part of the interaction and gets driven away. In the Rice-Thomson theory one writes

$$f_{disl-crack} = f_i + f_l + f_a \qquad (1)$$

where f_i = the attractive image force between the crack and the dislocation.

f_l = the attractive force between the disl and the ledge which is created when the disl is created

f_a = the repulsive force exerted by the shear fields of the tip trying to drive the disl away

The authors evaluate the total force when the applied $\sigma = \sigma_f$ the Griffith stress. The critical radius is the value of r which makes $f = 0$

$$f(r_c) = 0$$

this gives, r

$$\mu b\left[-\frac{1}{4\pi\xi_c(1-\nu)} - \frac{2}{\pi\eta^2\beta'}\frac{\alpha}{\xi_c^2+\alpha^2} + \frac{1}{\eta\beta}\sqrt{\frac{1}{2\pi(1-\nu)\xi_c}}\right] = 0 \qquad (2)$$

where

$\xi_c = r_c/b$, $\alpha = e^{3/2}\xi_0/2$, $\xi_0 = r_0/b$

$\underline{b}$ = BURGER VECTOR , $\beta = \sin\phi\cos(\phi/2)$

$\frac{1}{\beta'} = r_0/b \sin\phi$, $\eta^2 = \mu b/\gamma$.

Neglecting the ledge interaction (middle term) one gets

$$r_c = \frac{1}{8\pi(1-\nu)}\beta^2\frac{\mu b^2}{\gamma} \qquad (3)$$

Applying this equation to the two dimensional triangular lattice and for a first neighbour $\mathcal{L}$-ϕ potential, gives

$$r_c = \frac{(1+\nu_{2D})}{8\pi}\beta^2\frac{\mu b^2}{2\epsilon/\alpha} \qquad (4)$$

Where ϵ is the depth of the potential, α is the nearest neighbour distance. In writing (4) the correspondence

$$\frac{1}{1-\nu_{3D}} \longrightarrow (1+\nu_{2D}) \qquad (5)$$

has been used (Dally & Riley 1965) ν_{2D} is the Poisson ratio in two dimensions. For an isotopic medium

$$\nu_{2D} = 1/3$$

For a slip system making an angle of 120° or 60° with a

<110> crack and a Burger's vector $b = a$, r_c will be

$$r_c = \frac{8}{\pi\sqrt{3}} = 1.47\,a$$

From Esbjorn and Jensen (1976)

$$r_0 = (1.7 \pm 0.2)\,a, \quad (1.5a < r_0 < 1.9a)$$

The ductility criterion $r_c < r_0$ is satisfied. One expects the probability of dislocation emission to be quite high, although brittle behaviour could sometimes result because the criterion is only barely satisfied.

If the ledge term is included it will increase the value of r_c and might cause the system to stop satisfying the ductility criterion.

Thus according to the Rice-Thomson theory this system is expected to show a behaviour in between the two extremes, or it might show only one of the two types of behaviour in different situations depending on the dynamic details of the loading process.

I G DYNAMIC EFFECTS

Introduction

Continuum theories predict the occurence of bifurcation and bending for cracks propagating in isotropic or near isotropic materials. For cracks which do not undergo bifurcation or bending, such theories predict an upper limit of C_S (shear wave velocity) or C_R (Rayleigh wave velocity) for the velocity of the crack.

The main assumptions which are used to arrive at these predictions are thermodynamic in nature and are of such general validity that the predictions based on them are qualitatively very sound. Moreover a large literature of experimental results on a wide variety of materials agrees with such predictions in a qualitative way. In particular, the upper limits on the velocity mentioned above seem to be experimentally obeyed quite well. The high upper limits are attained in the fracture of single crystals which have a preferred weak cleavage plane (Gilman 1959, Hull et al 1965,1966). On the other hand experimental studies on isotropic solids (glasses mainly) have indicated that the crack velocity behaves in one of the following ways (Schardin 1959, Beebe 1966, Carlsson 1963). The velocity increases until it attains the terminal velocity which is independent of the applied loads, and changes with composition. Under certain loading conditions the crack does not reach its terminal

velocity but bifurcates at a much lower velocity v_B . The crack bends either before or after bifurcation. The length at which this bifurcation occurs being determined by the loads. The maximum attained velocity v_B before bifurcation has been found to lie between $\cdot 3\, C_s$ & $\cdot 6\, C_s$. The maximum velocity $\cdot 6 C_s$ predicted continuum mechanics agrees well with these experimental results (approximately $\cdot 6\, C_s$)

The work which is outlined in this section has been carried out by Yoffe (1951), Craggs (1960), Broberg (1960), Baker (1962), and Barenblatt et al (1962)

THE DYNAMIC CRACK PROBLEM

In the dynamic case one seeks the displacement field $\underline{u}(t)$ and the length $2\ell(t)$ of the crack by trying to solve the dynamic equations of the continuum simultaneously with an energy balance equation. This one has to solve

$$(\lambda+\mu)\sum_{\beta}\frac{\partial^2 u_\alpha}{\partial x_\alpha \partial x_\beta} + \mu \nabla^2 u_\alpha + F_\alpha = \rho \frac{\partial^2 u_\alpha}{\partial t^2} \qquad \alpha = 1, 2, 3 \qquad (1)$$

with

$$\frac{dU}{dt} = \frac{dU_k}{dt} + \frac{dU_\Sigma}{dt} + \frac{dU_s}{dt} \qquad (2)$$

where

$$\frac{dU}{dt} = \iint_S \sum_{\alpha=1}^{3} \sigma_{\alpha\alpha} \dot{u}_\alpha \, dS + \iiint \sum_{\alpha=1}^{3} F_\alpha \dot{u}_\alpha \, dR \qquad (3)$$

$$\frac{dU_E}{dt} = \iiint_S \sum_{\alpha\beta} \sigma_{\alpha\beta} \dot{\varepsilon}_{\alpha\beta} \, dR \tag{4}$$

$$\frac{dU_k}{dt} = \iiint_R \rho \sum_{\alpha} \dot{u}_\alpha \ddot{u}_\alpha \, dR \tag{5}$$

After expressing the σ's & ε's in terms of u equations (1) & (2) become four equations for the four unknowns u_1, u_2, u_3, l. All the terms in the above equations have been previously defined except for R & S. R is the volume of the body and S the total surface.

$$S = S_0 + A$$

Where S_0 is the external surface and A is the crack surface. Clearly (3) contains the boundary conditions through the first integral and since S is a function of time, its form would not be known except after a solution is obtained. The region R is also a time dependent region in this problem. This makes equations (1) & (2) an integro-differential equation of variable time dependent limits. Moreover one has to make special assumptions about the shape of the crack as a function of time in order to be able to find dU_3/dt in (2).

Mathematical methods for solving (1) & (2) in their most general form are not available. The complexity of the problem is simply beyond the power of analytical methods. A solution for $l(t)$ for arbitary loads could not be obtained and thus the way a crack accelarates under particular conditions is not available.

Instead the time dependence of ℓ must be specified in advance. The work done up to date has concentrated on the case

$$\ell = v_c \, t \qquad \text{(Craggs and Broberg)}$$

Similarly Yoffe considered the case of a crack of constant length moving with uniform velocity. Barenblatt has studied the accelerated motion of a crack by considering subsequent time intervals during each of which the velocity remains constant. It should be mentioned that all the mathematical difficulties mentioned above hold for brittle fracture. For ductile materials an additional complication is encountered. One needs to include a plastic dissipative term in $\mathcal{U}_s$, this term could moreover be velocity dependent.

As mentioned above the Craggs and Broberg treatments treat the case of a constant velocity. These theories consider a crack moving with a velocity v_c without considering how the crack got accelerated to this velocity. The theories do not furnish a relation which determines what loads or what material properties give rise to a particular v_c. The basic result is that the stress σ_{yy} near the tip is given by

$$\sigma_{yy} = \sqrt{\frac{\ell}{r}} \, \sigma \, F(v)$$

$$= \sqrt{\frac{c_s t}{r}} \, \sigma \, F(v) \qquad (6)$$

where $v = \frac{v_c}{c_s}$ & r is the small distance ahead of the tip

at which the stress is being measured, t the time. $F(v)$ is a function which is complicated in form but has the following graphical appearance

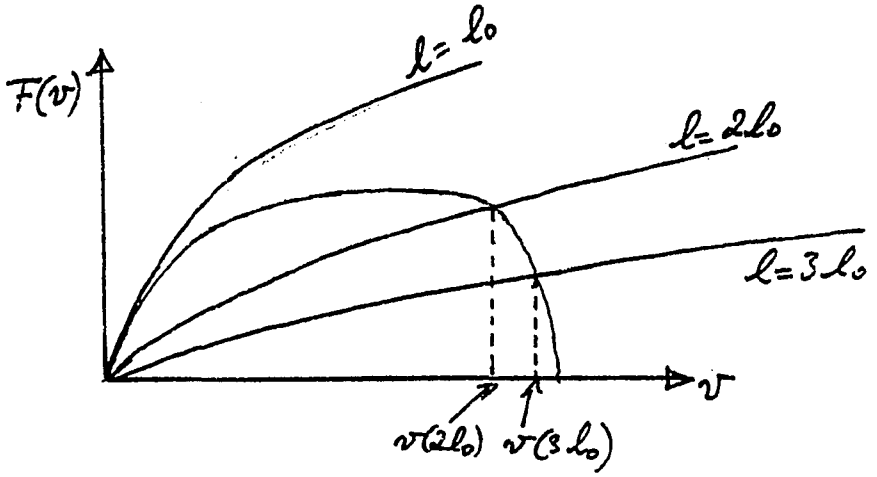

FIG. 1-4

Barenblatt made use of the Graggs result by assuming that at each instant an accelerated crack is in a stationary motion, and by requiring that the total stress σ_{yy} at the tip be finite. This requirement he satisfied by equating the dynamic stress intensity factor of Craggs to the cohesive modulus of the material K_0 (see the appendix for a description of the Barenblatt fracture criterion). Then Barenblat put

$$K_{dynamic} = K_0 \tag{7}$$

This gives

$$F(v) = \frac{K_0}{\sigma\sqrt{l}}\sqrt{v} \tag{8}$$

To find the velocity at a given length ℓ (or time t one has to find the intersection of the curves given by the right and left hand sides of (8). If one assumes that the crack starts from rest then $\sigma\sqrt{\ell_0} = K_0$ and one has to find the intersection of

$$f(v) = \sqrt{\frac{\ell_0}{\ell}}\sqrt{v} = \sqrt{\frac{t_0}{t}}\sqrt{v} \qquad (9)$$

with $f(v)$. Clearly, the longer ℓ is, the larger the velocity v_c at which the intersection happens. In other words as t increases v is increasing and the crack accelerates. As shown in the figure the maximum velocity is $C_R \sim 0.95 C_s$, and the prediction of the sound velocity as the maximum attainable crack velocity is clearly satisfied.

The same upper limit is derivable from consideration of the minimum load σ_M necessary to maintain a velocity v_c, or from consideration of the energy release rates at the tip. The prediction is (see Yoffe's for example) that σ_M goes down as v_c goes up. For $v_c = C_s$, one gets $\sigma_M = 0$. This means that one does not have to supply energy (do work) on the solid in order to maintain the processes of bond breaking, surface creation, and plastic deformation which are happening at the tip. Such a state of affairs would violate the first law of thermodynamics. One thus concludes that $v_c = C_s$ is an unphysical result in the first place and that the sonic velocity C_s is not attainable.

The prediction of branching and bending come about in the following way. The mechanistic approaches enable one to conclude that for small crack velocities, a crack which starts propagating along the x-direction will have directional stability and will remain moving along that direction. This could be understood via a stress argument or an energy one. The stress argument is based on the assumption that the tearing of bonds occurs perpendicular to the direction of crack propagation. The tearing happens along the direction (θ) of $\sigma_{\theta\theta}$ at which that stress attains a maximum. If the maximum of $\sigma_{\theta\theta}$ is sharp, then there will be a predominant direction for propagation, if not then the several possible directions will compete with the possible occurence of branching, bending, or surface roughening. For low velocities the dynamical solutions indicate a very sharp maximum of $\sigma_{\theta\theta}$ at $\theta = 0$. This explains the initial directional stability about $\theta = 0$. As the velocity increases, the $\sigma_{\theta\theta}$ vs θ curve flattens out for a while and then a shifted maximum appears. The shift in the maximum tends to produce a sharp bend, but the inertia of the motion tends to keep the initial motion going. This effect postpones the bending or branching for a while, but by the time the shifted maximum appears either or both phenomena take place.

Most continuum treatments estimate a velocity v_B (the maximum vel. before branching or bending) of $0.6\, C_s$. Either phenomena might occur before this limit because of

flattening, but by the time v_B is reached one is guaranteed the occurence of either. v_B would thus be given by the value of the velocity at which the maximum starts shifting. From the dynamical solution

$$\left.\frac{\partial \sigma_{\theta\theta}}{\partial \theta}\right]_{\theta=0} = 0 \qquad \& \qquad \left.\frac{\partial^2 \sigma_{\theta\theta}}{\partial \theta^2} < 0\right]_{\theta=0}$$

for $v_c/c_s \leq 1/\sqrt{3}$. This gives $v_c \leq .57 c_s$. For higher v_c the maximum starts shifting and thus branching or bending must occur for

$$v_c > 0.5\, c_s$$

giving

$$v_c \approx 0.6\, c_s$$

The competition between several directions of propagation for some velocities can result in the crack going in one direction, then in another for a short period, and so on. This results in surface roughness, which increases the surface energy. This increase in the surface energy with velocity has been observed experimentally in brittle fractures although the effect is usually masked by the more dominant decrease in the plastic part of the surface energy with velocity.

Finally it should be mentioned that the above dynamical effects are less likely to appear in crystals which have a weak cleavage plane. In such crystals the initial propagation remains the dominant one until much higher velocities

are reached. Only if there is another weak cleavage plane having a small angle with the first, could the branching and bending take place.

CHAPTER 2

2 A MOTIVATIONS FOR ATOMISTIC CALCULATIONS

Although continuum mechanics offers an approximate description of fracture, the essence of any fracture process is atomic in nature. One therefore expects that a satisfactory theory of fracture will have to include the details of atomistic processes occuring at the tip. The mechanisms of bond breaking and atomic gliding will ultimately determine the mechanical strength and brittleness (or ductility) of a cracked solid.

Atomistic calculation of crack problems can handle some aspects of the crack problem which are completely inaccessible to the continuum methods. For example, continuum theories do not distinguish between the cases of pre and postloading, although these two modes give rise to different critical stresses. Atomistic calculations which include the distinction can be made.

Dynamic atomistic calculations can handle the acceleration phase in the motion of a crack in a natural way. The assumptions made in the Mott theory, make this theory incapable of handling the acceleration phase. In particular the quasistatic assumption about the fields of a propagating crack, make the conclusions of value only in the final stage of stable propagation. The other dynamic treatments (e.g.

Craggs) mentioned in section I G can handle the special case of uniform propagation only. The Barenblatt dynamic theory (section I G)considers the accelaration phase as a collection of consecutive periods of uniform propagation. On the other hand, dynamic atomistic treatments do not have to make any of these special assumptions about the motion. The behavior of cracked systems can be found without any ad-hoc assumptions about the way in which the crack starts its motion.

In section IA it has been mentioned that accurate values of the stress concentration factor $\mathcal{F}$ are not available. As mentioned in that section, this is due to the unavailability of a solution of the elastostatic boundary value problem of a crack (because the boundaries are not known except after a solution is obtained). The corresponding elastodynamic initial value problem which can remove this unsolvability is too difficult to attempt. On the other hand an atomistic dynamic approach is ideally suited to the problem. A cut can be introduced and the time evolution of the lattice can be obtained. The motion of the boundaries (crack walls) to their final equilibrium positions of vanishing normal stresses can be obtained. The final equilibrium configuration of the system can be used to find accurate values for $\mathcal{F}$.

In addition to the above, atomistic calculations can serve as a test of the different assumptions which go into

the various continuum treatments. For example, quantities like the crack strain energy U_E can be easily calculated in an atomistic model, whereas there is no direct way to measure this quantity experimentally in a cracking solid. Thus one could test the assumption of $dW = 2\,dU_E$ for example, or the continuum result for $U_E (= \pi \sigma^2 \ell^2 / E)$. A criterion like the Griffith one could thus be tested in full detail. Stress (or force) concentration curves can be obtained and compared with the continuum curves (by Eringen for example).

Most continuum treatments of fracture are based on linear elasticity. The linear Hookean nature of the solid, containing no upper limit on the linearity, gives rise to the singularities mentioned in Chapter I.This is because the cracked system contains regions which are highly deformed, and should not be treated by linear elaticity. Instead, the linear constitutive relations of classical elasticity,should be replaced by non-linear ones in which the stress starts decreasing with large strain and ultimately vanishes. Including non-linear and finite strength effects in a continuum theory would indeed remove the stress and strain singularities. Such theories pose insuperable mathematical difficulties and progress in them is very slow. Instead, a more practical approach is to treat the parts of the system which do not suffer large deformations by linear elasticity, and the large deformation regions near the tips atomistically. This is similar to the approach employed in dislocation

theory. The far field information (stress, strain, or energy) derived on the basis of linear elasticity is not abandoned. The stresses, core energy, and configuration near the crack are obtained by performing an atomistic calculation after assuming an interaction between atoms which includes the non-linear and finite strength aspects. The near(atomistic) and far (continuum) solutions are then matched.

In the crack problem, it can be easily shown that linear elasticity always predicts infinite stress and strain fields in the vicinity of the tip, even when an infinitely thin crack is not assumed. Thus the value of using a discrete (atomic) description of the system near the tip is quite clear.

2 B PREVIOUS ATOMISTIC CALCULATIONS

Atomistic calculations have been attempted by several authors. The attempts have been in two different directions. Some work has been done on trying to simulate a crack in a real material. Kanninen et al (1970-1973) have simulated a crack in BCC iron using a Johnson empirical pair potential. On the other hand several other authors have studied cracks in highly idealized lattices in order to gain some insight into the consequences of the discretness. In some of these attempts the models have been formulated in such a way so as

to allow an analytic solution of the resulting equations. The Thomson et al calculations mentioned in chapter one are of this type. Other idealized models are formulated in such a way so as to resemble some simplified continuum model in order to fascilitate the comparison of the discrete and continuum results.

Three examples of previous atomistic calculations will now be given. The first two are of the idealized type. The third is of the type which tries to simulate a real material.

WEINER - PEAR

Weiner and Pear (1975) have carried out calculations on cracks in the so called Newel-Rosenstock model. A computer was used to find the dynamic behaviour of cracks in this idealized lattice. The reason for the choice of this particular model was to make a direct comparison between their results and the results of an analytic calculation performed by Sanders (1960). Earlier, Sanders had studied a crack in the same lattice with a linear potential (described below) and concluded that a crack in such a lattice cannot reach a terminal subsonic velocity. This conclusion was based on the fact that his cracks had an expanding elliptic shape in which the curvature at the tip was increasing. The increasing curvature offered an increasing stress concentration, which accelerated the crack continuously.

Weiner and Pear showed that, by modifying the potentials so as to allow for plastic deformation and dislocation emission at the tip, the continuous increase of the tip curvature stopped. The reason behind the Sanders' conclusion was thus shown to be invalid. They obtained subsonic terminal velocities after these modifications in the potential were introduced. For such propagations, the inclination of the crack face was found to be fairly constant giving a constant curvature and stress concentration. Dislocation emission at the tip and motion to the surface were observed during these propagations. For very high applied stresses supersonic velocities were observed both for the Sanders potentials (elastic) and the Weiner-Pear (plastic) potentials. For large values of the parameter which controls the plasticity of the solid, tip blunting occured and no propagation resulted.

The lattice employed consists of atoms placed on a square lattice in the x-y plane with rows parallel to the x - axis and columns to the y- axis. Motion is allowed only in the y - direction. Each atom interacts with its neighbours in the same column with a tensile force f_T and with its neighbours in adjacent columns with a shear force f_S.

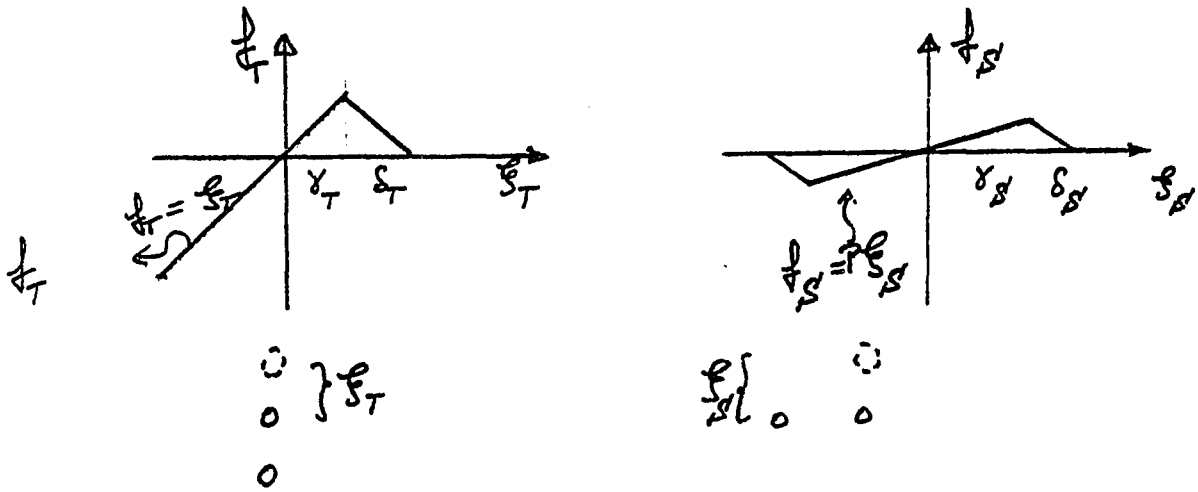

FIG. 2 - 1

P is the Shear modulus, and Young's modulus is $/$.

The Sanders potential is obtained from the Weiner-Pear one by letting $\delta_T = \delta_\beta = 0$. Runs for which this was done gave the Sanders results of continuous accelaration. The value of δ_β controlled the quantity and extent of plastic deformation. When this quantity was made large enough, tip blunting without propagation resulted. The effect of temperature on the terminal speed was also investigated and found to be small. The terminal velocities in the brittle propagations were found to be stress dependent.

Discussion

The Weiner-Pear results are in contradiction with the Mott terminal velocity result, and with the continuum result of the unatainability of supersonic velocities. The results

are quite valuable since they have established the role of the decreasing part of the force law in causing crystal plasticity. The same loading conditions which gave supersonic velocities when plasticity was prohibited, gave subsonic velocities when plasticity was allowed. This illustrates an important aspect in the simulation of crack propagation. When a possible energy dissipation mechanism is prohibited by an artificial aspect of the simulation, the energy which would have been dissipated in such a mechanism, is forced to be dissipated by another mechanism. The rate at which this other mechanism proceeds would thus be higher than if the available energy is shared between the two mechanisms. Thus Sanders prohibited plasticity by letting $\mathcal{E}_\beta = \mathcal{E}_\gamma = 0$. All the energy released from the loads and the strain field at the tip, was forced to be dissipated in surface creation by crack propagation rather than being split between surface creation and dislocation formation. This forced the velocity to be unrealistically high (supersonic). When the sharing was allowed, the velocity was found to subsonic.

This type of reasoning could be used to get an understanding of the supersonic velocities observed by Weiner-Pear in their high stress runs. The one dimensionality of their model prohibits crack branching (and bending). The propagation of the two new branches would necessarily involve bond tearing motions which have a horizontal component. Since these motions are forbidden in this model, branching

cannot occur. According to the continuum models discussed in section I G an accelerating crack will branch at a maximum velocity of about $0.6\,C_s$, and the two new branches will split the energy available for acceleration in between them and start accelerating from zero. If the branching is prohibited then all the acceleration energy is retained by the original crack, which would thus unrealistically be accelarated to supersonic speeds.

In the present calculation the crystal will be allowed to have two degrees of freedom so as to allow for branching.

ASHURST - HOOVER (1976)

This study was carried out on a two dimensional triangular lattice using central pair potentials of the parabola, parabola-linear, and double parabola types. This lattice is the simplest two dimensional lattice possesing shear stability in a first neighbour approximation. The simpler square lattice has shear stability only when second neighbours are included, and even then the shear modulus μ is still quite low. This lattice has the advantage that it is elastically isotropic(see the next Chapter), and thus comparisons between its properties and those of isotropic continuum theories are valid. For other lattices comparisons must be made with anisotropic elastic theories. The two dimensional triangular lattice has the same strain energy as a two dimensional continuum when first neighbour Hookian springs connect the

atoms. The energy of the continuum is computed by a finite element analysis in which the finite elements are triangles whose sides are the Hookian Springs (Hernnikoff 1941)

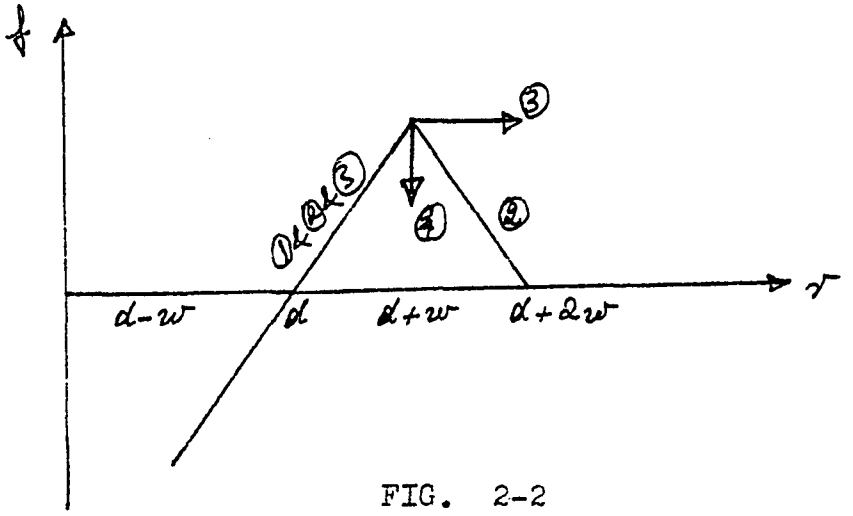

FIG. 2-2

FORCES USED IN THE ASHURST HOOVER MODEL

(1) Parabolic potential

(2) Double parabola potential

(3) Parabola linear potential

The similarities between the two dimensional continuum and this lattice, and the simplicity of the lattice made it a good starting point for fracture studies. Ashurst & Hoover used the central difference method to integrate the equations of motion. The force laws are sketched above. Their study started with fixed loads applied in the y - direction with periodic boundary conditions in the x - direction. The large horizontal surface deformations obtained, led them to switch to fixed displacement (grips) boundary conditions (with the x - periodicity removed and replaced by fixed vertical boundaries).

Their static calculations were done with the parabolic potential of type (1). In these calculations ($w \ll d$) (N.B. value of $(\frac{w}{d})$ was not mentioned explicitly in the paper for the static calculations). The results indicated that for small cracks the molecular dynamic energies can be as large as two times ~~as large as~~ the continuum predictions. The extrapolation of the molecular dynamic energies to the large crack length limit gave an energy very close to the continuum prediction. They obtained a correction to the continuum result in the form of an additive term linear in l for the energy U_E.

$$U_E = \frac{\sigma^2}{k}(0.68 l^2 + 0.6 l d) \qquad (1)$$

The ccefficient of the $\sigma^2 l^2$ term in (1) is predicted by linear elasticity to be π/E . For this force law, the appropriate two dimensional relation between the same parameters and E (see next Chapter) gives $E = 2k/\sqrt{3}$, which gives $\pi/E = 2.72/k$ as compared with the $0.68/k$ reported in equation (1).

The authors reported that their results agreed with the continuum result about the dependence of the critical stress on the length

$$\sigma_c \propto \frac{1}{\sqrt{l}} \qquad (2)$$

The agreement with the continuum result is understood to apply to the large ℓ limit only, otherwise an energy analysis of (1) would not lead to the simple form (2) but to a modified one inversely proportional to $\sqrt{\ell + A}$, A being a constant.

The authors reported observing an appreciable lattice trapping of $\sigma_+ / \sigma_- = 3.7$ (where σ_+, σ_- are as defined in chapter I).

The dynamic calculations were done in three stages, initialization, relaxation, and propagation. In the first stage the appropriate bonds were cut. In the second the atoms were critically damped for a hundred steps. In the third, the widths of the potential was adjusted so that the critical bond just broke. The results therefore, do not represent experiments done on the same solid, but rather on a set of different solids having the same elastic properties and different mechanical strengths. The authors reported crack velocities which are monotonic functions of the necessary w for types (1) & (2) force laws. The necessary w is the maximum w which will cause the critical bond to break. If the critical bond has a length of r_c for some applied strain ε, the necessary w will be infinitesimally greater than $r_c - d$. Since for any crystal below critical r_c is a monotonic function of ε, it follows that the necessary $w \left[= r_c(\varepsilon) - d \right]$ will be a monotonic function of the applied strain ε.

The Ashurst - Hoover results of the monotonic dependence of the crack velocities on the necessary w can be interpreted as indicating a monotonic dependence of v_c on ε . According to the Mott theory for these boundary conditions the terminal velocity (whenever it could be attained) is a material property independent of ε . In general this theory predicts that a crack under fixed ε will reach a terminal velocity only when the initial size is small with respect to the total area of the sample. Otherwise the crack will accelarate for a while,then deaccelerate and finally get arrested (Lawn 1975, p.97). The w (& therefore ε) dependence reported by Ashurst & Hoover is therefore not in agreement with the Mott prediction. The authors have extrapolated their terminal velocity data type (1) to the large l limit and find an extrapolated $v_T = .49 c_l$ (c_l = long sound velocity).The Mott theory predicts a $v_T = .38 c_l$. Their data also showed that type (2) potential gives lower terminal velocities than type (1) due to the extra attractive energy offered by the type (2) double parabola. Crack arrests have also been reported. The results indicated that the double parabola causes arrests more than the single.

The supersonic regime was investigated. Crystals were loaded to high strains and cracks were then introduced . Results were reported in terms of the parameter δ . The initial stretch of a bond across the crack plane (row in 2D) but away from the tip is $w - \delta$. The higher the applied

strain ε , the lower δ is. For a sample loaded to the ideal strength of the perfect (non-cracked) solid δ is zero. The authors reported terminal supersonic velocities linear in $\sqrt{\frac{w}{\alpha}}$ for small δ/w (i.e. high ε).
No dislocations were reported in this study.

Discussion

The reason for the occurence of supersonic velocities with the linear potential can be understood in the light of the Sanders and Weiner-Pear studies. As mentioned before in the discussion of these papers, the linear potential was found to prohibit plastic deformation. Thus here all the energy released from the loads and the strain field is forced to go into propagation, rather than being split between propagation and plastic deformation. This results in over-acceleration to supersonic velocities.

The snapping mechanism by which the propagations were initiated can help in understanding the absence of dislocations in the double parabola runs. The double parabola gives rise to a force law similar to the Weiner et al plastic potentials, and should have given dislocations. In the Ashurst-Hoover study the bonds are broken and then the crystal is only partially relaxed (with critical damping) for a hundred steps. At the end of the hundred steps $2w$ was reduced to that propagation starts. This process does not allow the lattice to perform all the deformation it wants to perform (in order to minimize the free energy). First, the way in

which the damping affects dislocation formation is not understood (it could oppose it because the rate of deformation is reduced). Second even if the system, inspite of the damping is proceeding towards a dislocation formation, the hundred steps of partial relaxation might not be sufficient for the dislocation to get completely formed. When the w is adjusted at the end of the hundred steps, surface creation (by propagation) is given an artificial preference over plastic deformation. The sample is thus forced to possess excess brittleness than it would have shown if it would have been left to evolve by itself under a fixed potential.

Finally, the fixed vertical boundaries could have prohibited motion parrallel to the crack (resulting from the non-negligible shear fields). This is because these boundary conditions fix the density in the x - direction and would thus resist any motion which tends to alter this density.

KANNINEN et al (1970 - 1973)

The work of the Kanninen group concentrated on BCC iron and used a Johnson potential. In a first paper (Gehlen & Kanninen 1970) a crack in the (100) plane (xy plane) was studied. A small number of layers were used. In order to simulate an infinite solid, periodic boundary conditions were employed in the direction perpendicular to the crack plane. The authors were unable to obtain a propagation even

when the stress intensity factor $K = \sigma\sqrt{\pi l}$ was raised far above the critical value $K_q = \sqrt{2\delta}$ predicted by the Griffith theory. The authors viewed the lack of propagation as resulting from their Z -periodic boundary condition. A crack motion in this situation must involve a motion along one of the body diagonals of the unit cell. The motion of the seperating first neighbours (at the tip) has a component in the Z -direction. Such a motion will thus reduce the average density in the Z -direction. The Z -periodic boundary condition tends to keep the average density (in Z -direction) fixed, and will thus oppose such a motion and help in locking the crack.

In a second paper (Kanninen & Gehlen 1971) tried to move the crack by introducing a jog in the crack line. They used two seperate small crystallites one containing a crack of length l and the other of length $l + \frac{1}{2}a$ where a is the lattice parameter. The two crystallites were placed together, thus forming a jogged crack. The closure and extension of this crack was studied as a function of stress level. No actual propagation or healing of cracks was studied. What the authors mean by extension and closure is the following. When the shorter portion of the crack whose length is l becomes of length $l + \frac{1}{2}a$ they consider the crack above critical and about to extend. When the $l + \frac{1}{2}a$ portion becomes of length l, the crack is considered below critical and about to heal. Thus their simulation (as noted by them in their

discussion) allows crack motion only by half a lattice spacing. The authors think that this jog mechanism would be self sustaining in a real crystal. In this study their ∓ boundary conditions was removed.

The authors have also observed a static dislocation-like deformation at their tip (at 45°). They attributed the lack of propagation of the dislocation to their fixed isotropic boundary conditions in the x-y plane.

In subsequent studies (1973) the authors have made their x-y boundary conditions flexible (and anisotropic). A crack propagation was obtained.

2 C MOTIVATION FOR THE PRESENT CALCULATION

As mentioned previously the W-P and A-H models have given some results which are in contradiction with the continuum predictions. In particular, the two models have obtained load dependent terminal velocities, and also supersonic velocities for high loads. It is of interest to know whether these continuum violations have resulted from the idealized nature of the simulation, or whether they are true consequences of the atomic discretness of the lattice. When the discussions of the W_P and A-H models were given, it was pointed out that restrictions in the models can indeed produce unphysical results. Thus the discussion of the W-P model

proposed an explanation of their supersonic velocity in terms of the one dimensionality of their lattice (which prohibits bifurcation). The discussion of the A-H model proposed an explanation of the supersonic velocity in terms of the absence of dislocations due to the particular way in which the propagations were obtained, and due to the nature of the potential.

A model will be used here which resembles the A-H two dimensional triangular lattice with the more realistic L-J potential. The basic goal is to remove all restrictions on the atoms and allow them to perform any preferred motion. The A-H periodic and fixed vertical boundary conditions will thus be removed. The model will be two dimensional so that the one dimensionality difficiency which is present in the W-P study will be absent.

A L-J potential (with forces between atoms whose distance is greater than 1.6α neglected) will be employed, so the results will refer to a single solid with a unique mechanical strength (not like the A-H model in which the strengths were different). For propagation studies, no damping will be used. The unrestricted time evolution after the introduction of the cut will be studied. In this way the lattice will deform in the mode which is energetically favorable. The time evolution will be carried out until all transient effects die out except when propagation results. In the A-H model

only a hundred critically damped time steps were done before inducing a propagation by adjusting w . This adjustment of w which helps the propagation to start before large deformations take place will not be repeated here. Instead the lattice will be allowed to deform as much as it wants before the critical condition of fracture initiation is reached. Damping will be employed only in the runs in which no propagation is observed in order to speed the approach to equilibrium. In some of the runs damping will be employed to see whether it would affect dislocation formation or not.

One of the basic goals of the calculation will be to study the time evolution of the different parts of the total energy (strain, kinetic, surface, and loads) to check the validity of the assumptions which go into the Griffith and Mott theories. The time evolution of these quantities has not been reported in the A-H study.

The model is not intended to correspond to any real material. It is believed that studies of such idealized models can still give valuable understanding of fracture before proceeding to more realistic three dimensional models.

Summary

Section 2A has described why atomistic calculations are of interest and importance in general. In 2B the details of previous molecular dynamic calculations have been given. In 2C some of the motivations for the present calculation have been given. Because the discussion has been rather detailed, it seems appropriate at this point to summarize the goal of the present calculation.

(1) Examination of the different assumptions which go into the Griffith and Mott theories.

1a. Checking the continuum expression for $\mathcal{U}_E$ for this type of loading and for these boundary conditions (i.e. free vertical boundaries),

1b. Checking the validity of the relation between the work and the increase in strain energy both at the start of the motion and later in the propagation.

1c. Examination of the Mott quasistatic assumption about the stress fields.

(2) Calculation of stress profiles for a long range potential and comparing them to the Eringen non-local profiles.

(3) Studying the time behaviour of the different parts of the total energy (surface, strain, kinetic, and work of loads)

(4) Studying the effects of stress level and crack length on the brittleness and ductility of the lattice.

(5) Studying the problem of the attainability of supersonic velocities in a lattice which is free to generate dislocations and to exhibit branching.

Molecular dynamics will be employed in the simulations.

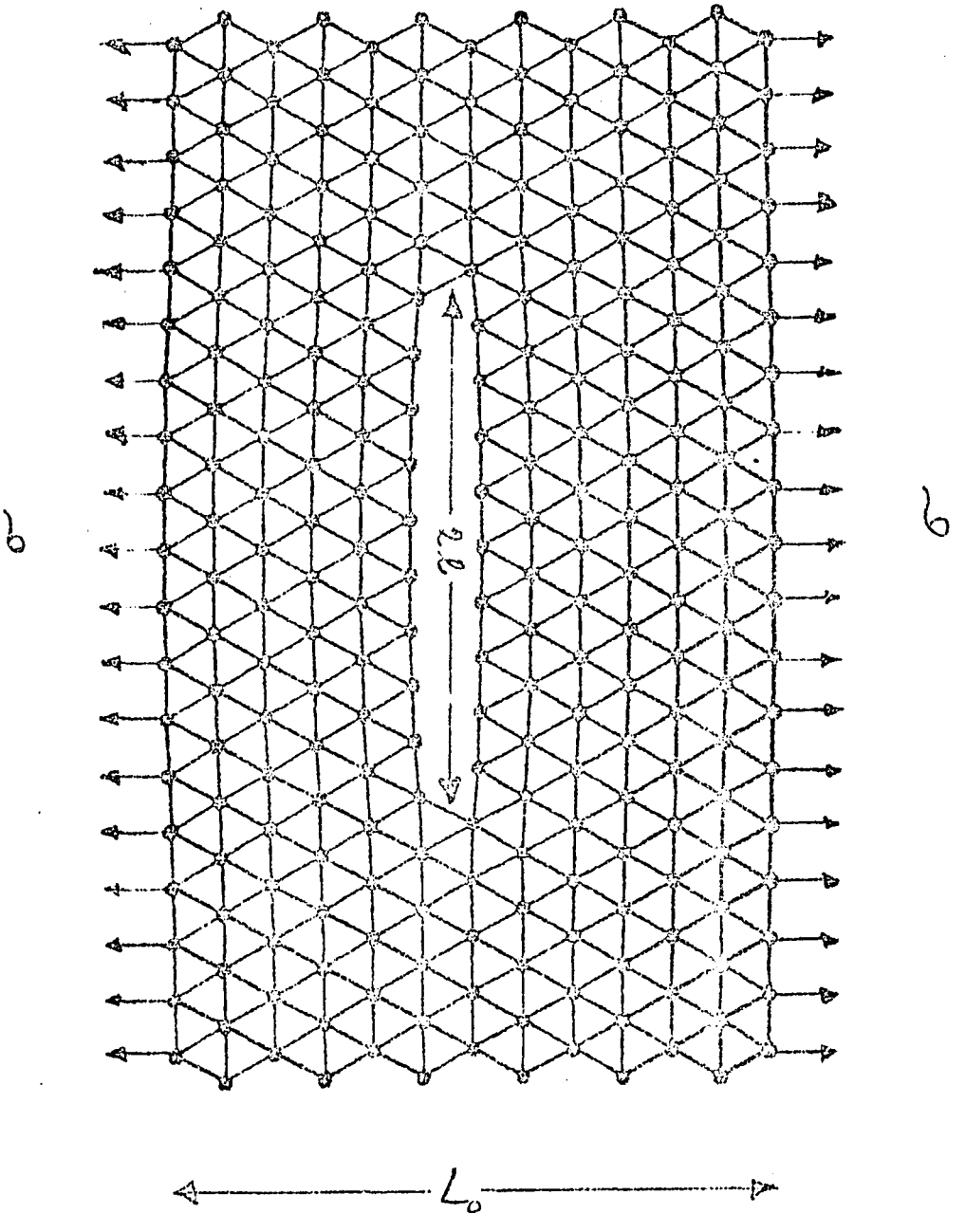

Fig. 2-3

CHAPTER 3

3A MOLECULAR DYNAMICS

Due to the fact that the technique of molecular dynamics has become well known (and fairly direct), no detailed description of it will be given here (for examples of molecular dynamic calculations see Paskin et al 1968 - 1978). Instead, some of the limitations of the technique and details pertinent to the present problem will be discussed.

The basic limitation of the technique is the small duration in time of events which ca be handled by the technique (10^{-10} sec.) This means that only phenomena in which the characteristic times are of this order can be studied by the technique.

Another serious limitation is the small number of atoms which can be handled (due to computer memory capacity). This limitation has led to the reduction of the present model to two dimensions. In many situations a large enough two dimensional model can lead to a clearer and more realistic understanding of the phenomenon, more than a much smaller 3-D model. This means that a 3-D model is not necessarily more realistic than a 2-D one. The Kanninen et al model is an example of this. Their whole sample is effectively a tip. The proximity of the boundaries produces small size effects which lead to

unnecessary complications in the problem.The size limitation can cause a serious size dependence in the results of some simulations. This point will be discussed further when the results of the present simulation are given. To reduce this finite size effect periodic boundary conditions are sometimes used. When this is done, the simulation sample is taken to represent a typical cell inside a solid composed of a periodic repetition of such cells. However one should be careful in the use of such boundary conditions specially in the simulation of lattice defects like dislocations or cracks. This is because such boundary conditions limit the average density in the direction which they are applied. This fixed density could inhibit some degrees of freedom of the system and would thus cause the system to behave in an unnatural way. An example is given by Gehlen & Kanninen (1971) in which the periodic boundary condition in the z - direction of a sample containing a crack in the x-y plane. This z periodic boundary condition prohibits the motion of the crack.

Molecular dynamics has been applied to look for equilibrium configuratıcns of defects, and also of monequilibrium phenomena. In cases in which the interest is in finding the stable states (equilibrium)various damping techniques are employed in order to speed the approach to equilibrium. This is done by removing kinetic energy from the system in some way. The damping technique employed depends on the

particular situation at hand. Using a ~~non~~ suitable damping technique could slow the approach to equilibrium rather than speed it. For example, in cases in which the atoms are approaching their final equilibrium positions via vibrational motions, the Beeler-Kulcinski technique is very suitable. This technique consists of setting the velocity of the i-th atom to zero whenever $\underline{v} \cdot \underline{a}$ becomes negative. However, if this technique is applied to problems in which the approach to equilibrium is via a collective motion (e.g. a crack problem) the result is a slowing down of the approach to equilibrium. Other damping techniques set the velocities of all the atoms to zero when the total kinetic energy reaches a maximum. Still other methods use a damping parameter to withdraw a fraction of the kinetic energy of each atom in every step. This damping parameter is varied until the most suitable value which satisfies some criterion (e.g. critical damping) is found. The main point which should be stressed here is that a moderate amount of damping is generally required. Too much damping slows the approach to a stable state and no damping slows down the process tremendously. Usually one needs a degree of experience with the system at hand in order to find the most suitable damping method.

The discussion in the previous paragraph referred to equilibrium states at zero temperature. If one wants an equilibrium state at finite temperatures then no damping

could be employed. To simulate temperature the atoms are given random displacements of some maximum magnitude. This maximum magnitude determines the value of the temperature which is simply the appropriate kinetic energy of the atoms.

The methods used to carry out the integration usually involve transforming the second order differential equations of Newton into a finite difference equation. The most commonly employed methods are the central difference method (Verlet), the generalized predictor corrector methods, and the Nordseik-Gear multistep methods (see Beeler & Kulcinski 1971) for an exposition of the different methods). The main difference between these methods is in the number of previous positions (or equivalently the number of higher order time derivatives) which are used to predict the new positions and thus in the computer memory requirments of the technique. Excluding some special cases, one could make the general statement, that the more memory used by a method,the higher the accuracy of the method.This is true provided the limit of the double precision word of the computer is not reached (N.B.This is not a serious restriction because stacking techniques could be used to pack groups of computer words together to produce larger words capable of giving higher accuracies). Thus, the higher the order of the method used the larger the time step one could use. Of course the larger the time step allowed the less computer time a certain job requires. Hence the choice between the various

methods available becomes dependent on the accounting practices of the computer system used. Thus for example, for the CDC 7600 system at BNL higher order methods turn out to be generally cheaper than lower order ones. There is however a practical consideration which favours the lower order methods when a large number of atoms is used. The large memory needed due to the large number of atoms plus the large memory required by the high order of the method add up and tend to slow the turn around time in obtaining the results in a serious way.

Originally when the present calculations were planned the Nordseik-Gear method of order seven was going to be used. Earlier, a comparison had been made between the central difference method and this method on a small FCC L-J solid. It was found that the same accuracy resulted when the Gear-Nordseik time steps were 4-6 times as large as the central difference time steps. When a cost calculation was performed it was found that the Gear-Nordseik was cheaper. However because of the turn around time problem mentioned in the preceeding paragraph, the central difference method has been used in the present calculation.

3 B THE PRESENT CALCULATION

The details of a calculation performed on a 2-D triangular lattice, using a first neighbour Lennard-Jones potential will now be given.

The interaction energy ϕ_{ij} between atoms i & j was assumed to be of the form

$$\phi_{ij} = \phi(r_{ij}) = \epsilon\left[\left(\frac{\alpha}{r_{ij}}\right)^{12} - 2\left(\frac{\alpha}{r_{ij}}\right)^{6}\right] \qquad (1)$$

where ϵ is the depth of the potential and α is the nearest neighbour distance (for a nearest neighbour calculation). The value of α is obtained by minimizing the free energy of the lattice at zero temperature and with no applied loads.

The Verlet central difference method has been used to integrate the equations of motion

$$\underline{r}_i(t+\delta t) = -\underline{r}_i(t-\delta t) + 2\underline{r}_i(t) - \frac{(\delta t)^2}{m}\underline{F}_i \qquad (2)$$

where m is the mass of an atom $\underline{F}_i$ is the force on it due to the other atoms. A value of $\delta t = 10^{-2}\alpha\sqrt{\frac{m}{\epsilon}}$ has been used. This value has been found to conserve energy to six places in previous studies on the same lattice.

The computer code for solving the problem consists of five parts, a main program called (CRACK) and four subrou-

tines called (PLACEM, NEBOR, DYNMOL, and FORCE).

The main program (CRACK) initializes execution by reading in the relevant parameters and calling on the subroutine PLACEM. The relevant parameters are the size of the sample, the length of the crack, the cut off of the potential, and the required number of steps.

The subroutine PLACEM places the atoms on the required lattice, and determines the shape of the crystallite. It then calls the subroutine NEBOR.

NEBOR conducts a search to find the neighbours of every atom in the crystallite and then places these neighbours in a table. In many problems (e.g. shock waves) one could form a reduced table using the first few planes in the sample (or first few rows in 2D). This reduced table could be used to find the neighbours of any atom in the sample by finding the member of the reduced table which corresponds to the atom. In other problems in which there are significant differences in the environments of atoms appearing in different parts of the crystallite, it becomes necessary to form a full table. This is the case for example in the crack problem. NEBOR calls on DYNMOL which in turn calls on FORCE where the forces of interaction $\underline{F}_i$ are computed. After the return to DYNMOL from FORCE the Verlet solution is carried out for every atom. When damping is required it is

done in the Verlet loop by introducing a damping parameter β in the velocity term in the Verlet equation (2)

$$\underline{r}_i(t+\delta t) = \underline{r}_i(t) + \beta\left(\underline{r}_i(t) - \underline{r}_i(t-\delta t)\right) - \frac{(\delta t)^2}{m}\underline{F}_i \qquad (3)$$

This corresponds to absorbing a fraction of the kinetic energy at $(t - \frac{1}{2}\delta t)$, $\beta =$ corresponds to no damping and $\beta = 0$ to full damping . As mentioned before the damping can slow or enhance the approach to equilibrium. Different damping parameters have been tried on the small sample. Continous damping every step for some fixed β, full damping every steps (100 or 200), and the Beeler-Kulcinski damping mentioned before have been tried. An optimum parameter β of 0.9875 has been found to give critical damping for the small sample. For this β fluctuations in the total potential disappeared. This value of β has been used in the large sample whenever damping was required.

When it is required to apply an external force to some of the surface atoms, the Verlet equation (3) for these atoms is modified as follows

$$\underline{r}_i(t+\delta t) = \underline{r}_i(t) + \beta\left(\underline{r}_i(t) - \underline{r}_i(t-\delta t)\right) - \frac{(\delta t)^2}{m}\left(\underline{F}_i + \delta\underline{F}_i^{\circ}\right) \qquad (4)$$

Where $\delta \underline{F}_i^{\circ}$ is the external force on the surface atom i . The application of the external forces could be done in one

step or as gradual as required.

The remaining part of DYNMOL consists of computing the quantities of interest from the coordinates just found. Time averages of the energies (PE & KE), strains, and Young's modulus are found and printed out.

In cases in which extensive deformation takes place as in the dislocation emmitting propagations, the initial table of neighbours does not contain the new interactions which come into significance by virtue of the deformation. In such cases, the table needs to be updated periodically in time. This is done, for most runs every twenty steps by a call from DYNMOL to NEBOR.

The subroutine FORCE which feeds the forces to DYNMOL operates as follows. A loop is constructed which goes through all the atoms to compute the force on each due to its neighbours. Use is made of the table formed in NEBOR. Use is also made of the equality of action and reaction to compute the interaction f_{ij} only once and then use it twice once for atom i & then for j.

The potential energy is also computed in FORCE. When it is required to introduce a crack, the interactions across the faces of the crack are set to zero (turned off).

FORCE also contains a small subprogram which calls on the DISSPLAY graphic system in order to produce a pictorial representation of the lattice. In most of the runs the small circular dots representing the atoms are removed and vectors connecting the atoms are drawn in order to indicate the interactions present. The vector connections are drawn at the instant the forces are computed.

A fifty percent saving in computer time can be obtained by using the left right symmetry of the cracked system. This requires a special treatment of the atoms lying near the central symmetry axis of the crystallite. One half of the crystallite is used but two columns of the neglected half are kept. These form a mirror for the last columns of the half which is retained.

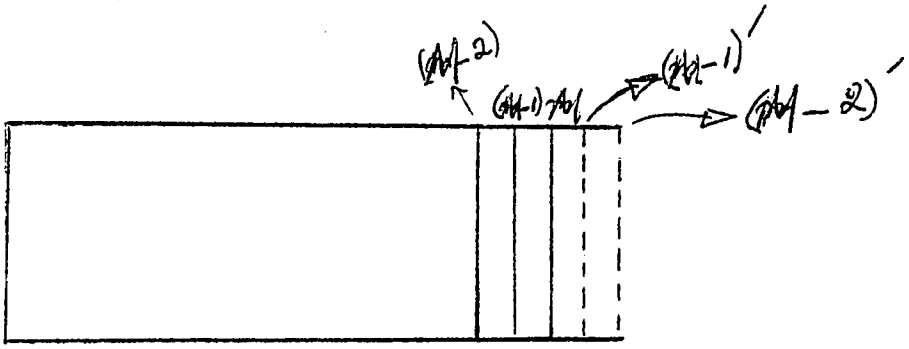

The coordinates of the first 2 columns in the neglected half crystal are found by reflection (e.g. $(M-1)'$ is the reflection of $(M-1)$ in (M)).

FIG. 3 - 1

The position of the mirror columns are found by reflecting m-1, m-2 in m. The use of these columns is to make the last few columns of atoms in the half crystallite behave as bulk atoms at the center of the sample and not as surface ones.

Finally the problem contains a part in DYNMOL which stores the final information in a run in such a way that continuation of the run is possible if required.

3 C MECHANICAL PROPERTIES OF THE TWO DIMENSIONAL TRIANGULAR LATTICE.

One of the goals of the present study is to carry out a careful comparison between the predictions of the continuum theories and the results of the molecular dynamic model. Some care should therefore be devoted to pick the continuum results which correspond to the two dimensional system at hand. Also the comparison will involve the use of Young's modulus E . One way to obtain E is directly from the results of the simulation. However one would also like to obtain E from the interatomic potential and the geometry of the lattice.

The Born theory (Born & Huang 1965) enables one to calculate the Lamé's parameters λ, μ . Classical elasticity supplies a relation for E in terms of λ, μ in 3-D.

If one wants to find E for the present system, the corresponding 2-D relation for E in terms of λ, μ has to be used.

Ashurst & Hoover (1976) as well as Esjborn and Jensen (1976) have realized that application of 3-D elasticity results to 2-D leads to inconsistencies. The conclusion of Esjborn & Jensen is that for 2-D the elasticity results of 3-D plane stress should be used. For the present calculation the numerical differences which result from using plane strain or stress are almost trivial. Here the application of the correct continuum form(plane stress) leads to a result 12.5% larger in the strain energy U_E, and 6% smaller in the Griffith stress σ_f, than if the incorrect form is used. Thus for the present system

$$U_E = \frac{\pi}{E}\sigma^2 \ell^2 \quad ; \quad \sigma_f = \sqrt{\frac{2E\gamma}{\pi \ell}}$$

Detailed analysis leads to the conclusion that λ, μ are equal for this lattice when the $L\text{-}J$ pair potential is used (any pair potential gives $\lambda = \mu$ for this lattice). The system is elastically isotropic. In 2-D it is found that,

$$\left[E = \frac{4\mu(\lambda+\mu)}{\lambda+2\mu}\right]_{2D} , \left[\nu = \frac{\lambda}{\lambda+2\mu}\right]_{2D} \qquad (5)$$

whereas the relations in 3-D are

$$\left[E = \frac{\mu(3\lambda+2\mu)}{\lambda+\mu}\right]_{3D} , \left[\nu = \frac{\lambda}{2(\lambda+\mu)}\right]_{3D}$$

Hence for the present case

$$E = \frac{8}{3}\mu \quad , \quad \nu = \frac{1}{3} \tag{6}$$

For the L_J potential this gives

$$\mu = 18\sqrt{3}(\epsilon/a^2)$$

$$E = 48\sqrt{3}\,\epsilon/a^2 = 83.14\,(\epsilon/a^2) \tag{7}$$

This value of E does not take care of the non-linear nature of the potential. It is expected to be close to the measured value only for small stresses. The measured values will be given with the result below.

Although the lattice is isotropic in the elastic properties, it has different mechanical strengths in the different directions. In the y - direction $\langle -1, 2\rangle$ the maximum local tensile stress, the lattice can withold is approximately

$$\sigma_{MAX} = 2 f_{MAX} \cos 30^\circ = \sqrt{3}\, f_M = 4.66\,(\epsilon/a^2)$$

where f_{MAX} is the maximum force exerted by a L J – bond at its inflection point $\left[= \left(\frac{13}{7}\right)^{1/6} a\right]$. In this estimate the decrease in the length of lateral bond (AC) has been neglected.

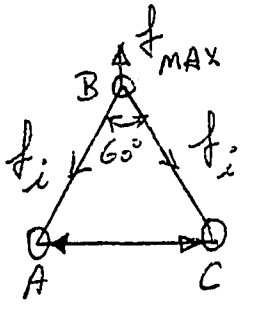

$$f_{MAX} = 2 f_i \cos 30^\circ$$

$$f_i = f\left(\left(\frac{13}{7}\right)^{1/6}\right)$$

All calculations were performed below this level.

3 D INTRODUCTION TO RESULTS

The computer simulations were done on samples containing 39 rows of atoms. The odd numbered rows contained 135 atoms and the even contained 136. The left-right symmetry was used throughout the large sample calculations. Each preloading simulation was done by loading the perfect sample to the required stress and then introducing the cut. In all such cases the perfect samples were brought to equilibrium $T = 0$ before cracking. This was done by using a damping parameter $\beta = 0.9875$. To save computer time, the perfect samples were prepared from previous ones by scaling the displacement fields. The scaling was always followed by a period of non-damped relaxation, and then the samples were damped to equilibrium. This was done in order to allow for a displacement field consistent with the non-linear force law.(N.B. The scaled displacement fields correspond to a linear force law.). For the preloading experiments no damping was applied after cracking. In order to study crack statics some of the cracked samples were damped with $\beta = 0.9875$.

The postloading simulations were done by taking a crack in equilibrium and increasing the applied stresses.

A table update was done every 20 steps with neighbours less than 1.6 α apart included. The time step was $10^{-2}\alpha\sqrt{m/\epsilon}$, where m is the mass of the atoms. α and ϵ have been defined before.

Potential, kinetic, surface, and strain energies were monitored throughout the runs. Surface strain ϵ, effective modulus E', and critical bond lengths were also monitered.

Brittle, semi-brittle, and ductile behaviours were observed depending on the crack lengths and loading parameters. Dislocation creation, annihilation, and motion were also observed. Healing experiments were conducted with no evidence found for lattice trapping. Static results indicated that the continuum predictions for the strain energy is always less than the molecular dynamic values for fixed loads.

The Griffith concept was tested. The continuum relation between work and increase in strain energy was not satisfied in general. In one case the sample behaved in a rigid fashion with $\alpha \mathcal{U}_E \approx 0$.

In general the Mott picture of a gradually accelerating crack was not observed. Instead the velocities increased more quickly.

Stress concentration curves were obtained both for the static and dynamic cases. The non-local continuum result giving a stress independent stress concentration factor did not agree with the results of the simulation. $\mathcal{F}$ was found

to be σ dependent. One propagation remained clean until the very end of the sample. Another ended in bifurcation, and a third in surface roughening and a region of extended damage.

The clean fracture was still accelerating at the time the end of the sample was reached. Some information about the possibility of attaining a supersonic velocity could have been obtained from this run if the sample had been longer.

It was not possible to investigate the supersonic regime because all highly stressed samples blunted by dislocation formation and plastic glide.

Before the large samples were studied preparatory runs on smaller samples were carried out. In these small sample experiments crystallites containing 253 atoms were used. The small samples consisted of 13 rows with the odd ones containing 19 atoms and the even ones containing 20 atoms. In general the small samples showed a great tendency to deform plastically and generate dislocations. It was not possible to obtain brittle fracture except by introducing a cutoff on the potential. The form of the fracture surface was found to be sensitive to the cutoff and damping technique (whenever damping was used). Because such small sample calculations were sometimes damped, the runs could not be used to obtain information about velocities (since the time

steps do not represent real time anymore). The samples were also too small to investigate an actual propagation. In some of the small runs the left-right symmetry was used. Most of the small sample simulations were for fixed loads but some fixed strain experiments were also done.

The goal of the small sample simulations was to gain familiarity with the system rather than to obtain accurate numerical information. Thus most of the quantities which were monitored for the large samples were not monitored for the small ones. When the small sample calculations were done an optimum damping technique had not yet been found. The experiments were thus done with different damping methods. Before presenting the results some definitions have to be mode. These are the definitions of U_E, E_{eff}, and W.

The strain energy due to a crack is defined by the relation

$$U_E(\ell) = \Delta V - U_s \qquad (1)$$

ΔV is the change in the potential energy and U_s is the surface energy due to the crack

$$\Delta V = V(\ell) - V(0) \qquad (2)$$

$V(\ell)$ is the potential energy of the system when the crack length is 2ℓ and $V(0)$ is the potential energy before cracking. Also $U_s = N_b \epsilon$ where N_b is the number of broken bonds, and ϵ is the depth of the L-J well. From now on all energies will be given in units of ϵ, distances in α, stresses in ϵ/α^2, and time in $10^{-2}\alpha\sqrt{m/\epsilon}$.

Comparisons will be made between U_E^{MD} (strain energy obtained by molecular dynamics) and U_E^c (by continuum mechanics).

Another quantity of interest is the effective Young's modulus (Berry 1960). To define this, one writes the total strain energy for a cracked sample

$$S.E. = \frac{\sigma^2 A}{2E} + \frac{\pi \sigma^2 \ell^2}{E}$$

where A is the area. If one assumes that the sample as a whole behaves in a linear fashion with an effective modulus E' then

$$S.E. = \frac{\sigma^2 A}{2E'}$$

Comparing the two expressions for the strain energy gives

$$E_{eff} \equiv E' = \frac{E}{1+\alpha_0} \quad ; \quad \alpha_0 = 2\pi \ell_0^2 / A \qquad (3)$$

One could also test the continuum predictions by comparing the change in strain ε for fixed loads (or stress σ for fixed strain) due to the crack. Using (3) one gets

$$\sigma' = \sigma - \frac{\alpha_0 \varepsilon E}{1+\alpha_0} \qquad (\text{fixed } \varepsilon) \qquad (4)$$

where σ is the stress before and σ' after the introduction of the crack. Also

$$\varepsilon' = \varepsilon + \frac{\alpha_0 \sigma}{E} \qquad (\text{fixed } \sigma) \qquad (5)$$

Of course continuum theory predicts (3),(4),and (5) only for an equilibrium situation.

In the large sample data which follows, the W is the work done by the loads in straining the sample from the unstrained perfect state to the present state.

$$W = \sigma \varepsilon A = 135 f_a \varepsilon L_o \qquad (6)$$

where $L_o = 38\sqrt{3}/2$ is the zero stress length of the sample, f_a is the applied force on a surface atom. To check conservation of energy in a time interval one should compare the change in W to the sum of the changes in U_E, U_{SP}, and U_K.

There is an error in W introduced by neglecting forces between atoms beyond a certain maximum distance. As mentioned in the description of the calculation, a table of neighbours is formed at the beginning and updated every 20 steps. Only forces between members of the table are included in the calculation. The table includes atoms whose distance apart is less than or equal to 1.6 . The force between two seperating atoms will be included even if their distance apart exceeds 1.6 provided a new table update has not yet been reached. The runs have indicated that forces are usually included up to a separation of $r_{MAX} = 1.6 + \Delta$, where $0 \leq \Delta \leq .04$. Thus for a pair of atoms the force is included for $r < r_{MAX}$ and then suddenly drops to zero for $r > r_{MAX}$

This is equivalent to using a L-J which drops to zero discontinously at $r = r_{MAX}$, figure (3-2(a))

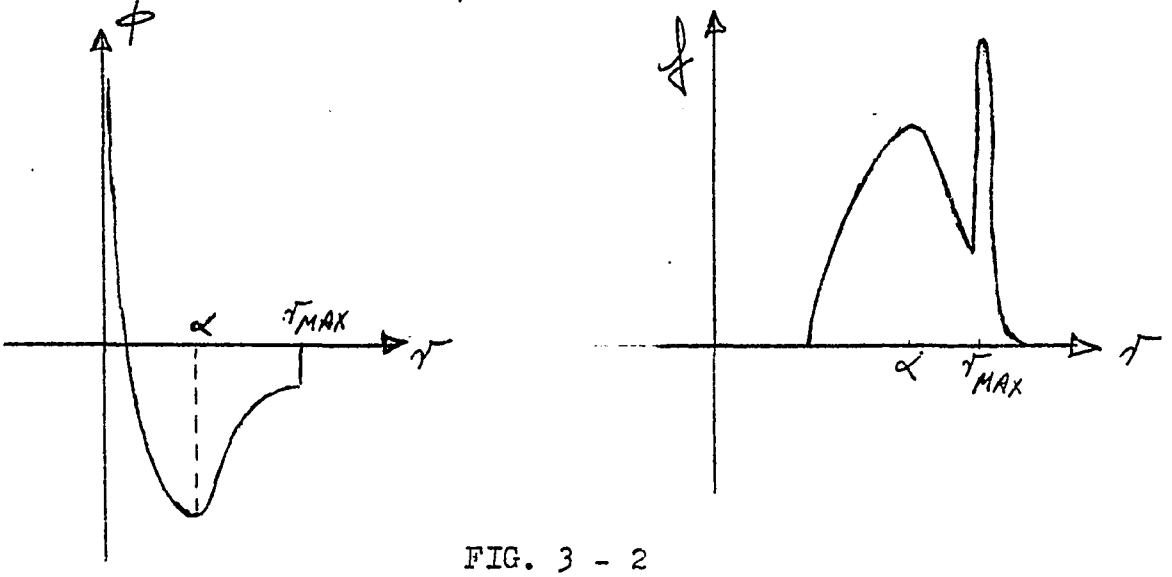

FIG. 3 - 2

In the calculation, neglecting the energy for $r > r_{MAX}$ is equivalent to neglecting the work done in separating the atoms through r_{MAX} . In the vicinity of r_{MAX} the potential is approximately a step function, giving a force in the form of δ- function (figure 3b).

$$f(r) = |\phi(r_{MAX})|\,\delta(r - r_{MAX})$$

for $r_{MAX} - \delta' < r < r_{MAX} + \delta'$, $\delta' \to 0$.

The neglected work is thus the r integral of this delta force which is $|\phi(r_{MAX})| \cdot$

$$|\phi(r_{MAX})| = \left| \int_{r_{MAX}-\delta'}^{r_{MAX}+\delta'} f(r)\,dr \right|$$

Thus once a propagation starts, one should correct the work done on the sample by adding $(N_b - N_b^0)\,|\phi(\sigma_{max})|$ where N_b^0 is the number of originally broken bonds, N_b is the number of broken bonds at the present time. Work corrections have been included in all large sample runs.

The dynamic stress fields of the propagating cracks were studied. Actually, force fields, the discrete analogue of the continuum stress fields, were studied. These will be referred to as stress fields from now on. The fields which can be calculated readily from an atomistic model and which are of interest here, are the tensile fields. These are σ_{yy} , σ_{xx} . In the dynamic case there is no guarantee that $\sigma_{yy}^{(+)} = \sigma_{yy}^{(-)}$ i.e. that the stresses up will be equal to or close to the stresses down. The equalities will hold in an approximate way only when the separation process is quasistatic. The same comments apply to $\sigma_{xy}^{(+)}$ & $\sigma_{xx}^{(-)}$ (σ to the left and to the right) At the beginning of the stress profile investigations the four quantities were monitored i.e. σ_{up} , σ_{down} , σ_{right} , σ_{left}. The equalities were found to hold almost exactly for atoms away from the tip. The quantities were close but not equal near the tip. In the results which follow the profiles will be given for σ_{right} and σ_{up} only although the maximum values of σ_{left} and σ_{down} will be quoted in tabular form. The stresses will be given for the four central rows 18,19,20,21 which lie above and below the crack. It is also of interest to know

the form of the stress profiles as a function of y. Thus σ_{right} is given for columns which are close to the tip. A column M includes all atoms which originally (in the stress free sample) had the same x-coordinate $=(M-1)\alpha$ and those which had an x-coordinate $=(M-1.5)\alpha$. Instead of σ_{up} or σ_{down} for the columns, a quantity of more interest σ_{open} (or σ_{close}) is given for the columns, where

$$\sigma_{open} = \begin{cases} \sigma_{up} & \text{for rows} > 19 \\ \sigma_{down} & \text{for rows} < 19 \end{cases}$$

A final remark about the stress fields is due. The longitudinal force fields $\sigma_{up}, \sigma_{open}$ correspond exactly to the real stress fields as defined in continuum theory. The transverse force fields should be multiplied by $2/\sqrt{3}$ to convert them to a continuum stress, since the linear density of atoms in the y-direction is less than that in the x-direction by $\sqrt{3}/2$. The conversion to real stress was not done in the results section.

In the small samples the crack investigated was between the 6^{th} & 7^{th} rows. It was formed of 118 broken bonds. In the large samples the crack was between rows 19&20.

Small sample experiments are referred to with an S (e.g. S4 will be the fourth small sample experiment).

Large sample simulations will be referred to with an L. A quantity

$$\mathcal{L}_X = (X)^C / (X)^{MD}$$

will be used to compare continuum theory and molecular dynamics for any quantity X.

RUN	σ	CUTOFF	DAMPING	COMMENTS
S 1	1.0	NONE	β = .9875	STATIC
S 2	1.5	NONE	EVERY 100 STEPS	D
S 3	1.25	NONE	"	-
S 4	1.35	NONE	"	D
S 5	1.35	NONE	"	HEALED
S 6	1.3	12%	"	B (UNEVEN)
S 7	1.3	12%	EVERY 50 STEPS	B (CLEAN)
S 8	1.3	NONE	EVERY 20 STEPS	STATIC
S 9	3.2	20%	EVERY 5 STEPS	B (CLEAN)
S 10	3.2	NONE	"	-
S 11-S 17	S E E T A B L E 3 - 3			
S 18	3.11	NONE	β = .9875	FIXED $\varepsilon = 5.047 \times 10^{-2}$
S 19	3.67	NONE	"	FIXED $\varepsilon = 6.56 \times 10^{-2}$
S 20	-	NONE	"	FIXED $\varepsilon = 8 \times 10^{-2}$

D = DUCTILE B = BRITTLE

TABLE 3-1

RUN	ℓ	σ	DAMPED	LOADING	COMMENTS
L 1	39	0.5	NO	PRE	RIGID TEARING
L 2	19	1.3	NO	PRE	SEMI BRITTLE
L 3	39	1.3	NO	PRE	ENDS IN BIFURCATION
L 4	39	0.5	YES	-	EQUILIBRIUM
L 5	19	0.5	YES	-	"
L 6	9	0.5	YES	-	"
L 7	19	1.3	YES	-	"
L 8	9	1.3	YES	-	"
L 9	39	0.5	NO	-	BONDS RESTORED (HEALING)
L 10	19	1.3	NO	-	"
L 11	39	0.5	NO	POST	CRACK STABLE
L 12	39	0.55	NO	POST	NO PROPAGATION
L 13	39	0.6	NO	POST	"
L 14	39	0.65	NO	POST	PROPAGATION
L 15	39	0.55	YES	-	EQUILIBRIUM
L 16	39	0.6	YES	-	"
L 17	19	3.0	NO	PRE	DISLOCATION BLUNTING
L 18	9	3.0	NO	PRE	"

SUMMARY OF RUNS

LARGE SAMPLES

TABLE 3-2

3E RESULTS

RUN S1 (FIXED LOADS) ($\ell = 9$)

The perfect sample was stressed to $\sigma = 1.0$. The potential energy V for the unstressed sample was (-696). The stressed perfect sample had a potential energy of(-694.7), giving a strain energy

$$(S.E.)^{MD} = 1.3$$

The value predicted by linear elasticity is

$$(S.E.)^{C} = \left(\frac{\sigma^2}{2E}\right) A$$

$$= \frac{(1.0)^2}{2 \times 76.9} \left(12\frac{\sqrt{3}}{2} \times 18.5\right) = 1.25$$

The two values are thus quite close, giving

$$f_{S.E.} = (S.E.)^{C} / (S.E.)^{MD} = 0.96$$

The crack was introduced at time step 8800. In order to choose the optimum damping technique a set of calculations were made for different damping parameters and for the Beeler -Kulcinski damping. The results are given in figure 3-3. The value $\beta = 0.9675$ was found to be the optimum one. This value was used in all large sample experiments which needed damping. Here the different damping methods converged to a value of -337.025 for the half sample. This gives

$$U_E^{MD} = \Delta V - U_S$$

$$= (-674.05 - 694.7) - 18$$
$$= 2.66$$

$$\mathcal{U}_E^c = \frac{\pi}{76.9}(1.0 \times 4.75)^2 = 0.92$$

This gives $\frac{f}{\mathcal{U}_E} = 0.35$

RUN S2 (FIXED LOADS)

The desplacement field of an equilibrated crack at σ=1.0 was scaled linearly to 1.5. The initial values of the positions of the atoms was determined from this scaled displacement field. A stress of σ=1.5 was applied. A full damping every 100 steps was used ($T = 0$). The tip was blunted by dislocation formation, and the dislocation moved to the lower surface of the sample. The run started at 7900. Figure (3-4) to (3-6) show the lattice at three time instants.

RUN S3 (FIXED LOADS)

Same as S2 but for σ =1.25. No propagation or dislocation formation were observed. In S2 and S3 no table update was used and therefore some of the interactions which come into play as a result of the slip process (in S2) are

not included here but were included in later runs. These interactions are present at the core of the dislocation and in general help the glide process and therefore enhances dislocation emission. Also some of the interactions which were originally 1st neighbour have become second after the slip. To make the calculation consistent, these should be excluded. They have not been excluded in these two experiments since no table update has been used.

RUN S4

Same as S2 but for σ = 1.35. As in 2 plastic glide occurred. After a unit slip had occurred at 10180 (3-7) the sample was split into two uneven parts at 10980 (3-8).

RUN S5 (HEALING)

The sample mentioned in S4 was taken at 9000 (before the formation of the dislocation), and the cut bonds were restored.The crack healed.

RUN S6 (12% CUTOFF)

Similar to S2 but for σ = 1.3 and a 12% cutoff on the potential (i.e. all forces between atoms at a distance greater than 1.12 neglected). A propagation was obtained but the 6th row was split in two parts one adhering to the upper and the other to the lower part of the sample. Figure (3-9) to (3-12).

RUN S7 (12% CUTOFF)

Exactly same as S6 but with a full damping every 50 steps (instead of every 100). Clean propagation was obtained. Figures (3-13) and (3-14)

RUN S8 (HEALING)

Same as (S6) and (S7) but with a full potential and more frequent damping (every 20 steps). No propagation or plastic deformation were observed. Maximum stress at the tip was 4.2, at step 11520 giving

$$F^{MD} = 4.2/1.3 = 3.23$$

$$F^{ERINGEN} = 0.72\sqrt{2\times 4.75} = 2.22$$

$$f_F = F^c/F^{MD} = 0.69$$

The sample at 11520 was taken and the cut bonds restored. The crack healed in 960 steps (Figures (3-15) to (3-17). Run started at 7900.

RUN S9

Applied σ = 3.2 with a 20% cutoff and a full damping every 5 steps. Initial positions obtained by scaling from the σ = 1.0 . Clean propagation resulted (Figure 3-18). Started at 7900.

RUN S 10

Same as S9 with no cutoff or damping. Plastic deformation resulted. (Figure 3-19).

RUN S 11 TO S 17

Table 3-3 summarizes the results of runs (S 11) to (S 17) and gives the parameters used in the runs.

RUN S 18 (FIXED STRAIN)

This is a preloading simulation at $\mathcal{E} = 5.047 \times 10^{-2}$. The average σ on the surface was 3.11 giving $E = 61.6$. For this strain

$$u_E^{MD} = 6.34$$

$$u_E^{C} = \frac{\pi}{61.6}(3.11 \times 4.75)^2 = 11.12$$

$$f_{u_E} = 1.75$$

This fraction was always less than 1 for fixed σ both for the large and small samples

$$(E')^{MD} = 35.6 \qquad (E')^{C} = 35.5$$

$$[\sigma - \sigma']^{C} = \frac{\alpha_0 E E}{1+\alpha_0} = 1.32 \Rightarrow (\sigma')^{C} = 1.79$$

It was found that $(\sigma')^{MD} = 1.79$. The continuum and atomistic calculations are quite close in this case.

RUN S 19 (FIXED STRAIN)

Same as S 18 but for $\varepsilon = 6.56 \times 10^{-2}$. The average stress before cracking was 3.67, giving $E = 55.94$.

$$u_E^C = 17.06 \quad , \quad u_E^{MD} = 10.44$$

$$f_{u_E} = u_E^C / u_E^{MD} = 1.63$$

which is again greater than 1.

$$(E')^C = 32.2 \quad , \quad (E')^{MD} = 30.4$$

$$(\sigma')^C = 2.11 \quad , \quad (\sigma')^{MD} = 2.01$$

N.B. RUN S 18 & S 19 were damped with $\beta = 0.9875$ after it was ascertained that no propagation would result.

RUN S 20 (FIXED STRAIN)

Same S 19 but at $\varepsilon = 8 \times 10^{-2}$ and no damping. The purpose of the experiment is to study a propagation at fixed strain. The sample showed the same tendency to form dislocations as the fixed stress samples. At about 13900 the dislocations got away from the tip and the tip was blunted. The size of the sample was too small to continue the run. Figures (3-26) to (3-34)

RUN L1 (PRELOADING)

The sample was stressed to $\varepsilon = 0.5$. At equilibrium the surface strain ε was 0.00616, giving $E = 81.13$. A crack of 39 bonds was introduced at step 4500. The build-up period of the crack stress field was about 1300 steps. At the end of this period propagation started. This fracture was brittle throughout the sample. The different quantities of interest are given below.

Figure 3-35 gives W, U_S, U_E, and U_K as a function of the time t . These quantities are computed for the half crystal.

To compute the W correction mentioned in the introduction, the propagation was examined between the tip positions $x_T = 42.25$ and $x_T = 38.25$ (inclusive). For the 9 bonds which break in this interval, the maximum bond length included before updating was found to have an average of 1.6139. This gives a correction of .1099 per bond. This correction was used throughout the large sample propagations.

As is clear from Figure 3-35 the strain energy is not changing with length, and the work is. Hence $\frac{dU_E}{dW} \approx 0$. Linear elasticity predicts a value of 0.5 for this quantity, and this result is used in the Griffith and Mott theories.

Because $d\,U_E \approx 0$ this fracture will be called a rigid fracture. A simple model for analysing this special case will be given later. However it should be understood that the term rigid applies only in a very approximate and non-rigorous sense. If the upper and lower parts of the sample were exactly rigid the propagation velocity would be infinite. (N.B. See the discussion on the rigid tearing mode). Hear the region left behind the propagating tip is relaxed and hence its strain energy drops. The region ahead of the tip gets strained as the tip approaches it. The rates of strain energy decrease and increase in these two regions cancel each other and the total strain energy remains fairly constant.

Figure (3-36) gives the time evolution of the first five bonds across the crack faces. As apparent from the diagram the behaviour of the consecutive bonds is quite similar. The time rate of increase of these bonds is almost constant after they reach a length of approximately 1.16 (or 1.28 according to another estimate). Figure (3-37) gives the behaviour of the first four bonds and the eleventh bond in the range 1.45 - 1.6. The bond length vs time curves are almost parrallel indicating that the rate at which bond lengths increase between 1.45 and 1.6 is increasing very slowly. In Fig. (3-38) the variation of crack velocity with crack half length ℓ is given. In this figure a crack is considered to be at a certain bond when the bond length exceeds 1.45. This figure also shows some other estimates of the variation of v_c with ℓ . These will be discussed

later. Figures (3-39) to (3-44) show five pictures of the half lattice. In these and in subsequent pictures arrows connect all atoms which are interacting (up to r_{MAX})

Figures (3-45) to (3-73) show the ten stress profiles of interest at three different time steps 6900, 7620, 8800. The stresses σ_{up} and σ_{right} (defined in the introduction) are given for rows 18,19,20, and 21. Also σ_{open} and σ_{right} are given for the column closest to the tip. All these fields are given here in order to show that the dynamic fields at different times are qualitatively very similar. The stress profiles in the other two propagations were also tested as a function of time and the same qualitative similarity between the profiles was observed. Table (3-4) gives the maximum stresses on the four rows at different times. These maxima do not necessarily occur on the same atom of a particular row. As will be evident, when the static fields are presented, there are some differences between the static and dynamic stress fields. A discussion of the main differences will be postponed until the static fields are given.

RUN L2 (PRELOADING)

The number of originally broken bonds was 19. This simulation is similar to L1 but for a higher stress of 1.3. The surface strain ε for the perfect sample was 0.01633, giving $E = 79.6$. The crack started propagating at about

3400, which is 600 steps after the introduction of the cut. The propagation was initially brittle. By step 3700 dislocations were trying to form at the tip. The picture of the lattice at 3700 shows dislocations trying to form both above and below the tip. At 3700 the crack had a length of 13.25, the tip being at $x_t = 52.75$. As the tip moved to the left ($x_t = 52.75$ at 3800) the strain field at the old tip position ($x_t = 53.75$) is relaxed. As a result, the dislocations which had been formed (or which were trying to form) at the old tip position, got annihilated. This is apparent at 3800 where the dislocations which appeared below the tip at 3700 have disappeared. The same process of creation and annihilation of dislocations is repeated several times. This goes on until step 4400. In the language of the Rice-Thomson theory presented in chapter 1, the dislocations were trying to overcome the attractive force which pulls them to the tip by reaching the critical seperation radius r_c . This resulted in a dislocation cloud accompanying the tip. By step 4200 the dislocation below the tip had already been formed and seperated itself from the tip. However although it was already fully formed it got annihilated between 4200 and 4300. At 4400 two dislocations above and below the tip were formed and escaped the tip region travelling towards the outer surface. By 5100 these two dislocations were 5 and 6 rows from the top and bottom surfaces respectively. At this stage the tip had been somewhat blunted but the fracture was still quite brittle. By 5700 multiple slip had already occurred.

Two edge dislocations had arrived to each of the upper and lower surfaces. At the tip, surface roughening appeared and the originally sharp appearance of the crack disappeared.

Figure (3-74) shows the time evolution of W, u_s, u_E, and u_f. u_s also gives the length of the crack (in bonds). This figure also gives $(\Delta u_E/\Delta W)$ as a function of time. As apparent from the figure the elastic value of 0.5 for this coefficient is not observed. The value of the coefficient decreases with time (or crack length) so that in the long length limit $(\Delta u_E/\Delta W) \to 0$. This means that in this limit the rigid body picture might be a useful one for studying the propagation. The same conclusion can be derived from figure (3-75) in which W, u_s and u_f are given as a function of u_E. Linear elasticity predicts a straight line for W vs u_E with slope equal to 2. The molecular dynamic simulation gave a curve concave upwards with

$$\lim_{l\to\infty} \frac{dW}{du_E} \approx \infty \quad \text{or} \quad \lim_{l\to\infty} \frac{du_E}{dW} \approx 0$$

This indicates that in the limit, variations in u_E may be neglected with respect to dW, du_f, and du_s (rigid régime).

The decreasing value of du_E/dW might be understood in terms of the dislocation emission and motion. As the shear strains in the tip vicinity increases, the strain

energy U_E also increases. When a dislocation is formed and moves towards the surface, the shear strain is relaxed and U_E decreases. The energy released from the shear strain field goes into kinetic energy. This means that when work dW is done on the sample dU_E would be smaller if dislocation emission and motion take place than if such processes do not occur.

Thus one could arrive at the same conclusion of $dU_E \approx 0$ in two ways. By considering the fracture to be rigid in the long length (because in this limit $dU_E \approx 0$) limit, or by considering it to be highly plastic (with increasing dislocation emission) in this limit. The two pictures are physically very distinct. One could choose the appropriate one only when the probability of dislocation emission is known as a function of velocity. If dislocation emission increases or stays constant with crack velocity the plastic picture must be employed, if not the rigid one is appropriate.

Figures (3-76) to (3-91) give the pictures of the fracturing lattice between 3300 and 5700. Figures (3-92) to (3-107) give the stress profiles σ up, σ right for rows 18,19,20,21 at 3840 and 4500. Figure (3-108) gives the time dependence of crack velocity. In this figure the crack is considered to be at a certain bond when the bond is completely broken i.e. when its length is r_{MAX} (as defined in the introductory section preceeding the results)

Figure (3-74) shows that U_E and U_S are almost parallel implying that $dU_E = dU_S$. Since U_S is by definition proportional to the half length ℓ, the above equality indicates that U_E is proportional to ℓ in this run. Linear elasticity gives an ℓ^2 dependence instead.

Table (3-5) gives the maximum stresses near the tip on the different rows for steps 3160, 3840, 4500.

RUN L3 (PRE LOADING)

This experiment is similar to L2 except that the number of originally broken bonds is 39 giving $\ell = 19.75$. The tendency to form dislocations which was observed in L2 did not appear here. Instead the fracture was completely brittle until step 4000 when bifurcation associated with dislocation formation took place.

Figure (3-109) gives the time evolution of W, U_k, U_S, and U_E. Figure (3-110) gives W, U_k, and U_S as a function of U_E. W vs U_E is almost a straight line with an average slope of 2.85. This is quite close to the elastic value of 2.0. The behaviour here is quite different from L2 where (dW/dU_E) was always increasing. The constancy of (dW/dU_E) agrees with the assumption made in all continuum energy balance theories.

The u_y vs time curve is approximately a straight line with an average slope giving a crack velocity $v_c = 2.9\sqrt{\epsilon/m}$ where m is the mass of the atoms, and ϵ the depth of the well. This is gives

$$v_c / c_s = 0.59$$

Bifurcation occurs before this velocity is exceeded. This agrees with the continuum prediction for bifurcation velocities $v_B = 0.6\, c_s$.

It should be mentioned that the behaviour of the crack in this experiment is in contradiction with the Mott expectation regarding the acceleration period. As discussed earlier the Mott theory predicts a gradual increase in velocity. For example a crack needs to double its length in order to be accelerated to 50% of its terminal velocity. Here the terminal velocity is reached right after the propagation starts. Figures (3-111) to (3-125) give the pictures of the fracturing lattice, and figures (3-126) to (3-139) the stress profiles at 3760. This is about 200 steps before bifurcation starts. Of special interest are figures (3-134) to (3-139) which give the profiles for σ_{open} and σ_{right} for columns 40, 41, 42 about the tip. As apparent from these figures the profiles are broad. This will be more apparent when these profiles for the static cases are presented later. The broadening in the profiles indicate that the highly strained region extends above and below the central rows (19 & 20). This increases the probability of initiation of two

fractures above and below the central rows and explains why bifurcation occurs later.

RUN L4 (DAMPED EQUILIBRIUM)

The sample used in L1 was damped with $\beta = 0.9875$. The potential energy of the perfect half crystal was -7749.07 . The final potential energy at step 9900 was -7703.82 . This gives

$$U_E^{MD} = \Delta V - U_S$$

$$= 2 \times [45.25 - 39]$$

$$= 12.5$$

$$U_E^C = \frac{\pi}{E} \sigma^2 \ell^2 = \frac{\pi}{81.13} (0.5 \times 19.75)^2 = 3.78$$

with

$$f_{U_E} = 0.3$$

The effective modulus at the end of the run was

$$(E')^{MD} = 30.6$$

Using equation (3) of section 3D one gets $(E')^C = 52.2$. Linear elasticity predicts a new value for the surface strain given by (5). This gives

$$(\varepsilon')^C = .00616 + (0.5537)(0.5)/(81.13)$$

$$= .0096$$

The observed value of $\mathcal{E}'$ is

$$(\mathcal{E}')^{MD} = .01633$$

The value of $\mathcal{U}_E^{MD}$ quoted before (12.5) is derived from the potential energy at the end of the run (9900). When the damping was introduced at 5400 the potential energy moved towards a maximum at 5850 and then kept decreasing from 5850 tc 9900. Over the last 400 steps the rate of decrease in potential energy was (2.6×10^{-6}%) per step. An exponential extrapolation based on the last 2500 steps gives a potential energy at infinity of -7704.49 which gives a value of $\mathcal{U}_E$ equal tc 11.15 instead of the 12.5 obtained at 9900.

The stress concentration factor $\mathcal{F}$ for this run was

$$\mathcal{F}^{MD} = 4.46/0.5 = 8.92$$

This was obtained at step 9460. Table (3-6) gives the maximum stress on the different rows. The Eringen estimation of $\mathcal{F}$ for this case is

$$\mathcal{F}^{ERINGEN} = C(\nu)\sqrt{2\ell/a}$$

$$= .72\sqrt{2 \times 19.75} = 4.53$$

$$[C(\nu) = .72 \quad FOR \quad \nu = .33(2D)]$$

The critical bond at 9900 was 1.109 long.

Figures (3-140) to (3-151) give the stress profiles. Of particular interest are the profiles of column 48. The sharpness of these should be compared with the broadened profiles in L3 (Fig. 3-134 & 3-135) which gave rise to bifurcation. Of interest also is the fact that the ratio of maximum transverse stress to maximum longitudinal(vertical) stress is about 0.76 . This is contrasted with the corresponding ratio for the dynamic case at the same stress. From table (3-3) this ratio is .97 at 8280 and 1.004 at 8800.

RUN L5 (DAMPED EQUILIBRIUM)

A (19) crack was introduced in a perfect half crystal at σ =0.5 at step 4500. The system was left to evolve without damping for 1100 steps. In this time period the critical bond attained a maximum length of 1.0633 at 5400 and then started decreasing. This indicated that this crack (9.75 in length) was below critical. A damping of β = 0.9875 was introduced at 5600. The system reached an equilibrium in 400 steps. Between steps 6000 and 6300 the potential energy remained constant to six places. The decrease in the critical bond length in this period was 8.7×10^{-2}%. The constant value of the potential energy was -7729.21 . This gives

$$\mu_E^{MD} = 1.72$$

For this σ & ℓ $\mu_E^C = .92$

Also $f_{.} = 0.54$

$(E')^M = 66.49$ $(E')^C = 71.5$

$(\mathcal{E}')^{MD} = .00752$ $(\mathcal{E}')^{EQ} = .00699$

$\mathcal{F}^{MD} = 2.55/.5 = 5.1$ $\mathcal{F}^{ERINGEN} = 3.18$

Table 3-7 gives the maximum stress on the different rows. These are taken at step 6280. Again the ratio of maximum transverse to maximum longitudinal stresses at the tip in this static situation is 0.56 . Again this ratio is much smaller than the corresponding dynamic ratio for the same crack at $\sigma = 0.5$. The dynamic ratio at 3760 was .98 and at 4500 was .89.

RUN L6 (DAMPED EQUILIBRIUM)

Same as L5 but for 9 originally broken bonds ($\ell = 4.75$).

$(E')^{MD} = 79.62$ $(E')^{C} = 78.62$

$(\mathcal{E}')^{MD} = .00628$ $(\mathcal{E}')^{C} = .00635$

$\mathcal{F}^{MD} = 1.53/.5 = 3.06$ $(\mathcal{F})^{C} = 2.22$

$\mathcal{U}_E^{MD} = .36$ $\mathcal{U}_E^{C} = .218$

The stress concentration factor given above is for step 6500. The other maximum stress at this step are given in table (3-8).

The strain energy above is derived from the values at 6100. V remained constant to 6 places, and the critical bond to 5 places between 6100 and 6500. The run was started at 4600.

RUN L7 (DAMPED EQUILIBRIUM) ($\sigma = 1.3$)

This is another damped experiment in which the number of broken bonds is 19. Cracking was done at 2800. Until step 4800 the potential energy was still varying appreciably. ($\Delta V = .14$ in a 100 steps). An exponential extrapolation of the increasing potential energies based on values from step 3800 to 4800 gives a potential energy of -7700.31 .This gives

$U_E^{MD} = 16.78$

$U_E^{C} = 6.34$, $f_{U_E} = .38$

$F^{MD} = 4.45/1.3 = 3.42$

$F^{ERINGEN} = 3.18$

$(E')^{MD} = 61.91$ $\quad (E')^{C} = 70.14$

$(\dot{E}')^{MD} = .021$ $\quad (\dot{E}')^{C} = .019$

is from step 6240.

RUN L8 (DAMPED EQUILIBRIUM)

The perfect sample at $\sigma = 1.3$ was cracked with a crack of length 9 broken bonds at 2800. The sample was run for 2600 steps. During this time the critical bond achieved a maximum of 1.0927 at 4500 and then started decreasing to a value of 1.0566 at 5300. Damping was introduced at 5500, and another 1000 steps were run. During the last 100 steps (6400-6500) the potential energy of the half sample was constant to six places (= -7717.77). The critical bond was decreasing at the rate of $4.7 \times 10^{-4}\%$ per step during this interval.

$$U_E^{MD} = 3.86 \qquad U_E^{C} = 1.51$$

$$f_{U_E} = .39$$

$$(E')^{C} = 77.13 \qquad (E')^{MD} = 74.71$$

$$(\varepsilon')^{MD} = .0174 \qquad (\varepsilon')^{C} = .0169$$

$$\mathcal{F}^{MD} = 3.65/1.3 = 2.81$$

$$\mathcal{F}^{ERINGEN} = 2.22$$

$\mathcal{F}$ is obtained at 6500 and the profiles are given in Figures (3-152) to (3-155).

RUN L9 (HEALING)

It will be recalled that the Thomson et al model predicts that if a crack of length 2ℓ has a critical stress σ_c it will heal only if σ is lowered to σ_-. This model predicts that $(\sigma_c - \sigma_-)$ will be of the order of magnitude of σ_c. According to this model if the applied σ is lowered slightly below σ_c the crack will not heal and will be lattice trapped. As mentioned in chapter 2 Ashurst & Hoover observed a trapping of 2.7 $(= \sigma_+ / \sigma_-)$. It is the objective of this experiment to show that for a long ranged potential no such trapping will occur and that a stable track will heal whenever it

is allowed to do so. It will be shown below that no reduction of σ is necessary to obtain healing.

The stable crack of run L4 (σ=0.5, 39 broken bonds) was used. At step 9900 the broken bonds were restored. The crack healed. At the instant of restoration the critical bond was 1.10879 long. This bond connects atoms 48 & 49 in rows 19 & 20 respectively. Table (3-9) gives the time evolution of the critical bond and the first seven restored bonds for the first 150 steps after restoration. The equilibrium length of a bond between rows ~~18 & 19~~ 19 & 20 in a non-cracked sample at this stress level (σ= 0.5) is about 1.02. Thus the table indicates that the crack healed by 6 bonds in 150 steps. This process goes on until the whole crack closes completely.(N.B. This experiment was continued for another 100 steps only. In this additional period another 5 bonds healed)

Thus the results of (L9) indicate that a stable crack will heal when permitted to do so. In the language of the Thomson model this experiment has shown that $\sigma_- = \sigma$ for a stable crack. This indicates the absence of trapping.

From experiment (L1) σ_c (PRELOADING)= .5 . At an applied σ of 0.5 the crack will propagate in a preloading experiment and at the same applied σ it will heal if brought to equilibrium and restored. No wide range of σ is thus

required to produce healing and extension.

As will be evident from the coming experiments the σ_c (postloading) $\approx$ 0.625. This means that static crack of (L4) will be stable against propagation when the applied σ of 0.5 is raised to any value in the range (0.5 - 0.625). This just indicates that σ_c (postloading) $>$ σ_c (preloading). The relatively large difference between the two does not indicate any trapping. This is because at any σ in the range (0.5 - 0.625) a preloaded crack will propagate, and if suitably damped and restored will heal.

RUN L 10 (HEALING)

Run (L9) was repeated for a higher stress of 1.3 Healing resulted here too. The run started at 6240. The critical bond decreased from 1.25 at 6240 to 1.05 at 6350.

RUN L 11 (STABILITY AT σ = 0.5)

It is interest to know whether the damping forces the cracked system to go into a meta_stable state or whether the configuration arrived at with the help of damping is a true equilibrium configuration. The question is especially important in cases where the applied σ is close to the critical value. In the case of the long crack (39) a stress of 0.5 caused propagation in preloading (L1) and equilibrium when damped (L4). Here the system at 9900 (from L4) was used to

check whether propagation would result when damping is removed or not. The damping was removed and the system was run for 1200 steps. No propagation was observed. Actually the potential energy of the system decreased uniformly during this interval (gained attractive energy). The decrease in potential energy was 1.15. The run was stopped at 11200. In this interval the critical bond decreased by .018. If the run would have been continued both potential energy and critical bond would have oscillated about some average equilibrium values.

Thus the $\sigma = 0.5$ (39) crack was found to be stable, and σ_c (POSTLOADING) > 0.5.

RUN L 12 (POST LOADING) $\sigma = 0.55$

This experiment as well as the next two were performed with the objective of finding the critical postloading stress σ_c for the (39) crack at $\sigma = 0.5$. The applied stress was increased from 0.5 to 0.55 at step (9900). The sample was run until step 11800. The critical bond decreased from 1.109 at 9900 to a minimum of 1.108 at 10100. It then attained a maximum of 1.153 at 11300 and then started decreasing. At the end of the run the critical bond was 1.143 (at step 11800) It was concluded that σ_c (POST LOADING) > 0.55 for this system.

RUN L 13 (POST LOADING AT $\sigma = 0.6$)

The stress on the sample of experiment L 12 was raised to 0.6 at step 11900. The critical bond increased slowly and performed small fluctuations while increasing. It reached a maximum at 13500 and then started decreasing. The maximum was 1.2308. At the end of the run (step 13850) the bond was 1.2049 long. It was concluded that σ_c (POSTLOADING) > 0.6 for this crack.

RUN L 14 (POST LOADING AT σ = 0.65)

The stress on the sample of L 13 was increased to 0.65. Propagation was obtained. Thus σ_c (POST LOADING) ≤ 0.65.

RUN L 15 (σ = 0.55 DAMPED)

The sample in experiment L 12 was damped starting from step 11200. The run was continued to step 12500. At the end of this run the critical bond length was decreasing at a rate of 1.8×10^{-4}% per step, and the potential energy was also decreasing (becoming more negative) at the rate of 2.6×10^{-6}% per step. The final value of the potential energy was -7701.74, of the critical bond length 1.1387. To compute U_E^{MD} the potential energy of the strained lattice is needed. Since no run was done for a strained uncracked lattice at $\sigma = 0.55$ the value was obtained from the $\sigma = 0.5$ run by assuming a strain energy of the form given by linear

elasticity i.e. proportional to σ^2. The strain energy at 0.5 was 3.43 hence at 0.55 it is $3.43(0.55/0.5)^2 = 4.15$. This gives the potential energy of the uncracked half sample at $\sigma = 0.55$ as -7748.39. This gives

$$u_E^{MD} = 15.3$$

Also $u_E^C = 4.56$ which gives

$$f_{u_E} = .29$$

Table (3-10) gives the maximum stresses on the different rows at 12520.

$$F^{MD} = 4.55/.55 = 8.27$$

$$F^{ERINGEN} = 4.53$$

RUN L 16 ($\sigma = 0.6$ DAMPED)

The sample of (L 14) was damped starting from step 13900. The behaviour was the same as in (L 15). The rate of decrease of critical bond length at the end of the run (step 15750) was 6.6×10^{-4}% per step and its length was 1.2079. The rate of decrease of potential energy of the half crystal was 2.6×10^{-6}% per step and its value was -7699.06. This gives

$$u_E^{MD} = 19.00$$

$u_E^c = 10.88$

$f_{u_E} = 0.57$

$F^{MD} = 4.39/0.6 = 7.32$

$F^{ERINGEN} = 4.53$

Table 3-11 gives the maximum stresses.

RUN L 17 (DUCTILE FRACTURE)

In order to study the supersonic regime a perfect sample was strained to $\sigma = 3.0$. A 19 crack was introduced. Instead of propagation the tip blunted by dislocation emission. Several such emissions occurred before any extension took place. The main difference between this sample and the ones which resulted in propagation was that the highly strained region was relatively larger here. In the cases which resulted in propagation the bonds which suffered the largest extension always lay across the crack faces(i.e. between rows 19 & 20). Here it was found that after the initial extension takes place in the first two bonds the highly extended bonds are not the ones at the tip but are one row above and below it. At 7100 for example the extension state is

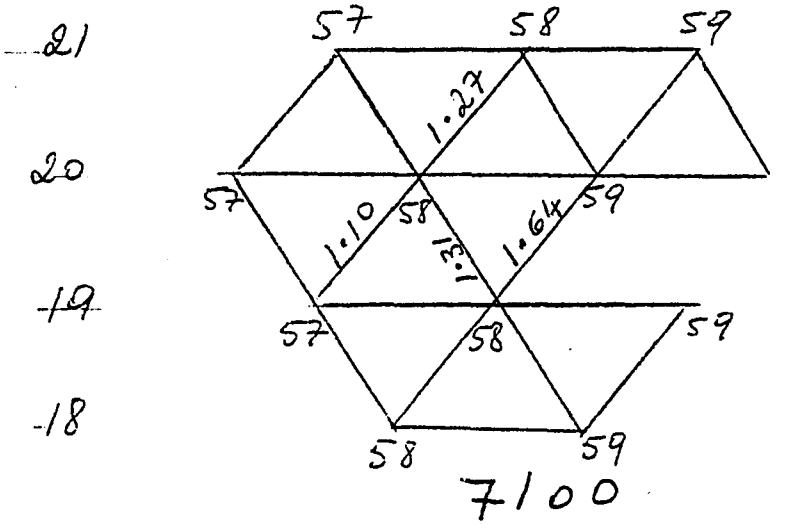

FIG. 3-156

In the propagation cases the next highly extended bond after (19-20, 58-59) was (19-20,58-58). Here instead of this(18-19, 58-57) and (20-21, 58-58) have a larger extension.

At 7150 this situation recurs with the extension of the off tip bonds increasing and a new interaction (20-21,57-59) coming into play.

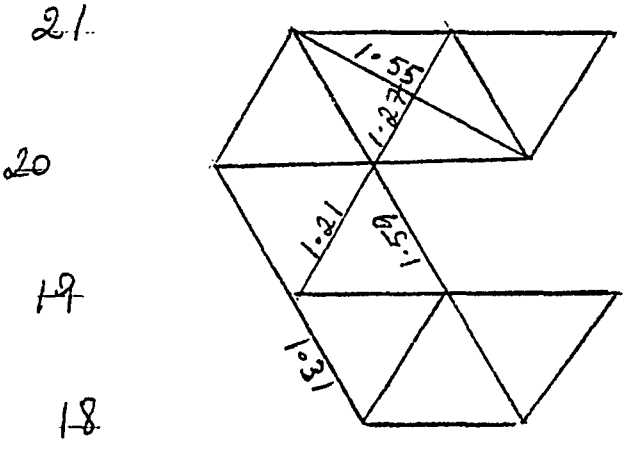

FIG. 3-157

At 7200 another new interaction has come into play(18-19, 57-58), These two new interactions help the glide process.

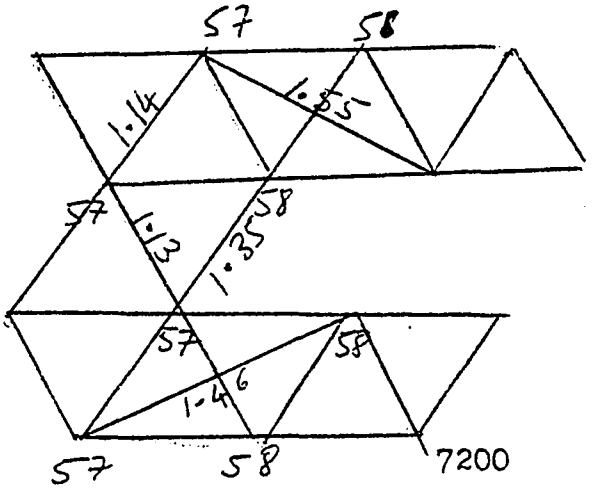

FIG. 3-158

Figures 3-159 & 3-160 show the lattice at two instants.

RUN L 18

Same as L 17 but for a smaller crack 9 bonds. Again ductile behaviour was observed. Figures (3-161) to (3-167) give the pictures of the lattice.

DISCUSSION

3F. THE GRIFFITH THEORY

The theory has been tested in detail for the case of fixed loads with free vertical boundary conditions. While the basic idea of the Griffith approach is thermodynamic in nature and cannot be wrong, the assumptions which have to be made in order to achieve some progress are not always valid for this type of loading.

In particular the use of the Inglis expression for the strain energy of an elliptic hole to represent the strain energy of a crack was found to yield values smaller than the strain energies obtained by molecular dynamics. Table (3-12b) summarizes the results and gives the continuum (Inglis) strain energy as percentage fraction of the molecular dynamic strain energy. The fraction varies from 29% to 61%. Excluding the last entry in the table (which might not have arrived to complete equilibrium) the results indicate that the differences between the continuum and molecular dynamic energies increase with σ for the same ℓ and with ℓ for the same σ. This is to be expected since the Inglis result is derived on the basis of linear elasticity and implicity includes the assumption of small displacements. Since the displacements increase with σ & ℓ it is expected that the Inglis result will be less valid as σ & ℓ increase. As will be shown below this inaccuracy in the theory can cancel out

with the inaccuracy in the relation between work and increase in strain energy in some cases. In such cases the Griffith estimation of the critical stress might not be far from the correct one. This might explain the initial success of the Griffith theory in spite of the fact that some of its assumptions are not generally valid. Table (3-12) compares the Griffith estimations of the critical stresses with the ones obtained by molecular dynamics. The comparisons are only meaningful in the cases of postloading.

The assumption of $\alpha U_E / dW = 50\%$ was also tested. At the beginning of the motion it was found that this fraction was 0%, 80%, and 33% in runs L1, L2, L3 respectively. In L1 this fraction was the same throughout a large fraction of the motion. In L3 it was constant until bifurcation took place, and in L2 it decreased monotonically as the crack propagated. The behaviour of the sample at the beginning of fracture in L2 & L3 is thus qualitatively similar to the Griffith expectation (of 50%) although the 50% assumed by Griffith is not obeyed. The 0% observed in (L1) is very different from the Griffith expectation. This so called rigid tearing mode will be analysed further in a subsequent section.

It should be mentioned that in some instants the Griffith critical stress can be obeyed accidentally because the errors made in the strain energy U_E and the error in the work cancel each other. To see this one writes the relation between dW and αU_E in the general non-linear case.

$$dW = a_W (dU_E)$$

In the linear case $a_W = 2$ but in general a_W can be smaller or larger than 2 as indicated by L2 & L3. The case of interest here is when a_W is less than 2(e.g. L3). For the strain energy one can define a coefficient a_E to describe the deviation from elastic behaviour

$$U_E^{MD} = a_E (U_E^C)$$

If a Griffith type energy analysis is done one gets

$$\sigma_C = \sqrt{\frac{2E\gamma}{\pi l a_e (a_W - 1)}}$$

Since for the case of interest ($1 < a_W < 2$), $(a_W - 1)$ will be less than 1. For fixed loads $a_E > 1$ and the quantity $a_E(a_W - 1)$ can be close to 1 in which case the Griffith stress σ_G will be accidentally close to the critical stress σ_C.

As commented previously the case of fixed strain gave Inglis values for U_E^C which are larger than U_E^{MD}. The Griffith theory has a better chance of success in the case of fixed strain since the work done by the loads is by definition zero. Hence there is no need for the work relation which is necessary for fixed loads. By conservation of energy all the strain energy goes to surface energy in the

brittle cases of fixed strain. The only inaccuracy in the Griffith theory would be the one resulting from the continuum expression for U_E. The case of fixed loads posseses one more degree of freedom than that of fixed strain.

3G. THE MOTT THEORY

Since the theory uses the two basic assumptions used by Griffith (i.e.the expression for U_E and the work relation) it cannot be obeyed (except accidentally). Since these two assumptions have been shown to be not satisfied in general. Indeed there are several other assumptions made in the Mott theory which are also not valid.

Mott assumes that the $dW = 2\,dU_E$ relation holds throughout the motion. Run L2 for example shows that $\frac{dU_E}{dW}$ keeps decreasing with crack length and that even if this Mott assumption is approximately valid at the beginning of the motion it will not be satisfied as the propagation proceeds. In (L3) the constancy of $\frac{dU_E}{dW}$ was satisfied.

The expression for U_k used by Mott which gives an l^2 dependence for U_k was also not satisfied in general. In run L1 for example the change in U_k was quite negligible (2ϵ) as $(l-l_0)/l_0$ varied from 0% to 21%. In L2 the increase was (4ϵ) as $(l-l_0)/l_0$ increased from 0% to 79%. Actually equation (1C-3) indicates a dependence of U_k stronger than l^2. This l dependence comes from assuming

that the static Griffith energy expression is valid for the dynamic case (i.e. $U_E \approx \frac{\pi}{E}\sigma^2 l^2$ dynamically). The much weaker l dependence observed in the present simulations indicate clearly that this assumption is not valid. Indeed in (L1) there was no dependence of U_k & U_E on l for a large part of the motion. The same conclusion about the dynamic situation can be derived from consideration of (1C-6). To evaluate the integral in (1C-4) Mott assumed that the displacement fields of the dynamic case are given by the static result (1C-5). The present simulation indicates that (1C-5) does not describe the dynamic fields. Instead u_x, u_y, have a weaker l dependence than that given by (1C-5) and therefore $\frac{\partial u_x}{\partial l}$ & $\frac{\partial u_y}{\partial l} \approx 0$. This leads to a small initial U_k.

The picture of a gradually accelerating crack has not been observed in L1,L2, L3. In L1 where the approach to a terminal velocity was the most gradual one in the simulations, the Mott expectation for the acceleration period was much higher than the observed one. To show this one needs to extend the Mott expressions in order to cover the case in which the applied stress is higher than the Griffith one(or equivalently when $l > l_g$). A direct integration of the Mott velocity leads to

$$v_T\, l = l + \frac{l_0}{m}\left\{\ln\left(m\frac{l}{l_0} - 1\right) - \left(m + \ln(m-1)\right)\right\}$$

where $l_0 = m l_g$ & m is some number slightly larger than 1.

For the σ =0.5 if one assumes $m \simeq 1.11$ this would give a period of 42400 steps required by the crack to double its length, which is of course much larger than the observed period. If m = 1.05 then the period is 52000 steps. The main difficiency of the Mott theory results from the errors in the Griffith theory, and from the quasistatic assumption.

3H. THE RIGID BODY REGIME

Ll has indicated that sometimes $d\,\underset{\sim}{u}_E \approx 0$. As commented in that experiment this could be dealt with as a rigid body fracture . As mentioned there, the term is only meant to apply in an approximate fashion since a real rigid fracture would propagate with an infinite speed. In sample containing a crack on its external surface a rigid tearing mode with a finite speed can occur. This is because the rigid motion can be performed by two rigid rotations of the upper and lower parts. If the crack is an internal one, as the case of interest here no rigid rotation is possible because there is an incompatability between the four rotations required and therefore the only possible rigid tearing motion has to proceed with an infinite speed (see 3-168(C)).

To analyse this special case one assumes that the form of the stress distribution in the vicinity of the tip does not change appreciably in time. Indeed the stress distribution presented in Ll make this assumption a plausible one. A tip force can be defined in the following way.(Fig. 3-168)

If the maximum value of the stress distribution occurs at A, and if the stress exceeds σ only in the region AB in the medium, and if the region in the crack in which the stresses are non zero extends from D to A then a tip force f_t is defined by

$$f_t = 2\left[\sum_{DA} \sigma_{yy} + \sum_{AB} (\sigma_{yy} - \sigma)\right]$$

In terms of f_t the equation of motion of the upper half sample can be written as

$$2\sigma l - f_t = M\ddot{y}^{\circ} \qquad (1)$$

Where M is the mass of each of the upper and the lower parts. This is because the forces on the portions BC of the half crystal are balanced so that they do not need to be considered. And because the force on the portion ABB'A' is

$$F \text{ on } ABB'A' = \sigma(AB) - \sum_{AB} \sigma_{yy}$$

$$= -\sum_{AB} (\sigma_{yy} - \sigma)$$

And

$$F_{oDD'C'} = \sigma l - \sum_{DA} \sigma_{yy}$$

Adding these two forces one gets (1). From (1) $f_t = 2\sigma l_o$ where l_o is the length at the beginning of the motion. This relation follows because fracture starts when $2\sigma l$ exceeds f_t so that initially $\ddot{y}^{\circ} = 0$. Since each half of the sample is considered rigid here y can be chosen as the CM of the upper half of the crystal. (1) thus becomes

$$2\sigma(l - l_o) = M\ddot{y}^{\circ} \qquad (2)$$

FORMATION OF AN EQUATION OF MOTION FOR ℓ.

If one writes an energy balance equation for the whole system (upper & lower halves) one gets

$$0 = d\mathcal{U} = d\mathcal{U}_k + d\mathcal{U}_E + d\mathcal{U}_S + d\mathcal{U}_L$$

$$d\mathcal{U}_k + d\mathcal{U}_E + d\mathcal{U}_S - dW_L = 0 \qquad (3)$$

In the present case the rigid body assumption leads to

$$d\mathcal{U}_E \approx 0 \quad \& \quad d\mathcal{U}_k = 2\,d\left(\tfrac{1}{2}MV^2\right) = 2MV\,dV \qquad (4)$$

where $V = \dot{y}$. When (4) is substituted in (3) and $\mathcal{U}_S = 4\gamma\ell$ is used one gets

$$dW_L = 2MV\,dV + 4\gamma\,d\ell$$

By definition

$$dW_L = 2F\,dy = 2(2\sigma w)\,dy = 4\sigma w\,dy$$

this gives

$$4\sigma w = 2MV\left(\frac{dV}{dy}\right) + 4\gamma\left(\frac{d\ell}{dy}\right)$$

or

$$MV\frac{dV}{dy} = M\ddot{y} = 2\left(\sigma w - \gamma\frac{d\ell}{dy}\right) \qquad (5)$$

Using (5) in (4) gives

$$2\sigma(\ell-\ell_0)=2\left(\sigma w-\gamma\frac{\partial l}{\partial y}\right)$$

$$\gamma\left(\frac{\partial l}{\partial y}\right)=\sigma\left[w-(\ell-\ell_0)\right] \tag{6}$$

$$\sigma\left[w-(\ell-\ell_0)\right]\dot{y}=\gamma\dot{\ell} \tag{7}$$

Diffrentiating (7) with respect to time gives

$$\sigma\left[w-(\ell-\ell_0)\right]\ddot{y}-\sigma\dot{\ell}\dot{y}=\gamma\ddot{\ell} \tag{8}$$

Using (7) in (8) gives

$$\ddot{y}=\frac{\gamma\ddot{\ell}\left[w-(\ell-\ell_0)\right]+\gamma\dot{\ell}^2}{\sigma\left[w-(\ell-\ell_0)\right]^2} \tag{9}$$

Using (9) in (3) gives an equation of motion for the crack

$$2\sigma(\ell-\ell_0)=\frac{M\gamma\ddot{\ell}\left[w-(\ell-\ell_0)\right]+\gamma\dot{\ell}^2}{\sigma\left[w-(\ell-\ell_0)\right]^2}$$

$$2\sigma^2(\ell-\ell_0)\left[w-(\ell-\ell_0)\right]^2=M\gamma\ddot{\ell}\left[w-(\ell-\ell_0)\right]+\gamma\dot{\ell}^2 \tag{10}$$

One could obtain a first integral of this motion (i.e. $v_c=v_c(\ell)$ or $\dot{\ell}=\dot{\ell}(\ell)$) in analytic form. Obtaining a second integral of the motion (i.e. $\ell=\ell(t)$) is not easy. To obtain $v=v(\ell)$

the following change of variables is performed

$$\phi = w - l \quad , \quad L = l - l_0$$

The initial condition is $\phi = \phi_0 = w$ and $\dot{\phi}_0 = -v_0$ when $t = 0$.

(10) becomes

$$M\gamma\left[\dot{\phi}^2 - \phi\ddot{\phi}\right] = 2\sigma^2(w-\phi)\phi^2 \tag{11}$$

(11) can be solved by the substitution

$u = \ln\phi$ with initial conditions

$u_0 = \ln w$ & $\dot{u}_0 = -v_0/w$

This substitution reduces (11) to

$$M\gamma\,\ddot{u}\phi^2 = 2\sigma^2(\phi - w)\phi^2$$

$$M\gamma\ddot{u} = 2\sigma^2(\phi - w) = 2\sigma^2(e^u - w) \tag{12}$$

$$\dot{u}\frac{d\dot{u}}{du} = \frac{2\sigma^2}{M\gamma}(e^u - w)$$

$$\frac{1}{2}\dot{u}^2 = \frac{2\sigma^2}{M\gamma}\int(e^u - w)\,du$$

$$\dot{u}^2 = \frac{4\sigma^2}{M\gamma}(e^u - w) + b \tag{13}$$

To evaluate b the initial conditions are used to give

$$b = v_0^2/w^2 - \frac{4\sigma^2}{M\gamma}(w - w\ln w)$$

which in turn gives

$$v = \sqrt{\frac{4\sigma^2}{M\gamma}\phi^2\left(\phi - w\left(1 + \ln\frac{\phi}{w}\right)\right) + v_0^2\left(\frac{\phi}{w}\right)^2} \tag{14}$$

In terms of ℓ & ℓ_0 (14) becomes

$$v = \sqrt{\frac{4\sigma^2}{M\gamma}\left[w-(\ell-\ell_0)\right]^2\left[w\ln\frac{w}{w-(\ell-\ell_0)}-(\ell-\ell_0)\right]+v_0^2\left(\frac{w-(\ell-\ell_0)}{w}\right)^2} \quad (15)$$

(15) gives the way in which v varies with ℓ for a given $v_0 = \ell_0^{\circ}$. The function (15) is given in figure(3-38)for v_0 =0.6, 0.8, 1.0. v_0=0.6 is close to the observed initial velocity of .65, v_0 = 0.8 corresponds to an initial velocity obtained by averaging over the first three bonds in the propagation. Actually a value quite close to the observed v_0 of 0.65 can be obtained from the atomic forces as will be done in the next section.

In order to account for the sharp decrease occurring in the observed velocity at about ℓ =33 an interference problem between the stress waves reflected from the outer surface has to be solved. These waves are being generated at the rupturing tip as this tip propagates. Such a solution might be attempted after the equation of motion of the tip(source) has been found. As mentioned in the introductory chapter(1), the compressive stress fields due to the reflected waves have been observed by Carlsson and Van Elst although there is some controversy in the literature about the interpretation of the data.

A simpler solution than (15) is obtained for the initial part of the motion in which $\alpha \ell_k \approx 0$ this is given by,

$$l - l_o = \frac{v_o}{\sqrt{\alpha}} \sinh \sqrt{\alpha}\, t \qquad \alpha = \frac{2\sigma^2 w}{M\gamma} \quad (16)$$

but this is valid only for the first few bonds (up to 20 bonds approximately). For example at 6950 $(l - l_o)^{MD} = 10.5$ and by equation (16) $l - l_o = 8.54$ for $v_o = 0.65$.

3I. ESTIMATION OF THE INITIAL VELOCITY

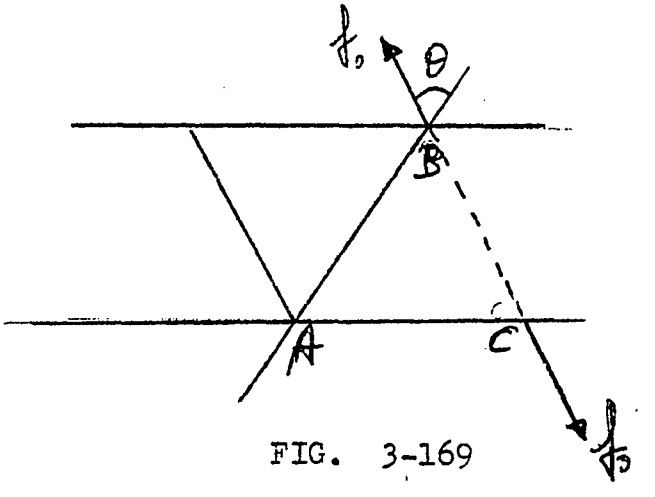

FIG. 3-169

When bond BC is cut the attractive force which was pulling atoms B & C together is lost. As a result each of these two atoms experiences a force f_o along BC. To find the initial velocity of the crack one needs to find the rate at which bond AB is extending. The force acting on B at the instant of cutting (along AB) is

$$f_B = f_o \cos\theta$$

From figure (3-36) it is clear that the bond is accelerating up to approximately 1.16 (or 1.28). From 1.16 on the

bond extends at a constant rate. This means that between the initial state and the state in which AB = 1.16 the lattice deforms in such a way so as to bring $f_{\vec{r}_B}$ to zero. One can take the average value of $f_{\vec{r}_B}$ during this period as

$$\langle f_{\vec{r}_B} \rangle = (f_0 \cos\theta + 0)/2$$

$$= (f_0 \cos\theta)/2$$

This means that the bond AB will get accelerated from zero to v_{AB}

$$v_{AB} = \sqrt{2\left(\frac{f_0 \cos\theta}{2}\right)\delta}$$

where $\delta = 1.16 - (AB)_0$, $(AB)_0$ initial length of (AB). In this case $(AB)_0 = 1.004$. This gives $f_0 = 0.276$. In the initial state $\theta = 60^\circ$. This gives

$$v_{AB} = \sqrt{\frac{.276}{2}(1.16 - 1.004)} = .15$$

This number is in fact the slope of the (AB) & the other critical bonds vs time curvesin figure (3-38) (in the approximate units). Thus the estimate agrees with the observed value. If one makes the judgement that the linear part of the bond vs time curves starts at 1.28 instead of 1.16 then

$$v_{AB} = .195$$

To get the initial crack velocity one finds the time τ required by the successive bonds to go through the extension process. It is noted from figure (3-37) that at the time a bond breaks, ($\sim$1.60) the next highly extended bond is at a length less than the breaking bond by a fixed amount Δ . Averages taken from the run have indicated that $\Delta \approx$ 0.12 (giving the next bond as 1.48). In order that the crack move from bond to another, the time τ required by the critical bond to extend from 1.48 to 1.6 has to ellapse.

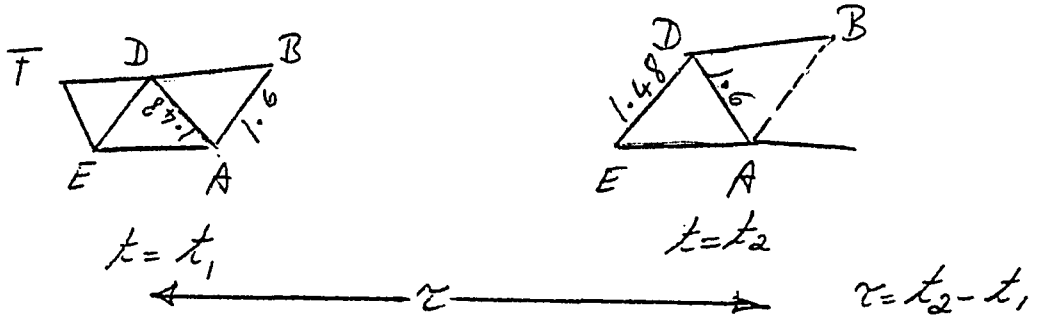

FIG. 3-170

Thus in figure 3-170 AD is 1.48 at t_1, and DE is 1.48 at t_2. In $\tau = (t_2 - t_1)$ the crack has extended by one bond (distance = 0.5).

Since the bond is extending at a rate $v_{AB} = .15$

$$\tau = \Delta / v_{AB} = .12/.15 = 0.8$$

$$(v_c)_o = 0.5/0.8 = 0.625$$

in quite good agreement with the observed value of 0.65 .

3J. STRESS PROFILES

The Eringen profiles and the ones obtained by molecular dynamics are qualitatively similar. Figures (3-171) to(3-173) below give a comparison of the two profiles. The non-local theory predicts the same stress concentration curve for the same crack length regardless of the applied stress. Instead the atomistic results indicate the $\mathcal{F}$ depends also on σ. The concentrations decrease with σ. This is clearly seen from figures (3-171) to (3-173), from the three columns of table (3-14). The decreasing $\mathcal{F}$ (with σ) in column 3 of this table can be explained using a two-bond tip picture as will be done in the next section. However column 1 of the table shows clearly that $\mathcal{F}$ has a real σ dependence even when the local stresses at the tip are far below the maximum. Such a stress dependence of $\mathcal{F}$ indicates that the stress fields of a crack are not linear functions of the applied loads σ as assumed in all elastic continuum treatments.

Examination of the first and ~~third~~ fourth rows of the table shows that the ℓ dependence of $\mathcal{F}$ predicted by non-local linear theory is not obeyed. The first row (applied $\sigma = 0.5$) gives $\mathcal{F}$ in the ratio

MD 1 : 1.67 : 2.92

ER 1 : 1.43 : 2.04

This indicates an ℓ dependence ~~weaker~~ stronger than $\sqrt{\ell}$ (i.e. $\ell^{\gamma}, \gamma > .5$)

However the third row gives the opposite conclusion (i.e. ℓ^{γ}, $\gamma < -5$) because

MD	1 : 1.13
ER	1 : 1.43

The results available are not sufficient to deduce an ℓ - dependence.

A note should be made about the comparisons which have been made between non-local linear predictions and the results of the present calculation. The available non-local results up to date have elastic modulus functions $\lambda'(|x'-x|)$ & $\mu'(|x'-x|)$ which have been obtained from a one dimensional lattice in which the atoms are connected by Hookean springs. The appropriate λ', μ' which are suitable for a two dimensional L-J lattice is not available and the non-local calculation has not been carried out. The use of the appropriate λ', μ' in a nonlinear Eringen theory might have yielded the σ dependence. Thus a fair judgment of the Eringen theory cannot be made at this stage, since this theory has not been extended to handle the case of the present calculation or of realistic solids. However the Eringen theory removes the singularity in a natural way and is capable of incorporating atomistic tip effects by using more realistic modulus functions obtained from phonon dispersion relations.

The parameter (a) in the Eringen relation $\mathcal{F} = C\sqrt{\frac{2\ell}{a}}$ is a measure of the size of the region (around a point) from which non-local contributions to the stress at the point are significant. As such it will differ from solid to solid and will depend on the details of the atomic force law and the effective ranges of these forces. In the (1D) first neighbour Hookian lattice which Eringen used (a) whould be equal to the interatomic seperation. In the present (2D) lattice a = 1.0 if only first neighbours are used. However it should be stressed that since the comparisons here are done for different situations the choice of (a) includes a degree of arbitrariness. A choice of a = 1.0 is a logical one since in the small deformation states all atoms seperated by more than 1.0 dc not affect each other. Hence the non-local region will have a dimension of approximately 1.0. This value has been used throughout the comparisons. Table B includes the Eringen predictions for a = 1.62 also. This value is an upper limit on a, since even in the most highly deformed states any atoms separated by 1.62 do not affect each other.

As clear from table 3-15 non-local theory underestimates $\mathcal{F}$ in all cases. This is because it is still a linear theory and does not cover large deformation effects.

Figure 3-171 indicates that atomistic profiles are wider than the Eringen ones when the maximum of both are close to each other.

The main difference between the static and dynamic profiles is the increase in the transvers fields in the dynamic case. This can help in understanding the origin of bifurcation. If an angle θ is defined by (fig 3-174)

$$\tan\theta = \frac{(F_{LONG})_{MAX}}{(F_{TRANSVERSE})_{MAX}}$$

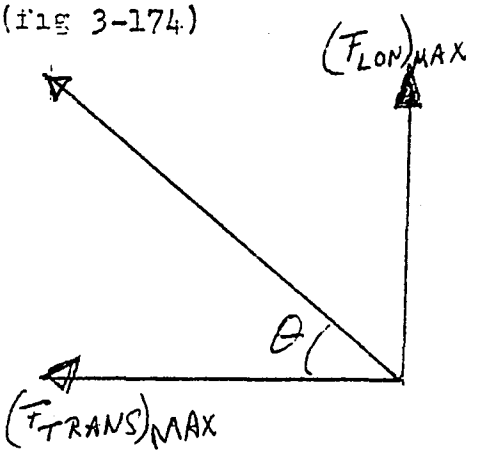

FIG. 3-174

If θ is about 60° then the force will be along the bonds between rows 19 & 20 and propagation along the original direction will result. If θ decreases then the crack will tend to bend. To understand the reason for this, one considers the extreme cases of $\theta = 90^{\circ}$ & $\theta = 0^{\circ}$. The first case gives propagation in the x - direction and the second gives two propagation in the y - direction in a continuum. Thus a decrease in θ (of 90° produces bifurcation and bending by 90°).

In the atomistic calculations it was found that θ for the static cases and for the cracks which were about to propagate was about 55° on the average. For the dynamic cases it was about 45°. Thus one expects the occurrence of bifurcation as the velocity increases.

Table 3-16 give a comparison of the molecular dynamic and Eringen profiles.

3K. THE ATOMIC TIP

There is an assumption which is common to all continuum treatments of fracture. It is that the local stresses at the tip are monotonic functions of the applied loads σ. As σ is increased the local tip stresses $\sigma_{yy}(l, o)$ near the tip also increase until the maximum allowed $\sigma_{yy}(l, o)$ is reached, at which point fracture starts. The atomic discretness of the tip and the particular geometry of that tip alter this picture appreciably. Instead of being monotonic in σ the tip stress $\sigma_{yy}(l, o)$ flattens out and becomes essentially constant over a wide range of applied σ's. This means that the factor $\mathcal{F}$ in this range will be a decreasing function of σ (because $\mathcal{F} = \sigma_{yy}(l, o)/\sigma$) as in column 3 of table 3-15 presented above.

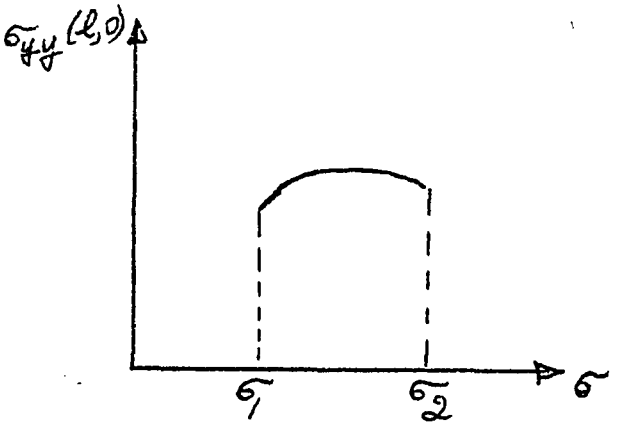

FIG. 3-175(a)

The simulation gave a width of this plateau of about 19% $\left\{ = [(\sigma_2 - \sigma_1)/(\sigma_2 + \sigma_1)] \times 100\% \right\}$ see figure 3-175.

This stability plateau is quite different from the stability considered in the Thomson lattice trapping models. In all cases considered here healing occurs when allowed. The occurrence of the atomic stability plateau does not depend in any way on the use of a short ranged potential, as in the Thomson models. Instead it is a consequence of the nature of the potential near the inflection point(maximum force seperation). The effect will thus be manifested for many other realistic force laws which are similar to the L-J in the vicinity of the inflection point. It will not be affected by the short range employed in the simulation. The origin of this flattening can be understood in terms of the atomic force laws as will be shown below.

As evident from 3-14 and from the results of the simulation, the maximum $\sigma_{yy}(\ell, o)$ of 4.66 is never attained. An explanation of this will also be given below.

Assume that AB = $r_i + \delta_1$, AC = $r_i + \delta_2$

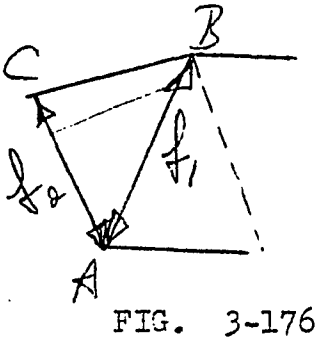

FIG. 3-176

where r_i is the inflection point (=1.1086), & δ_1 , δ_2, can be either positive or negative. The situation of interest

is that in which fracture is about to start, so that δ_1, δ_2, are very small. The stress $\sigma_{yy}(\ell,0)$ is given by

$$\sigma_{yy}(\ell,0) = [|f_1| + |f_2|]\cos\theta$$

where $\theta \approx 60^\circ$ (correction can be made in θ to include tip deformation).

$$|f_1| = \left|\frac{\partial\phi}{\partial r}\right|_{r=r_i^\circ+\delta_1} \quad , \quad |f_2| = \left|\frac{\partial\phi}{\partial r}\right|_{r=r_i^\circ+\delta_2}$$

A first order expansion in the δ's leads to

$$|f_1| = 12\left[\left(\frac{1}{r_i^{\circ 13}} - \frac{1}{r_i^{\circ 7}}\right) - \frac{\delta_1}{r_i^{\circ 2}}\left(\frac{13}{r_i^{\circ 12}} - \frac{7}{r_i^{\circ 6}}\right)\right]$$

and to a similar expression for $|f_2|$. Since $r_i^\circ = \left(\frac{13}{7}\right)^{1/6}$ the second bracket in the above expression vanishes. Thus to a first order in δ_1, δ_2, $\sigma_{yy}(\ell,0)$ remains at the maximum value 4.66 . This result is valid irrespective of the signs of the δ's (i.e. either before or after the inflection point is reached). To this order of approximation all applied σ's which give rise to small δ's cause a constant tip stress of

$$\sigma_{yy}(\ell,0) \simeq \sigma_{MAX} \ .$$

To get a more accurate picture of the behaviour of $\sigma_{yy}(\ell,0)$ one carries the expansion to second order in δ_1, δ_2. In the figure (3-177) f_1 & f_2 are given as functions of r_1 & r_2.

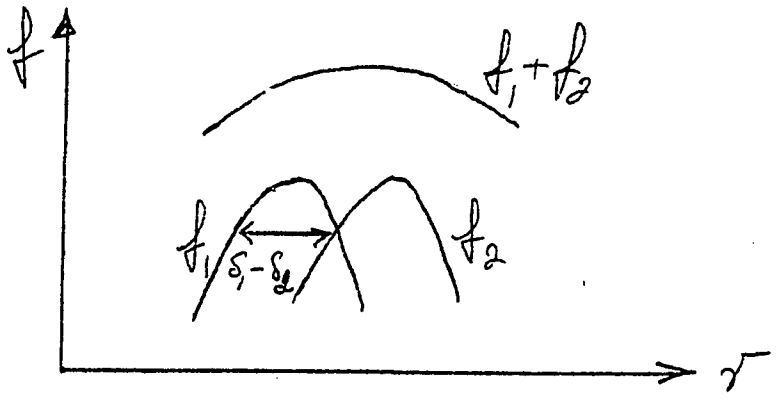

FIG. 3-177

As the first bond reaches the inflection point f_1 starts decreasing. At the same instant f_2 is still increasing. These two opposite trends tend to flatten $\sigma_{yy}(\ell,0)$ and therefore $\sigma_{yy}(\ell,0)$. A second order expansion of the f's leads to

$$\sigma_{yy}(\ell,0) = \left| \left[\left(\frac{1}{r_i^{13}} - \frac{1}{r_i^{7}} \right) \times 2 + \frac{12\times 21}{r_i^{9}} \left(\delta_1^2 + \delta_2^2 \right) \right] \cos\theta \right|$$

$$= \left| 4.657 - 86.24 \left(\delta_1^2 + \delta_2^2 \right) \right|$$

This is always less than the maximum no matter whether δ_1 , $\delta_2 > 0$ or $\delta_1, \delta_2 < 0$. For the σ = 0.55 for example the above equation predicts $\sigma_{yy}(\ell,0)$ = 4.44 (observed is 4.55).

3L. LATTICE TRAPPING AND HEALING.

Runs (L9 & L 10) have indicated the absence of lattice trapping in the present model. This is in contradiction with the Thomson et al results and with the results of the molecular dynamic study of Ashurst & Hoover who reported a large trapping parameter $\sigma_+/\sigma_- = 3.7$. Other workers in the field of brittle fracture have accepted lattice trapping as a real phenomenon which follows from the atomic discretness of the lattice (e.g. Lawn & Wilshaw 1975 and G. T. Hahn 1976).

It is the object of the present discussion to show that lattice trapping is not a real effect but has resulted from some unrealistic assumptions in these previous calculations. The origin of trapping in the Thomson et al energy calculation is different from its origin in their force calculation. The energy calculations will be discussed first and then the force calculations.

ERROR CALCULATIONS

In the Thomson energy calculations appreciable trapping will result only when η is small. For example to produce a trapping of $\sigma_+/\sigma_- = 3.3$, the value of η has to be equal to 0.1α. In the present simulation values of η obtained by fitting the bond energies to the Thomson energy expression gave values of σ_+/σ_- which produce only negligible trapping. If E_0 is the energy of the critical bond and E_1 of the first nonbroken bond then the Thomson expression gives

$$\frac{E_1}{E_0} = 1 - \frac{2}{\pi}\tan^{-1}\left(\frac{1}{\eta}\right)$$

This gives

$$\eta = \tan\left[\frac{\pi}{2}\left(\frac{E_1}{E_0}\right)\right]$$

For run (L9) table 3-17 gives

$$\eta = \tan\left[\frac{\pi}{2}\left(\frac{.08119}{.2113}\right)\right] = .6894$$

This gives

$$\sigma_+/\sigma_- = \cot(\pi\eta) = 1.027$$

For run (L 10) table 3-17 gives

$$\gamma = \tan\left[\frac{\pi}{2}\left(\frac{.22145}{.54495}\right)\right] = .742$$

giving $\sigma_+/\sigma_- = 1.019$

Thus the atomistic tip is too wide to produce appreciable trapping.

FORCE CALCULATIONS

In the Thomson et al work the assumption is made that the first broken bond (at E) is broken because its extension exceeds the allowed maximum of . Of course this is not the only case of interest in crack problems. The first broken bond can be broken because of the presence of a knife-like object or of some other external agent(e.g. corrosion). In such a case, that first broken bond could be within the allowable maximum range, and when the external agent is withdrawn the crack will start healing without reduction of the applied σ and there will be no lattice trapping at all. This type of process is however different from the situation discussed by Thomson et al. Instead their lattice static force calculations considers cracks with no external knife-like object. (N.B. Their situation does not represent a real one because as can be shown by a free energy argument, there are no static equilibrium situations of a crack system which does not have an external knife-like object).

If a $\sigma = \sigma_y$ is applied in a knife-like situation there can be two types of behaviour. When the knife is introduced the crack is above critical and extension takes place. If it is below critical an equilibrium will exist with the knife present. Once the knife is withdrawn then if the first broken bond is extended less than the maximum its atoms will be attracted toward each other and the healing process will start without a necessity for reducing σ. If the extension exceeds the maximum then the equilibrium of the atoms composing the first broken bond will not be upset by the withdrawal of the knife and one would have to reduce σ in order to obtain healing. Of course for a real material there is no cut-off in the potential and the attraction of the atoms of bond N will upset the equilibrium and healing will start immediately without need for reduction of σ. Real materials are thus not expected to exhibit trapping in the knife-like situation. In the two healing simulations conducted here the first broken bond had an extension less than the maximum (table 3-17) and therefore healing started immediately after restoration without need for σ reduction.

Finally it should be mentioned that the situation depicted by Thomson et al is less likely to occur if the cut-off δ is large. If this cut-off is larger than the extension in bond N then trapping will definitely be absent. In

order for trapping to occur δ must lie between $u(N)$ & $u(N+1)$ where u is the extension in a bond.

$$u(N+1) \leqslant \delta \leqslant u(N)$$

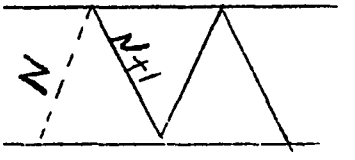

FIG. 3-178

Thus for σ =0.5 (39 BONDS) δ has to be lie between 0.11 & 0.29 and for σ = 1.3 (19 BONDS) it will have to lie between 0.25 & 0.42. Only a very artificial potential would satisfy these requirments for trapping. Even if one can imagine a substance for which the potential is very short ranged, it is still highly unlikely that the two inequalities above will be satisfied.

SUMMARY AND CONCLUDING REMARKS

The Griffith theory has been tested. In some cases it was found that the energy work relation which is assumed by this theory is approximately valid. In other cases the assumption was clearly violated. In one case the strain energy content due to a crack was almost constant during a large part of the propagation. This case which has been called a rigid tearing mode cannot occur in the case of fixed displacements.(See note at end of this section)

It has been possible in this case to work out an analytical expression for the velocity of the crack as a function of its length. This expression is in fairly good agreement with the results of the simulation. An estimation of the initial velocity in this case has also been possible. This has been done by considering the atomic process which takes place after the introduction of the cut.

The continuum predictions for strain energy have been found to be smaller than the atomistic strain energies for the fixed load cases which have been tested.

The Mott theory for crack velocities has also been examined. The basic assumption of the quasistatic nature of the dynamic fields has been found to be violated. This assumption implies that the strain energy of a moving crack

has the same ℓ dependence as a static one. Instead the dependence of U_E in the dynamic case has been found to be much weaker than the static ℓ^2 dependence. In one run U_E was almost a constant (independent of ℓ). The acceleration periods found from the simulations were much shorter than the Mott expectations. This was found to be the case even after the Mott result was modified to cover the case in which the loads are above critical.

The concept of lattice trapping has been tested. The results of the present simulation indicate the absence of any trapping. Analysis of the Thomson et al papers has led to the conclusion that the trapping reported by these authors resulted from the use of short ranged potentials in their force calculations, and from the use of unphysically small widths η in their energy calculations.

The stress (or force) environment of the tip has been investigated. The results have shown that fracture occurs when the force on the tip atom reaches a value slightly less than the maximum allowable for the perfect solid. In all cases the stress concentration factor F calculated by by Eringen has been found to be less than that calculated by molecular dynamics. The $\sqrt{\ell}$ dependence predicted by Eringen was not obeyed. Moreover F showed a clear load dependence contrary to the predictions of the Eringen theory and of other linear continuum theories. The profiles were qualitatively similar to the Eringen ones. When the maxima

of the two profiles were nearly equal, the atomistic profile was wider.

Consideration of energy and stress criteria has led to the conclusion that the latter is better for this type of loading. This is because of the considerable difficulties which face energy criteria, as outlined in the discussion of the Griffith theory for example. Methods for overcoming these difficulties are not available. For example there is no reasonable substitute for the work energy relation used in the Griffith theory. In the absence of such a relation no progress can be made using an energy theory. On the other hand there is a clear plan which can be outlined for formulating reliable fracture stress criteria. One can start by finding the maximum local force (stress) σ_{yy}^{MAX} a tip atom can withstand. This can be done by using a suitable pair potential. Once this is done then a set of calculations similar to the ones performed here can be carried out to yield the explicit dependence of $\mathcal{F}$ on ℓ & σ. Once an accurate $\mathcal{F}$ is available then it can be combined with the atomistic σ_{yy}^{MAX} to yield the critical σ for a particular ℓ or the critical ℓ for a particular σ by solving the implict equation

$$\mathcal{F}(\ell, \sigma) = \sigma_{yy}^{MAX} / \sigma$$

While the simulations have indicated that $\mathcal{F}$ decreases with increasing σ the number of static runs performed was not sufficient to propose an explicit form for the functional dependence of $\mathcal{F}$ on σ (or on ℓ).

Up to this point the present stress calculations have been viewed as a method for testing the Eringen calculation. Actually the present calculation includes less nonrealistic assumptions and is more accurate than the Eringen calculation. It can thus be used as a substitute for the Eringen formula and profiles. It should be remembered that the Eringen theory is still a linear one, and therefore does not include large deformations in the appropriate fashion.

The above comments on stress and energy criteria apply in particular to the case of fixed loads. For fixed displacements energy criteria stand a better chance of success than in fixed loads since no work energy relation is needed ($W = 0$). In this case the possibility of being a good approximation is better [illegible] because these loading conditions allow less deformation than fixed loads.

An interesting consequence of the atomicity of the lattice has been observed near the critical stress. The monotomic dependence on the local tip stress on the applied one is lost and the curve of $\sigma_{yy}(\ell, 0)$ vs σ flattens out.

This results in a range of ϵ's in which the crack is stable. This effect is a true consequence of the discreteness of the lattice and has nothing to do with the range of the potential, since it results from the nature of the potential near the inflection point.

Dislocation emission and blunting have been observed in some runs, in agreement with the predictions of the Rice-Thomson theory. According to this theory the ductility criterion is just barely satisfied and therefore dislocation emission is expected to occur only under special conditions.

It has not been possible to investigate the supersonic regime because all highly stressed samples deformed plastically i.e. by dislocation emission. The occurrence of plastic deformation rather than brittle propagation at high stresses is quite different from the Ashurst-Hoover result for this high stress level. In the Ashurst-Hoover and the Weiner-Pear high stress runs a supersonic velocity was achieved (very quickly in the W-P). The difference might be due to the potential, the boundary conditions, and the absence of any restriction on the motion of the atoms (as in W-P).

Bifurcation has been observed and is preceeded by a broadening of the column stress profiles.

Finally the case of fixed strain for this potential ~~and for~~ with free vertical boundary conditions remains to be investigated. The extension of the simulation to 3D for this type of loading (fixed) and for this sample size is also of interest.

NOTE:

As commented earlier the rigid tearing mode cannot occur for the case of fixed ~~loads~~ strains. This is because there is no additional room for a rigid separation of the two halves of the sample across the crack faces. In terms of energies, in the case of fixed displacements there is one source for the additional surface energy dU_S needed for crack motion. This source is the strain field. Thus for propagation

$$+ dU_S = - dU_E \qquad (\text{for } dU_k \approx 0)$$

In this case no propagation can occur in a rigid tearing mode ($dU_E \approx 0$) because the rigidity will necessarily imply that $dU_S \approx 0$ (i.e. no propagation). In fixed loads dU_E can be almost zero because the surface energy dU_S can be supplied from the loads i.e.

$$dW = dU_S \qquad (\text{for } dU_k \approx 0)$$

	CUTOFF	BEHAVIOUR	DAMPING	
S 11	45%	DUCTILE	EVERY 50	1.3
S 12	20%	BRITTLE UNEVEN	NO DAMP	1.35
S 13	30%	BRITTLE NEAT	NO DAMP	1.35
S 14	40%	BRITTLE	NO DAMP	1.35
S 15	42%	DUCTILE	NO DAMP	1.35
S 16	42%	DUCTILE	EVERY 20	3.2
S 17	45%	DUCTILE	NO DAMP	4.0

TABLE 3-3

STEP	ROW	σ up	σ down	σ right	σ left
5200	18	2.63	2.68	1.91	1.95
"	19	3.80	3.79	2.70	2.70
"	20	2.74	2.71	1.89	1.90
"	21	2.08	2.11	1.35	1.34
5360	18	3.21	3.20	2.08	2.05
"	19	4.37	4.39	3.41	3.39
"	20	3.33	3.34	2.18	2.16
"	21	2.59	2.59	1.59	1.56
6320	18	3.79	3.87	2.64	2.59
"	19	4.49	4.74	3.92	4.10
"	20	4.33	4.25	3.43	3.33
"	21	3.41	3.39	1.99	2.12
6960	18	3.36	3.48	2.45	2.48
"	19	4.39	4.34	3.89	3.84
"	20	4.59	4.33	3.83	3.87
"	21	3.82	3.72	2.35	2.38
8280	18	3.76	3.98	3.14	3.28
"	19	4.54	4.93	4.76	4.52
"	20	4.22	4.21	4.03	4.02
"	21	3.83	3.36	3.16	3.59
8800	18	3.89	4.08	3.53	3.71
"	19	4.62	4.85	4.65	4.40
"	20	4.80	4.25	4.47	4.87
"	21	4.49	4.01	3.39	3.12

σ = 0.5 39 BONDS

TABLE 3-4

STEP	ROW	σ_{up}	σ_{down}	σ_{right}	σ_{left}
3160	18	3.26	3.28	2.37	2.37
"	19	4.31	4.31	2.90	2.92
"	20	3.36	3.36	1.84	1.85
"	21	2.71	2.70	1.91	1.91
3840	18	4.17	4.15	3.06	3.63
"	19	4.59	4.73	3.49	3.98
"	20	-	-	3.39	3.57
"	21	4.21	3.85	2.99	4.04
4500	18	4.37	4.79	4.38	4.84
"	19	4.33	4.85	4.44	4.87
"	20	4.97	4.73	5.22	5.97
"	21	4.51	4.29	3.96	5.41

σ = 1.3 19 BONDS

STEP	ROW	σ_{up}	σ_{down}	σ_{right}	σ_{left}
3100	18	3.02	3.02	2.27	2.29
"	19	4.09	4.09	2.71	2.71
"	20	3.09	3.08	1.81	1.80
"	21	2.48	2.48	1.80	1.77
3760	18	4.31	4.50	4.47	5.59
"	19	4.62	4.89	5.53	5.49
"	20	4.66	4.38	5.13	5.13
"	21	4.63	4.16	4.25	4.33

σ = 1.3 39 BONDS

TABLE 3-5

STEP	ROW	σ_{up}	σ_{down}	σ_{right}	σ_{left}
9460	18	3.31	3.31	2.14	2.14
"	19	4.46	4.46	3.41	3.41
"	20	3.51	3.51	2.13	2.13
"	21	2.72	2.72	1.74	1.74

σ = 0.5 39 BONDS

DAMPED

TABLE 3-6

STEP	ROW	up	down	right	left
6280	18	1.75	1.75	1.55	1.55
"	19	2.55	2.55	1.47	1.47
"	20	1.76	1.76	1.31	1.31
"	21	1.38	1.38	1.20	1.20

σ = 0.5 19 BONDS

DAMPED

TABLE 3-7

STEP	ROW	up	down	right	left
6500	18	1.07	1.07	1.03	1.03
"	19	1.53	1.53	0.99	0.99
"	20	1.07	1.07	0.91	0.91
"	21	0.87	0.87	0.81	0.81

$\sigma = 0.5$ 9 BONDS

DAMPED

TABLE 3-8

BOND	STEP			
	9903	9950	10,000	10,050
48 - 49	1.109	1.028	1.009	1.027
49 - 49	1.283	1.034	1.051	1.031
49 - 50	1.364	1.125	1.0474	1.009
50 - 50	1.454	1.274	1.014	1.054
50 - 51	1.503	1.381	1.105	1.059
51 - 51	1.575	1.494	1.283	1.018
51 - 52	1.6	1.579	1.419	1.130
52 - 52	1.6	1.6	1.6	1.6

σ = 0.5 39 BONDS

BOND	STEP			
	6250	6300	6350	6400
58 - 59	1.250	1.170	1.033	1.056
59 - 59	1.419	1.290	1.127	1.051
59 - 60	1.516	1.412	1.299	1.141
60 - 60	1.597	1.524	1.446	1.311
60 - 61	1.658	-	-	1.454
61 - 61	1.717	-	-	-
61 - 62	1.762	-	-	-
62 - 62	1.808	-	-	-

σ = 1.3 19 BONDS

TABLE 3-9

ROW	σ_{up}	σ_{down}	σ_{right}	σ_{left}
18	3.50	3.50	2.20	2.20
19	4.55	4.55	3.51	3.51
20	3.81	3.81	2.37	2.37
21	2.97	2.97	1.90	1.90

39 BONDS (DAMPED) σ = 0.55

STEP 12520

TABLE 3-10

ROW	σ_{up}	σ_{down}	σ_{right}	σ_{left}
18	3.58	3.58	2.14	2.14
19	4.39	4.39	3.44	3.44
20	4.28	4.28	2.83	2.83
21	3.34	3.34	2.08	2.08

39 BONDS(DAMPED) σ = 0.6

STEP 15780

TABLE 3-11

ℓ	σ_z^1	σ_z^2	σ MD PRE
9	4.62	4.66	-
19	3.22	3.25	1.3
39	2.27	2.29	.5

TABLE 3-12(a)

RUN	ℓ	σ	u_E^{MD}	u_E^C	f_{u_E}
L6	9	0.5	0.36	0.218	61%
L5	19	0.5	1.72	0.92	54%
L4	39	0.5	12.50	3.78	30%
L7	19	1.3	16.78	6.34	38%
L8	9	1.3	3.86	1.51	39%
L15	39	0.55	15.3	4.56	29%
L16	39	0.6	19.0	10.88	57%

TABLE 3-12(b)

σ	$F = [\sigma_{yy}(\ell, 0)]_{MAX} / \sigma$		
	9	19	39
.5	3.06	5.1	8.92
.55	-	-	8.27
.6	-	-	7.32
1.3	2.807	3.16	-
ER (a = 1.62)	1.74	2.51	3.56
ER (a = 1.0)	2.22	3.18	4.52

TABLE 3-14

σ	σ_{local} (MAX)		
	9	19	39
.5	1.53	2.55	4.46
.55	-	-	4.55
.6	-	-	4.39
1.3	3.65	4.11	-

TABLE 3-13

F^E	F^{MD}	σ	σ^{MD}_{MAX}	SIZE
4.53	8.92	0.5	4.46	39
3.18	5.1	0.5	2.55	19
2.22	3.06	0.5	1.53	9
3.18	3.42	1.3	4.45	19
2.22	2.81	1.3	3.65	9
4.53	8.27	0.55	4.55	39
4.53	7.32	0.6	4.39	39

TABLE 3-15

W^{MD} (in ℓ)	W^{ER} (in ℓ)	σ	ℓ
.27	.15	1.3	19
.14	.15	.5	39
.09	.05	.5	39

W = width of profile at $F = (F^{MAX} - 1)/2 + 1$

Half widths of Force Profiles

TABLE 3-16

σ = 0.5 39 BOND CRACK

1ST BOND AHEAD OF TIP.	CRITICAL	1ST BROKEN	
1.05749	1.10879	1.28278	r
.08119	.2133	.6015	BOND STRAIN ENERGY

σ = 1.3 19 BOND CRACK

1ST BOND AHEAD OF TIP.	CRITICAL	1ST BROKEN	
1.11182	1.25028	1.41983	r
.22145	.54495	.7708	BOND STRAIN ENERGY

TABLE 3-17

$\sigma = 0.5$ 39 BOND CRACK

1ST BOND AHEAD OF TIP.	CRITICAL	1ST BROKEN	
1.05749	1.10879	1.28278	r
.08119	.2133	.6015	BOND STRAIN ENERGY

$\sigma = 1.3$ 19 BOND CRACK

1ST BOND AHEAD OF TIP.	CRITICAL	1ST BROKEN	
1.11182	1.25028	1.41983	r
.22145	.54495	.7708	BOND STRAIN ENERGY

TABLE 3-17

FIGURE CAPTIONS

FIG. 1-1 This figure gives the loading configuration investigated here (i.e. uniaxial tension), and the Inglis solution for the tensile field σ_{yy} in this situation.

FIG. 1-2 This figure gives the form used by Thomson *et al* in their energy calculations. The figure also defines the tip width η .

FIG. 1-3 The stress profiles obtained by Eringen are given here.

FIG. 1-4 The dynamic velocity function $\overline{f}(v)$.

FIG. 2-1 The tensile and shear force laws employed by Weiner and Pear are given here. ξ_T is the change in interatomic spacing of two atoms in the same column. ξ_S is the difference in y - coordinates of two atoms lying in different columns.

FIG. 2-2 The Ashurst-Hoover force laws. The three force laws agree up to an extension of w .

FIG. 3-1 This figure illustrates how a reflection about a central vertical axis of symmetry can be used to get a 50% saving in computer time.

FIG. 3-2 This figure gives the behaviour of the potential in the vicinity of r_{MAX} (as defined in 3D), and the origin of the W correction.

FIG. 3-3 This figure gives the behaviour of the potential energy of the half crystal as a function of time for different damping methods. (Run S 1)

X	$\beta = 1$
•	" = .99
△	" = .9875
⊙	" = .985
+	" = .975
o	BEELER- KULCINSKI

FIG. 3-4 to 3-25

give the pictures of the lattices of the small sample runs for fixed loads.

FIG. 3-26 to 3-34

same as above but for fixed strains.

FIG. 3-35 This figure gives the time evolution of the different energies in run L 1. Of special interest here is the constancy of U_E. The energies are in units of ϵ and are given for the half crystal. The time step is $10^{-2}\alpha\sqrt{m/\epsilon}$.

FIG. 3-36 Gives the time evolution of bonds across the crack faces as the crack propagates for run L 1. Bond lengths are in units of α .

FIG. 3-37 Same as 3-36 but for the large extension range.

FIG. 3-38 This figure gives the crack velocity as a function of half length ℓ . The solid line represents the results of the simulation. The dashed line (--------) gives the expectations of the rigid model for $v_0 = 1.0$, the dashed with dots (-.-.-.-.-.-.-) gives these expectations for $v_0 = 0.8$, and the dashed with x gives the velocity $v_0 = 0.6$ (-x-x-x-).

FIG. 3-39 to 3-44

These figures give the pictures of the cracking sample in run L 1.

FIG. 3-45 to 3-73

These figures give the dynamic profiles (as defined in 3D) (RUN L 2)

FIG. 3-74 The time evolution of the different energies together with the fraction $\frac{\Delta U_E}{\Delta W}$. (RUN L 2)

FIG. 3-75 Same as 3-74 but gives the energies as a function of u_E. The straight dashed line gives the elastic solution. (RUN L 2)

FIG. 3-76 to 3-91

The time evolution of the fracturing lattice (RUN L 2)

FIG. 3-92 to 3-107

The dynamic stress profiles. (RUN L 2)

FIG. 3-108 Crack velocity vs. time (RUN L 3)

FIG. 3-109 Time evolution of the energies. (RUN L 3)

FIG. 3-110 Energies as a function of u_E. (RUN L 3)

FIG. 3-111 to 3-125

Pictures of the fracturing lattice (RUN L 3)

FIG. 3-126 to 3-139

Dynamic stress profiles. (RUN L 3)

FIG. 3-140 to 3-151

Static (damped) profiles (RUN L 4)

FIG. 3-152 to 3-155 Static (damped) profiles. (RUN L 8)

FIG. 3-156 to 3-158 Bond lengths around the tip in L 17.

FIG. 3-159 to 3-160 Lattice pictures for the ductile fracture of run L 17.

FIG. 3-161 tc 3-167 Pictures of the ductile fracture of L18.

FIG. 3-168 This figure gives the details required in the definition of the tip force (a). In (b) the parameter used in the rigid body analysis are given. 168(c) illustrates why the only rigid tearing mode for this crack is the one with infinite speed.

FIG. 3-169 This figure gives the forces acting on the tip atoms when the cut is introduced. The dashed line represents the cut bond.

FIG. 3-170 This figure explains how the initial velocity v_5 was estimated.

FIG. 3-171 to 3-173 These figures give a comparison between the Eringen and the molecular dynamic profiles.

FIG 3-174 Definition of θ (the direction along which the maximum force is exterted).

FIG. 3-175(a),(b) This figure (a) shows the flattenning of the $\sigma_{yy}(\ell,\rho)$ vs. σ curve. In (b) the values obtained from the static σ =0.5, 0.55, 0.6 runs. Also given are the equilibrium lengths r_1 & r_2 of the first two tip bonds. (Fig. 176)

FIG. 3-177 The flattenning in the force on the tip atom.

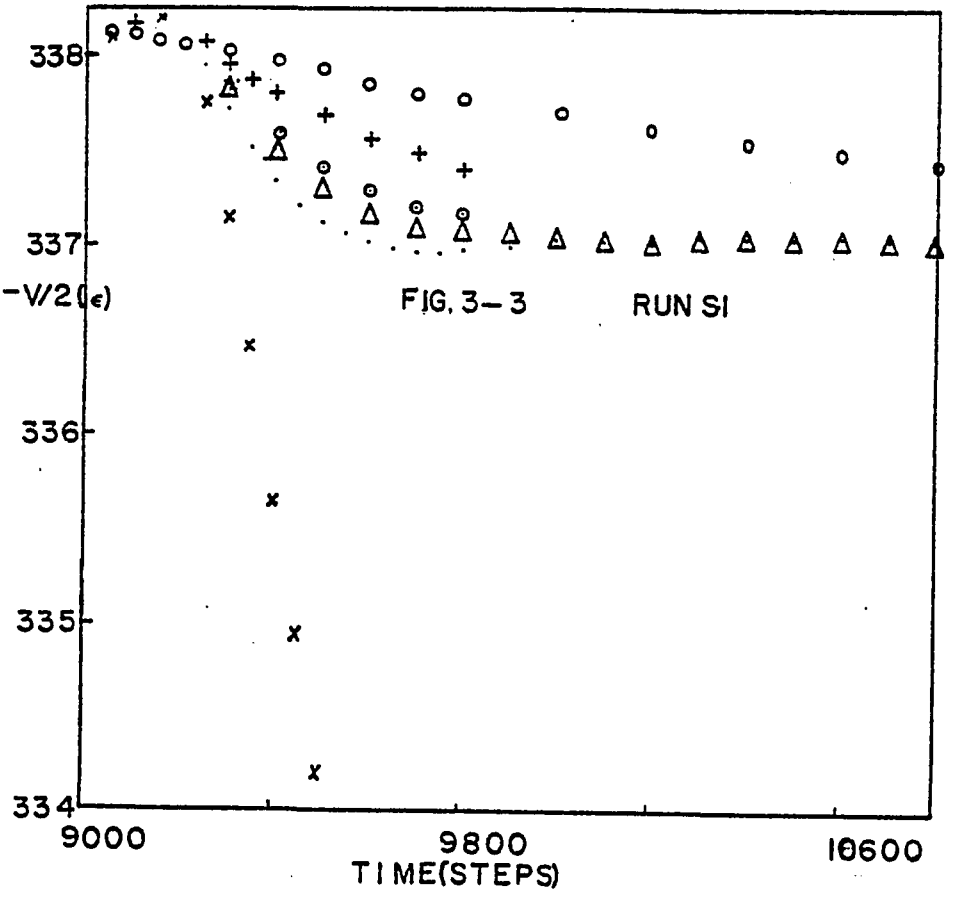

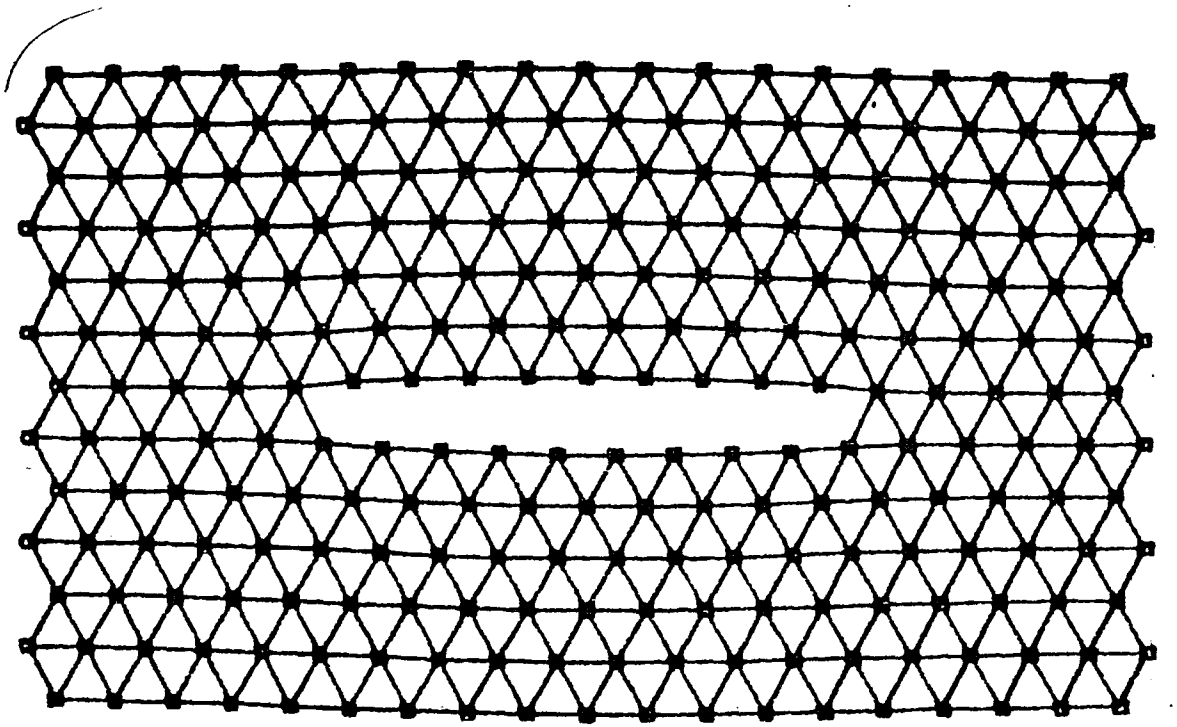

7920

FIG. 3-4

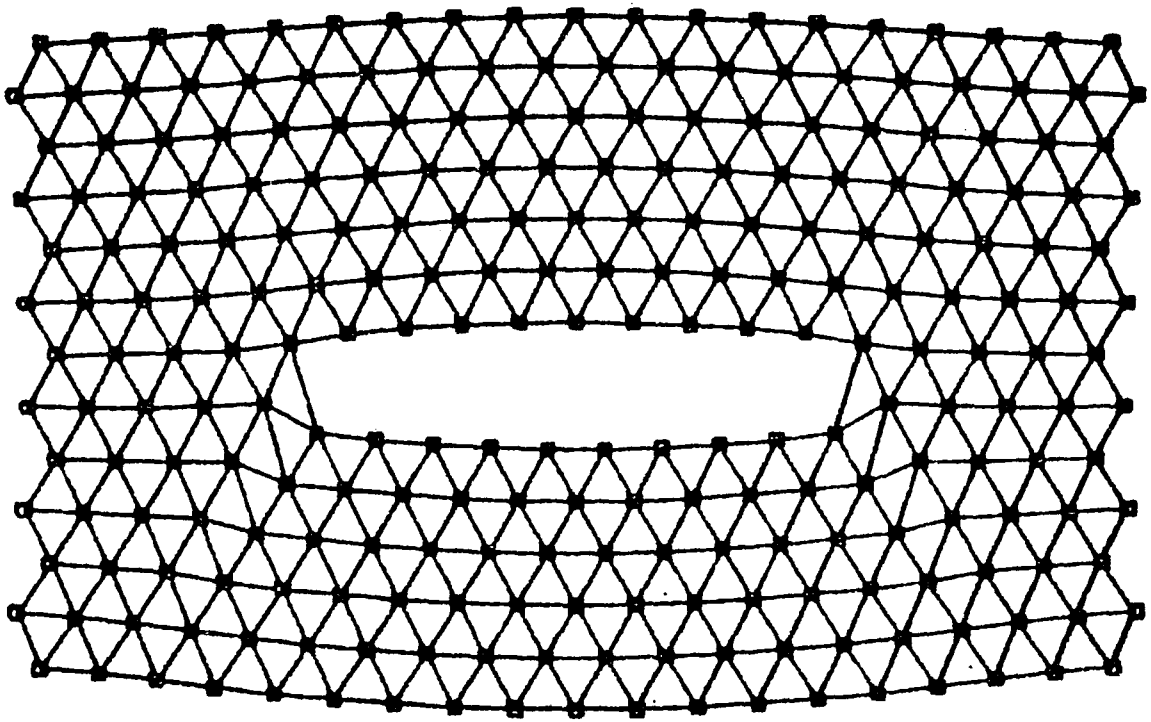

9120

FIG. 3-5

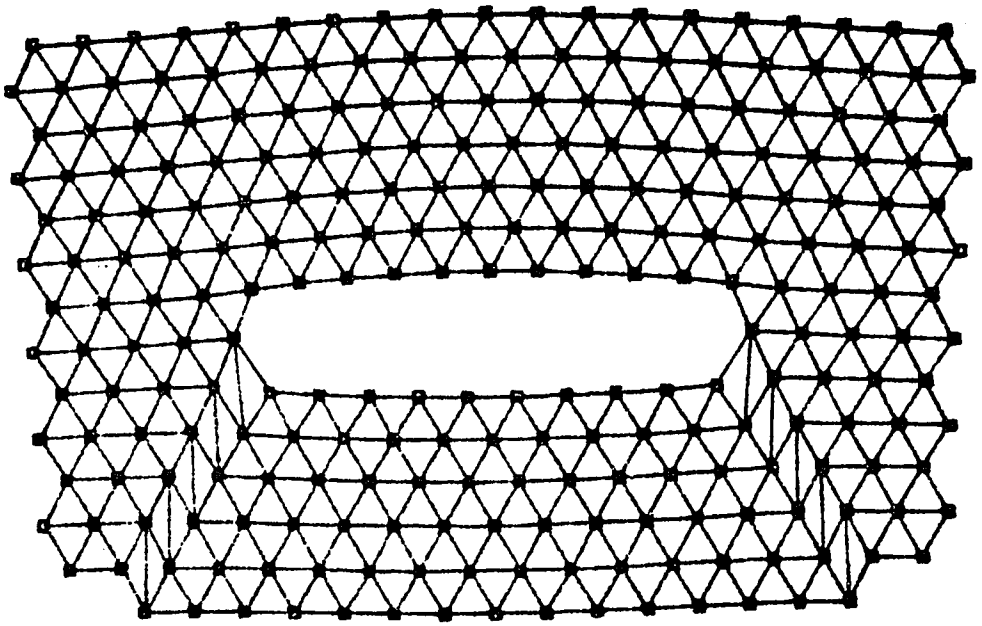

9920

FIG. 3-6

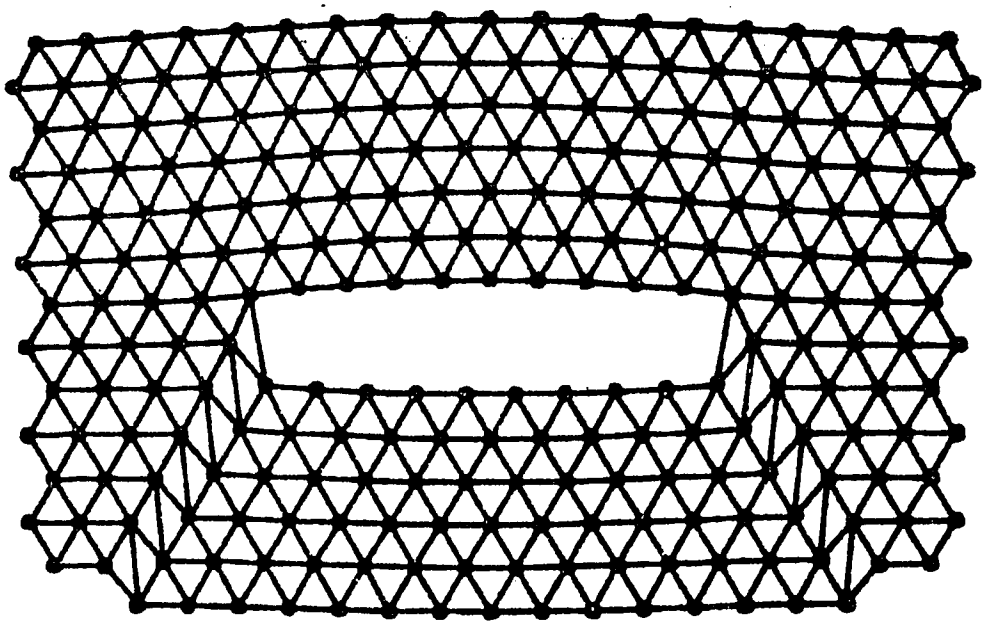

10180

FIG. 3-7

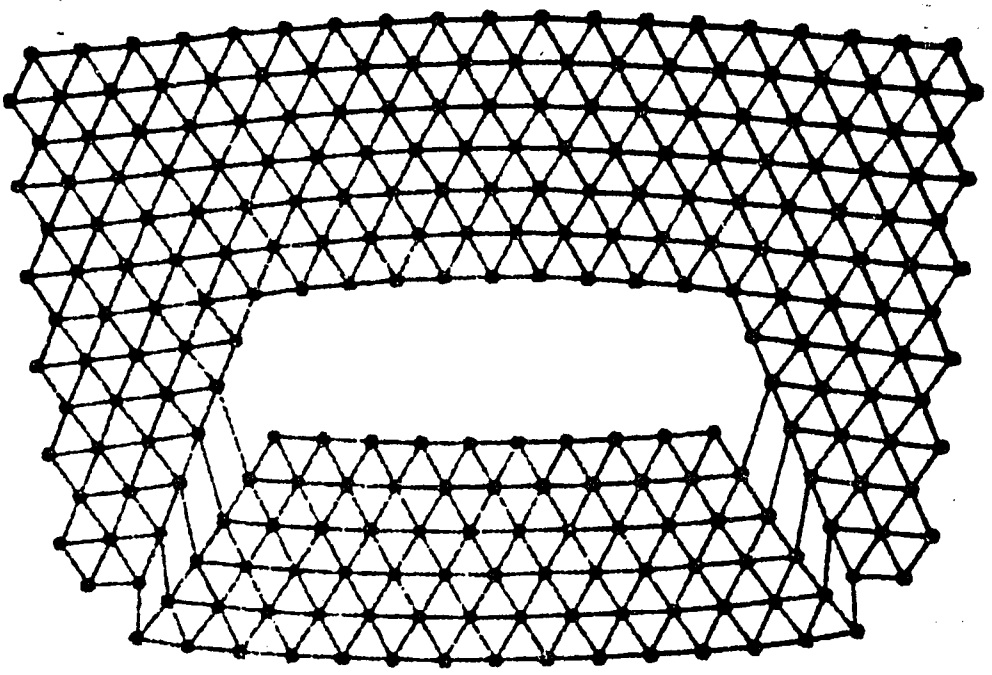

10960

FIG. 3-8

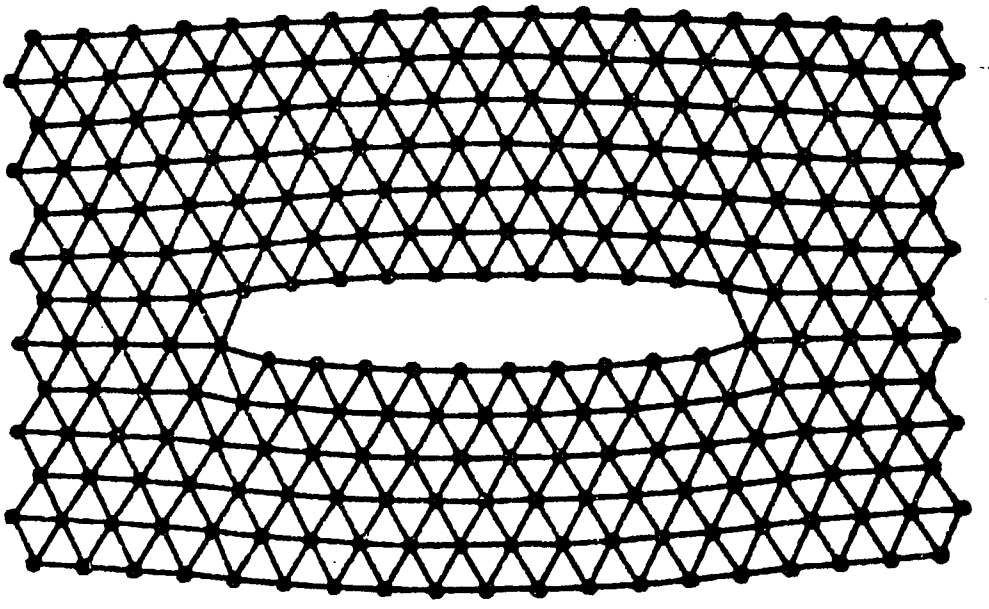

8700

FIG. 3-9

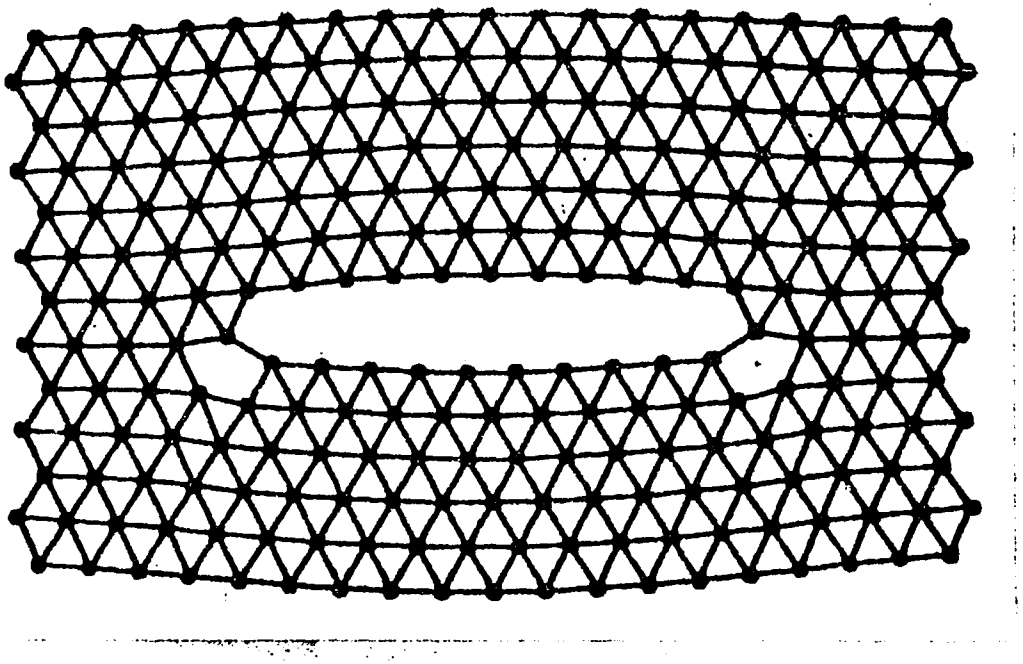

8800

FIG. 3-10

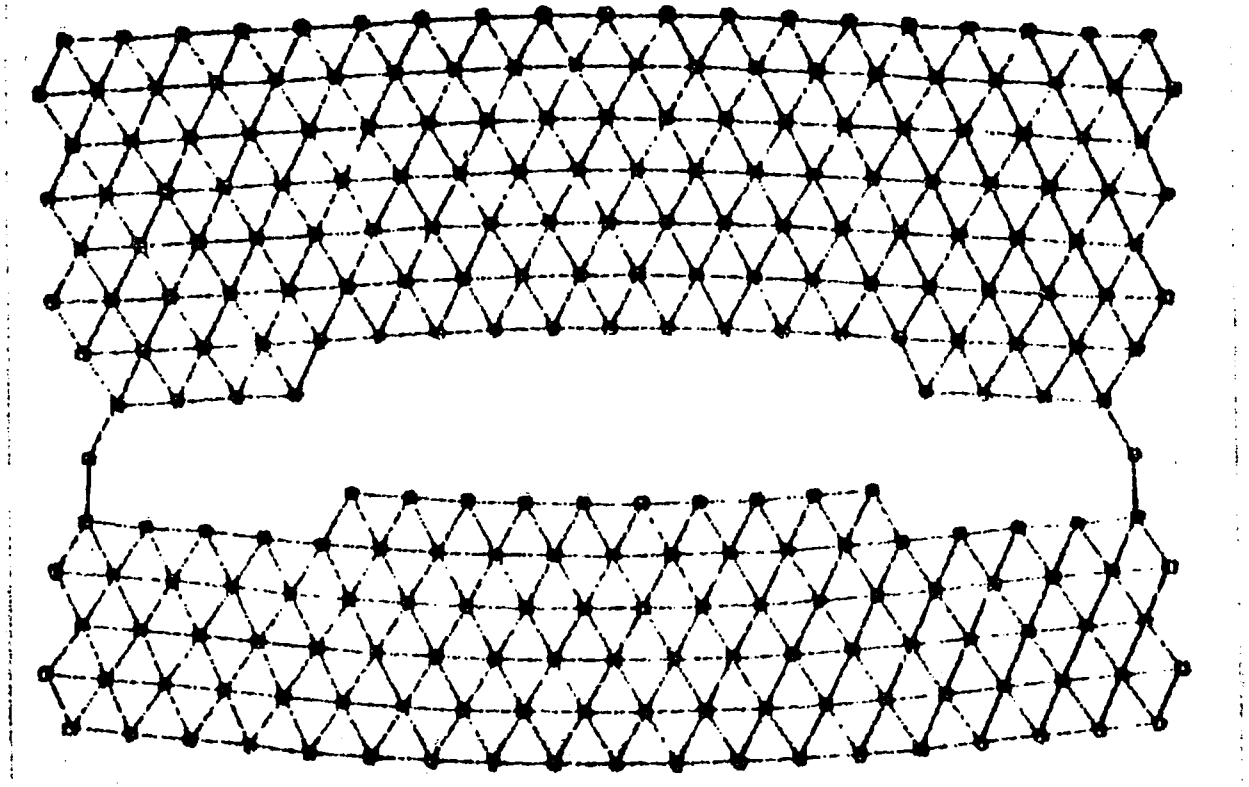

9400

FIG. 3-11

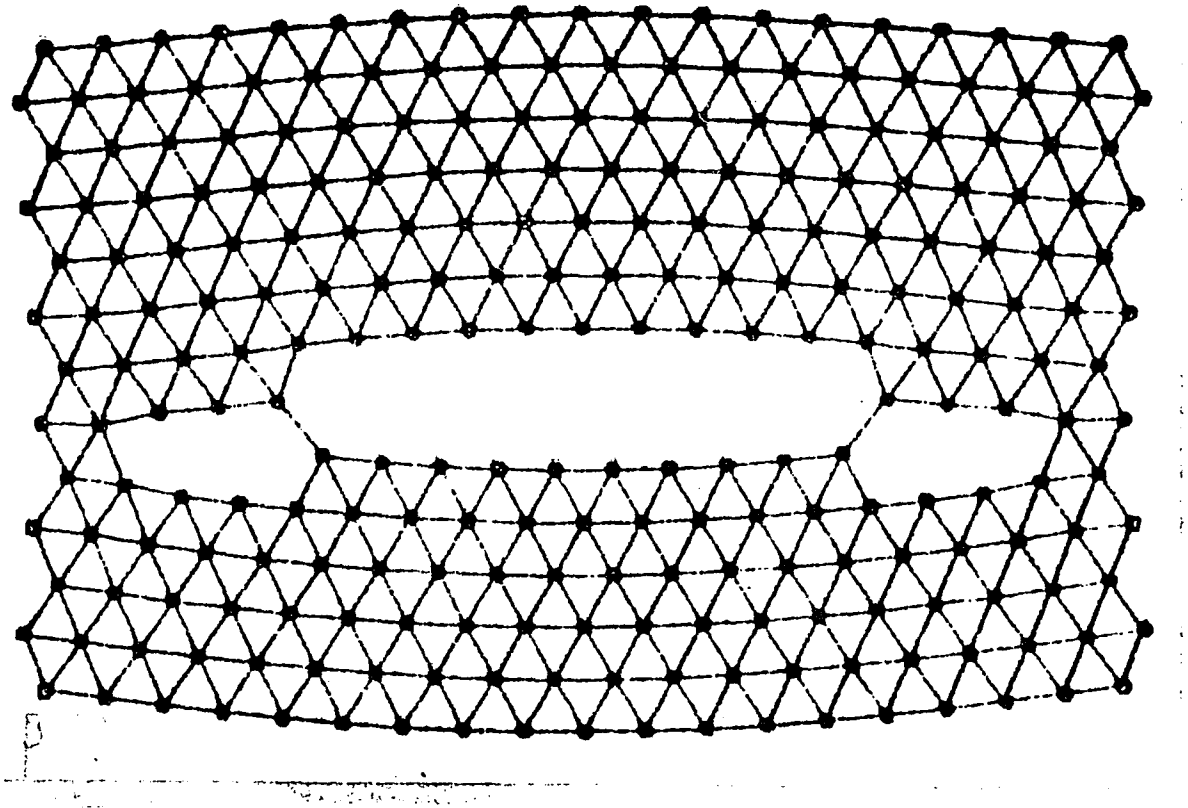

9100

FIG. 3-12

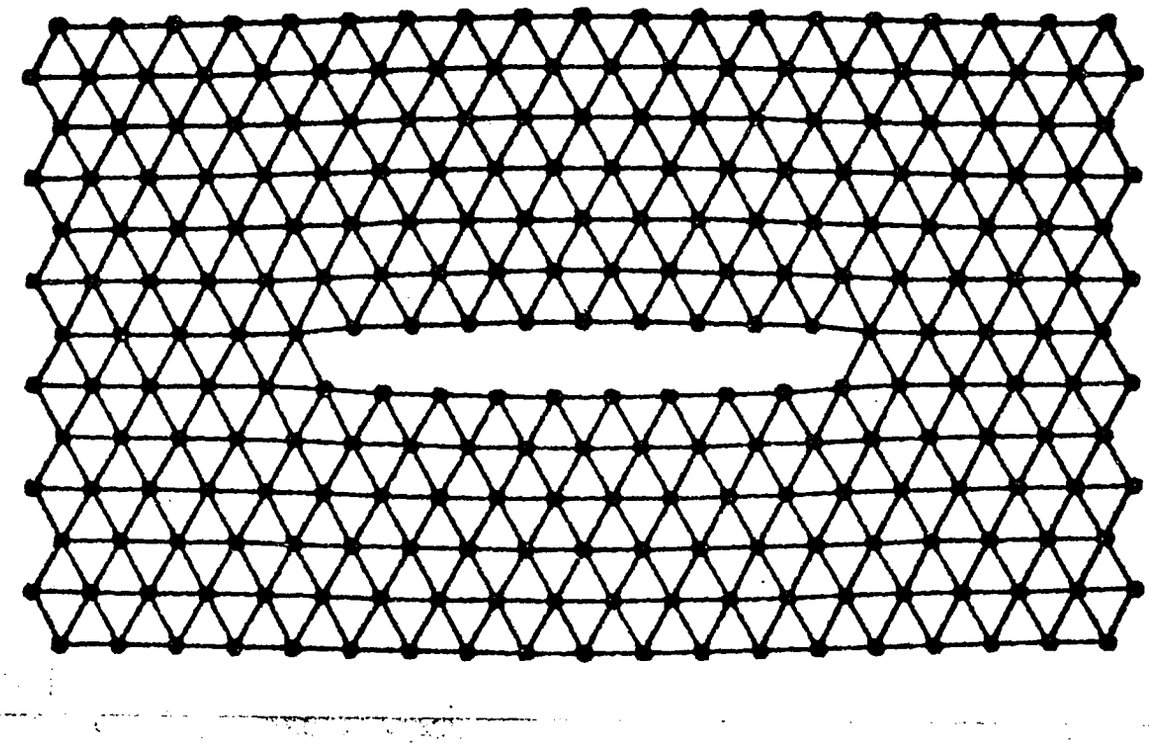

7950

FIG. 3-13

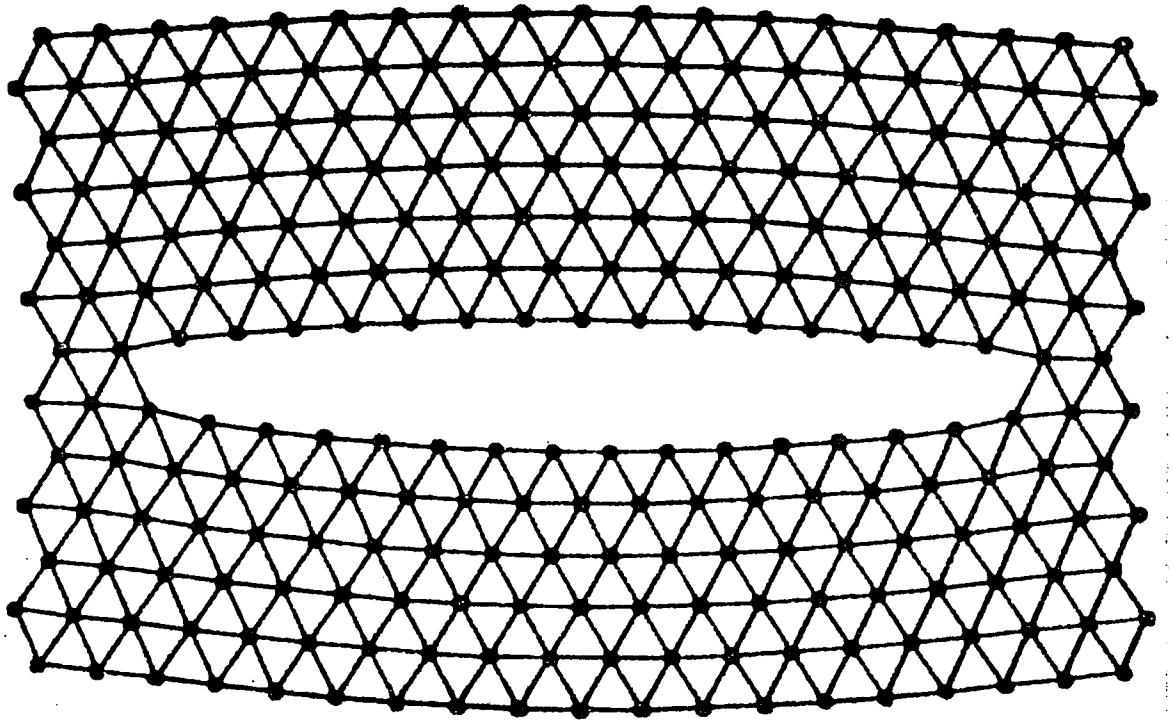

10700

FIG. 3-14

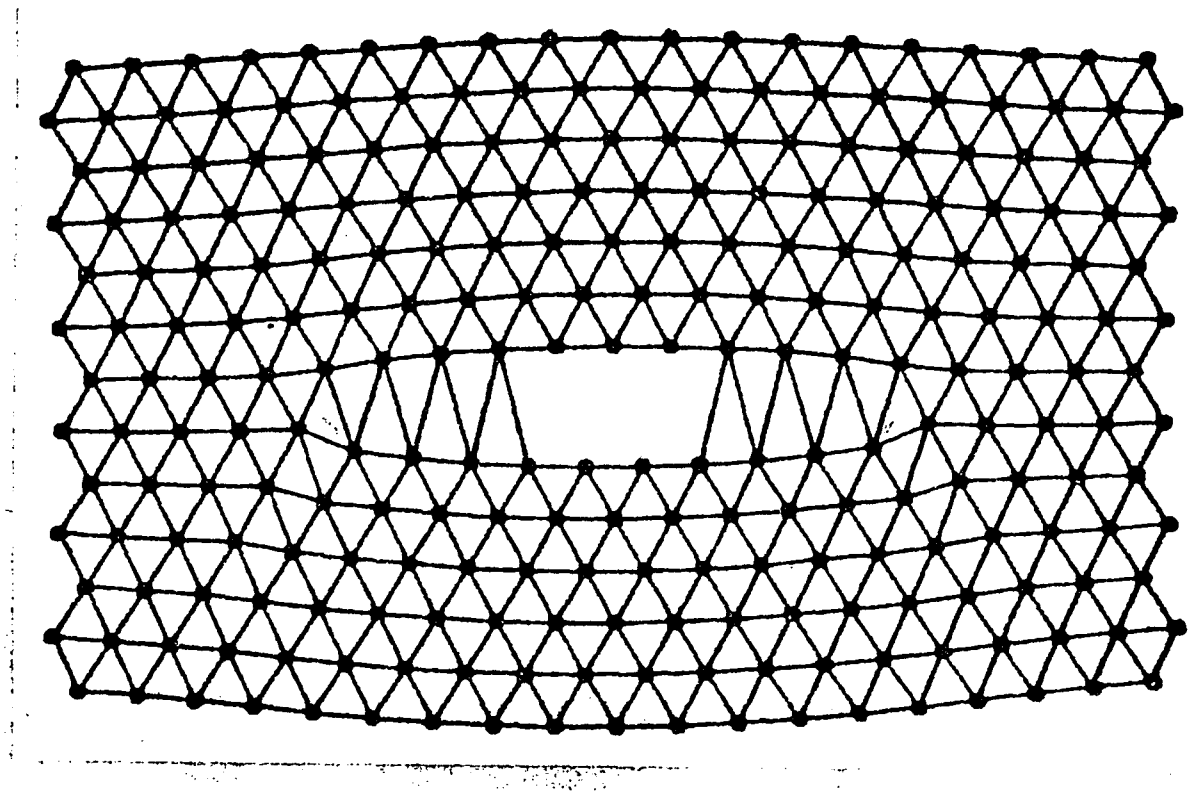

11520

FIG. 3-15

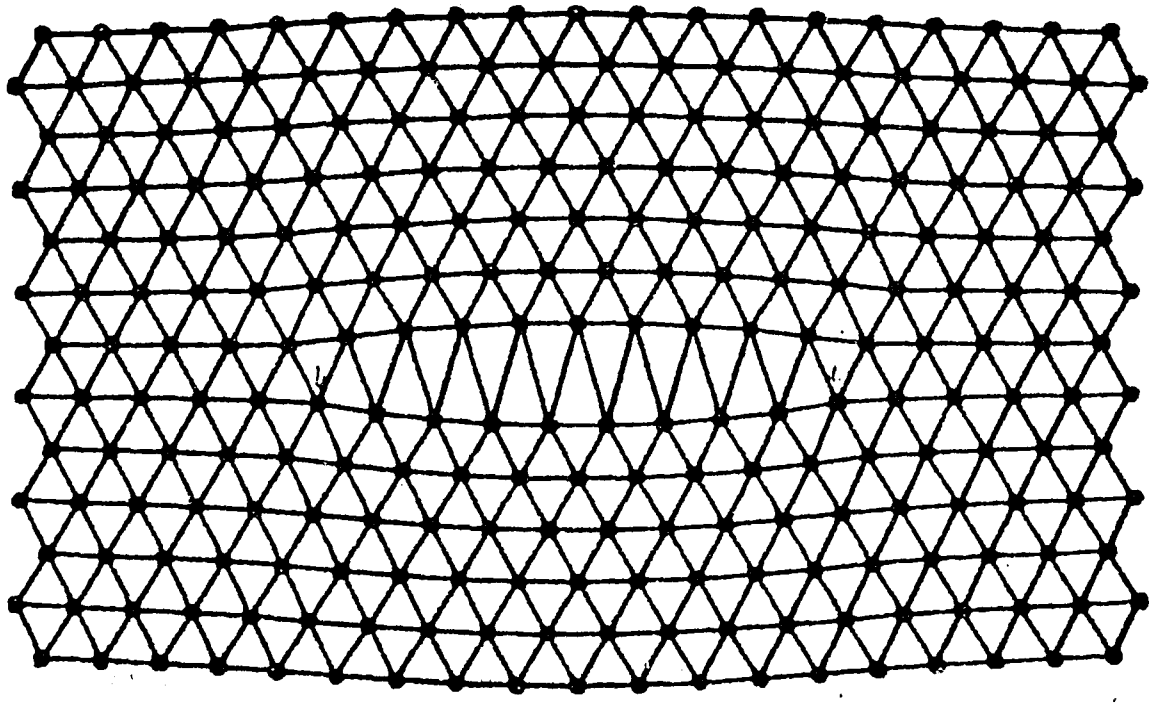

11920

FIG. 3-16

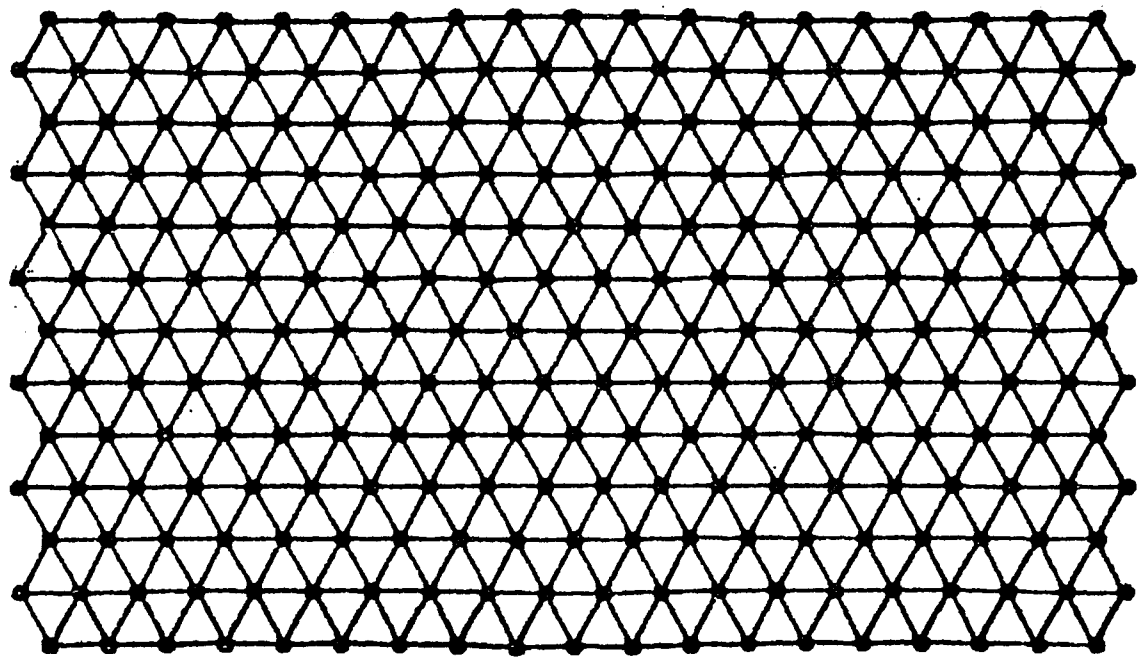

12480

FIG. 3-17

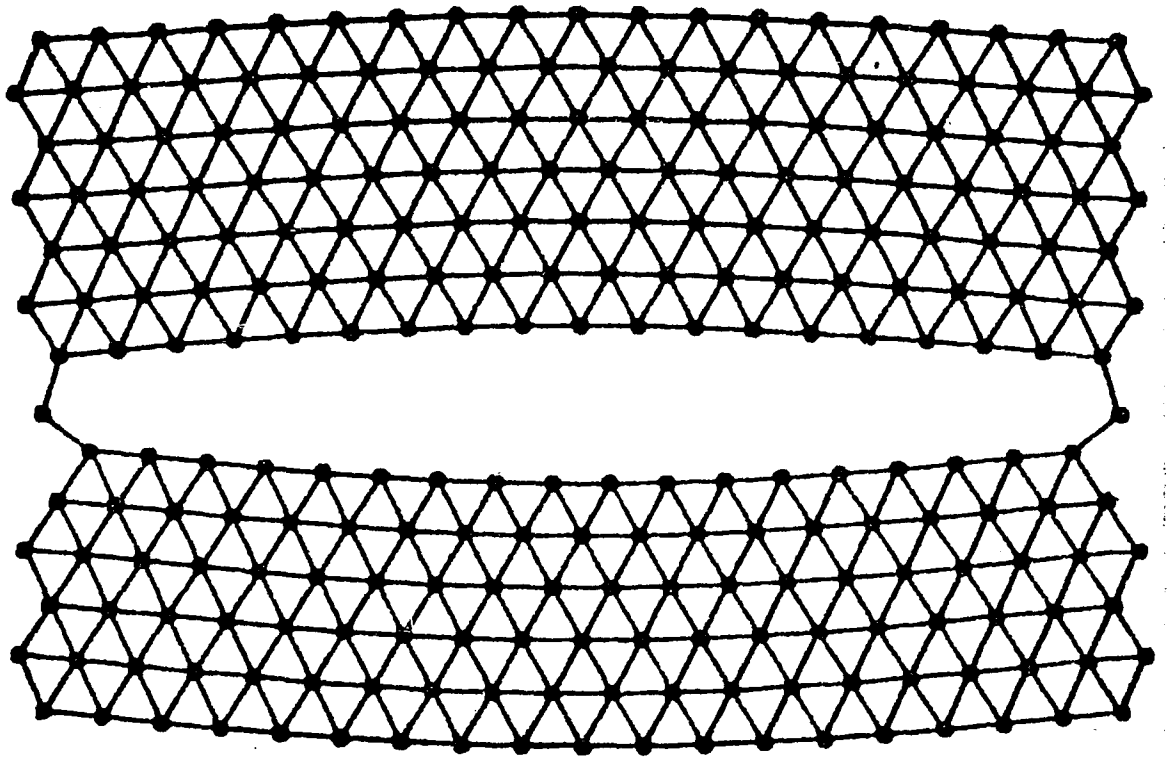

10150

FIG. 3-18

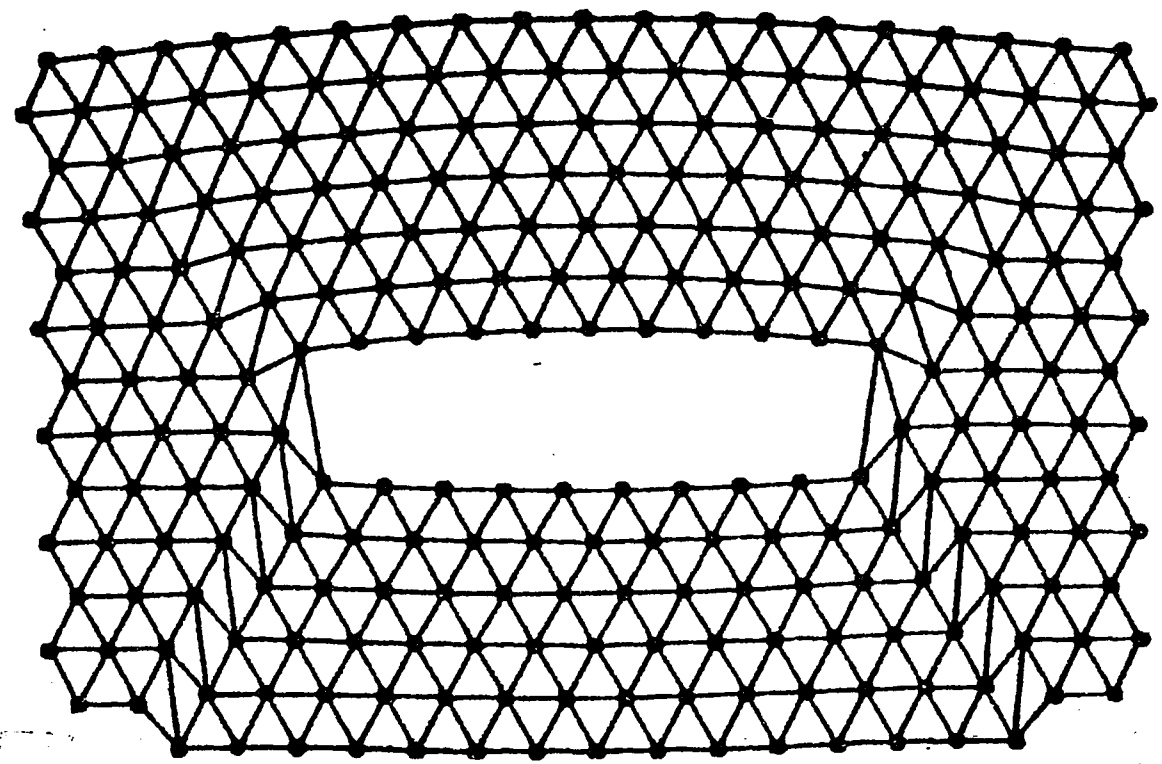

10650

FIG. 3-19

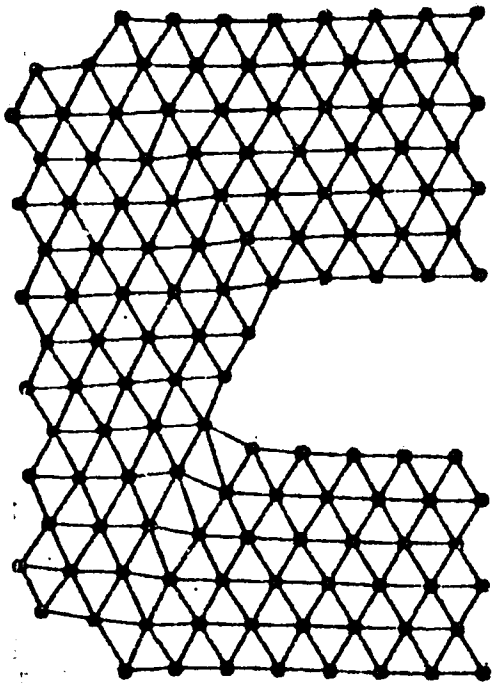

8150

FIG. 3-21

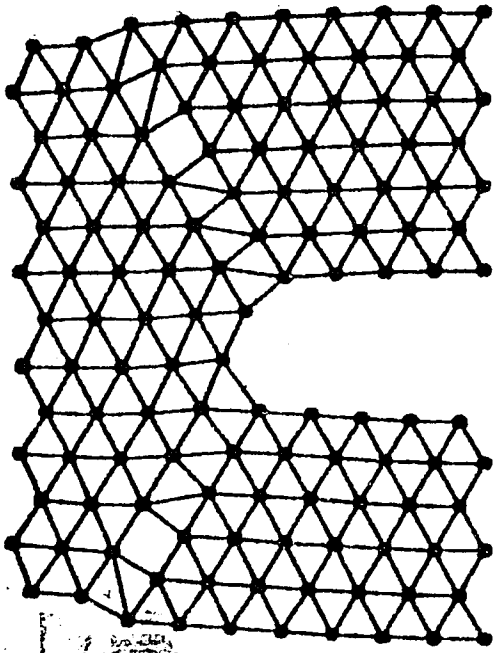

8100

FIG. 3-20

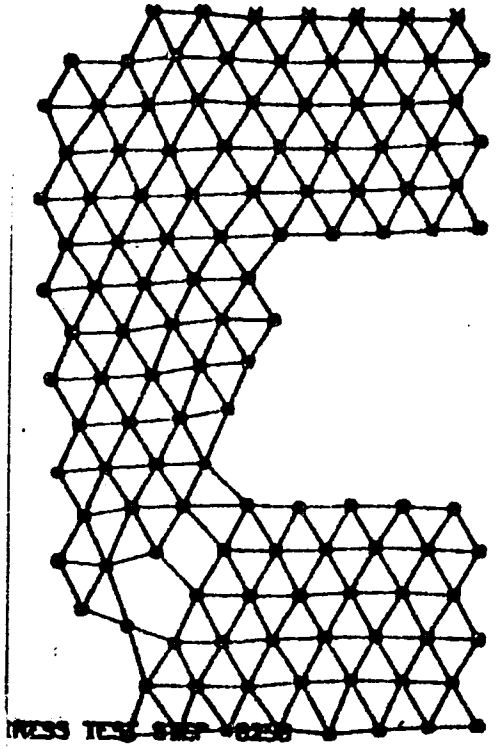

8250

FIG. 3-22

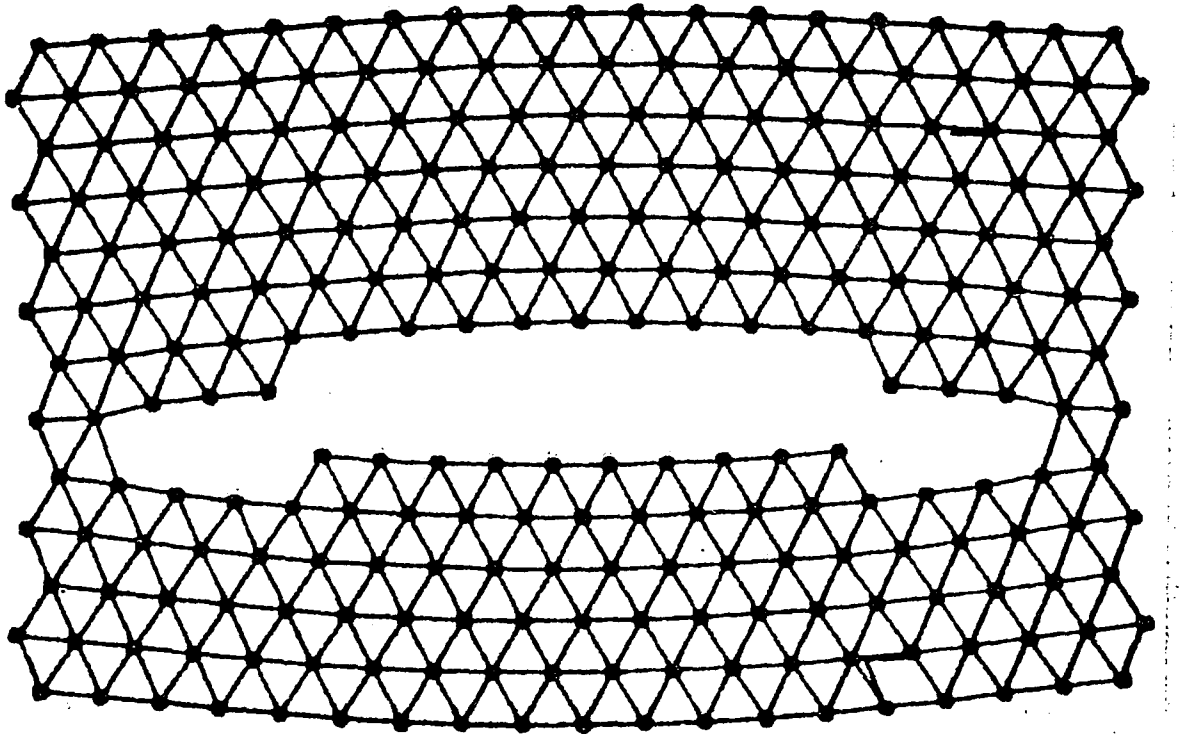

6650

FIG.. 3-23

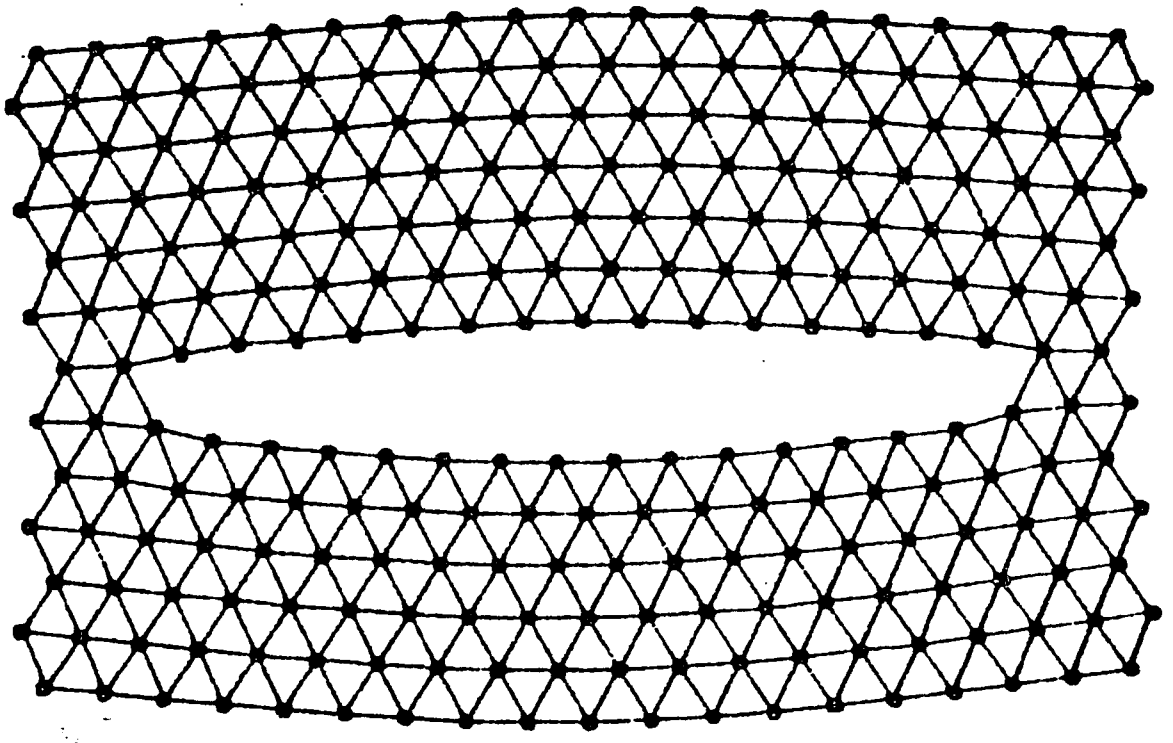

9200

FIG. 3-24

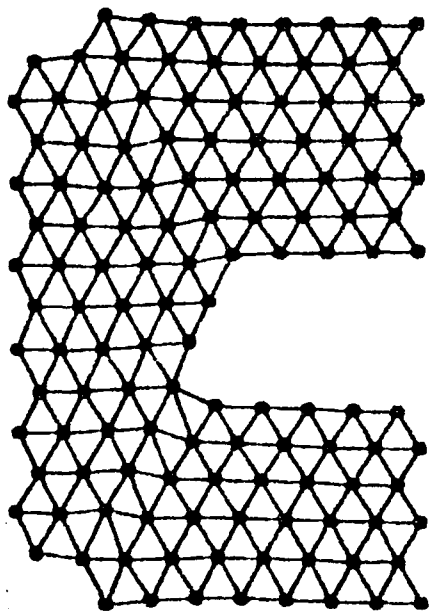

8100

FIG. 3-25

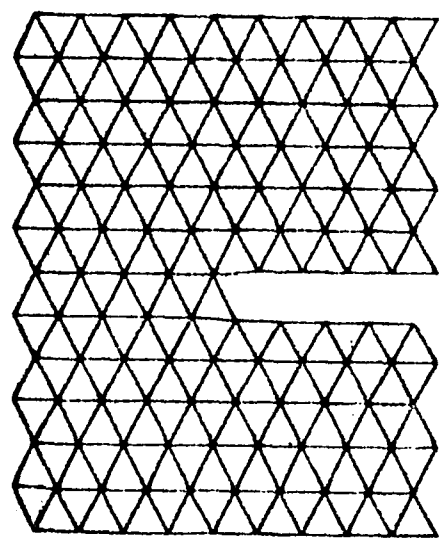

13500

FIG. 3-26

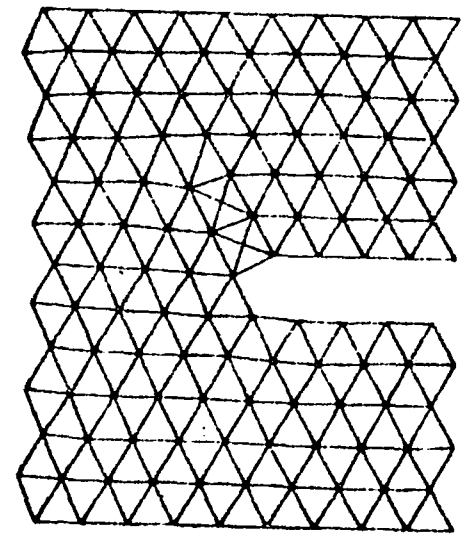

13700

FIG. 3-27

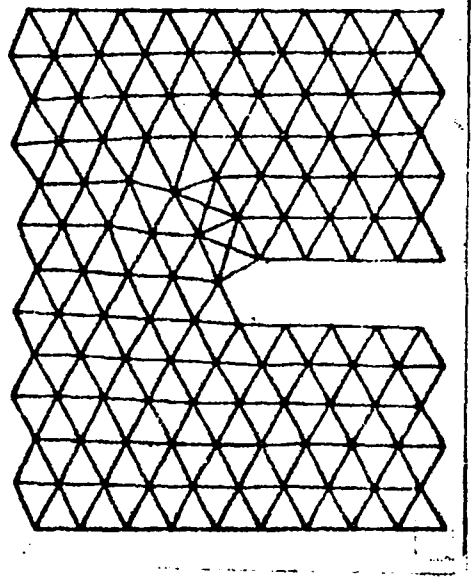

13750

FIG. 3-28

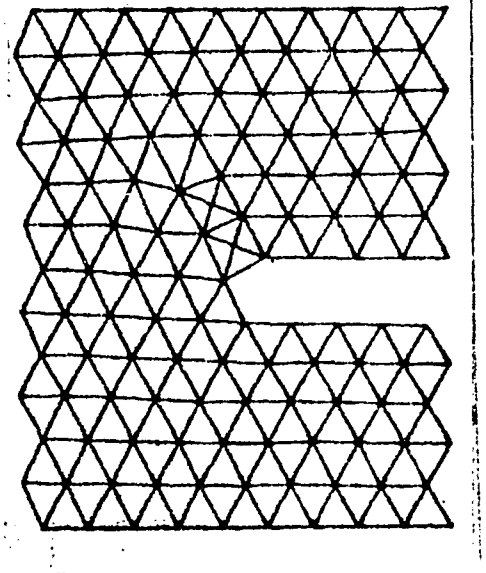

13800

FIG. 3-29

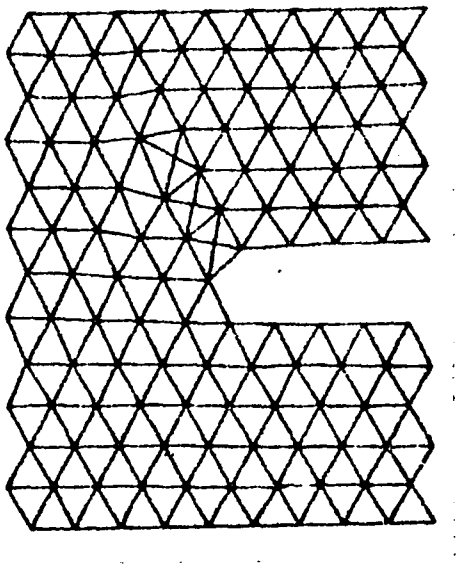

13850

FIG. 3-30

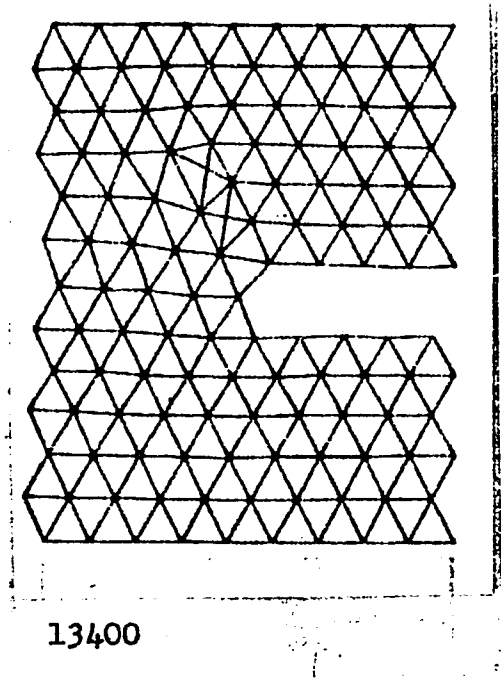

13400

FIG. 3-31

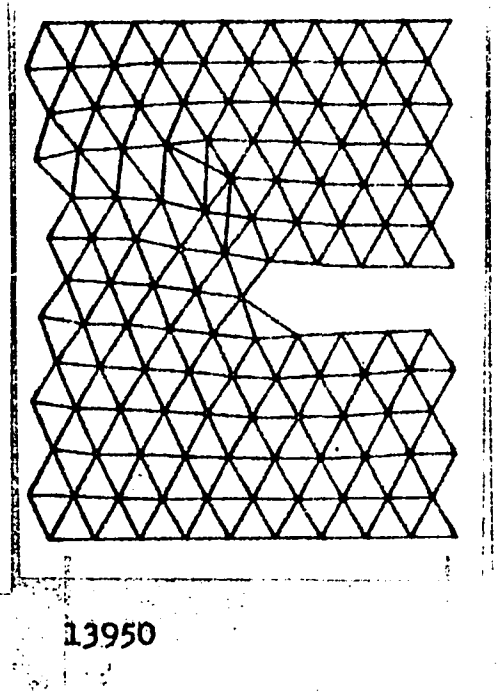

13950

FIG. 3-32

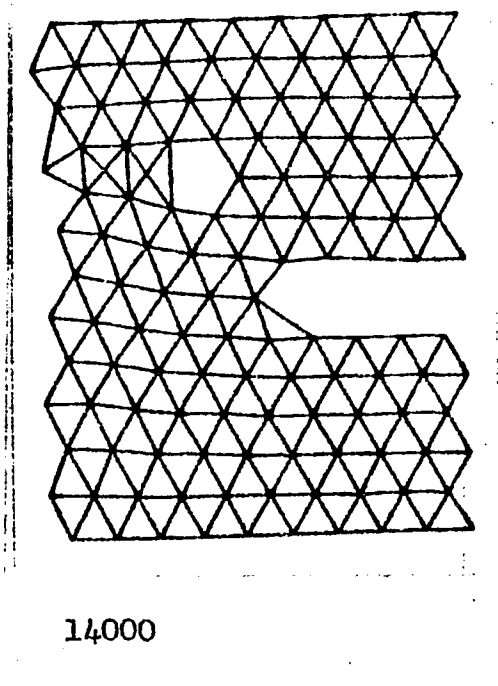

14000

FIG. 3-33

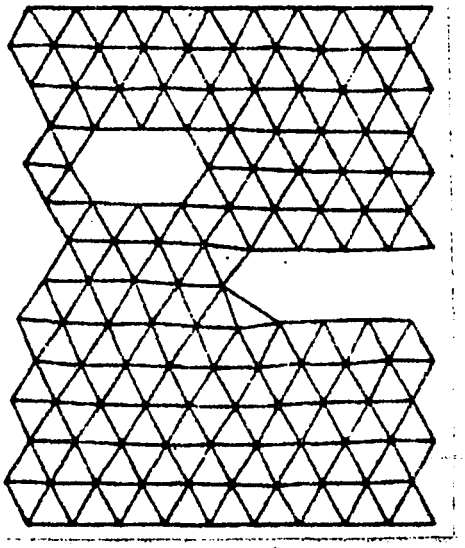

FIG. 3-34

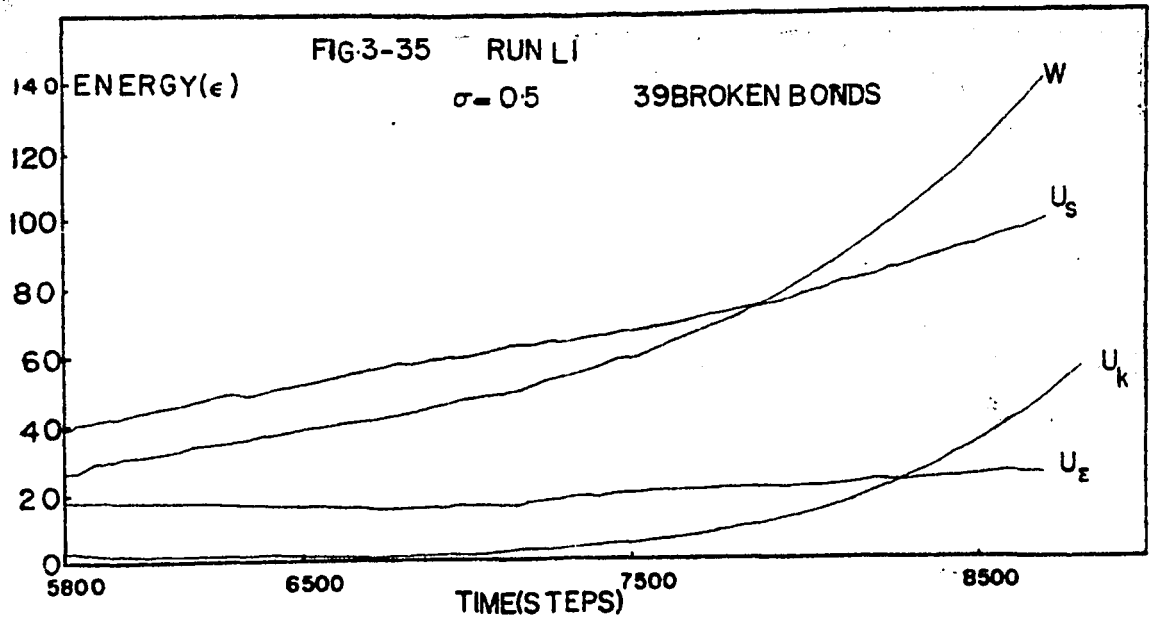

FIG. 3-35

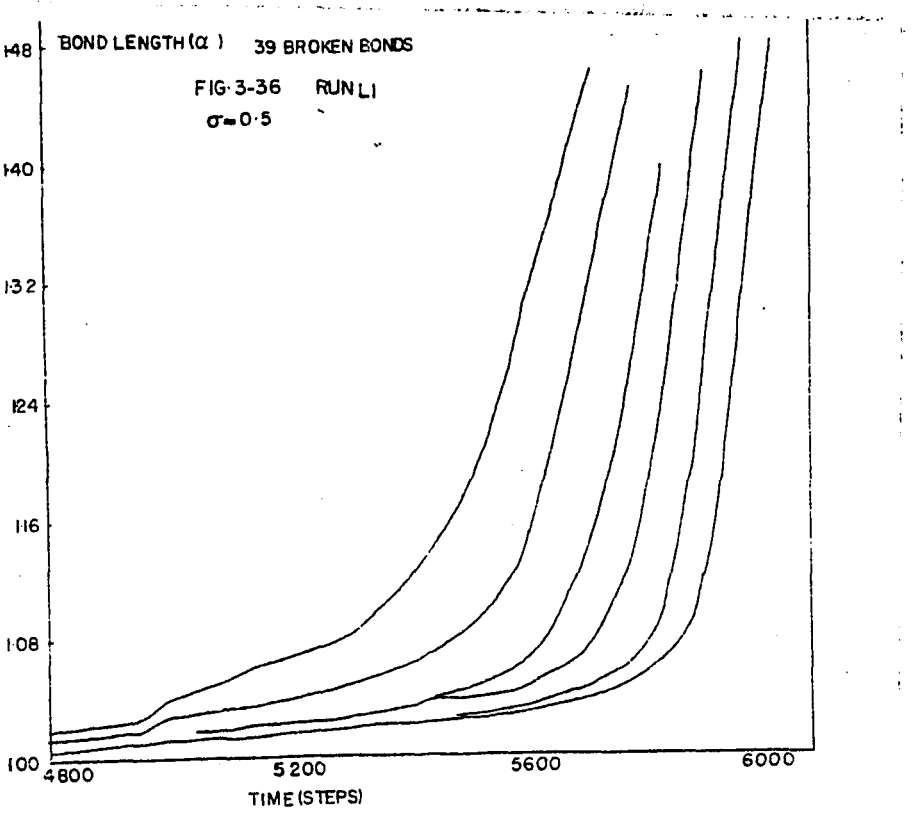
BOND LENGTH(α) 39 BROKEN BONDS
FIG·3-36 RUN LI
σ=0·5
1·48
1·40
1·32
1·24
1·16
1·08
1·00
4800
5200
5600
6000
TIME (STEPS)

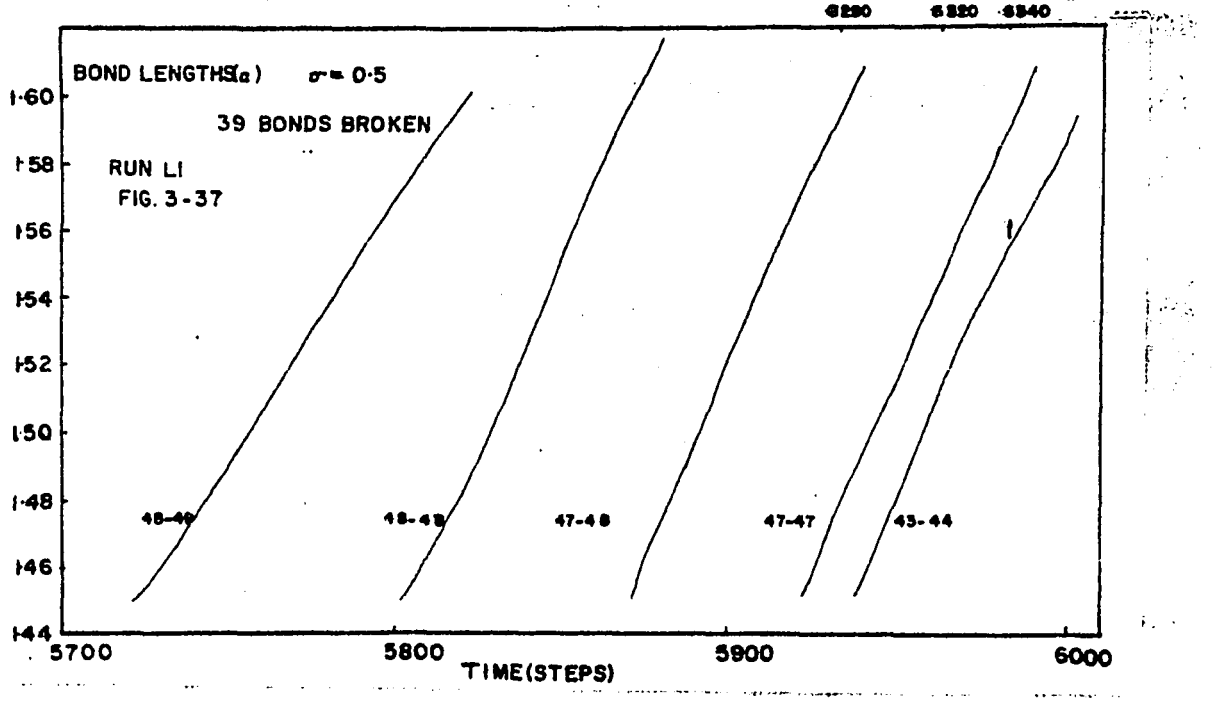
BOND LENGTHS(α) σ= 0·5
39 BONDS BROKEN
RUN LI
FIG. 3-37
1·60
1·58
1·56
1·54
1·52
1·50
1·48
1·46
1·44
48-48
48-47
47-48
47-47
45-44
5700
5800
5900
6000
TIME(STEPS)

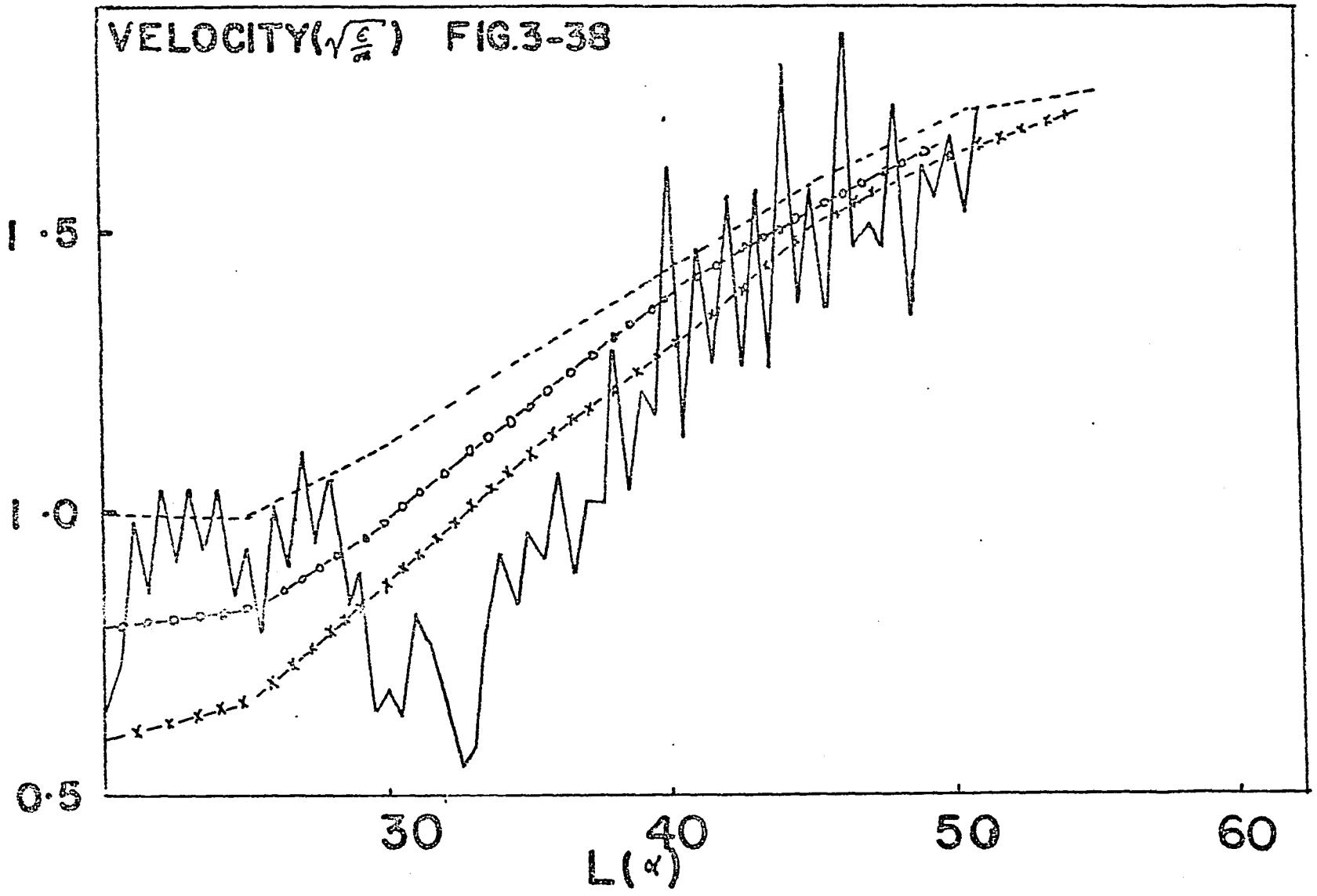
VELOCITY($\sqrt{\frac{\epsilon}{a}}$) FIG.3-38
1·5
1·0
0·5
30
40
50
60
L(α)

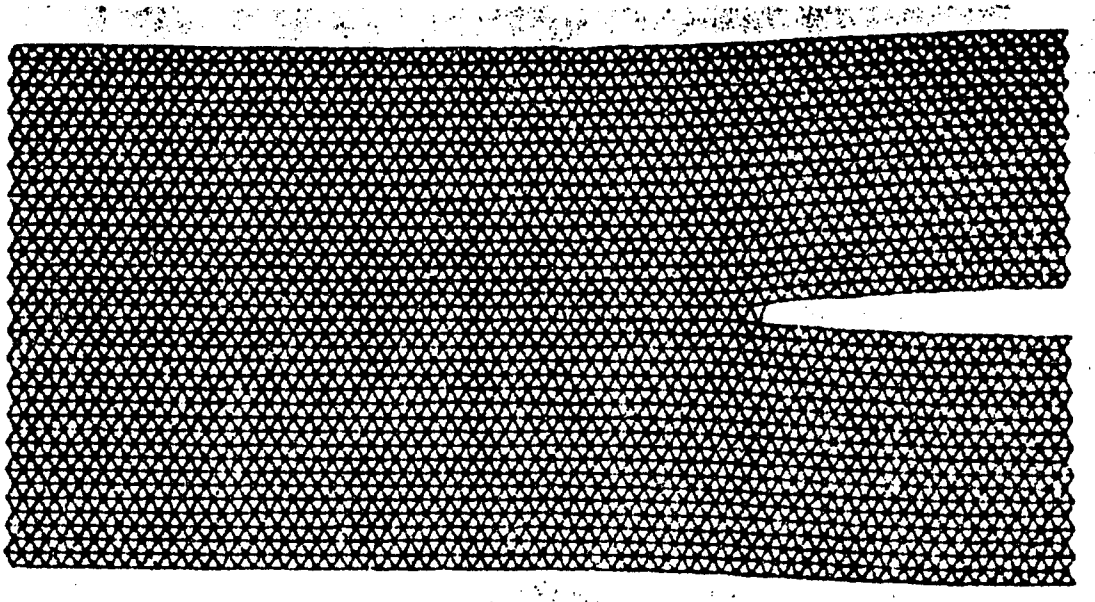

5700

FIG. 3-39

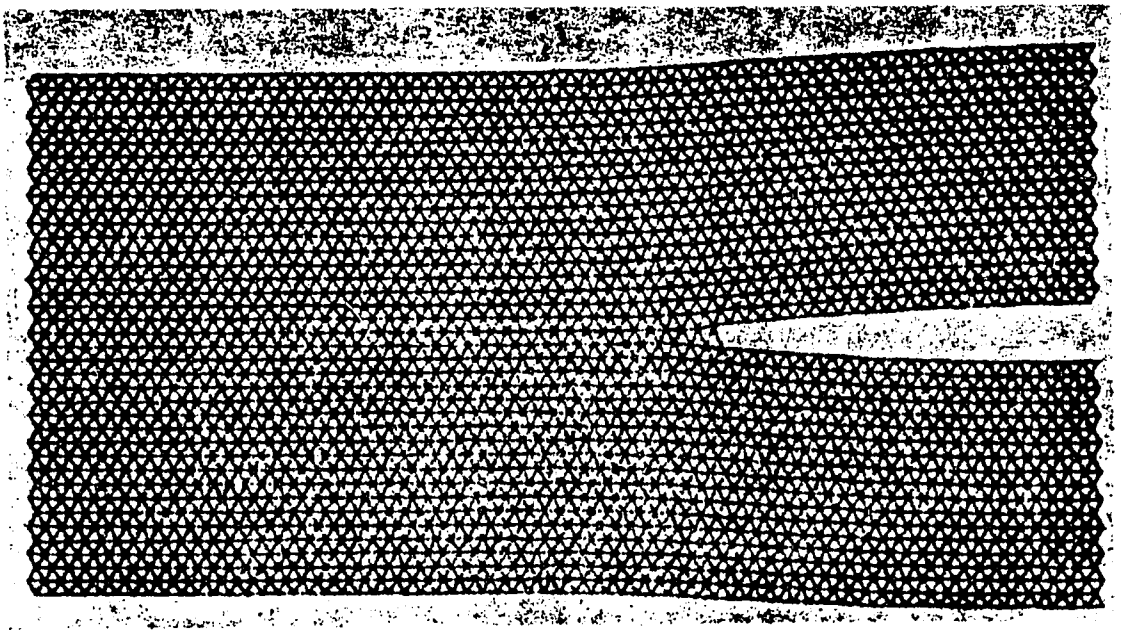

8300

FIG. 3-40

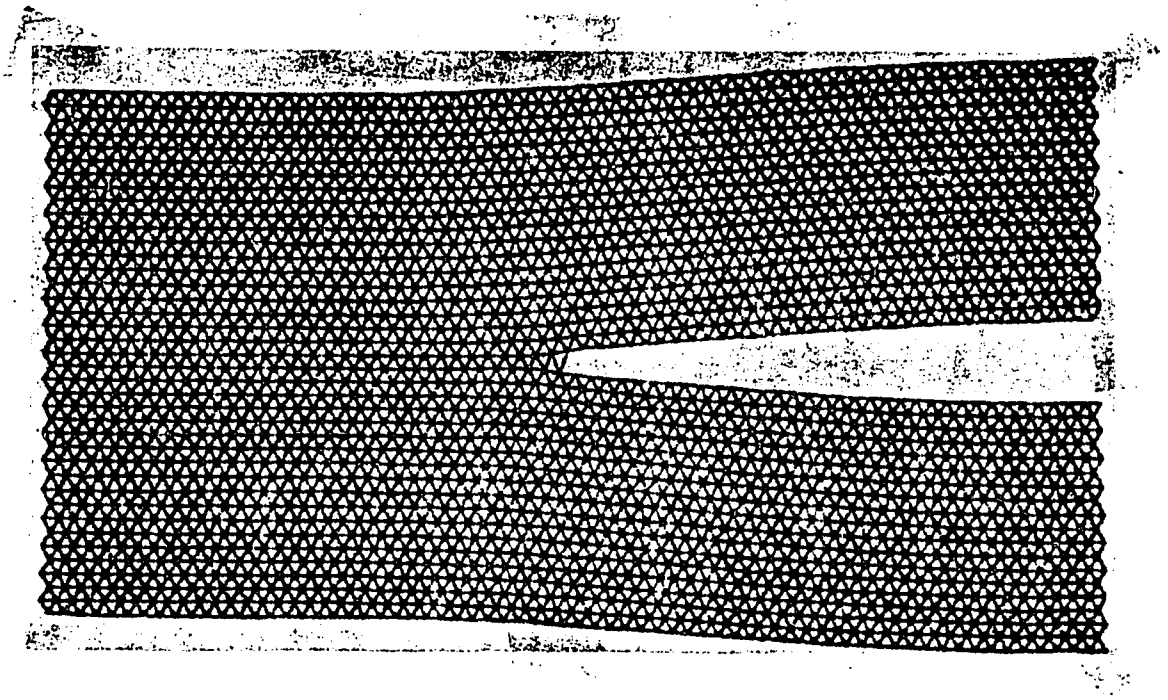

7600

FIG. 3-41

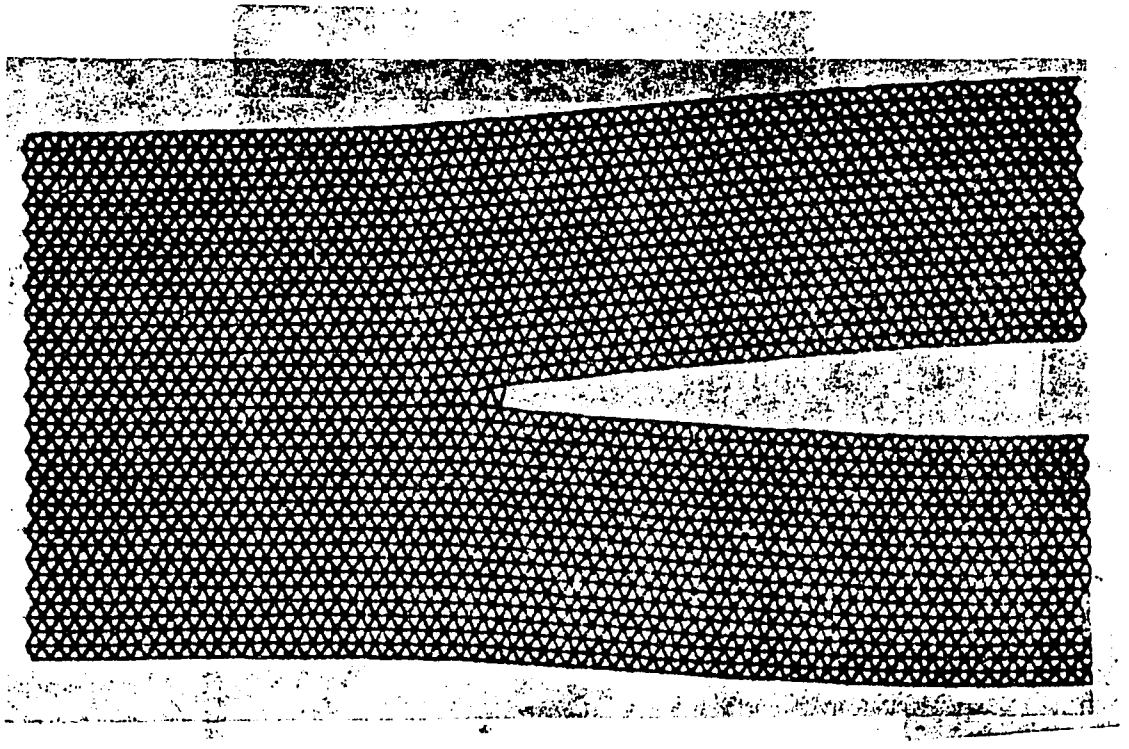

7900

FIG. 3-42

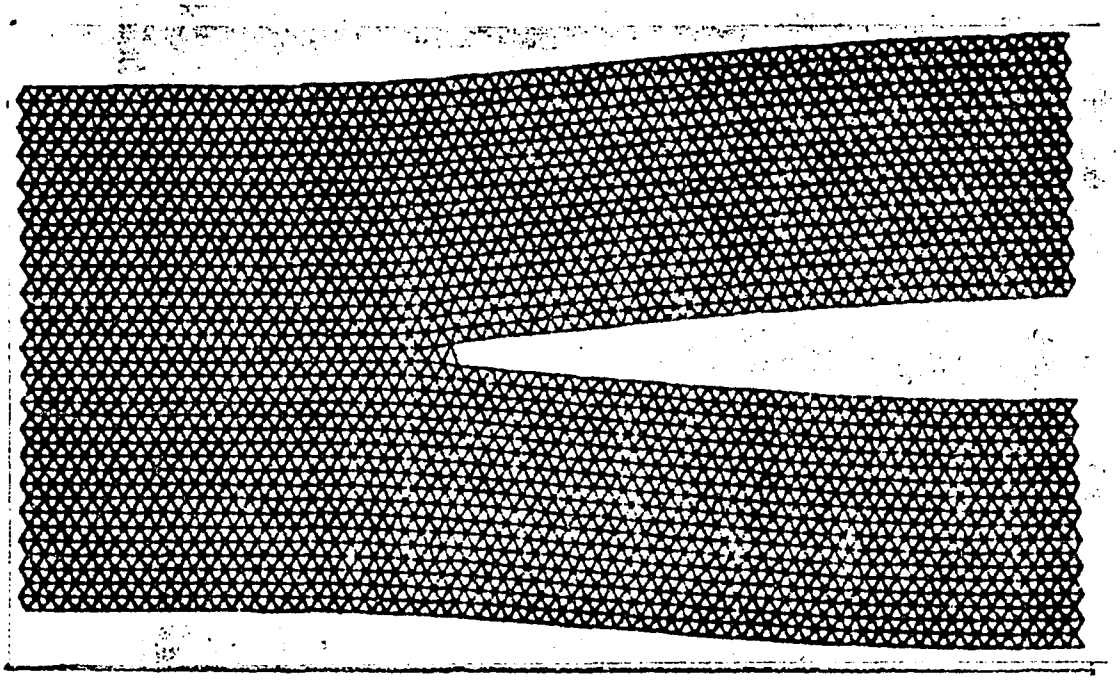

8100

FIG. 3-43

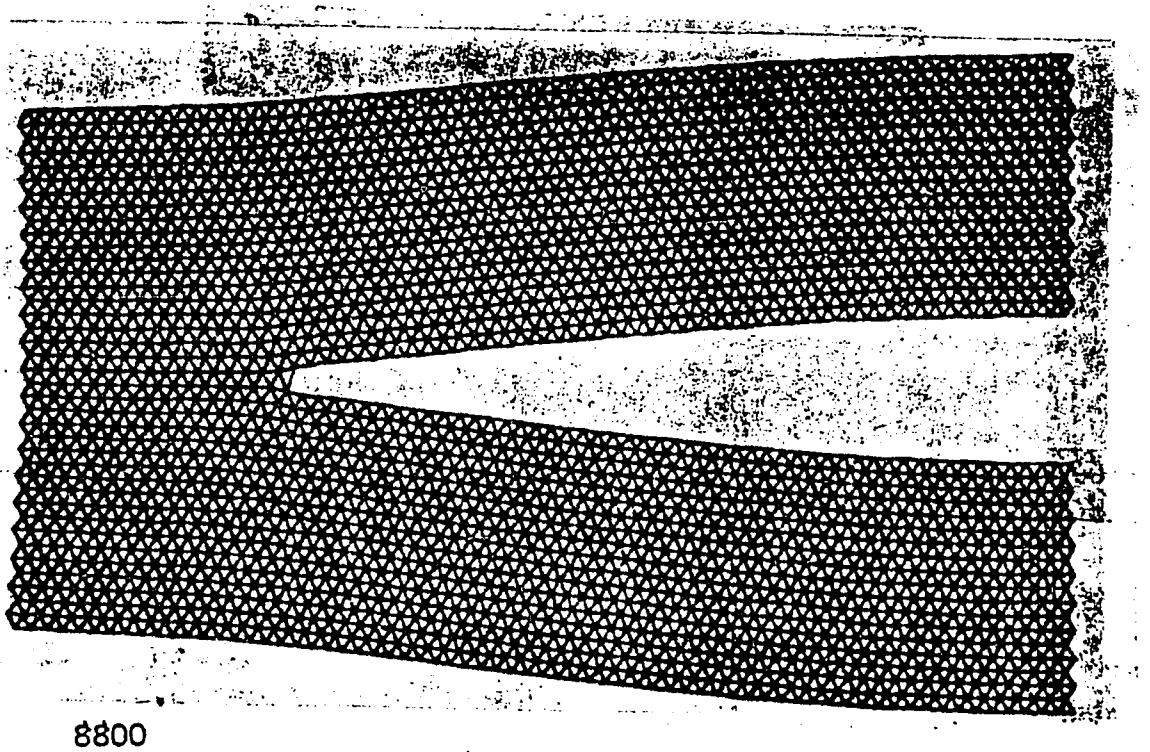

8800

FIG. 3-44

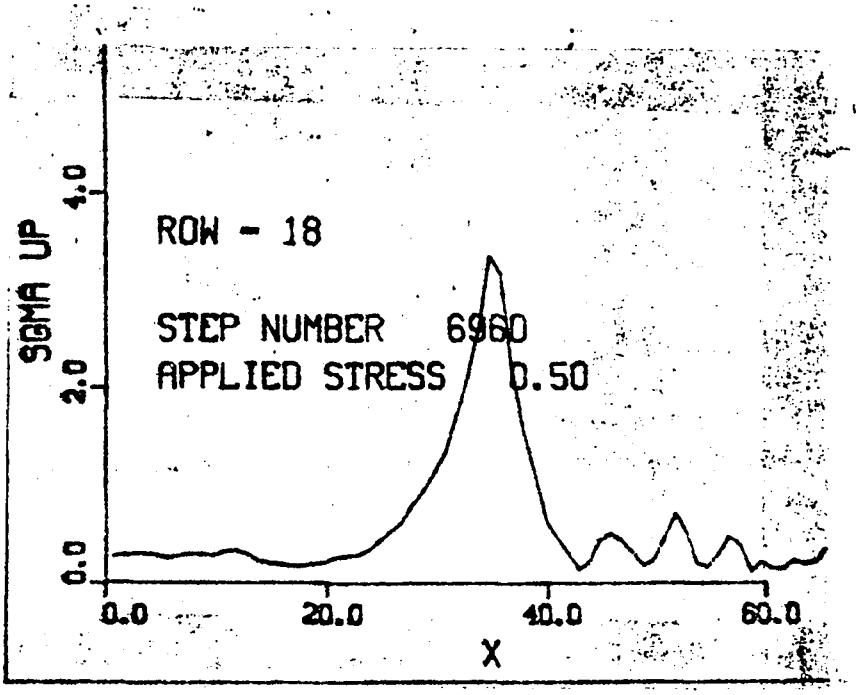

FIG. 3-45

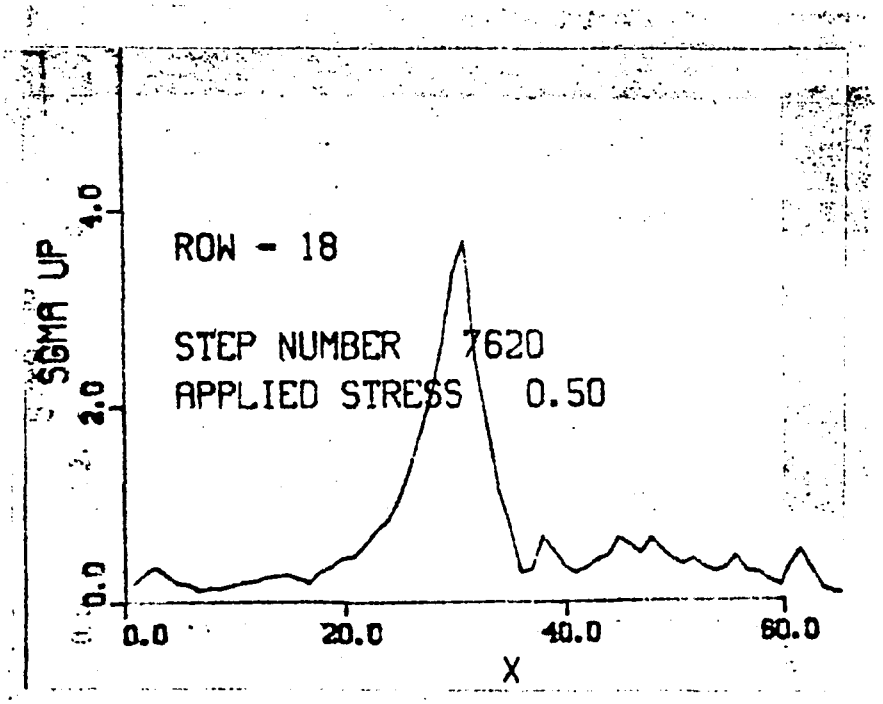

FIG. 3-46

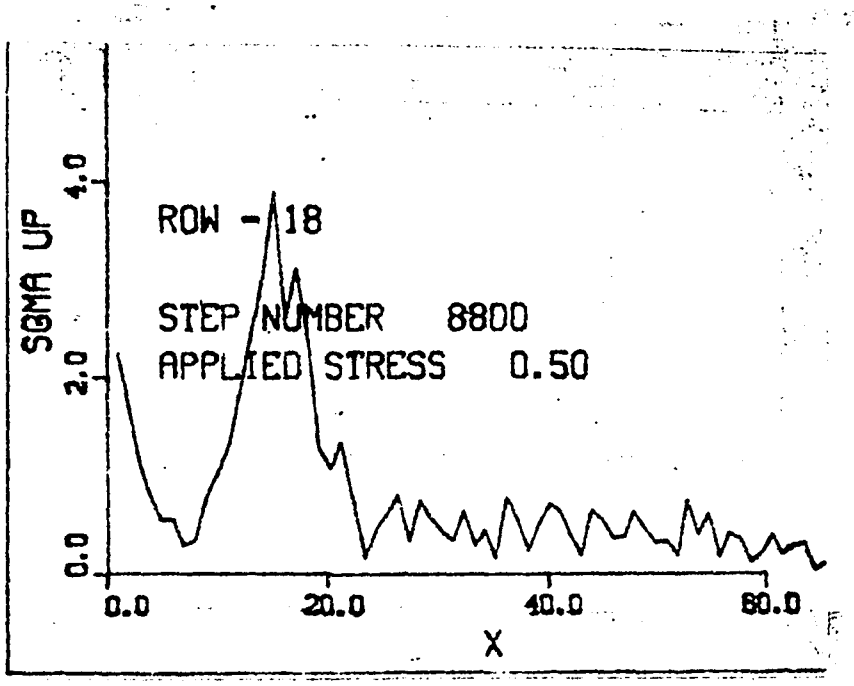

FIG. 3-47

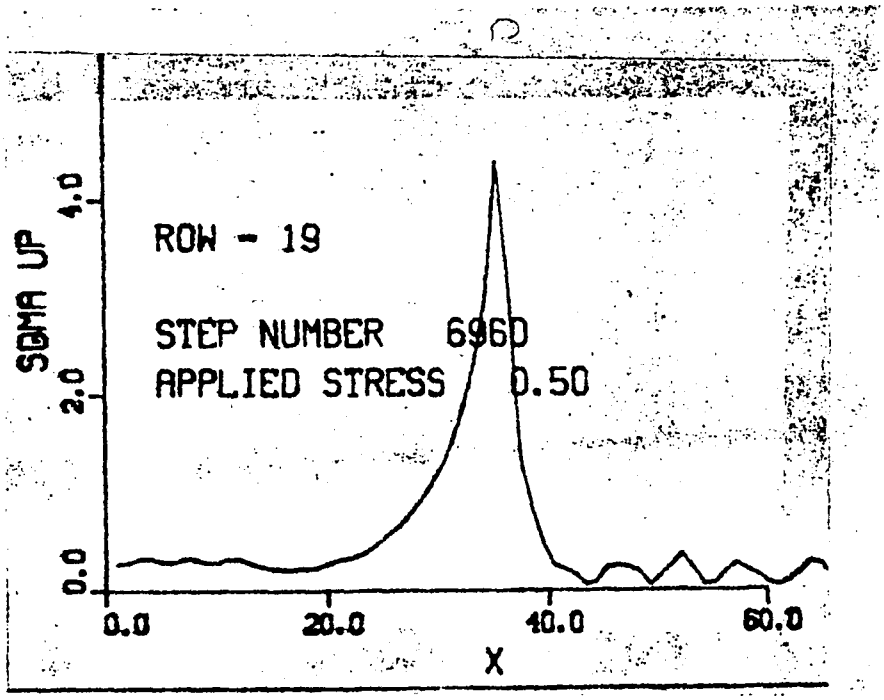

FIG. 3-48

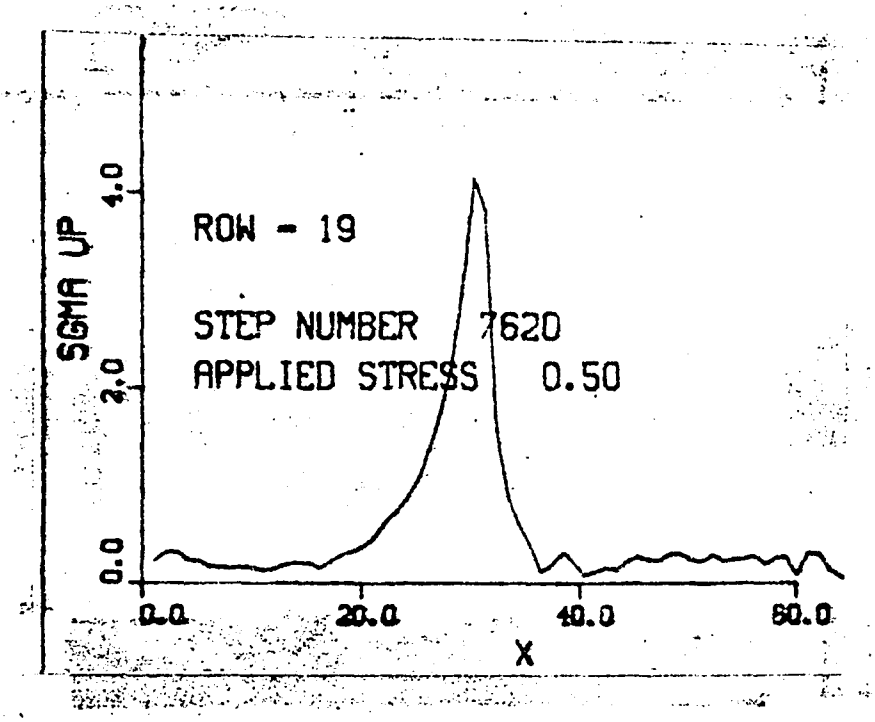

FIG. 3-49

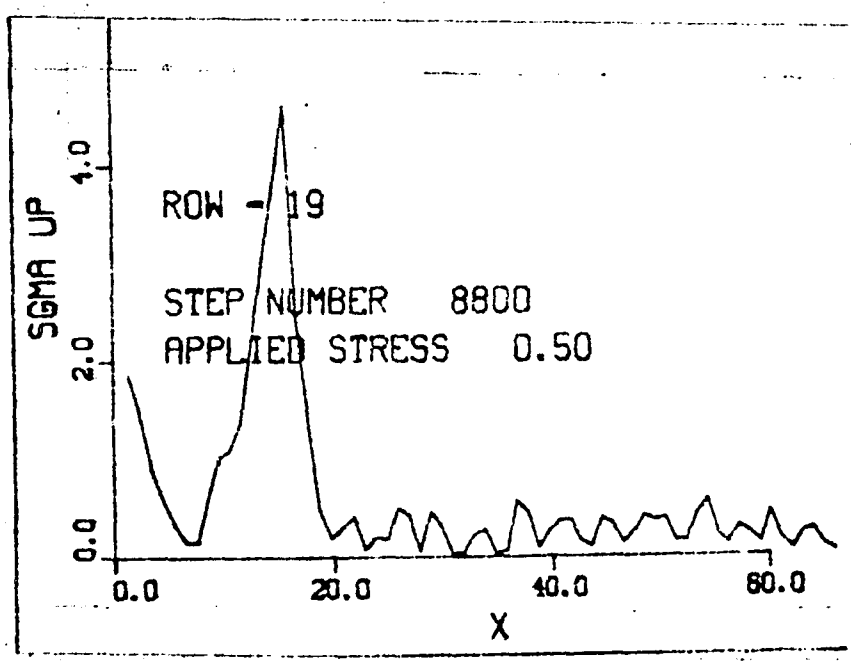

FIG. 3-50

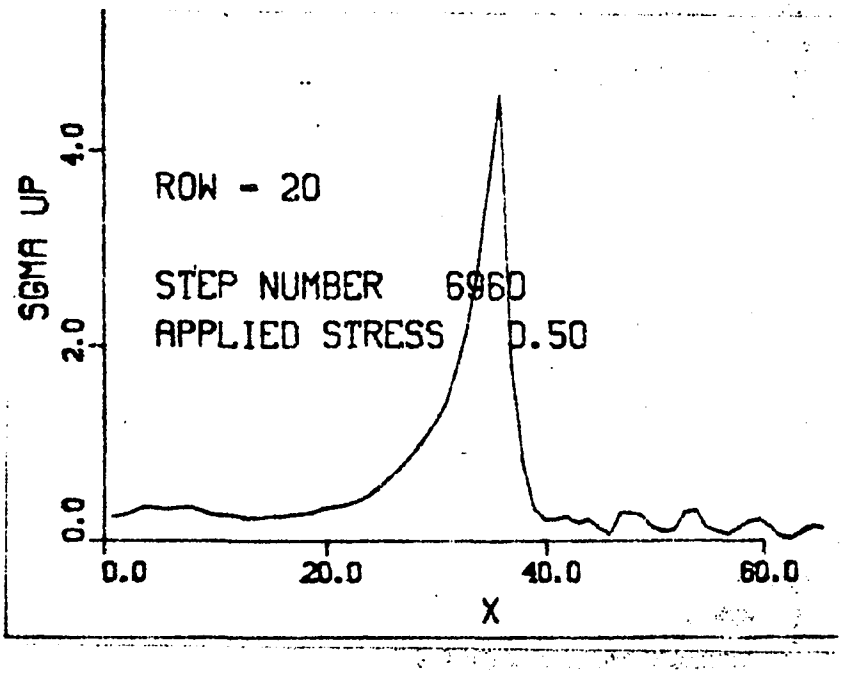

FIG. 3-51

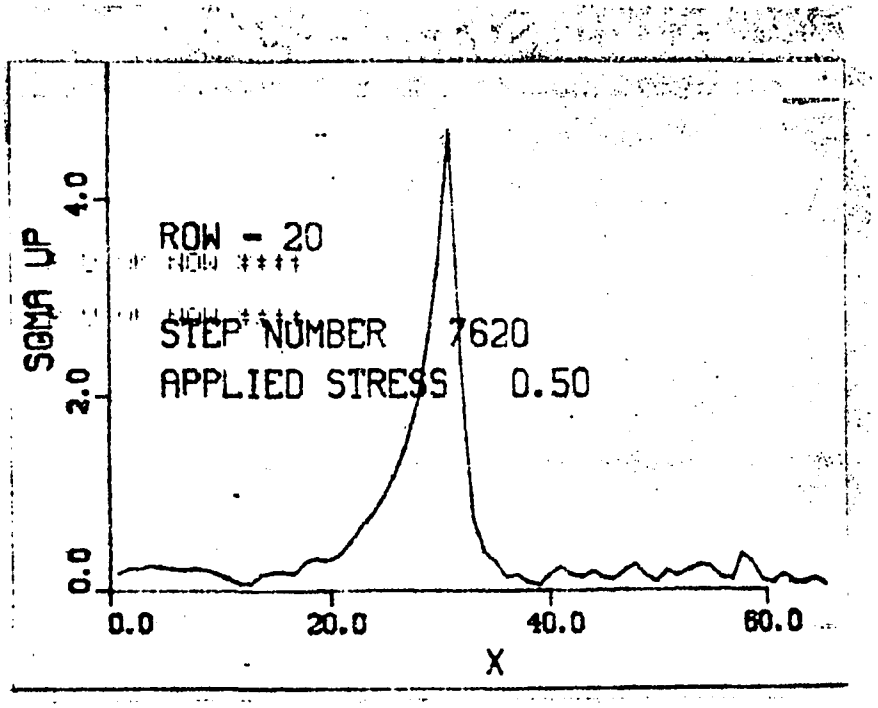

FIG. 3-52

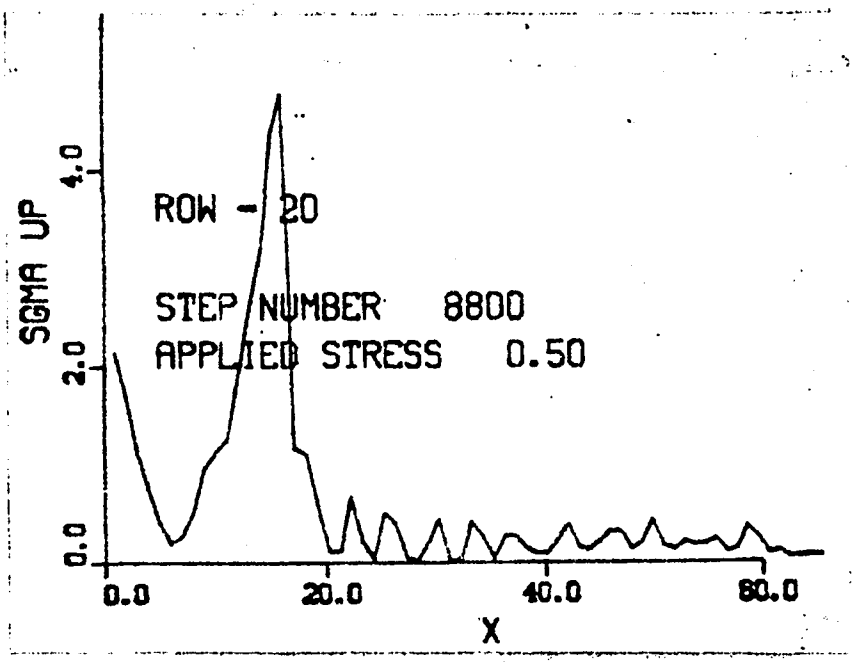

FIG. 3-53

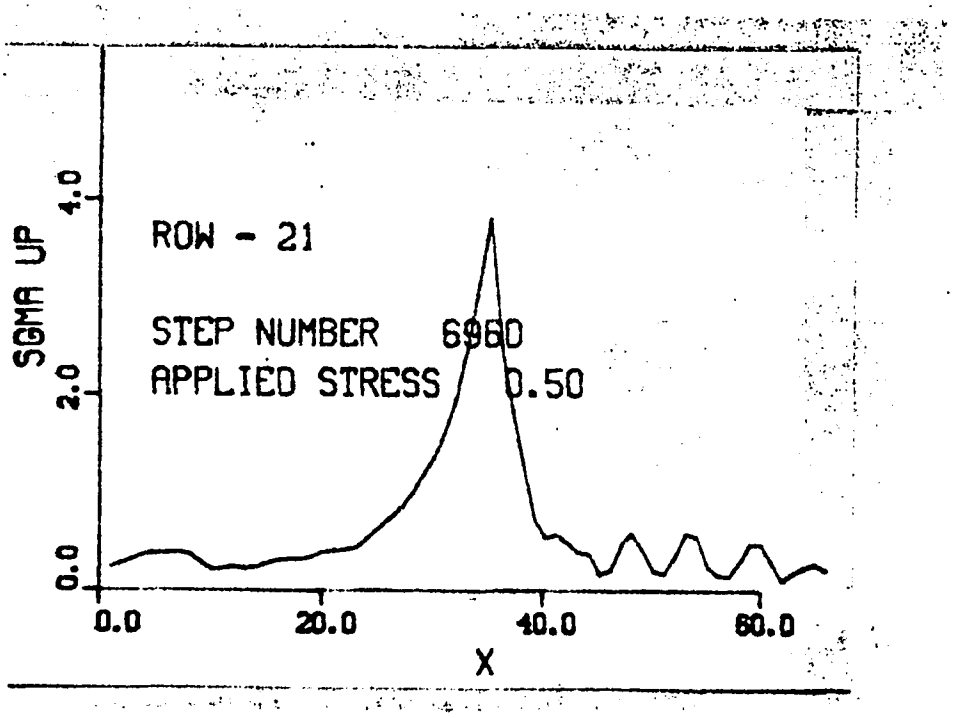

FIG. 3-54

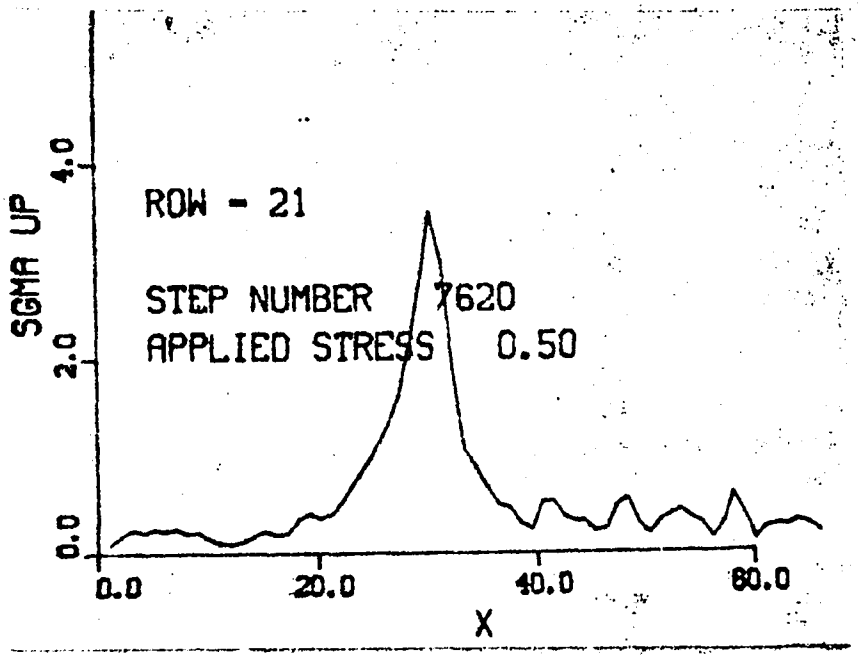

FIG. 3-55

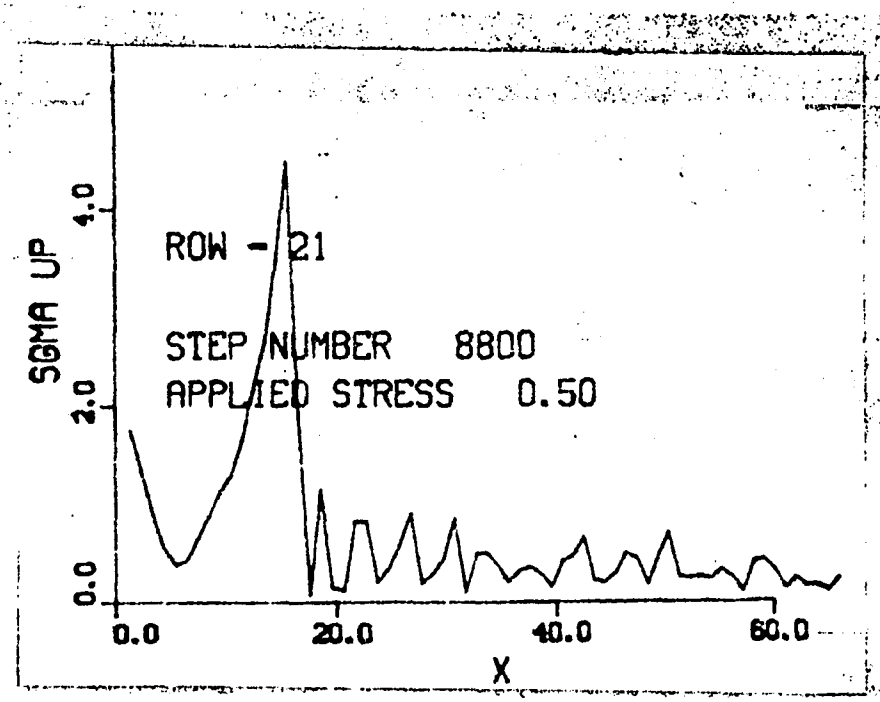

FIG. 3-56

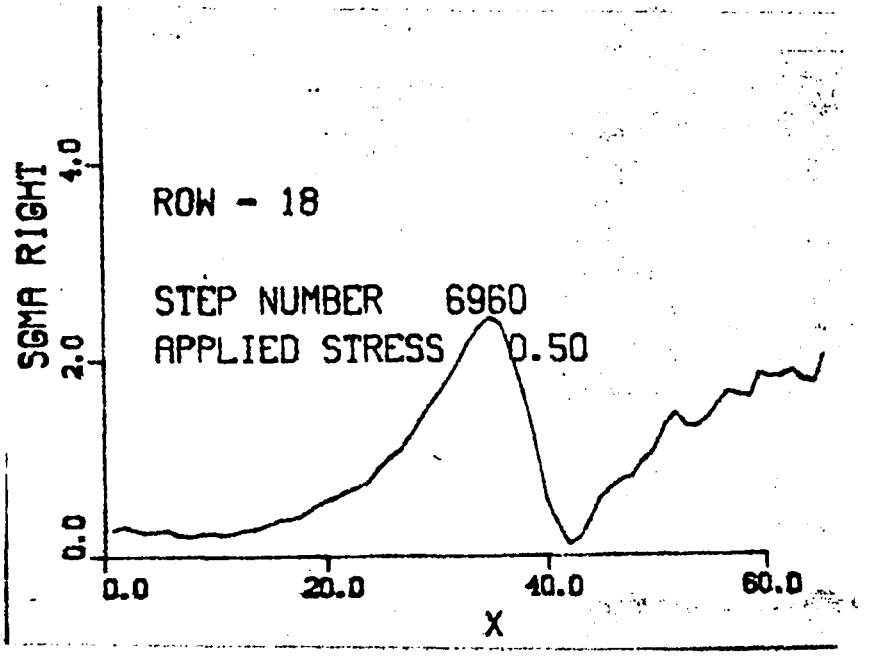

FIG. 3-57

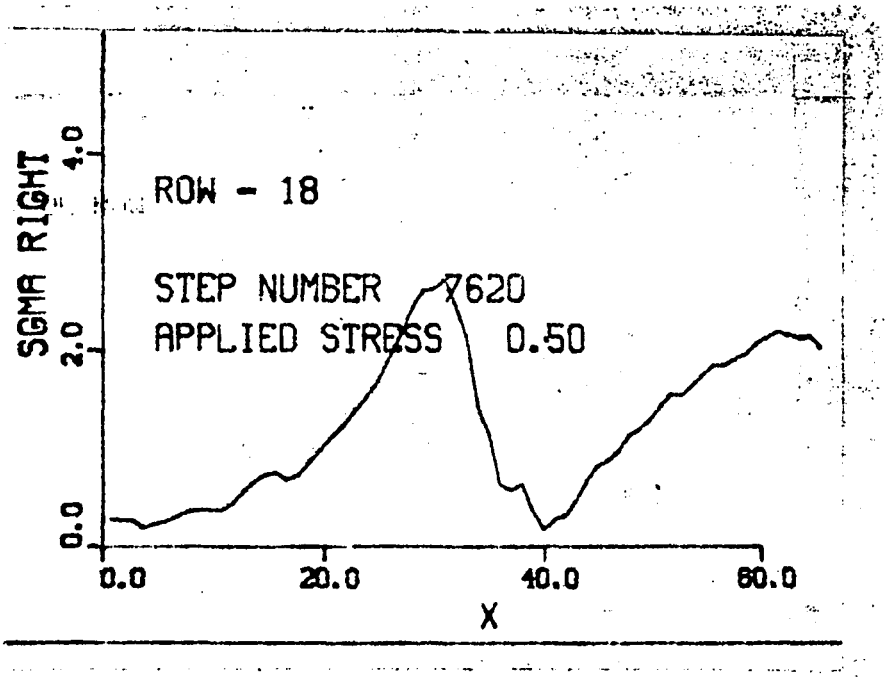

FIG. 3-58

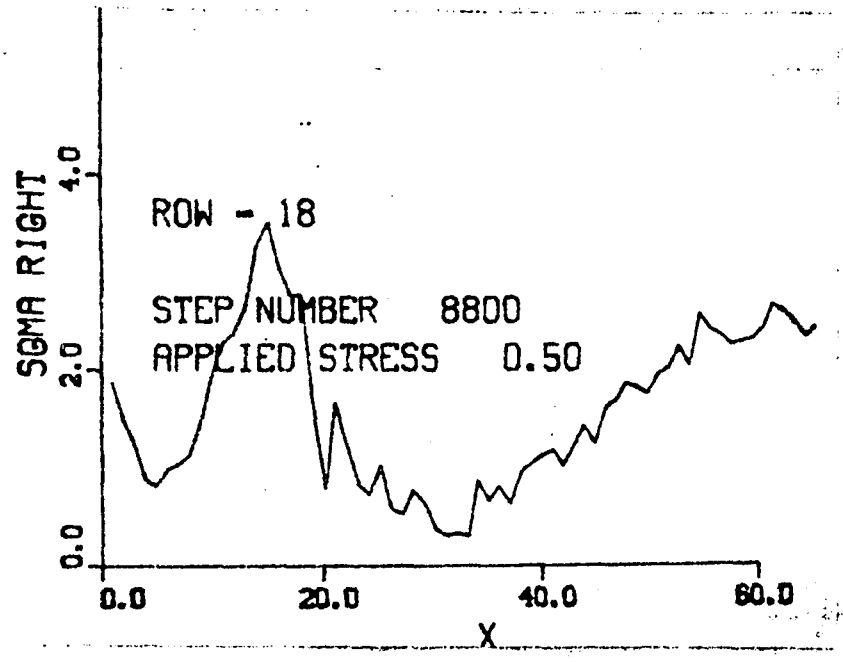

FIG. 3-59

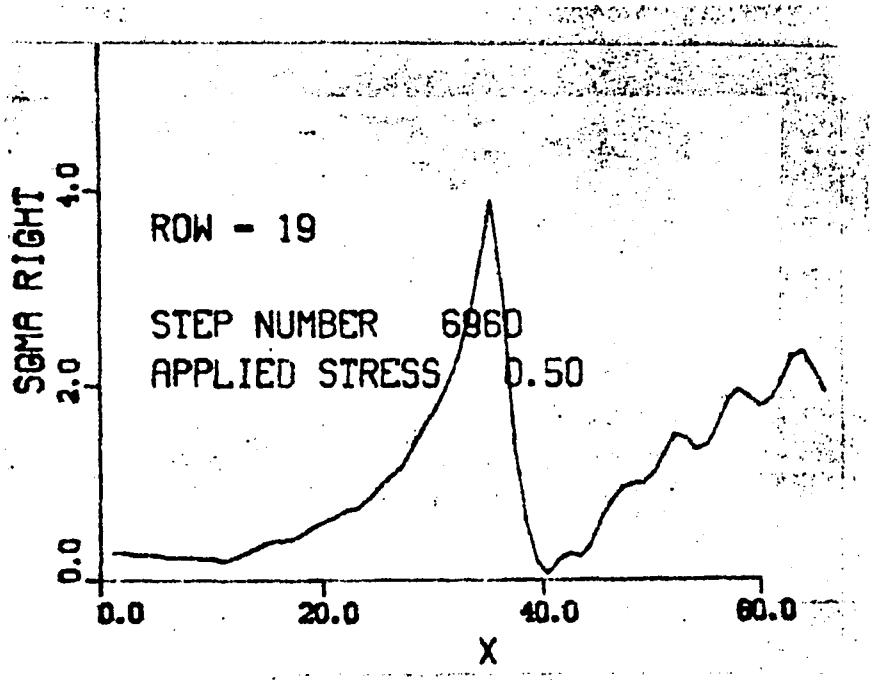

FIG. 3-60

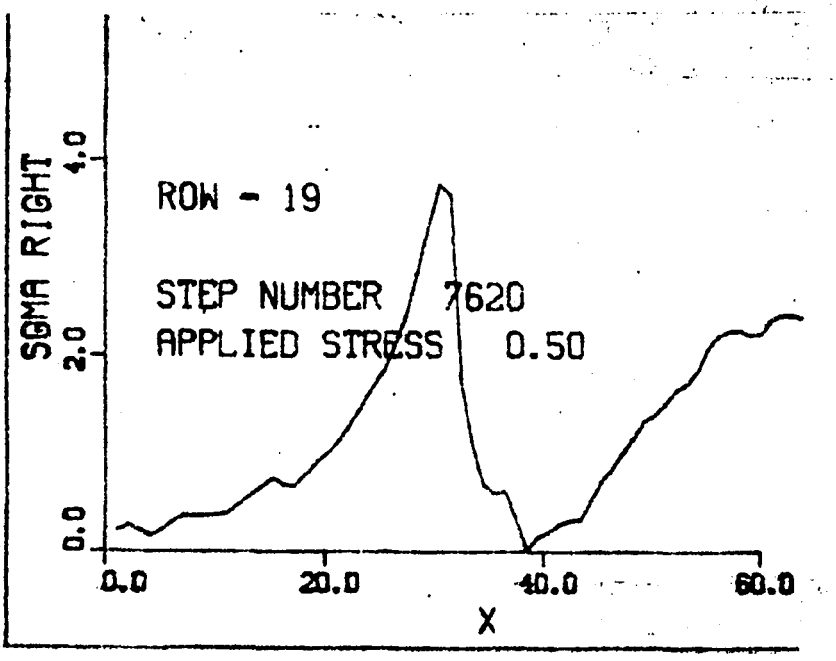

FIG. 3-61

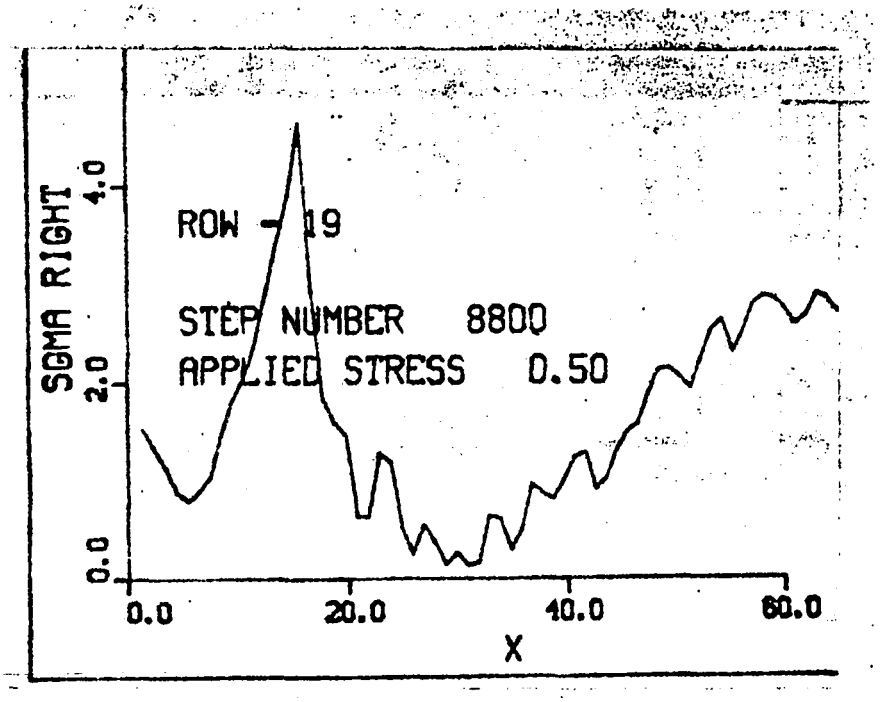

FIG. 3-62

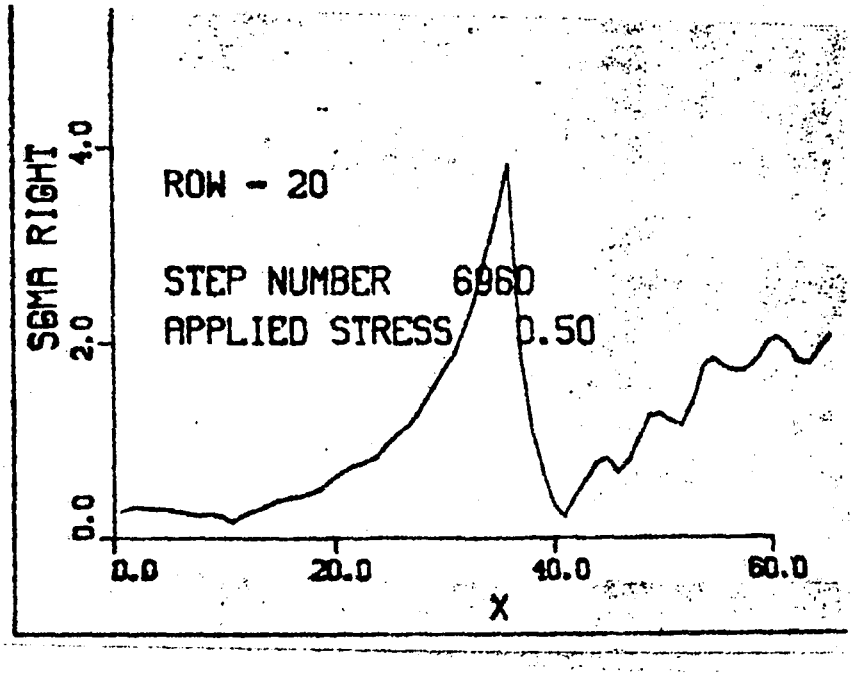

FIG. 3-63

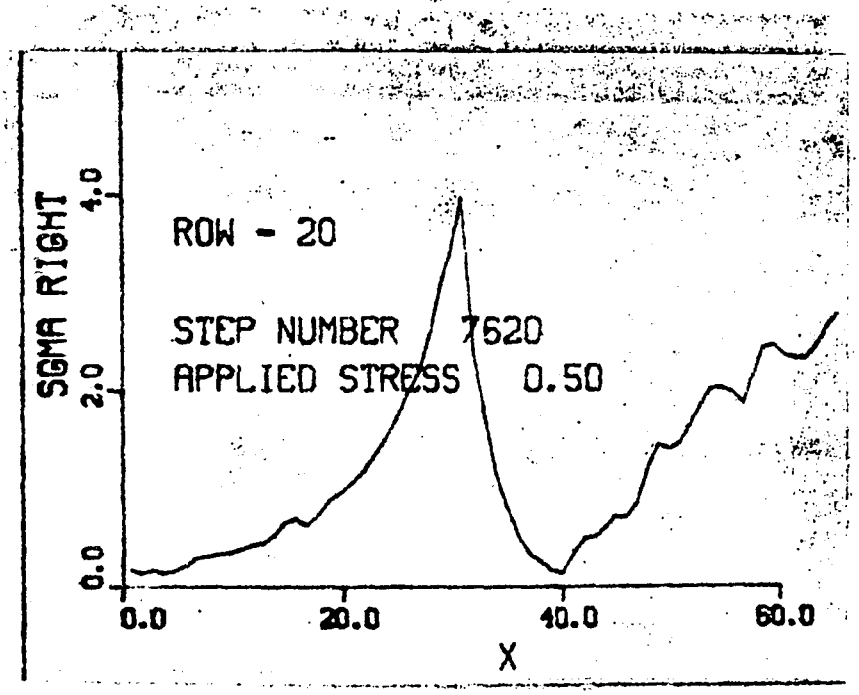

FIG. 3-64

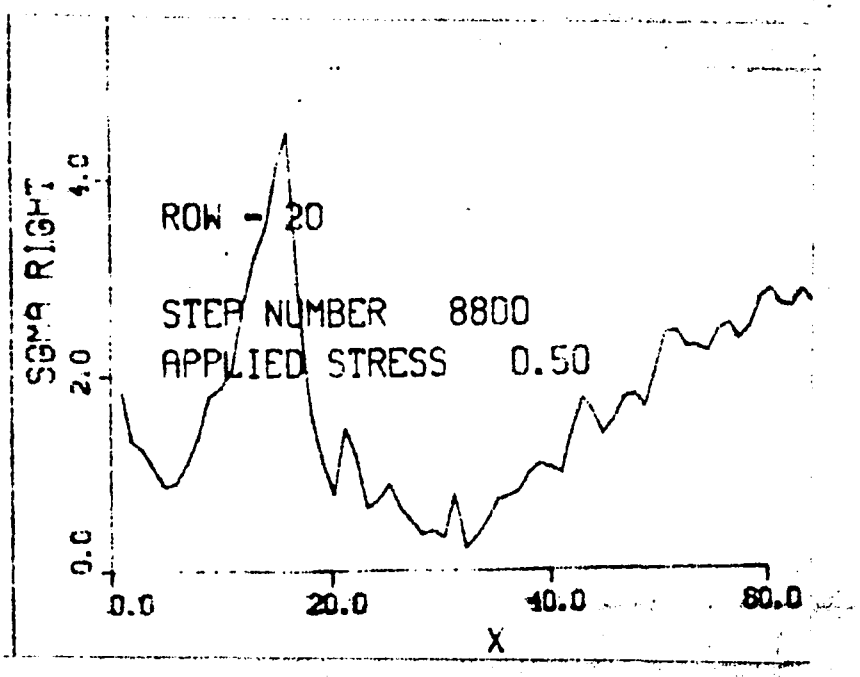

FIG. 3-65

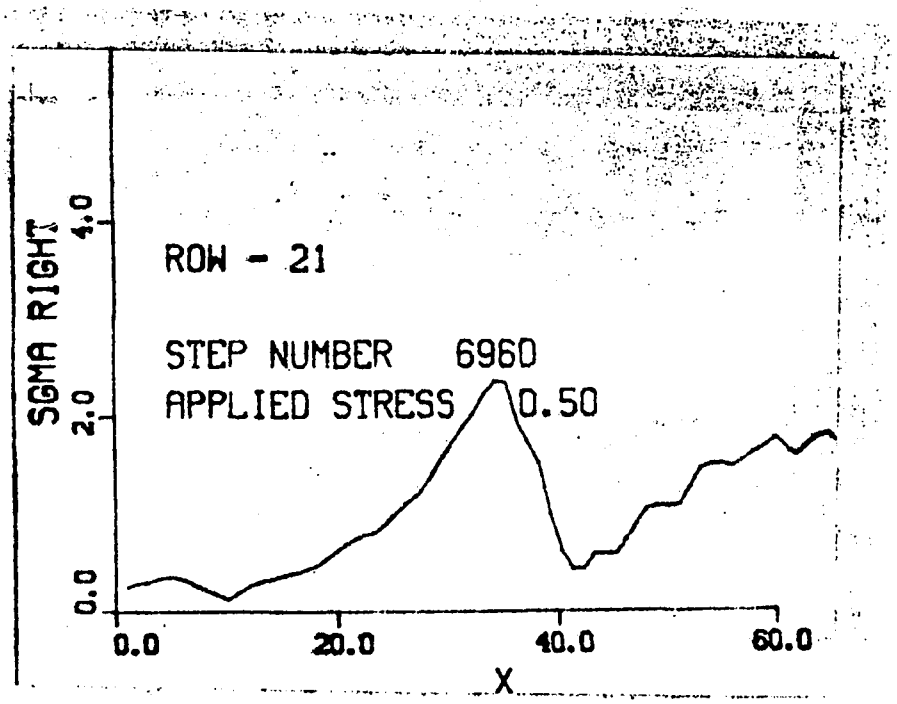

FIG. 3-66

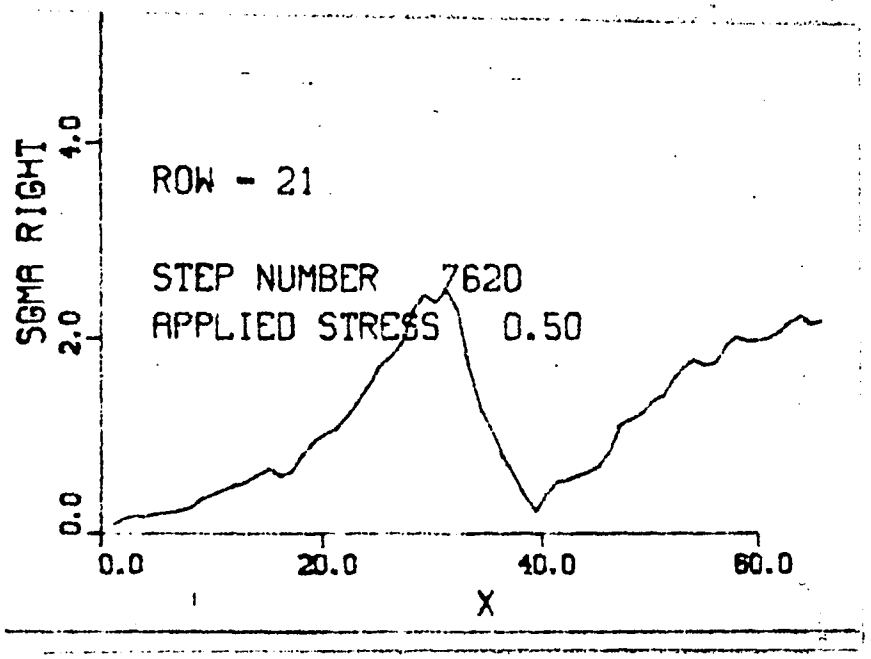

FIG. 3-67

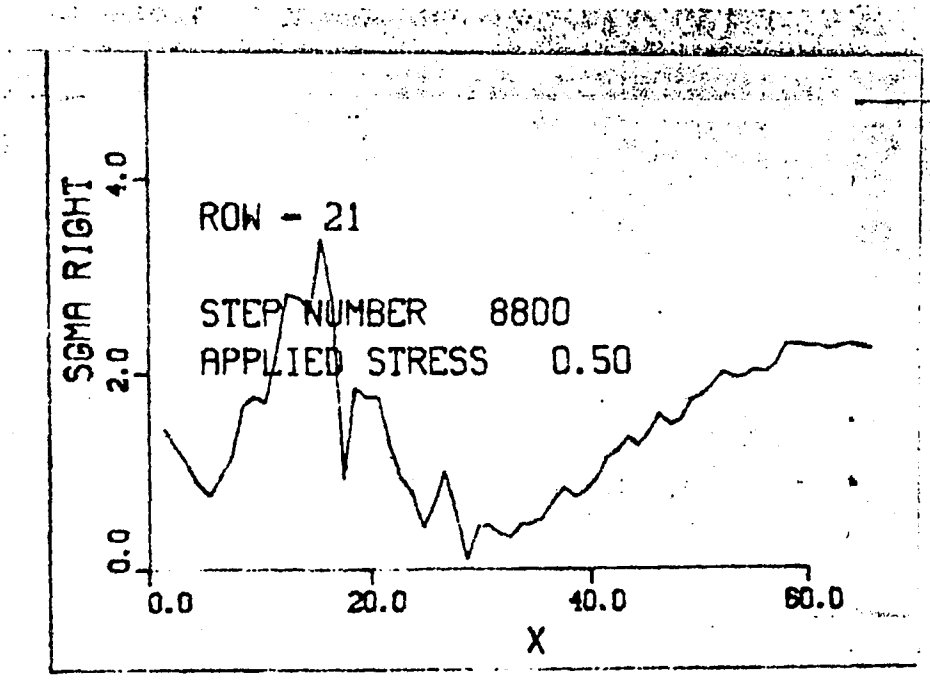

FIG. 3-68

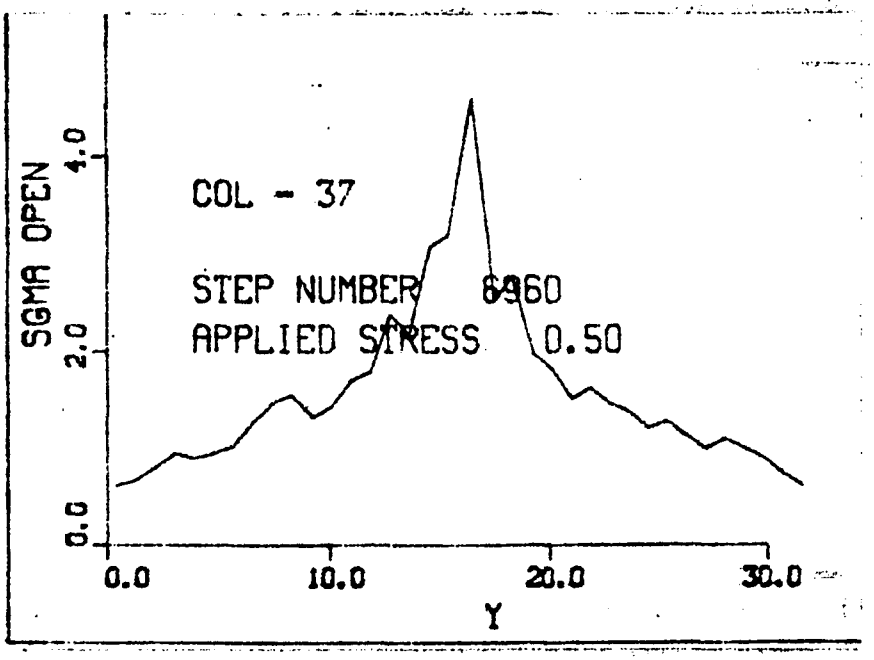

FIG. 3-69

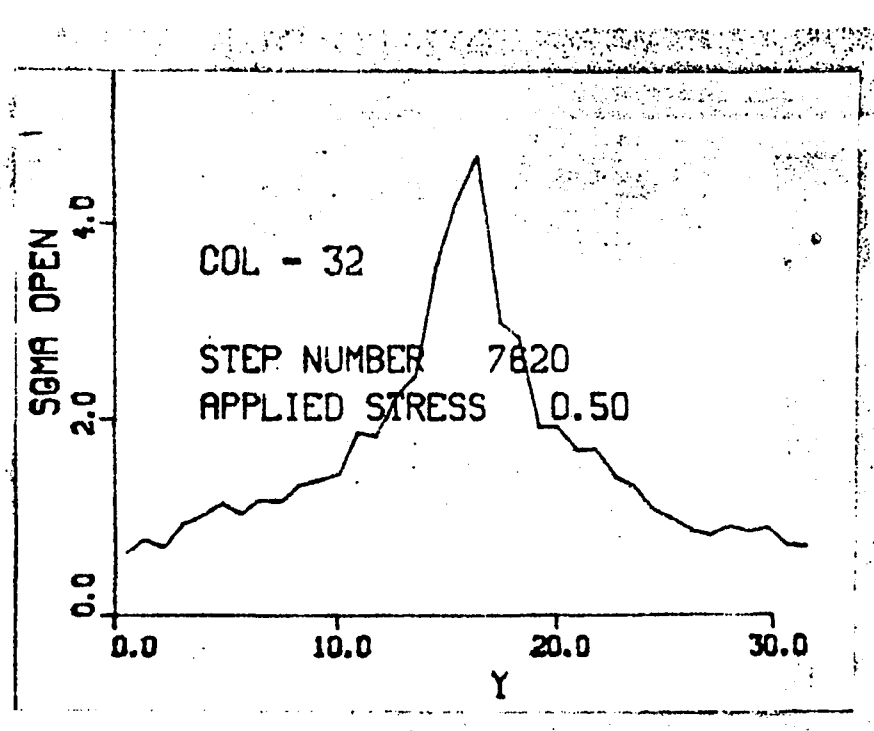

FIG. 3-70

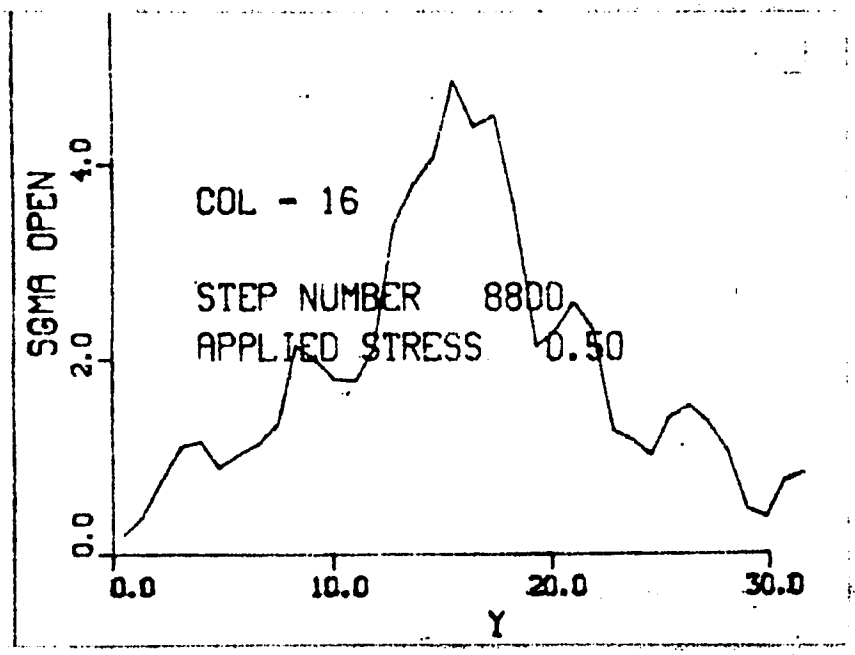

FIG. 3-71

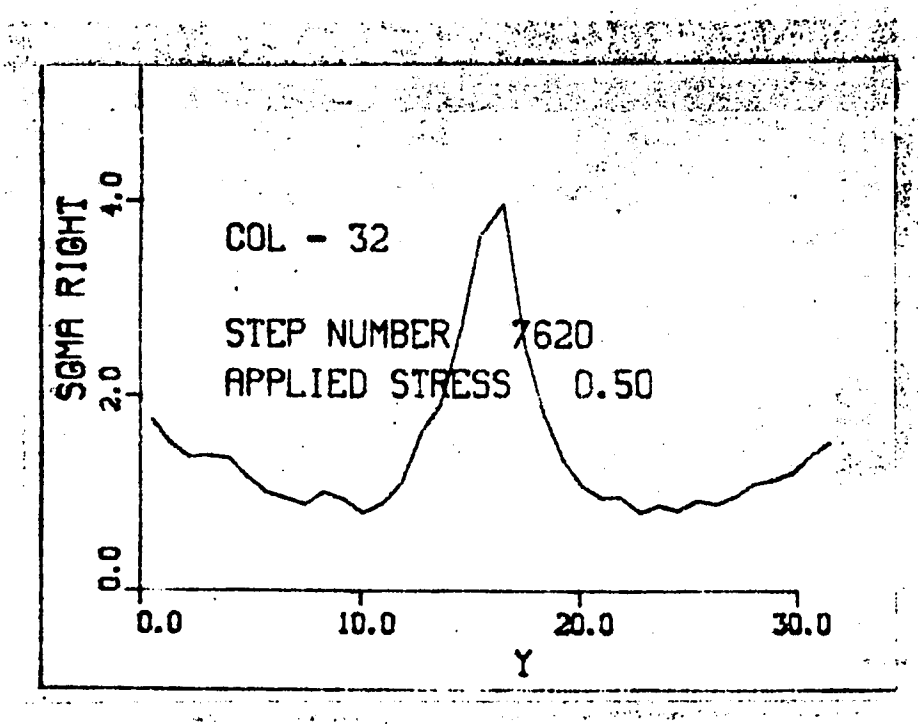

FIG. 3-72

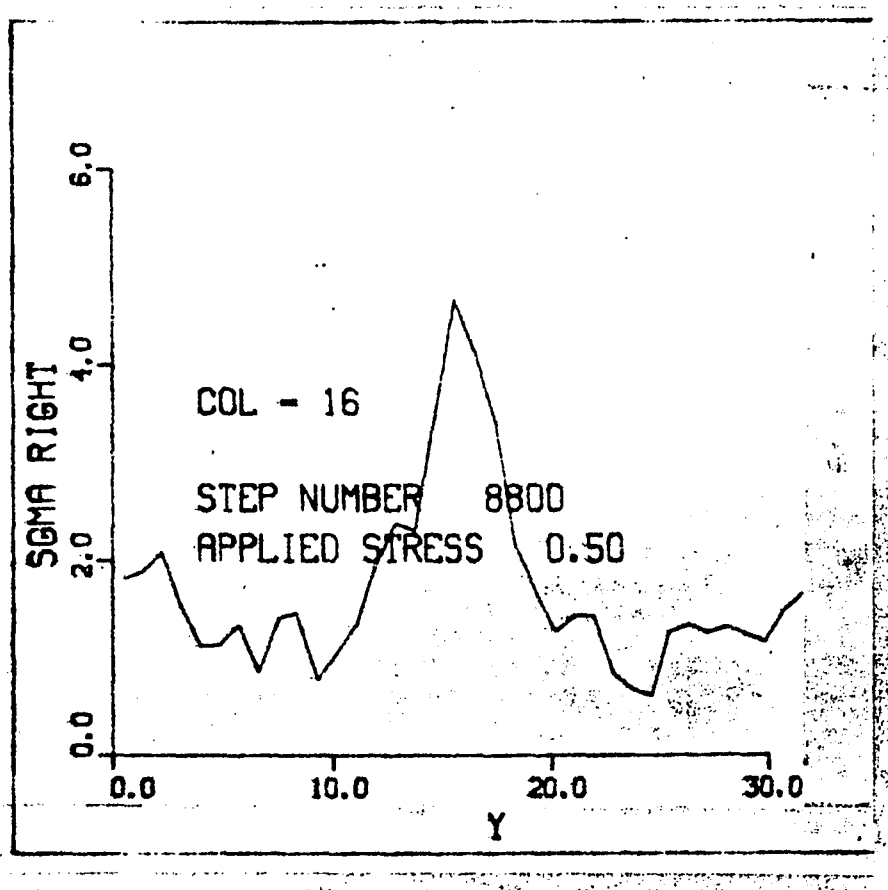
SGMA RIGHT
6.0
4.0
2.0
0.0
COL - 16
STEP NUMBER 8800
APPLIED STRESS 0.50
0.0
10.0
20.0
30.0
Y

FIG. 3-73

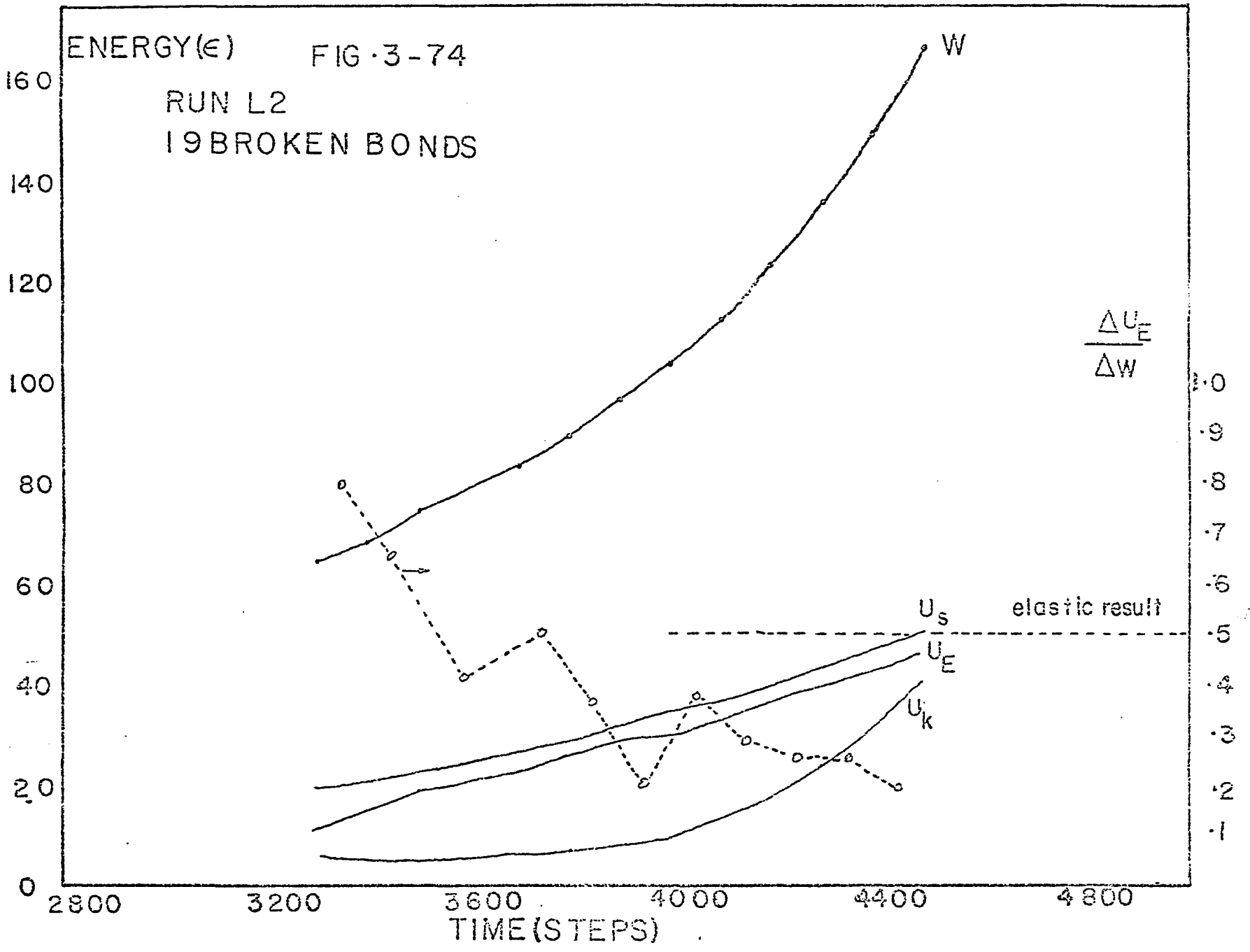
ENERGY(∈)
FIG·3-74
RUN L2
19 BROKEN BONDS
W
$\frac{\Delta U_E}{\Delta W}$
U_s
elastic result
U_E
U_k
160
140
120
100
80
60
40
20
0
2800
3200
3600
4000
4400
4800
TIME(STEPS)
1·0
·9
·8
·7
·6
·5
·4
·3
·2
·1

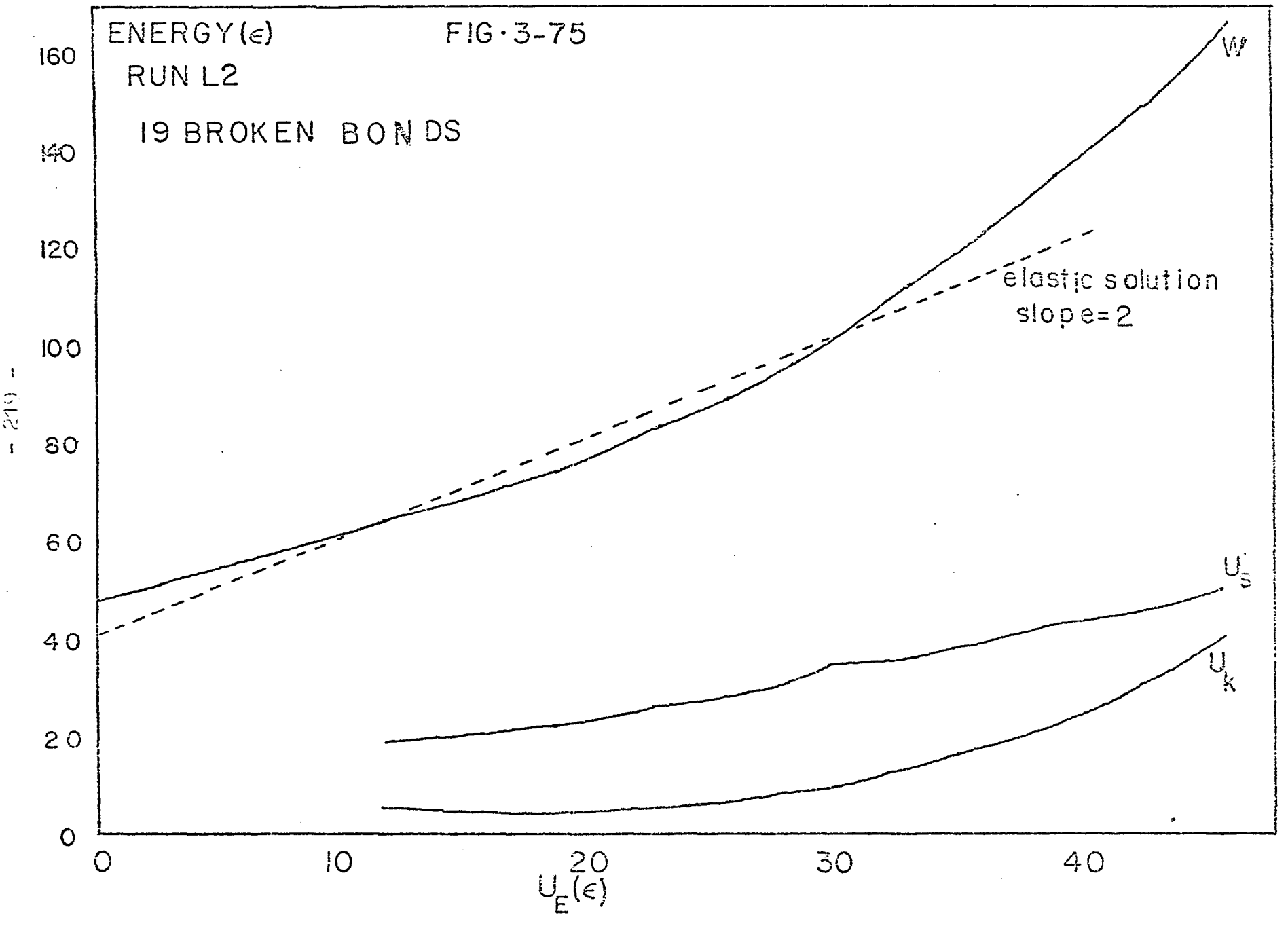
ENERGY(ϵ)
FIG·3-75
RUN L2
19 BROKEN BONDS
160
140
120
100
80
60
40
20
0
0
10
20
30
40
$U_E(\epsilon)$
W
elastic solution
slope=2
U_s
U_k

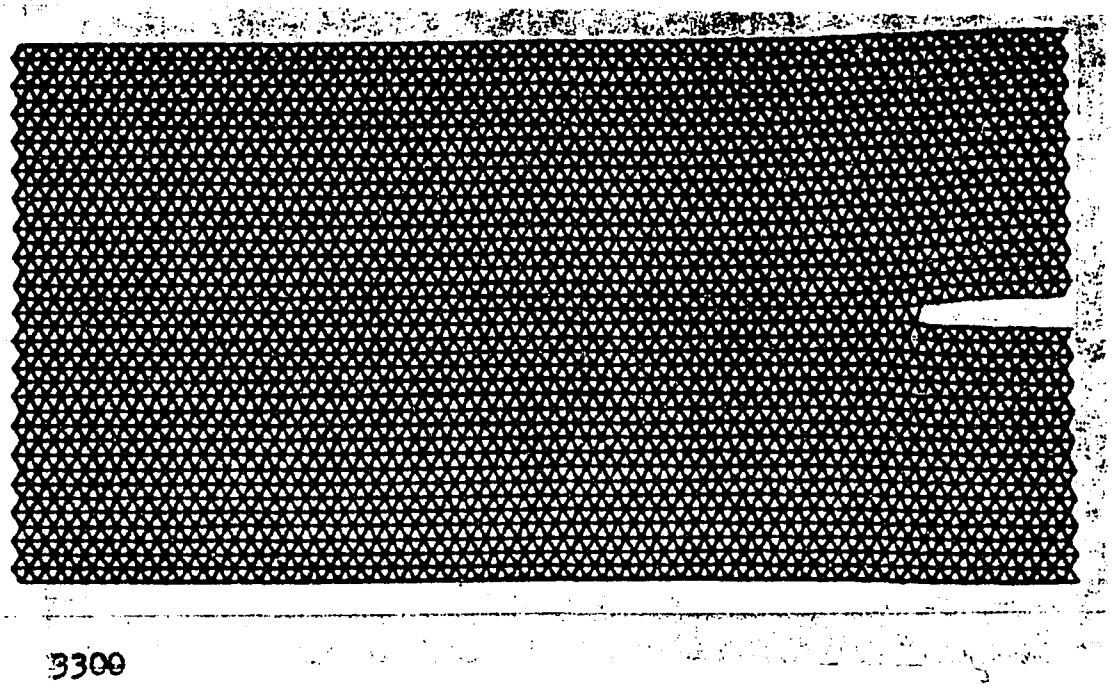

3300

FIG. 3-76

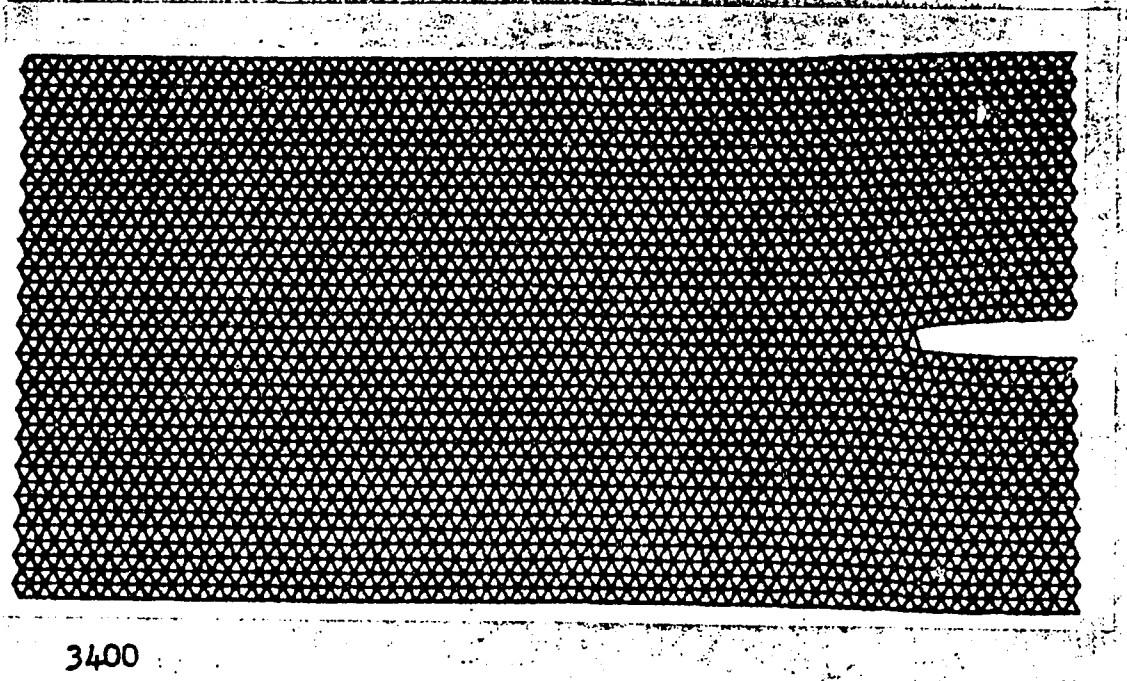

3400

FIG. 3-77

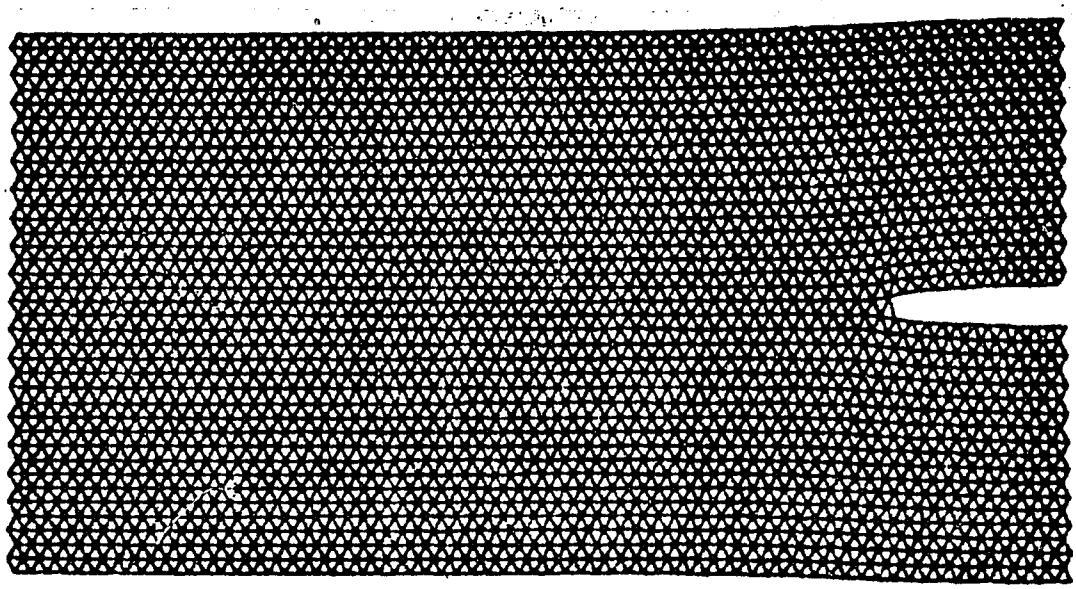

3500

FIG. 3-78

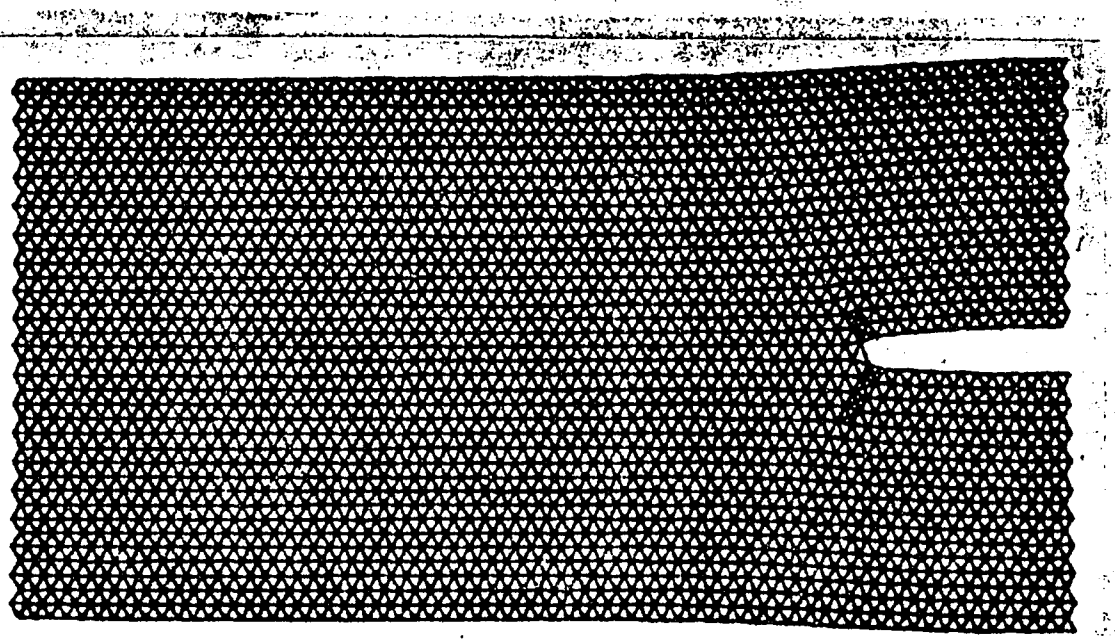

3700

FIG. 3-79

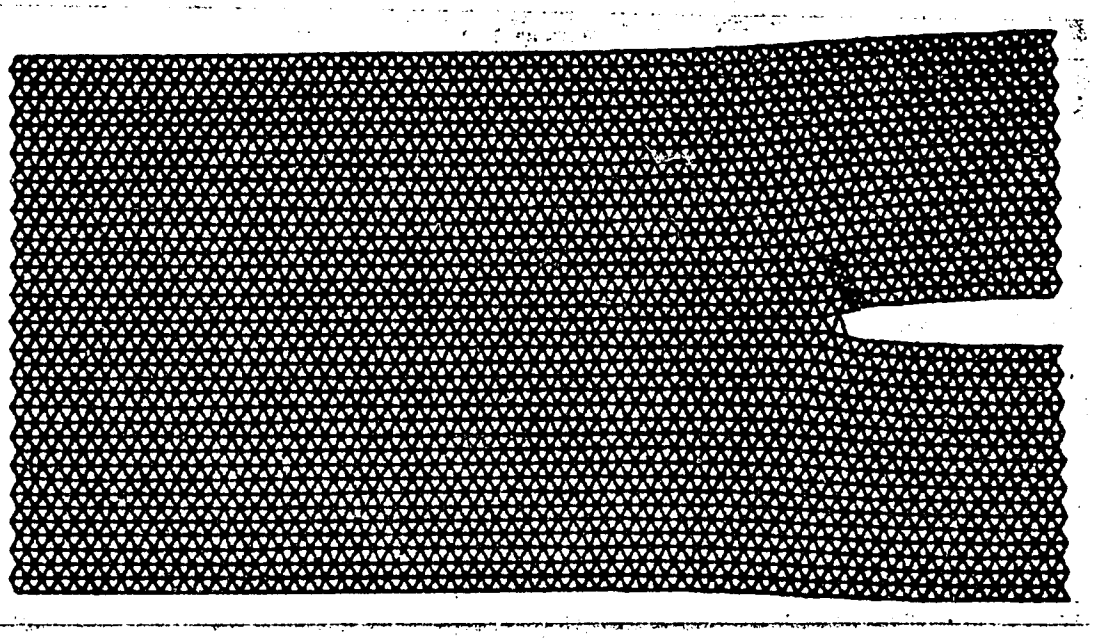

3800

FIG. 3-80

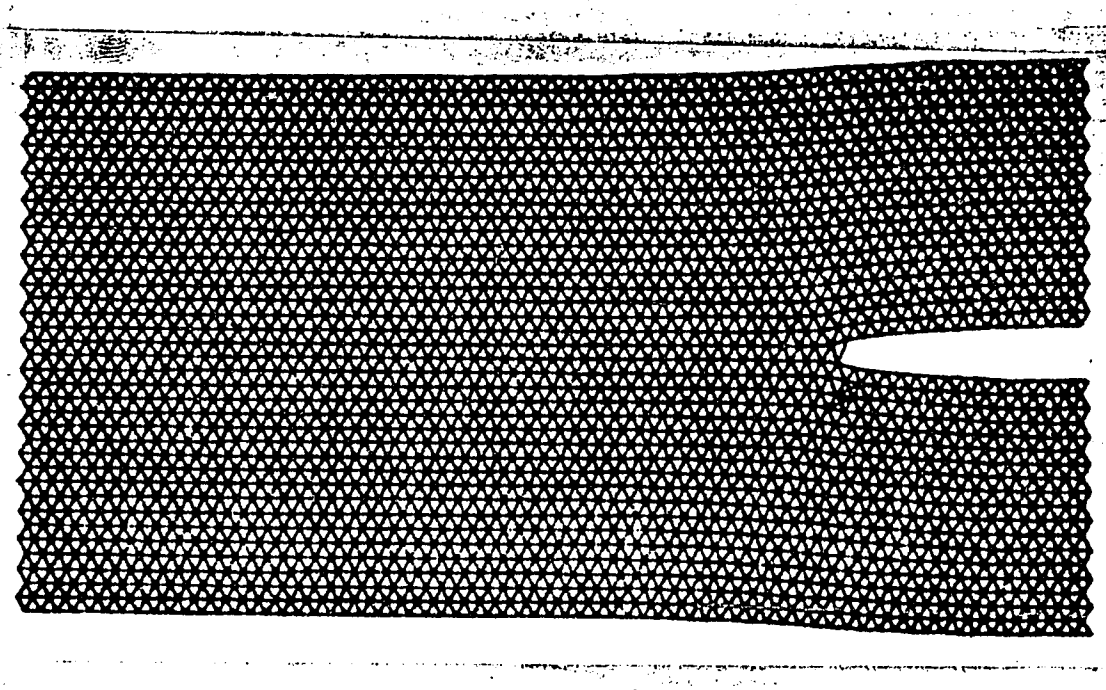

3900

FIG. 3-81

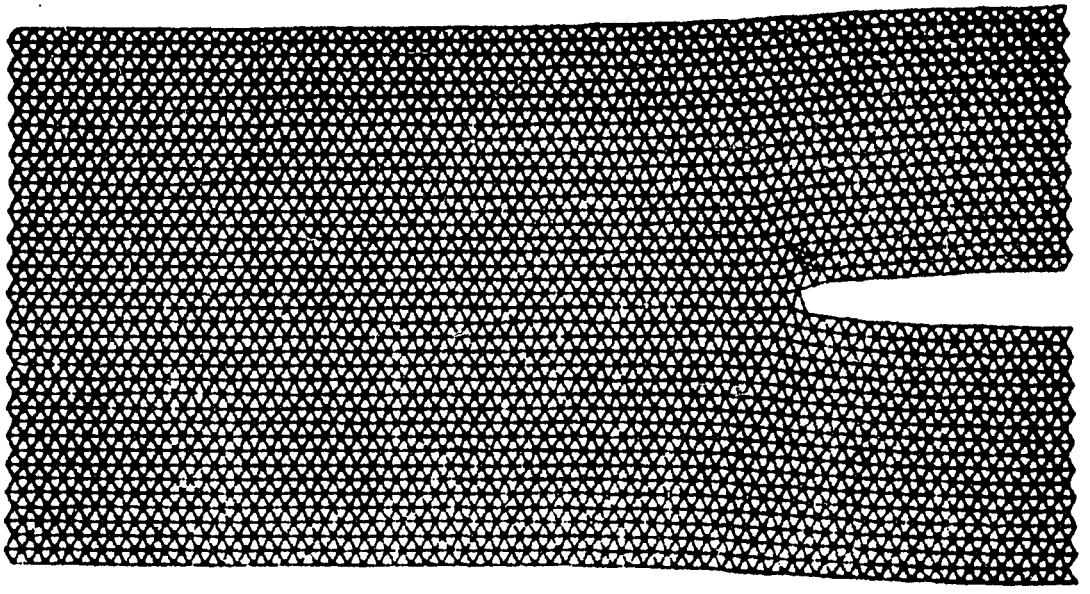

4000

FIG. 3-82

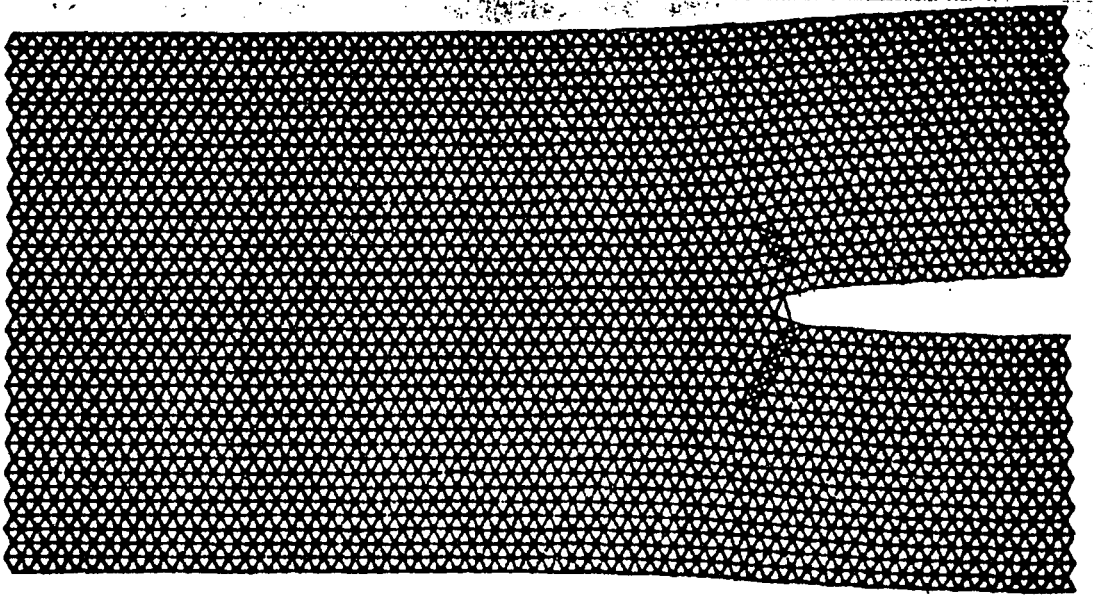

4100

FIG. 3-83

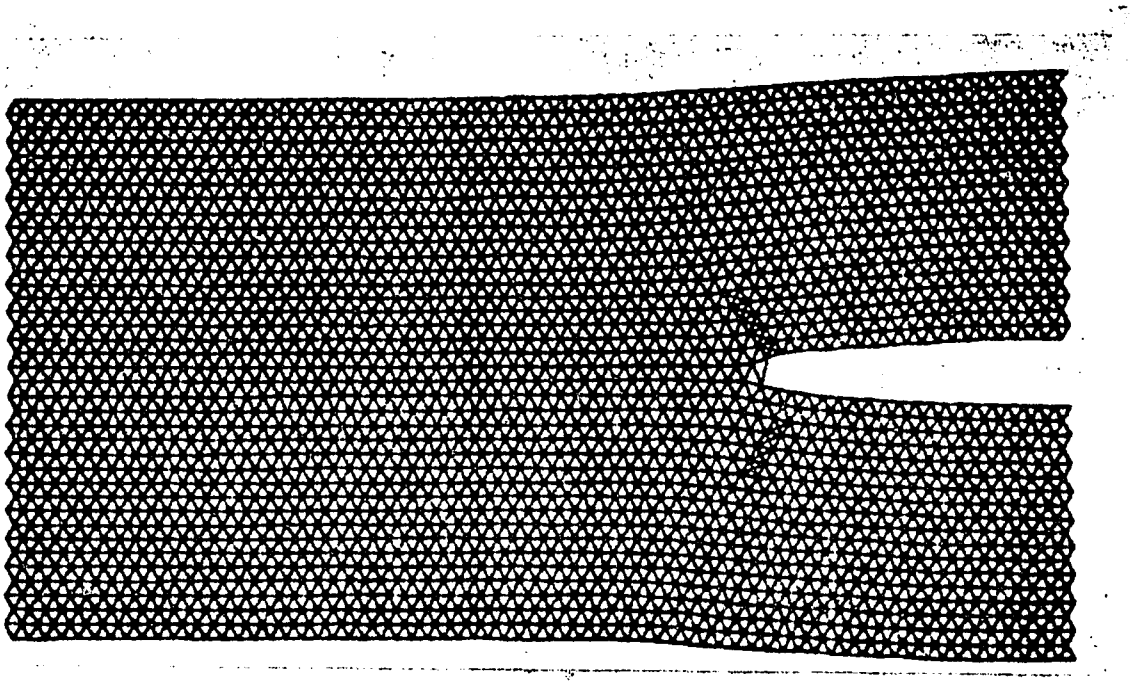

4200

FIG. 3-84 (a)

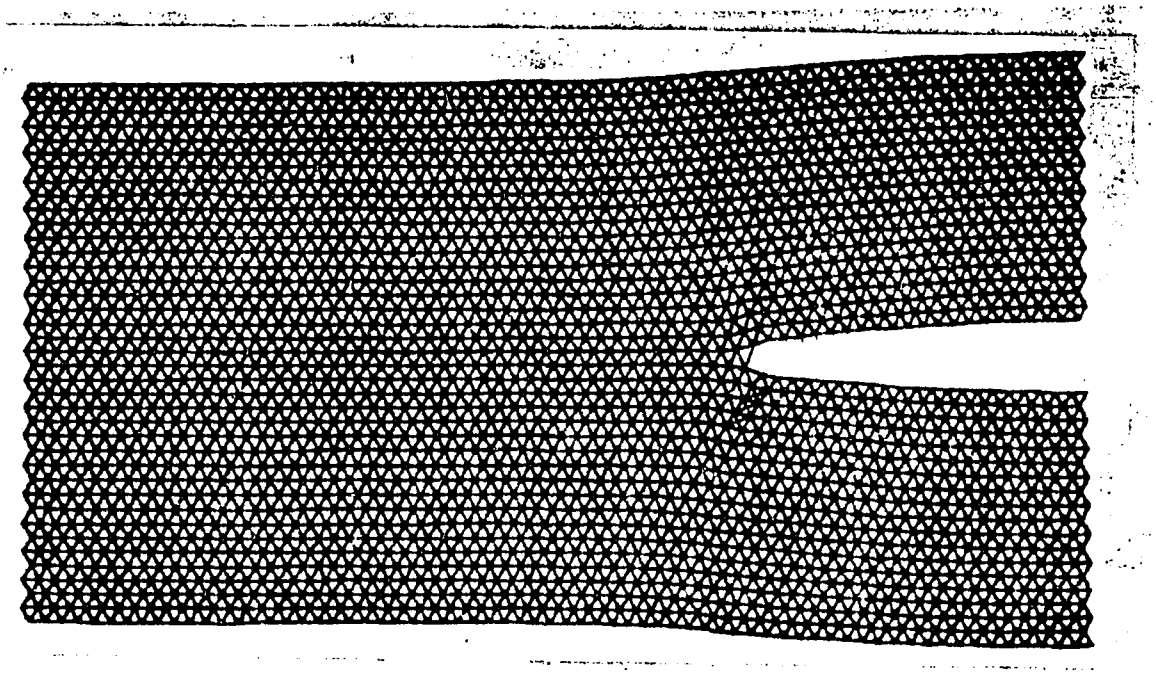

4300

FIG. 3-84(b.)

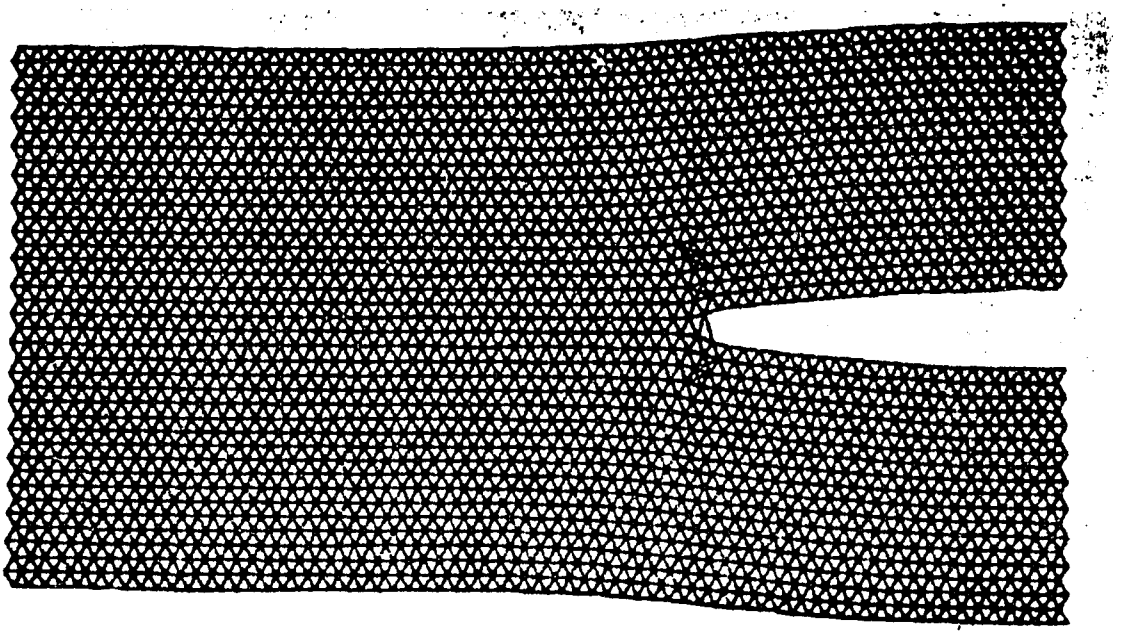

4400

FIG. 3-85

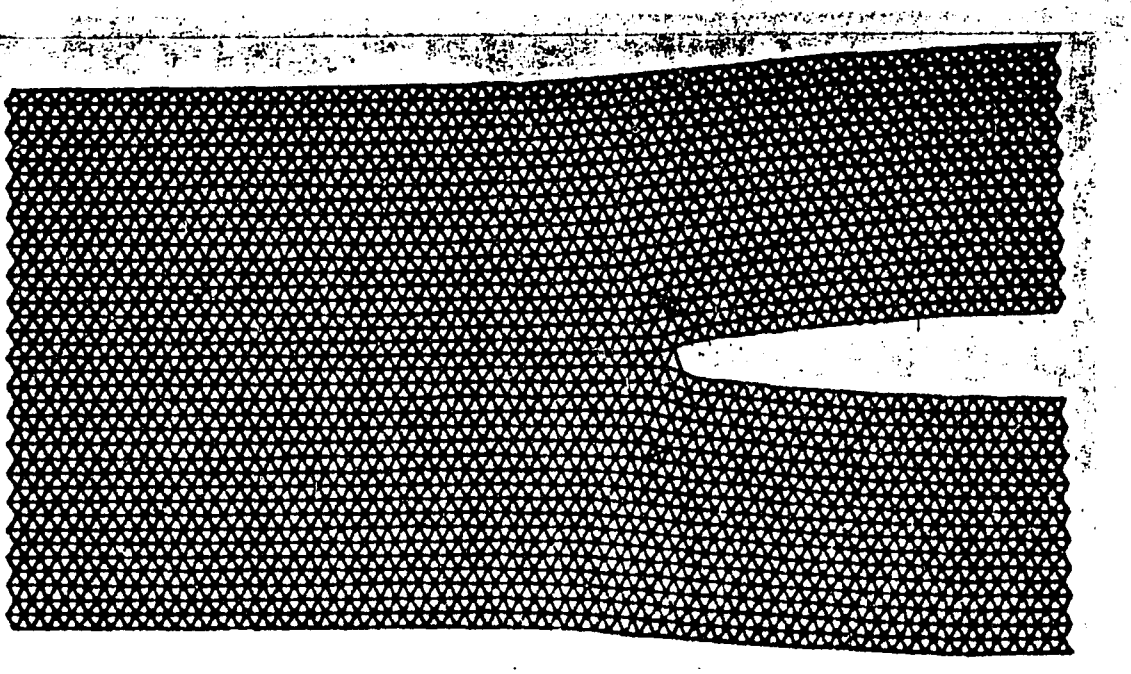

4500

FIG. 3-86

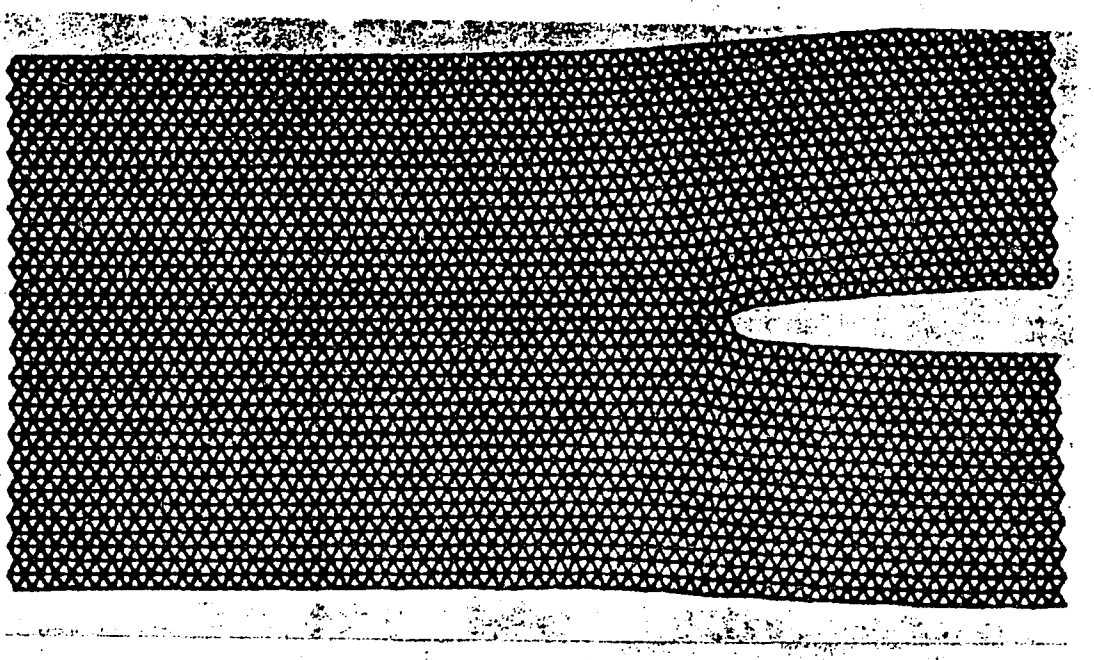

4200

FIG. 3-87

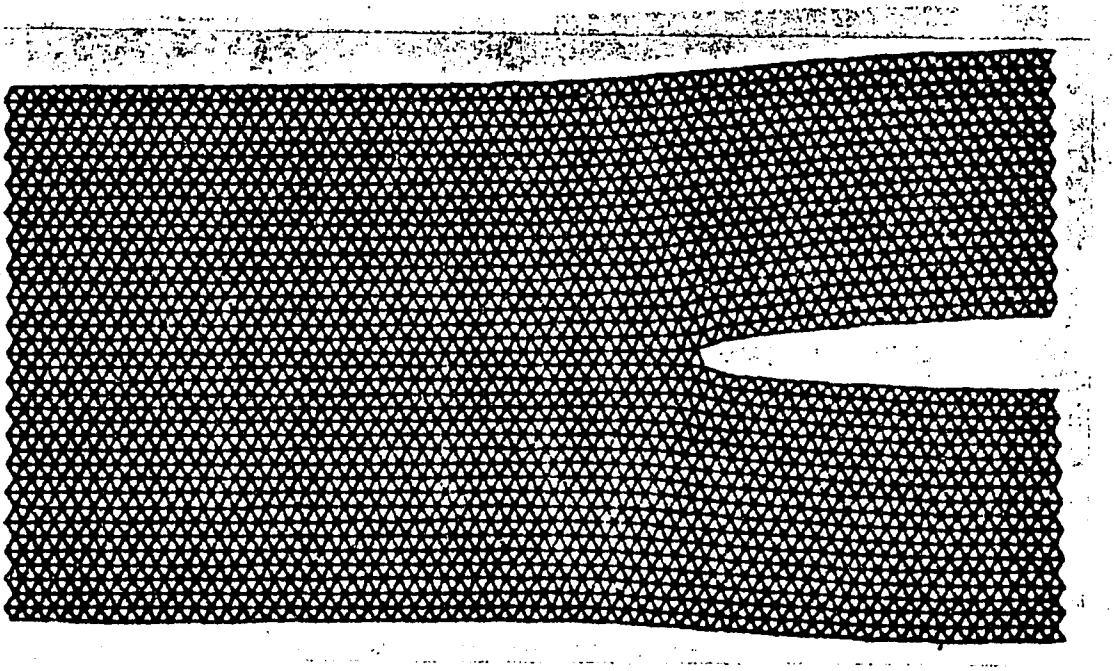

4300

FIG. 3-88

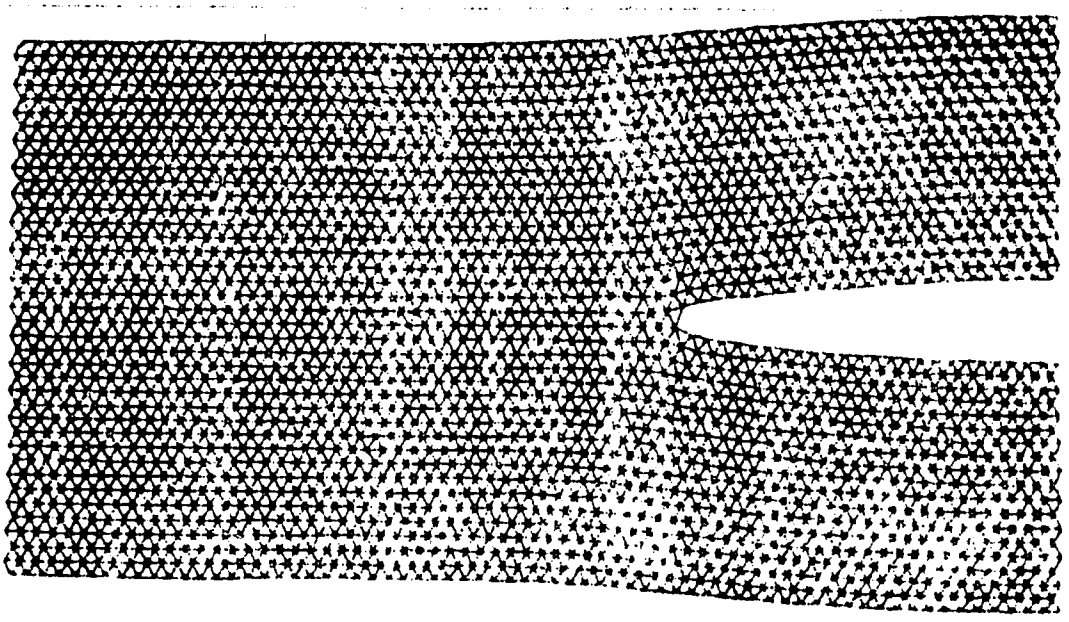

4400

FIG. 3-89

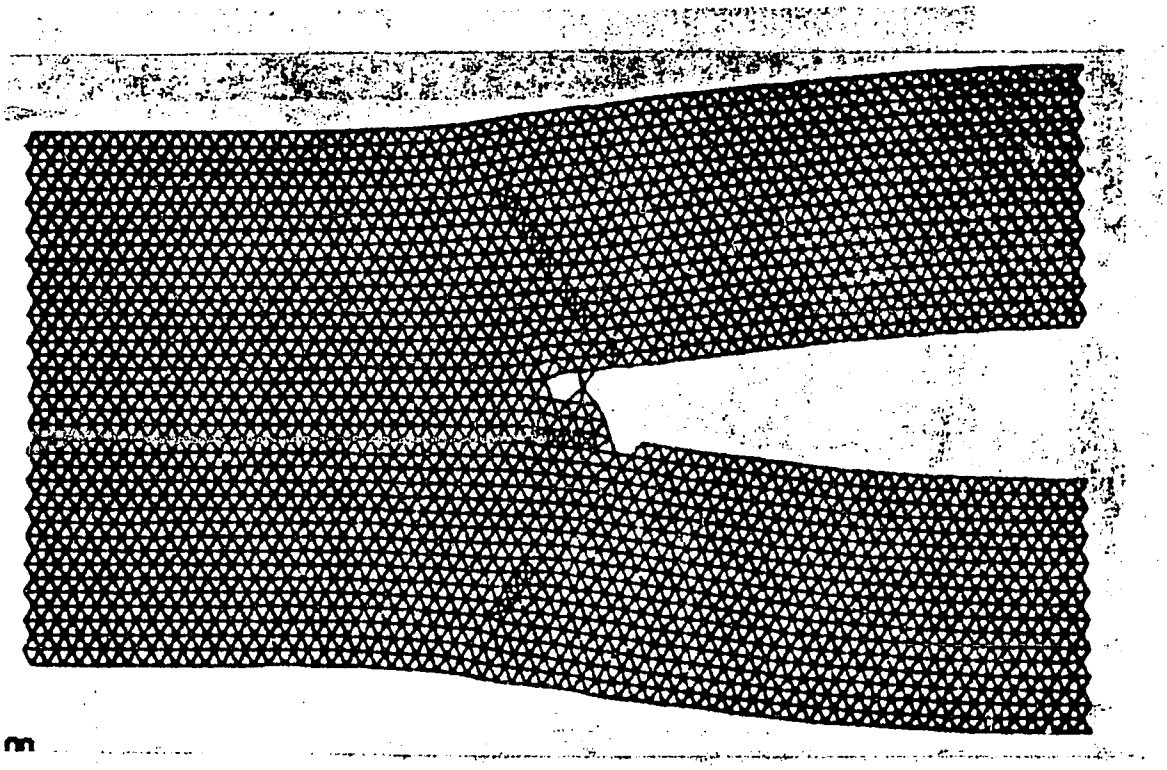

5100

FIG. 3-90

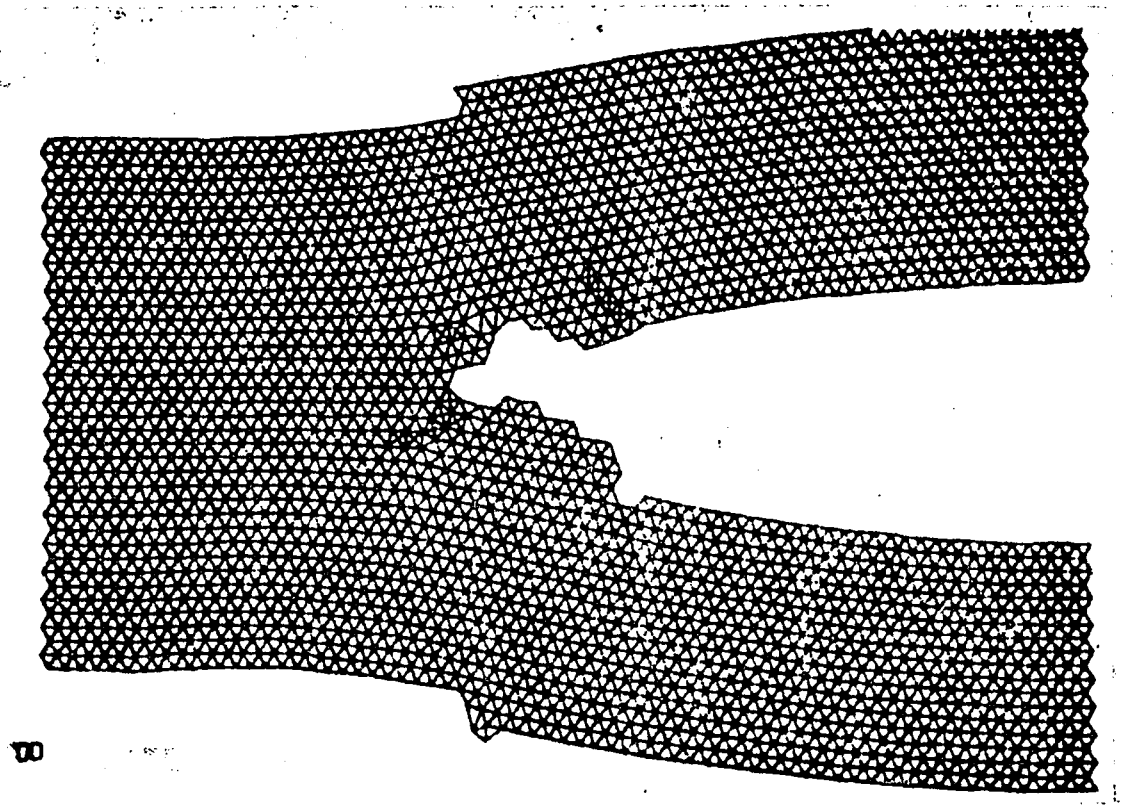

5700

FIG. 3-91

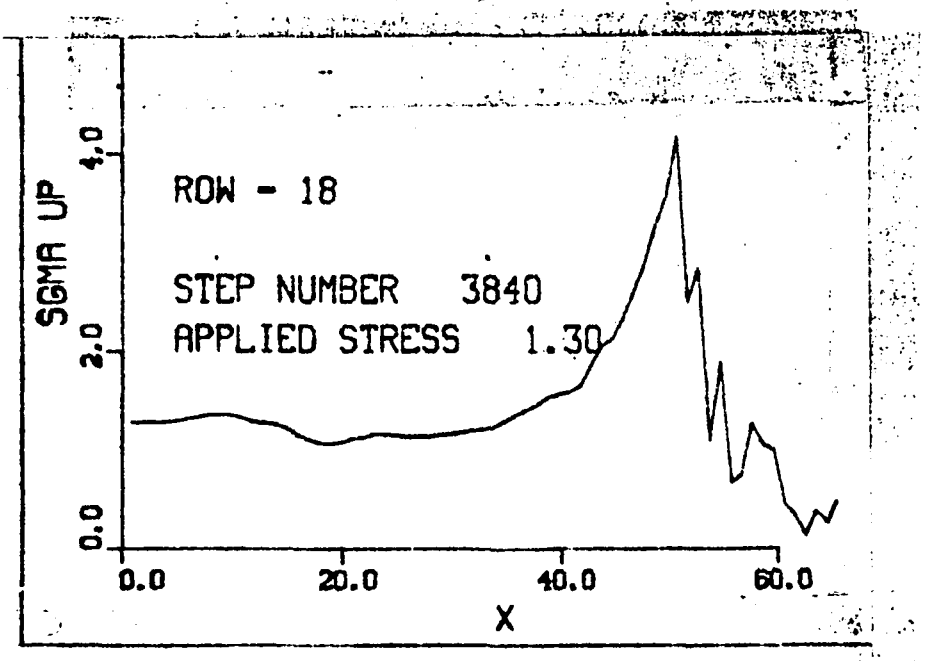

FIG. 3-92

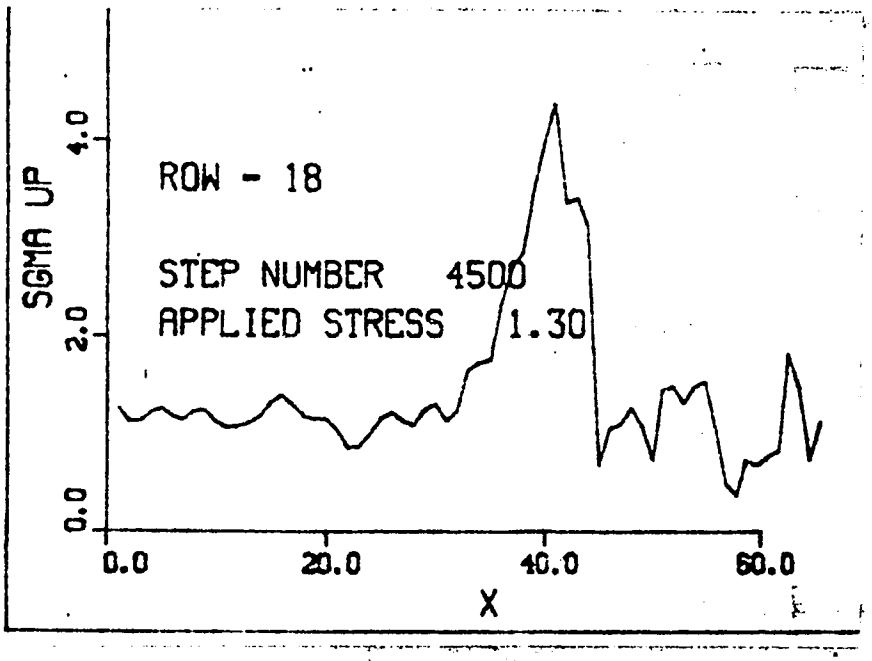

FIG. 3-93

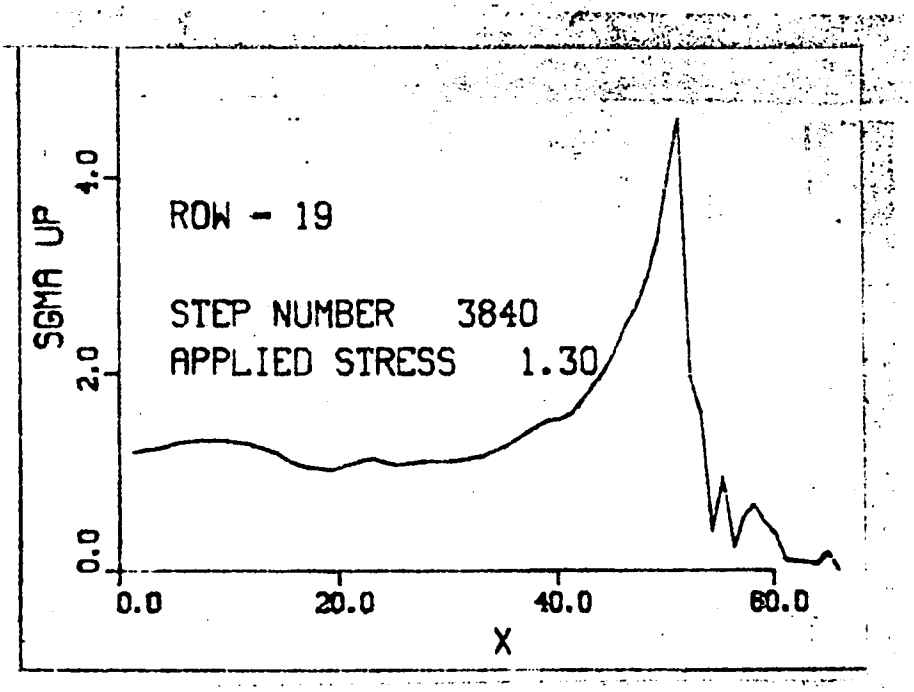

FIG. 3-94

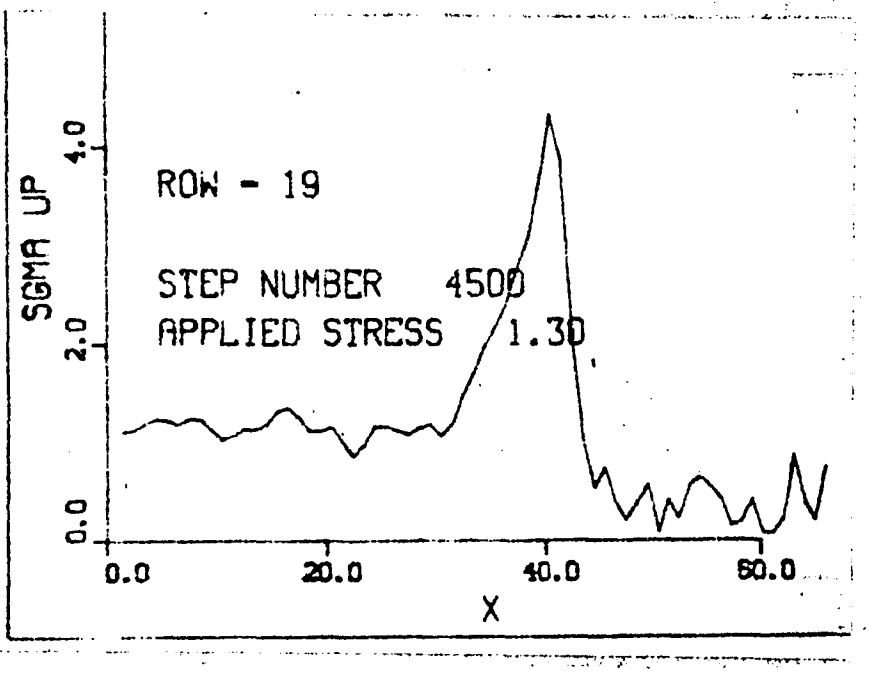

FIG. 3-95

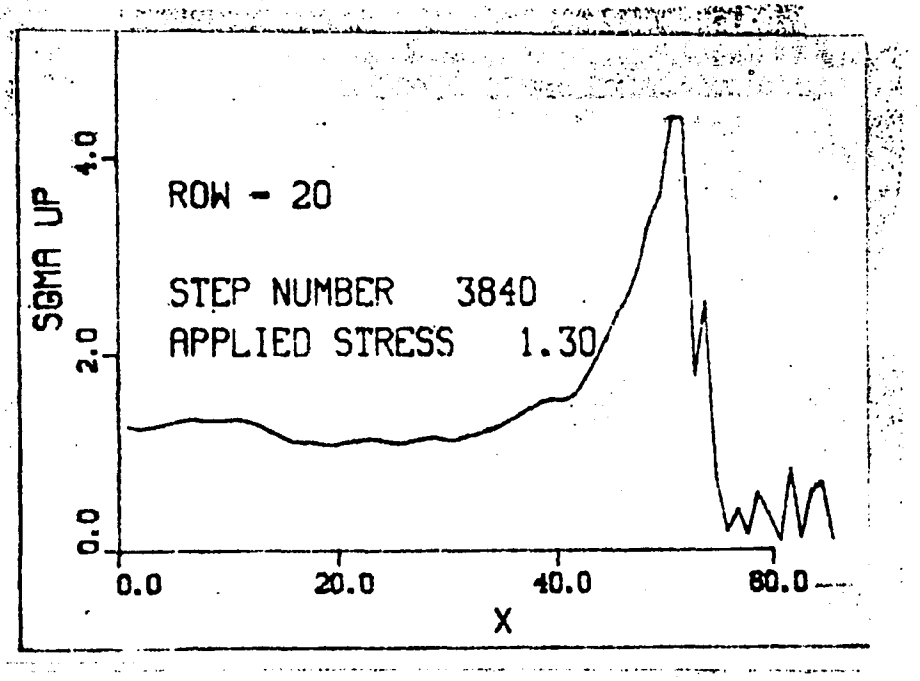

FIG. 3-96

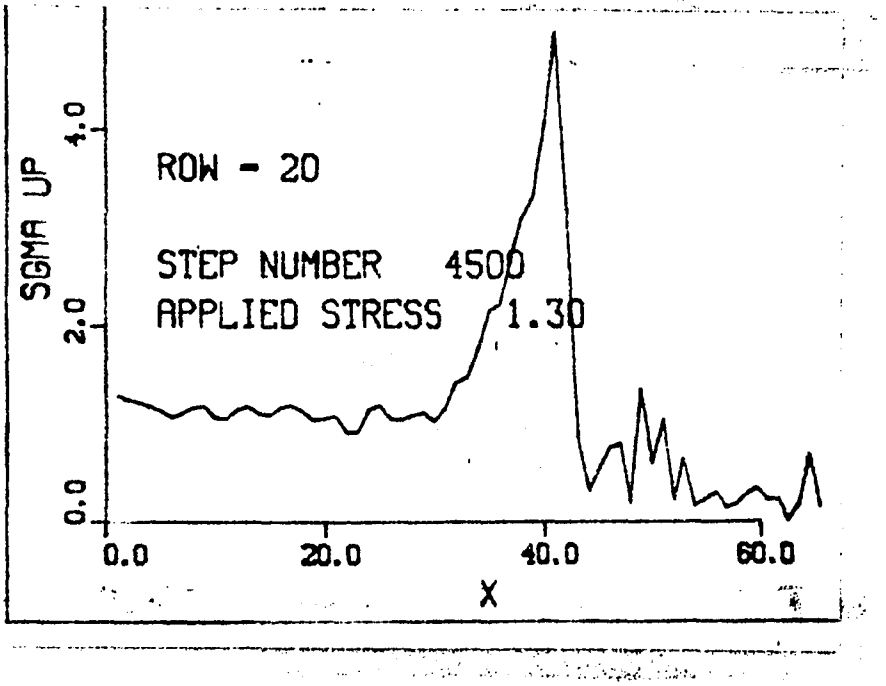

FIG. 3-97

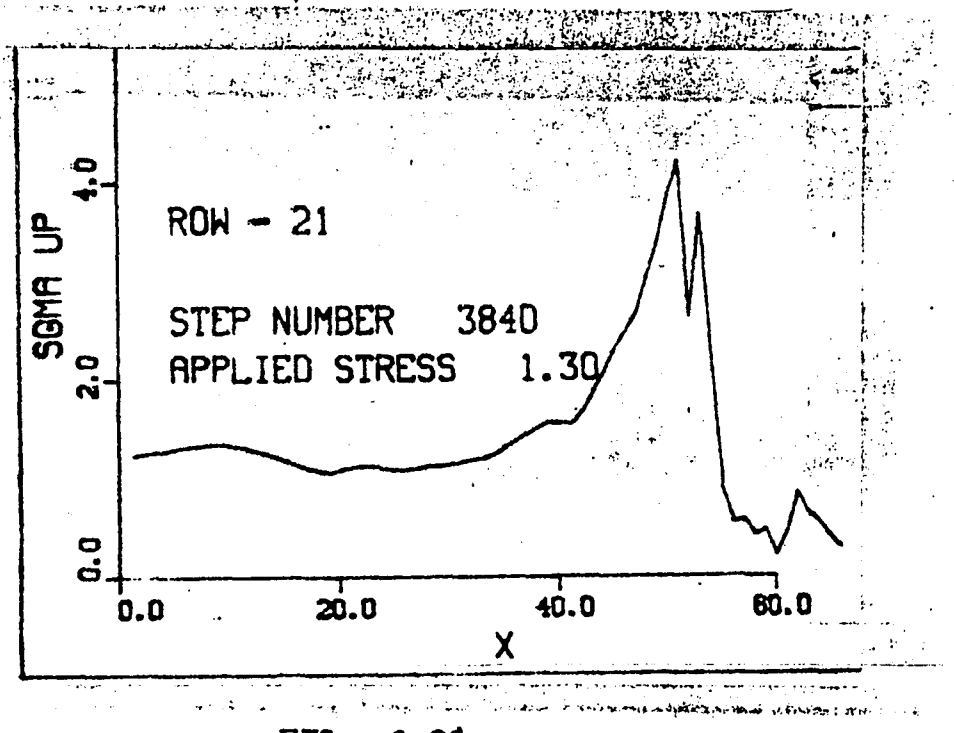

FIG. 3-98

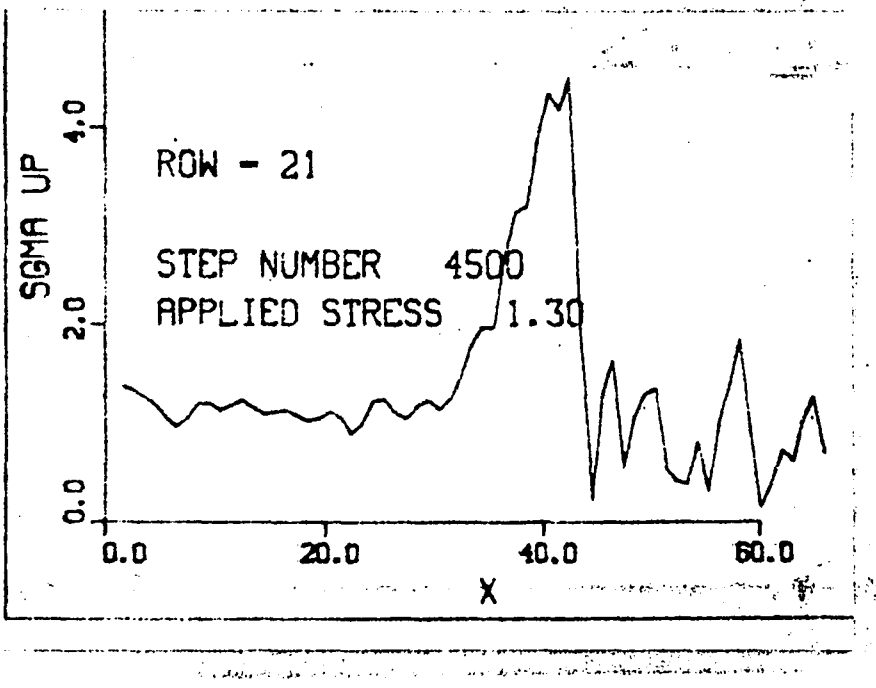

FIG. 3-99

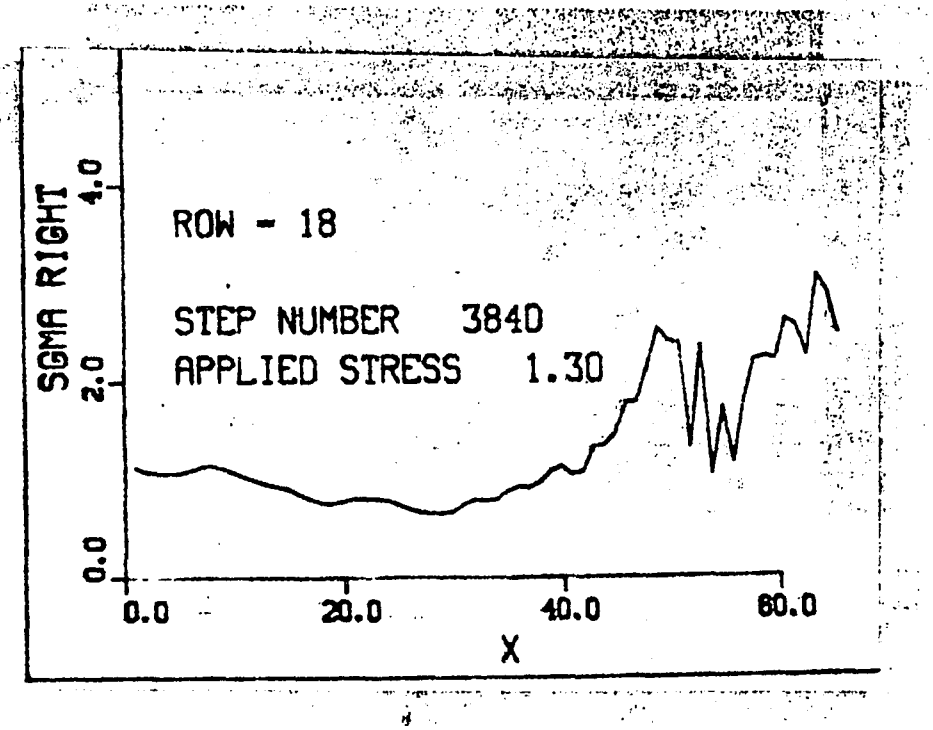

FIG. 3-100

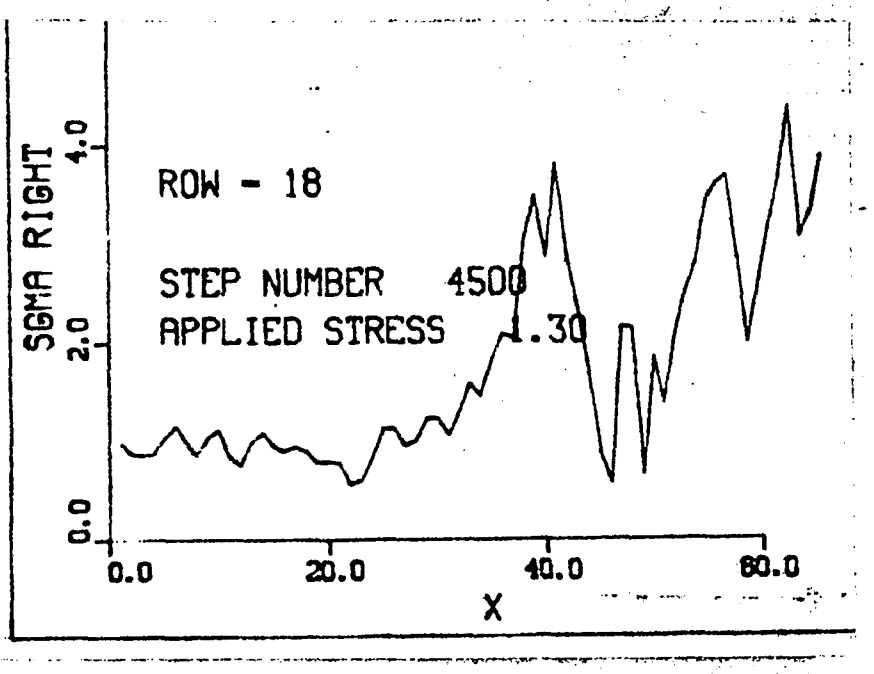

FIG. 3-101

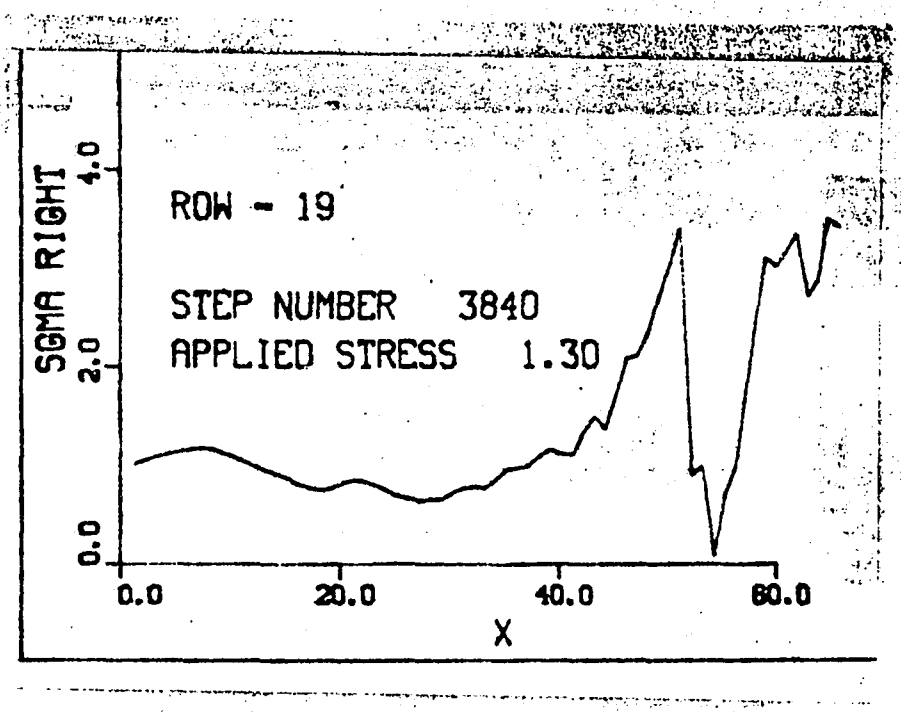

FIG. 3-102

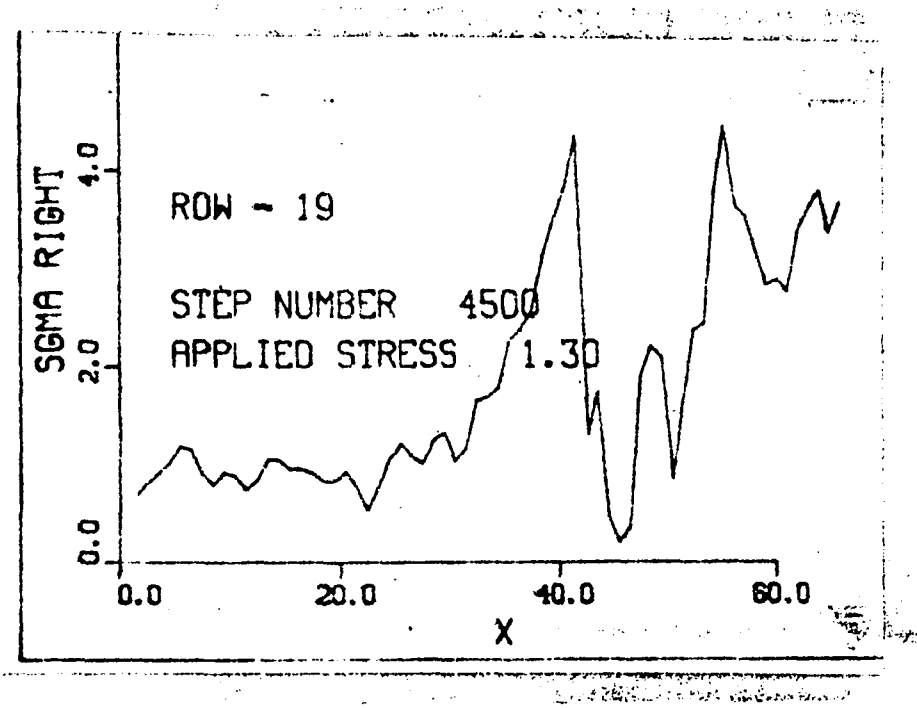

FIG. 3-103

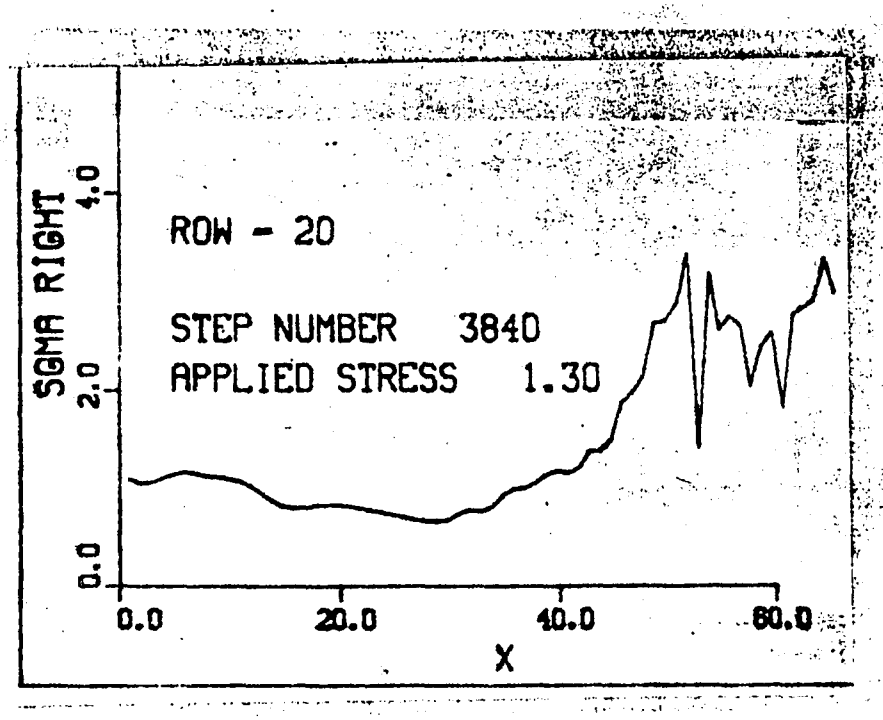

FIG. 3-104

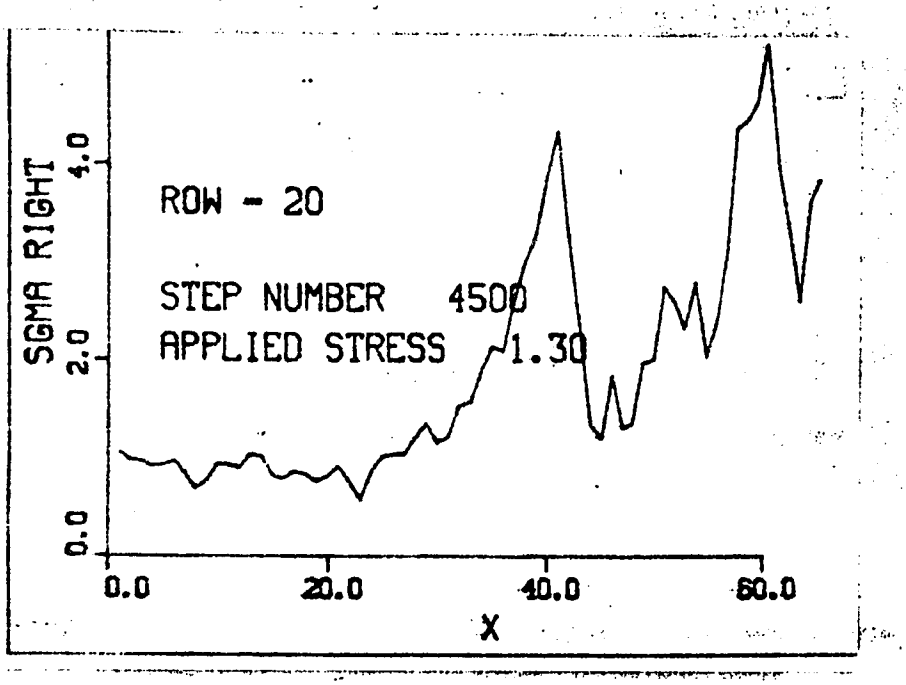

FIG. 3-105

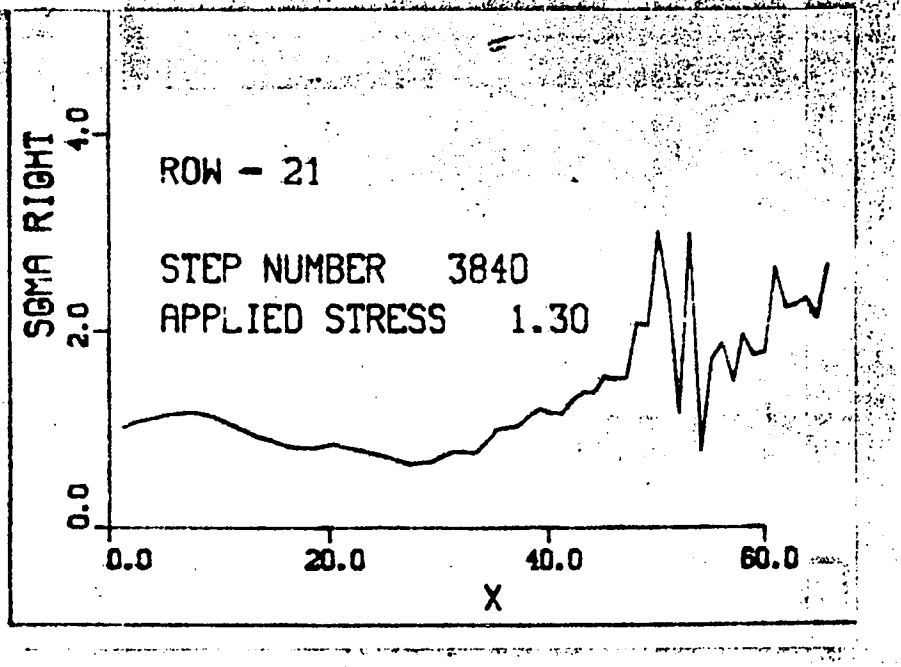

FIG. 3-106

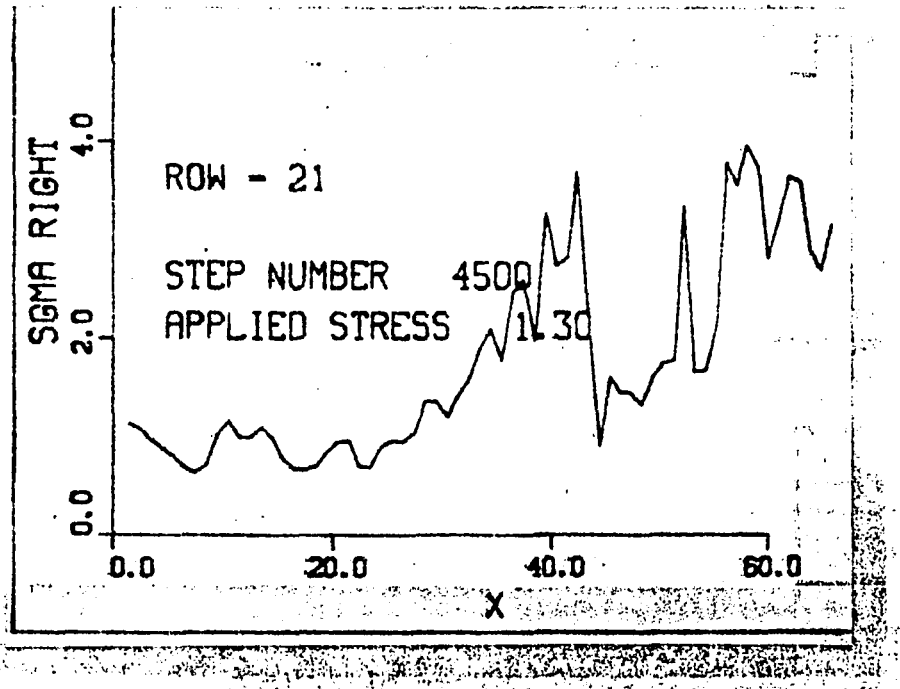
SGMA RIGHT
4.0
2.0
0.0
ROW - 21
STEP NUMBER 4500
APPLIED STRESS 1.30
0.0
20.0
40.0
60.0
X

FIG. 3-107

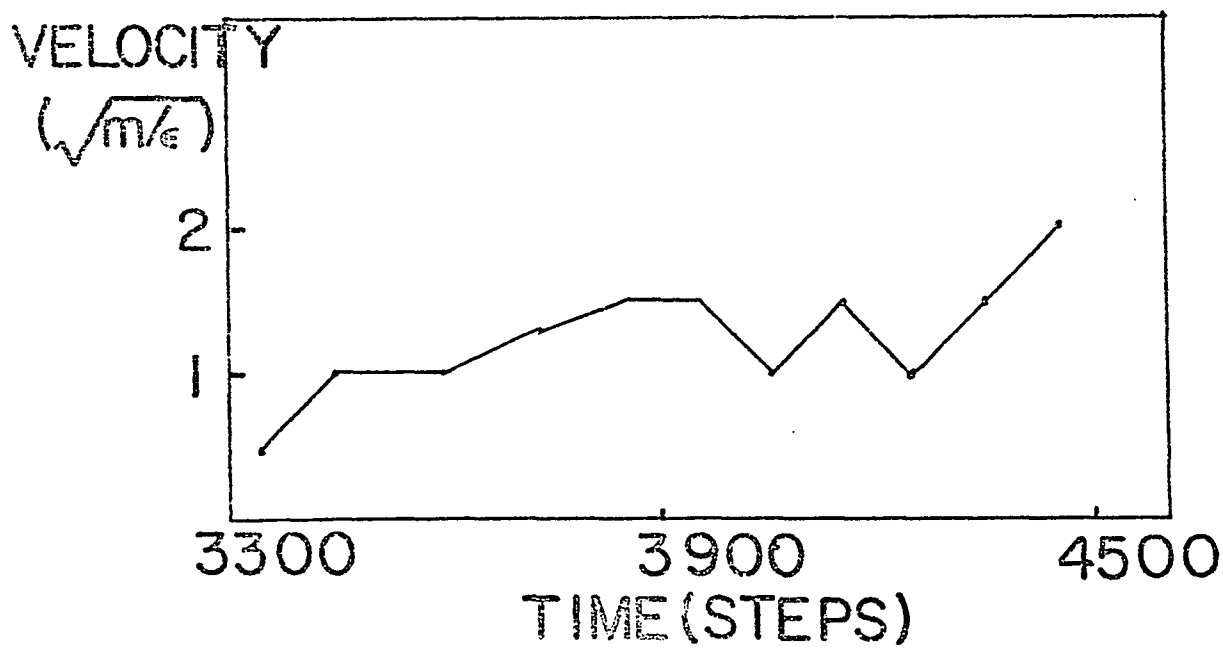

FIG.3-108

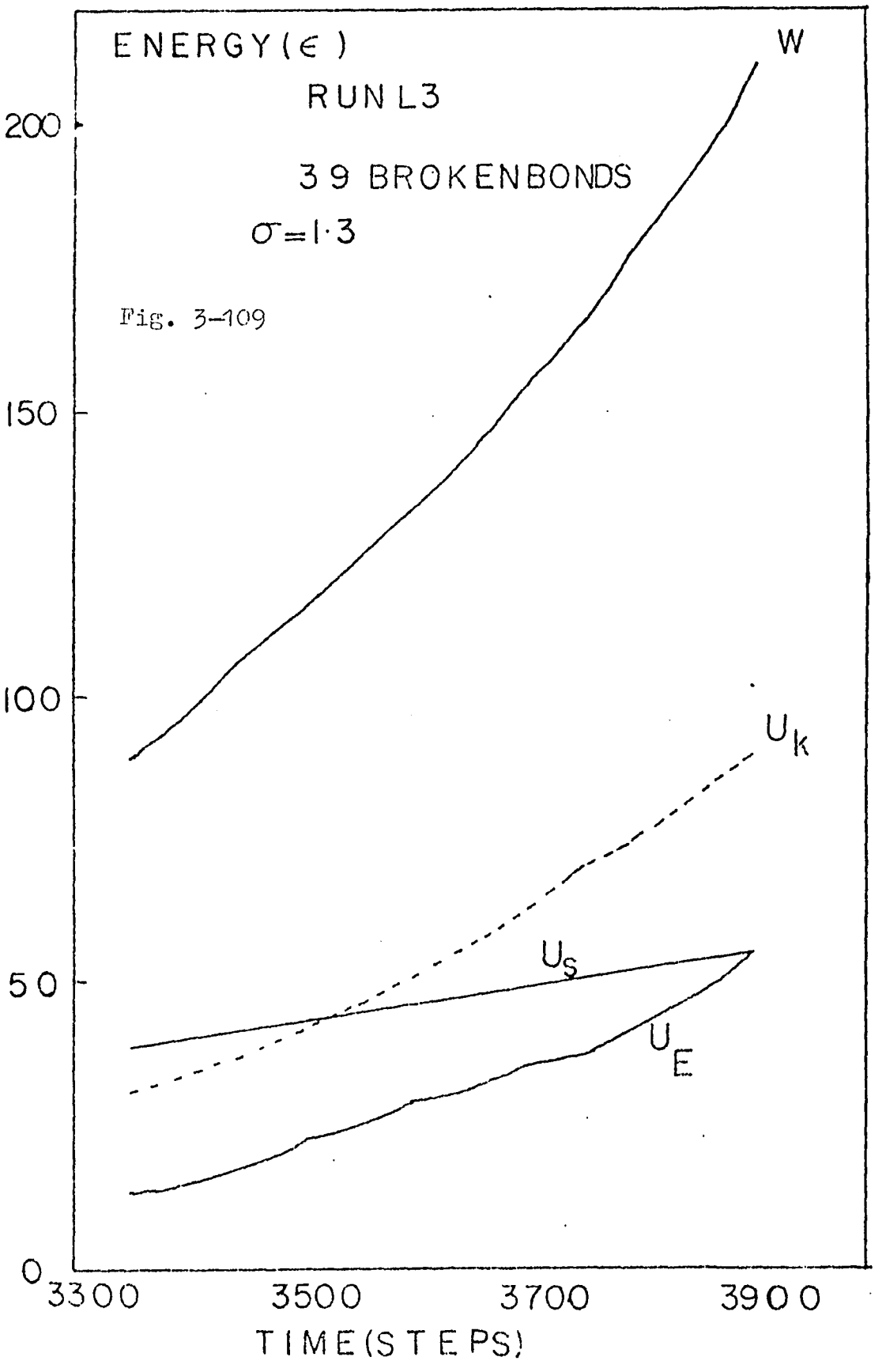
ENERGY(ϵ)
RUN L3
39 BROKENBONDS
σ=1·3
W
U_k
U_S
U_E
200
150
100
50
0
3300
3500
3700
3900
TIME(STEPS)

Fig. 3-109

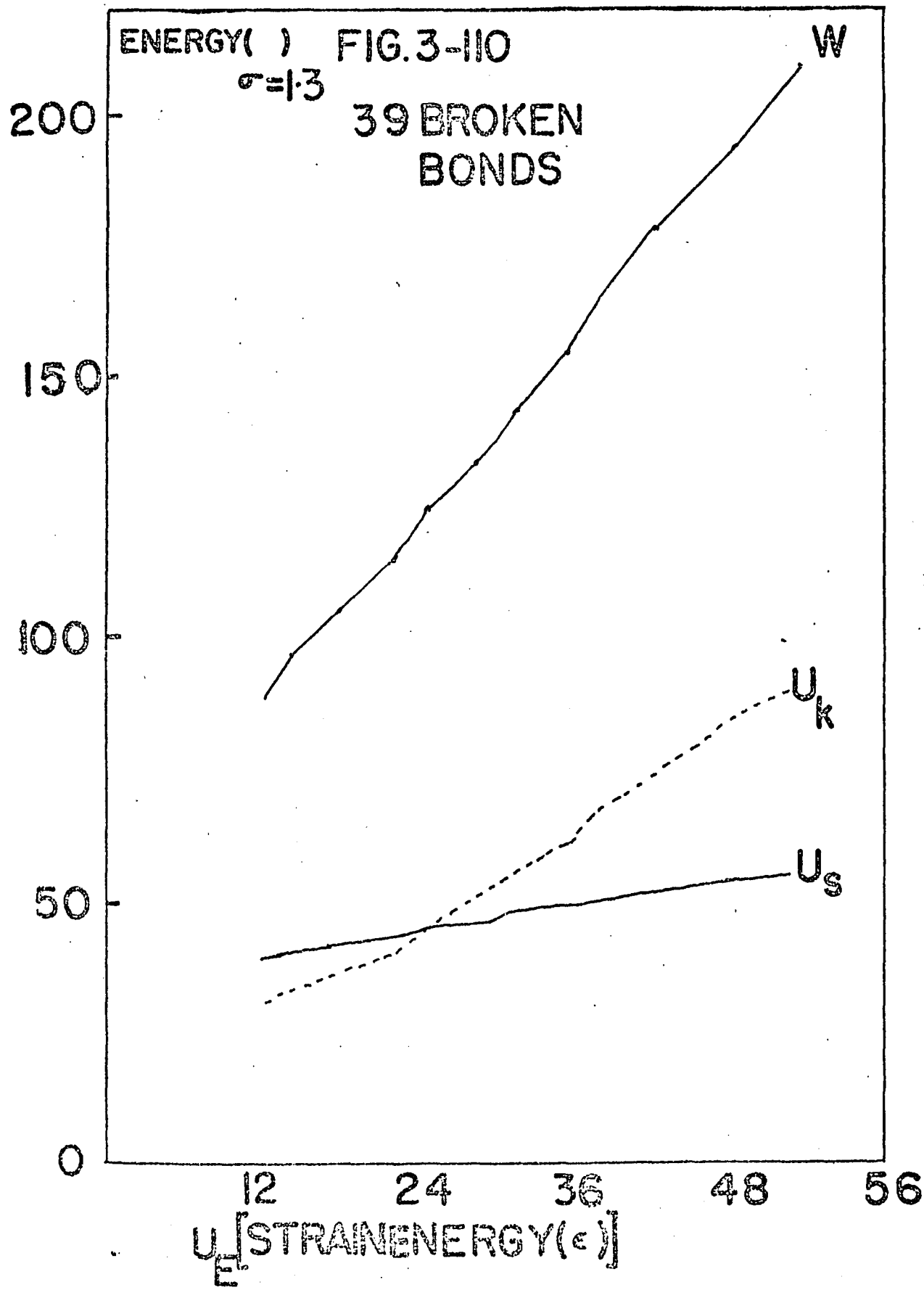
ENERGY( )
σ=1·3
FIG. 3-110
39 BROKEN BONDS
W
U_k
U_s
200
150
100
50
0
12
24
36
48
56
U_E[STRAINENERGY(ε)]

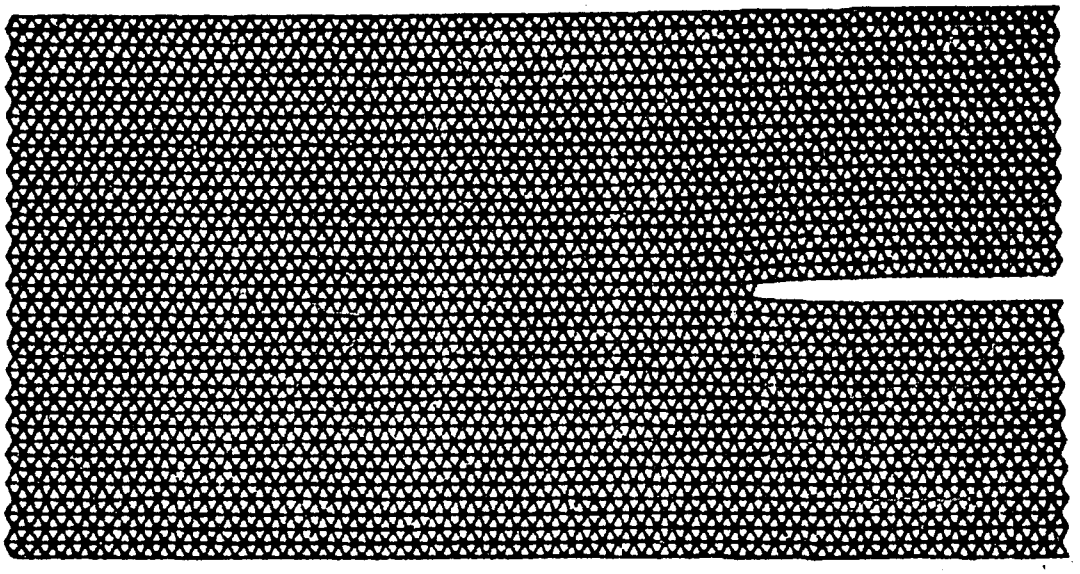

3100

FIG. 3-111(a)

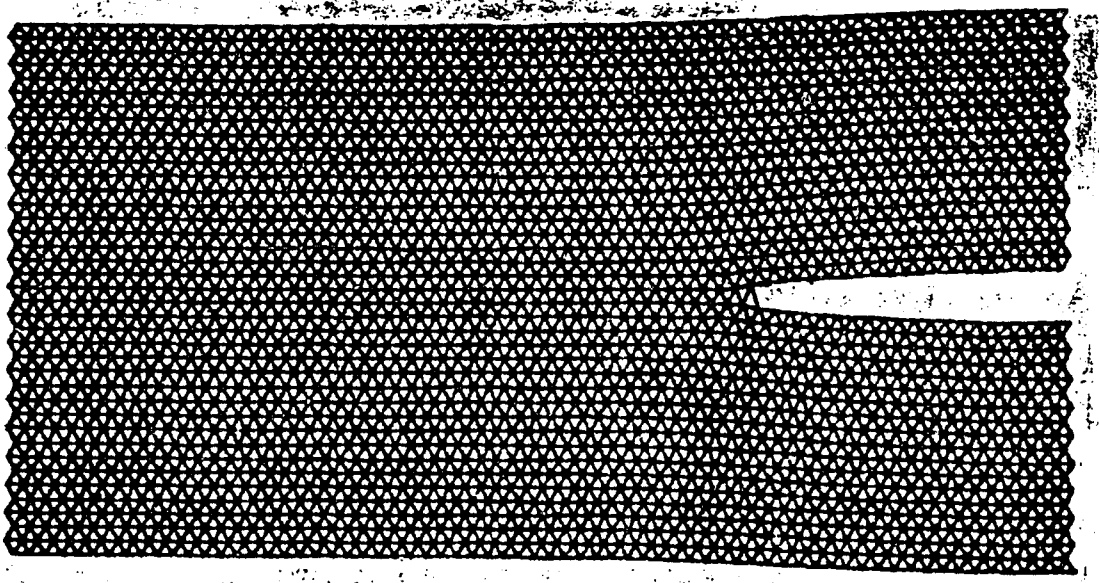

3400

FIG. 3-111(b)

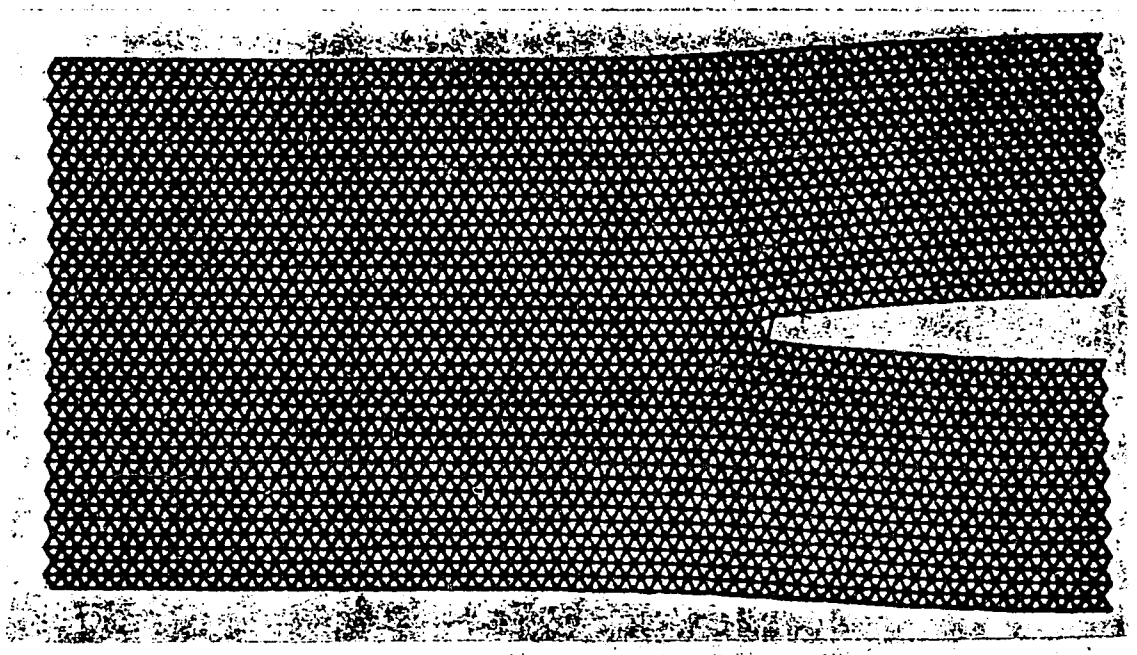

3500

FIG. 3-112

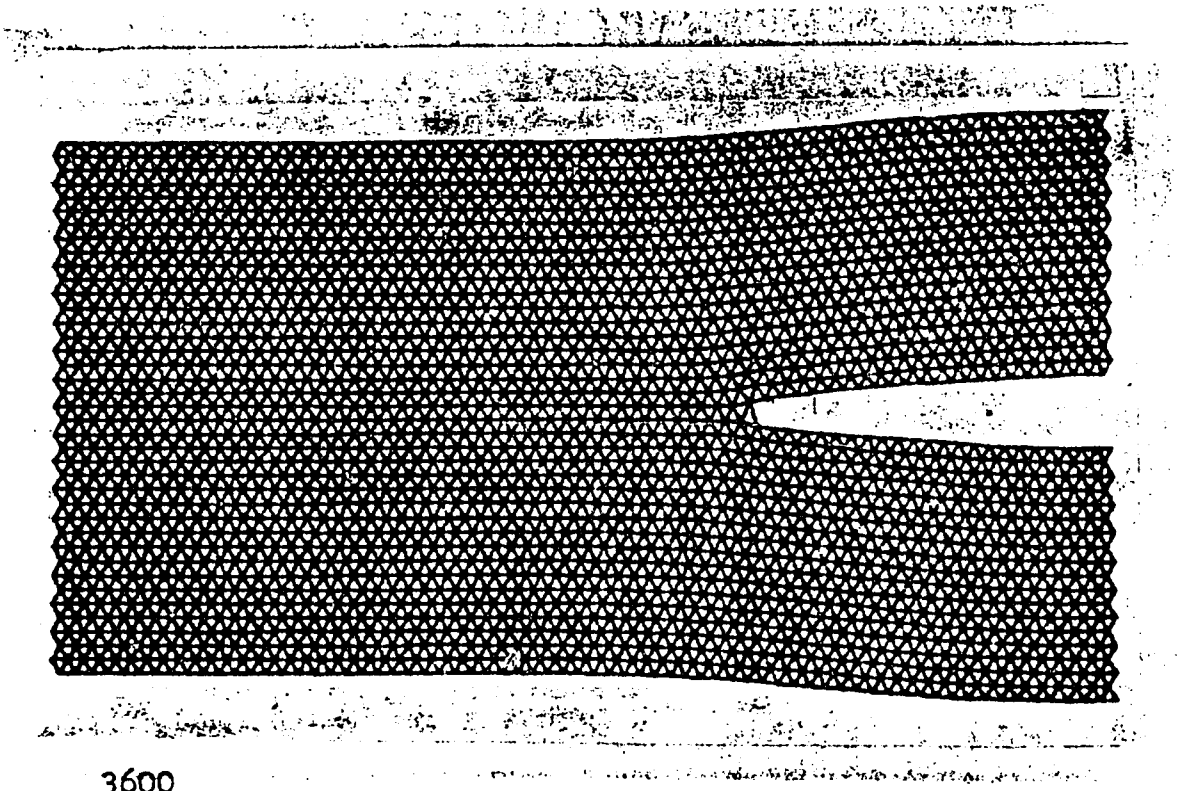

3600

FIG. 3-113

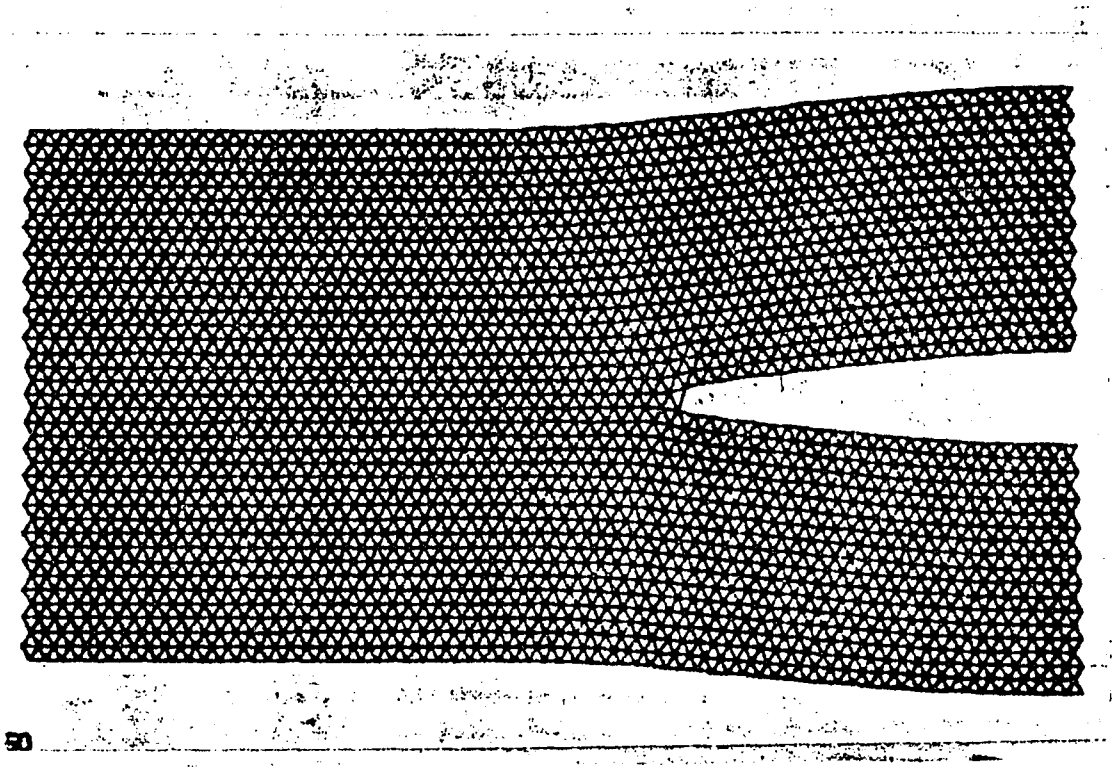

3750

FIG. 3-114

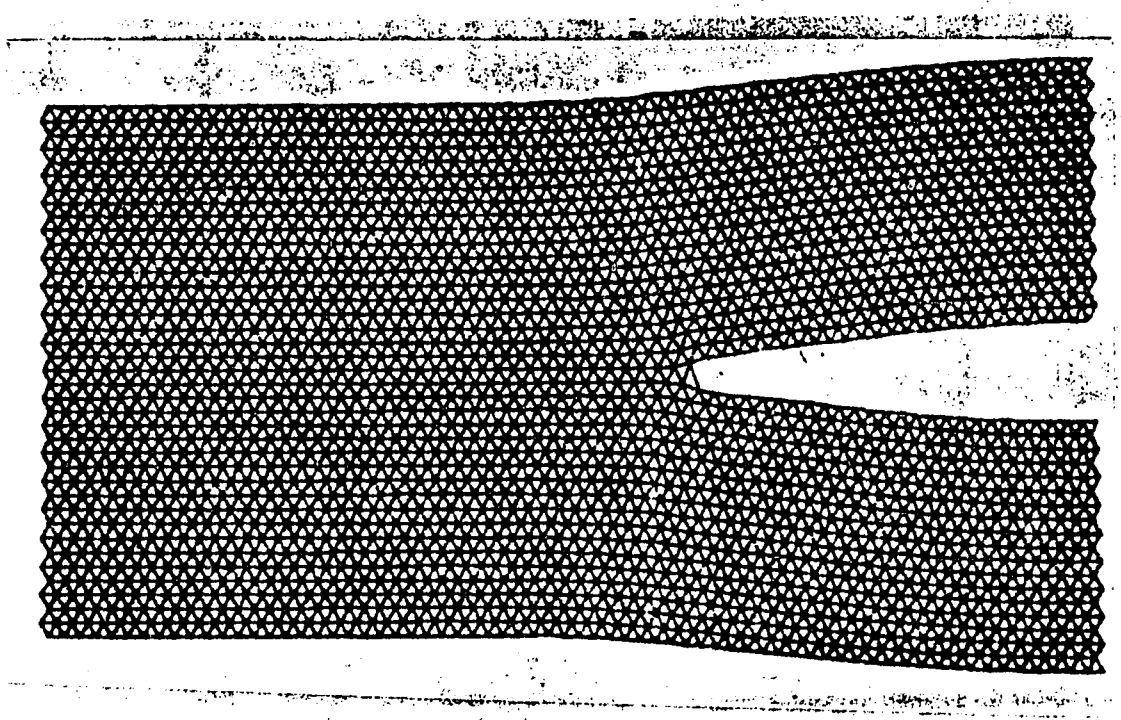

3800

FIG. 3-115

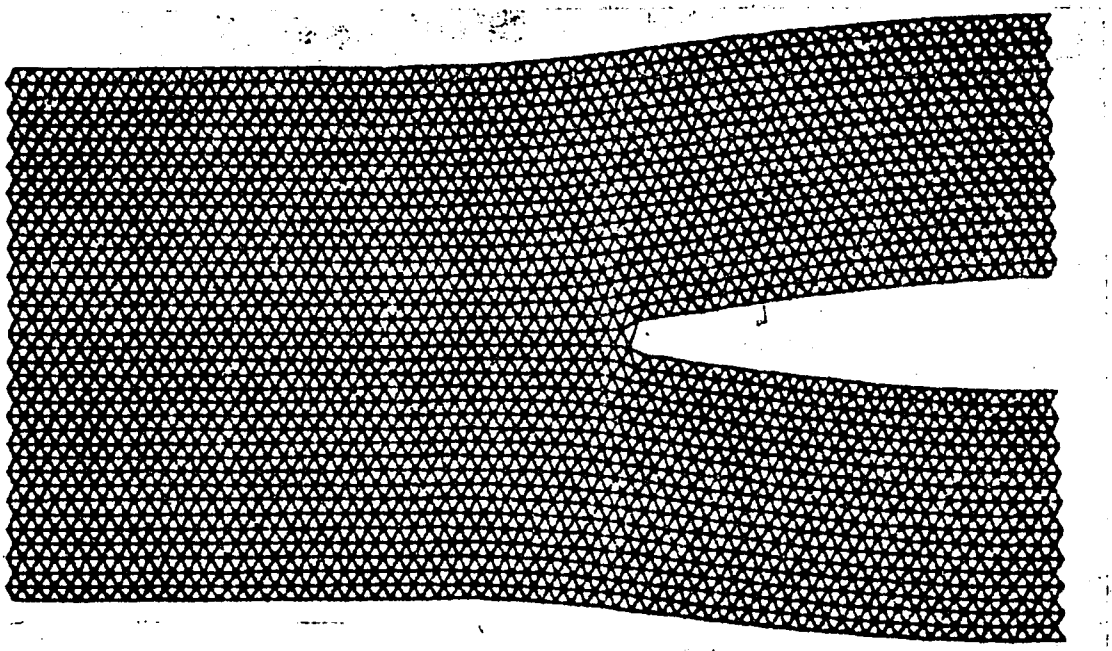

3900

FIG. 3-116

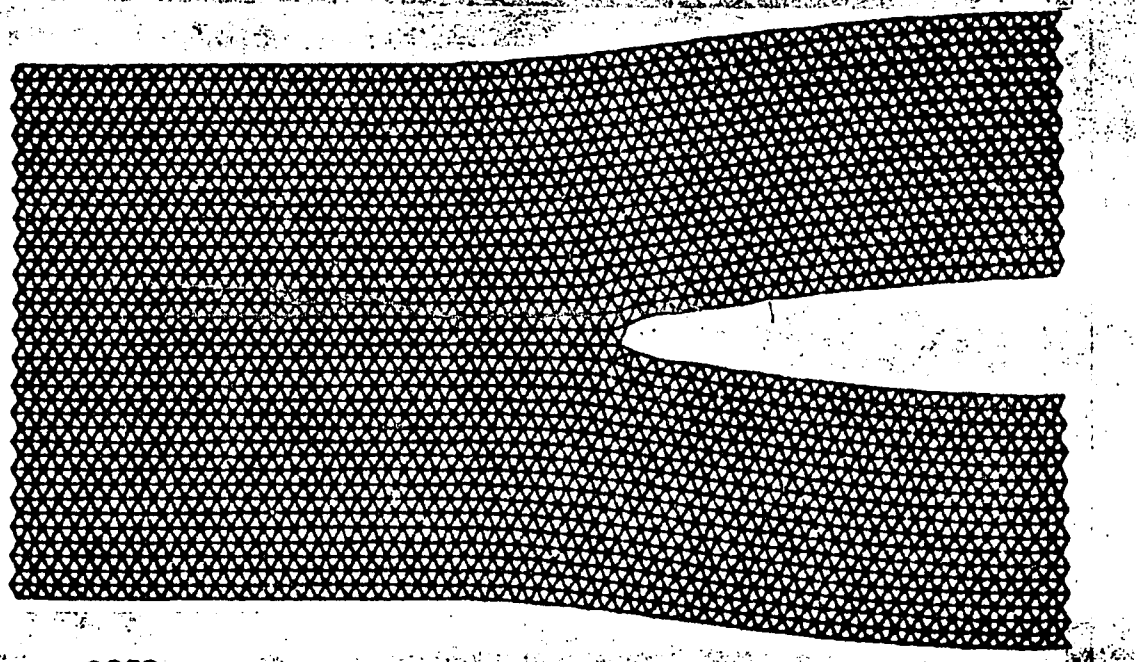

3950

FIG. 3-117

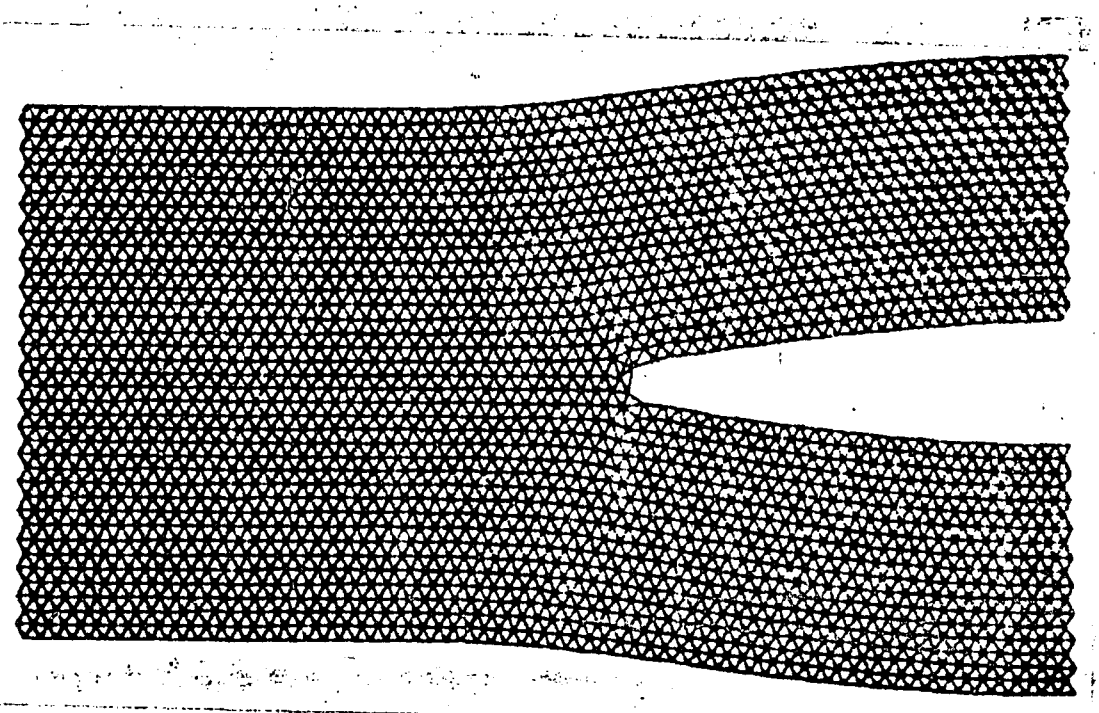

4000

FIG. 3-118

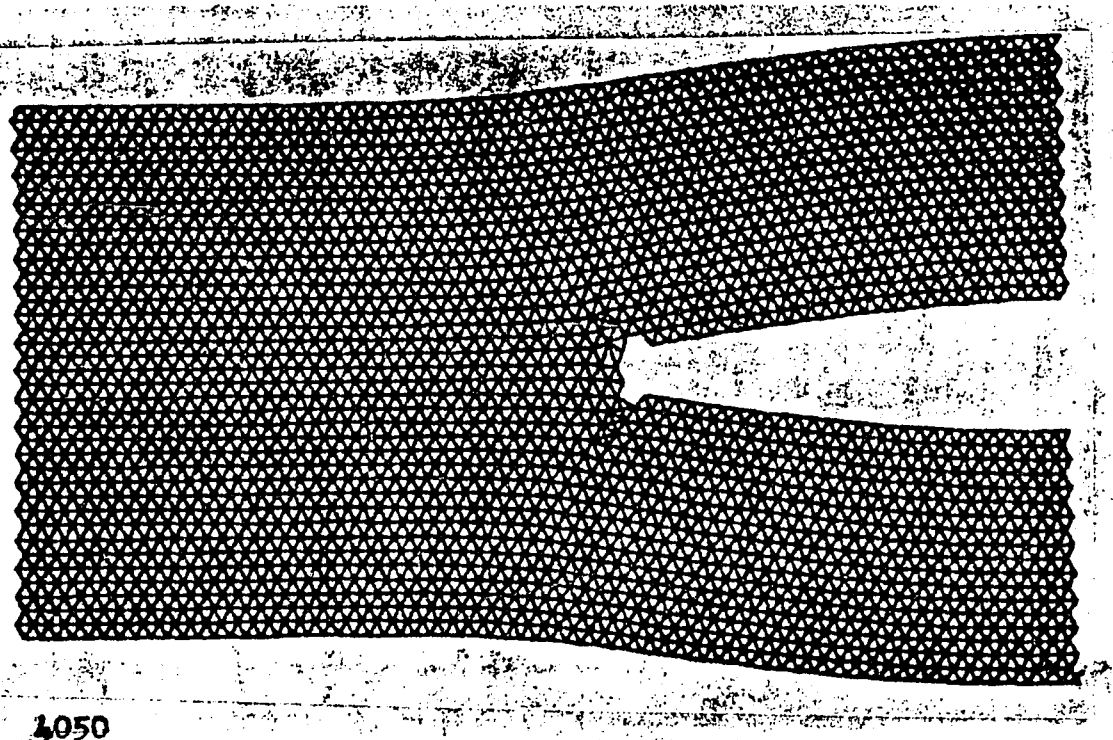

4050

FIG. 3-119

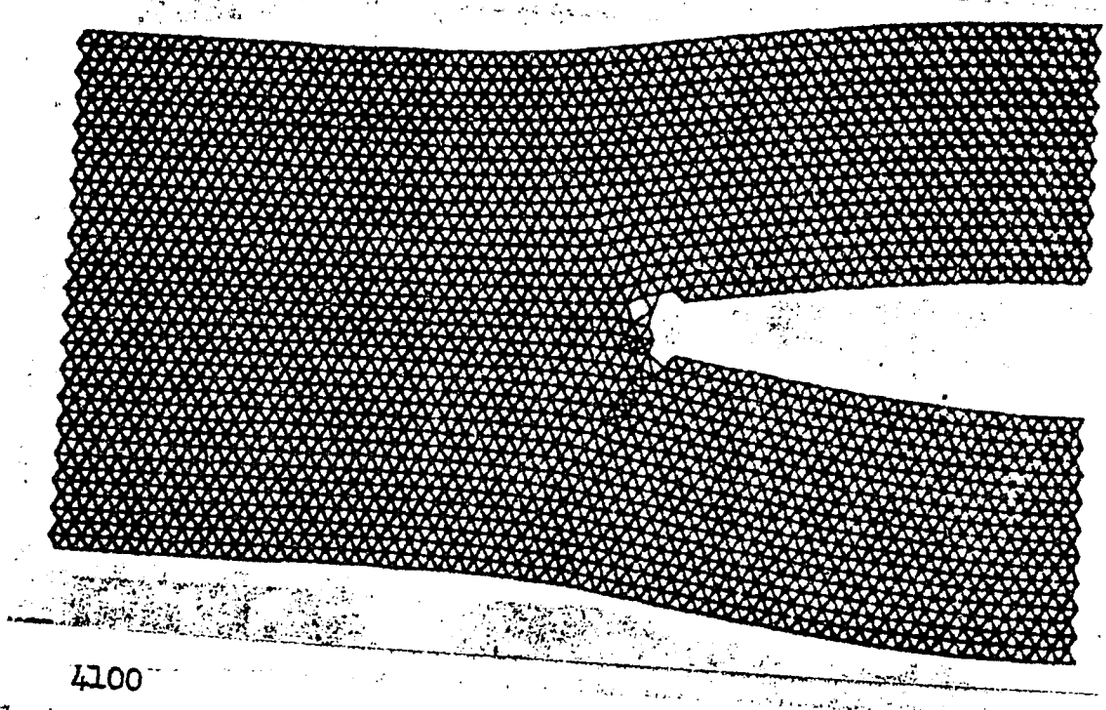

FIG. 3-120

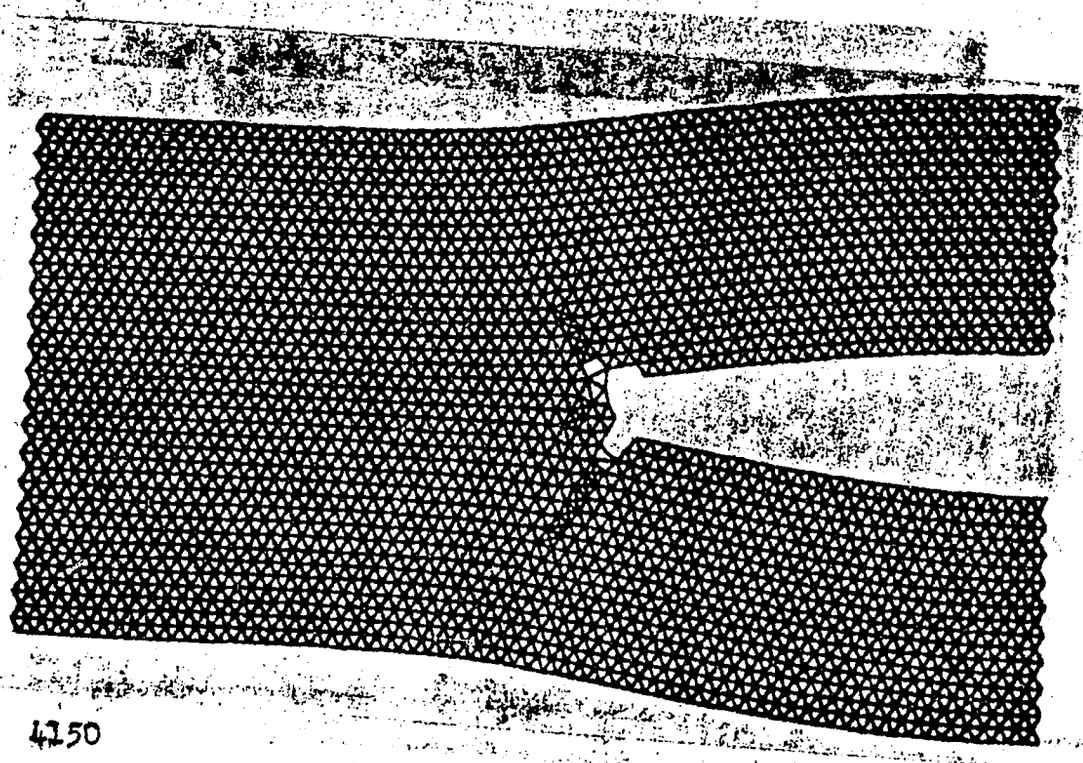

FIG. 3-121

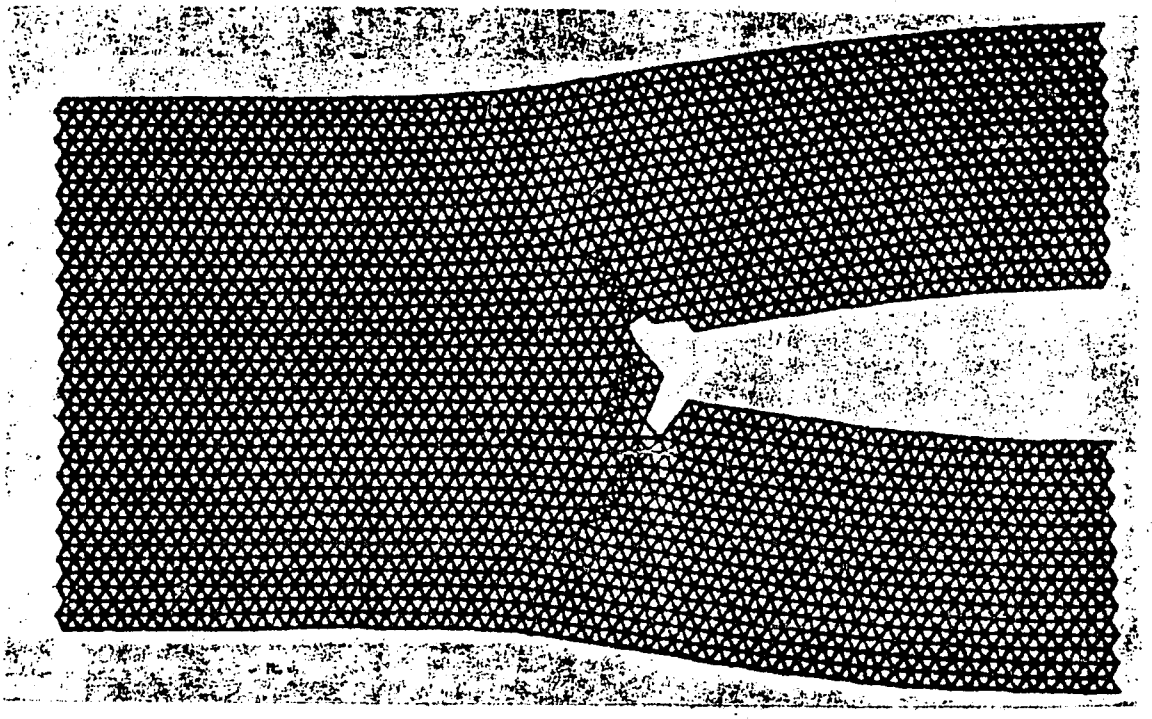

4200

FIG. 3-122

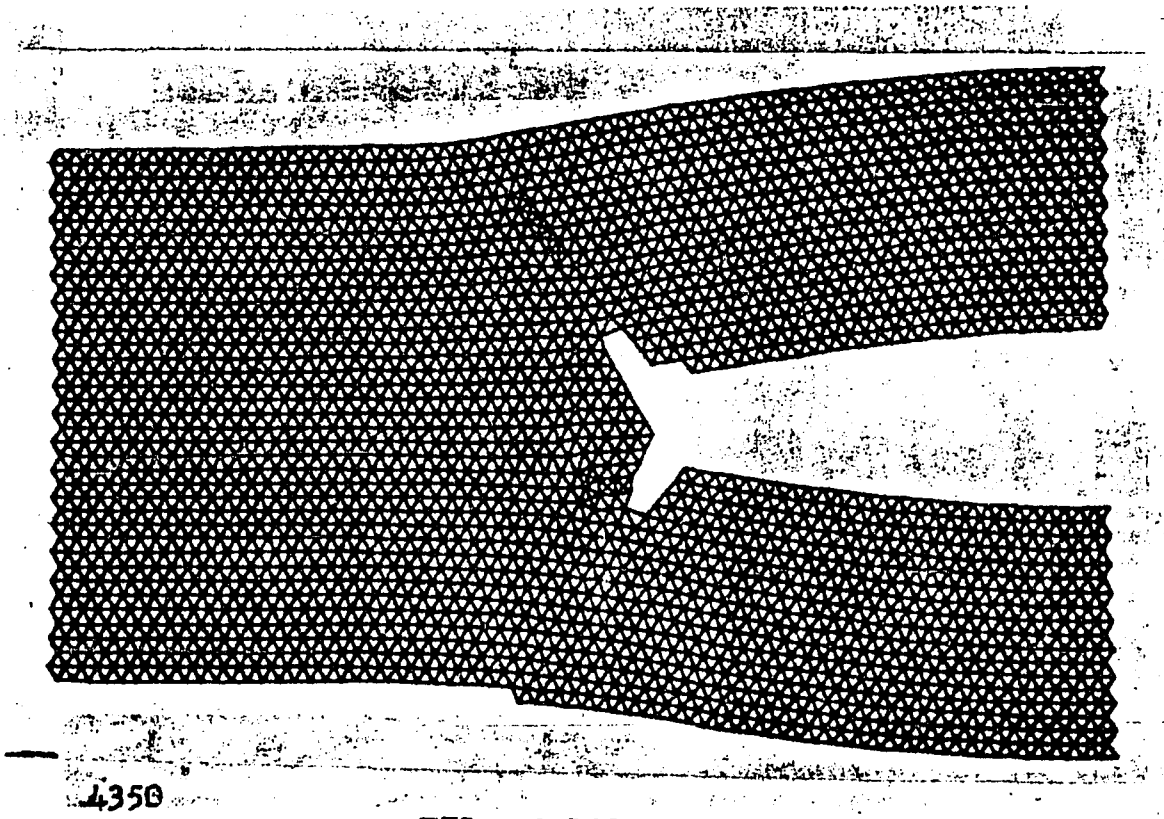

4350

FIG. 3-123

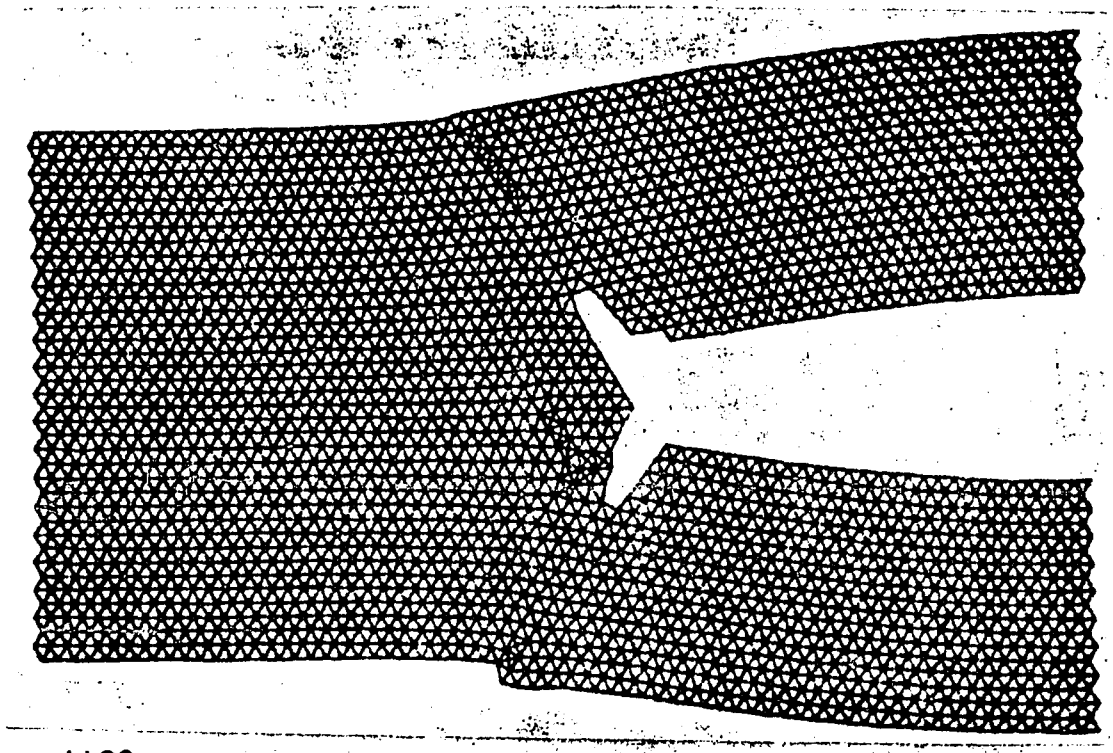

4400

FIG. 3-124

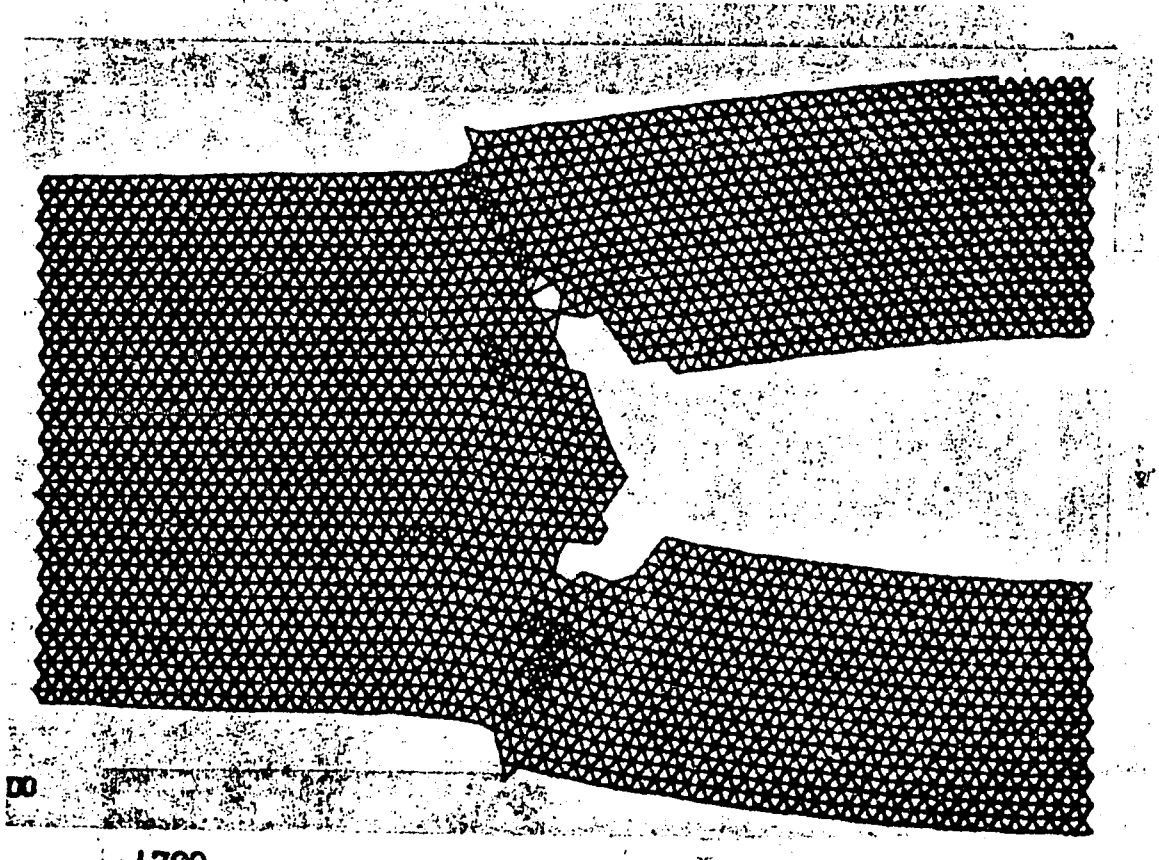

4700

FIG. 3-125

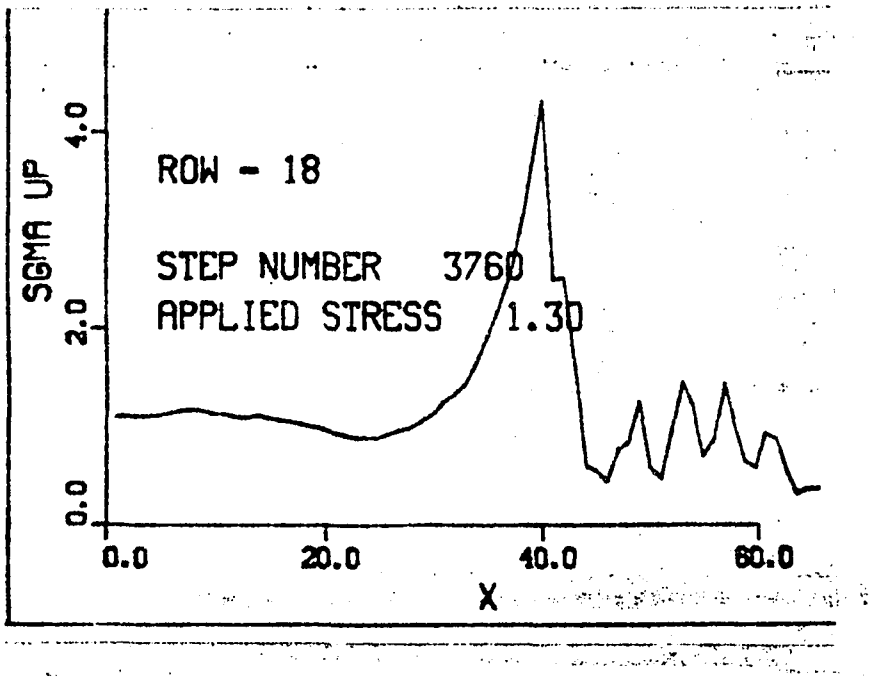

FIG. 3-126

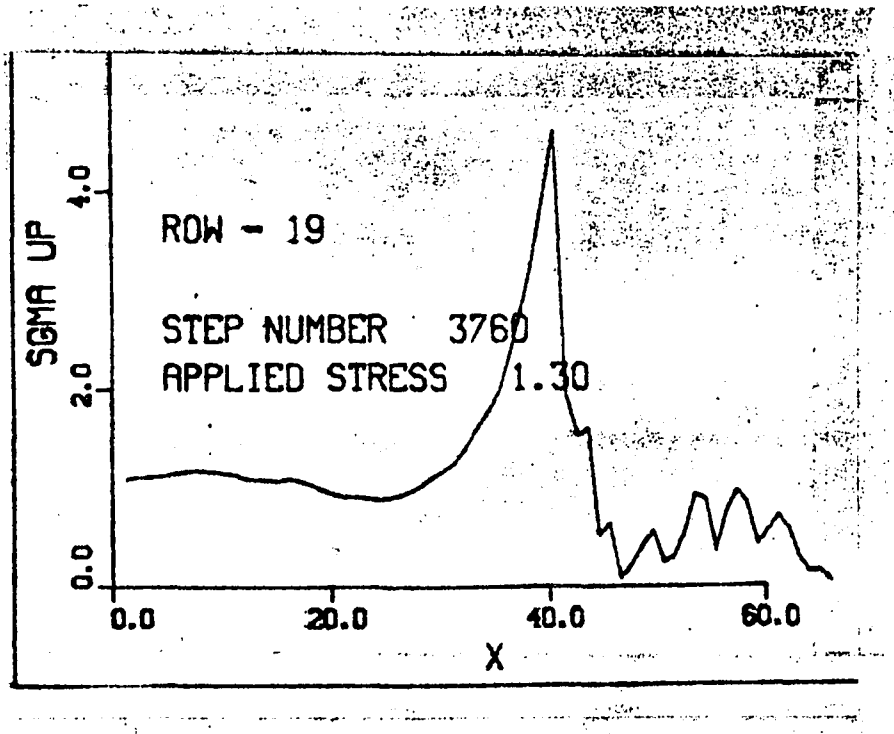

FIG. 3-127

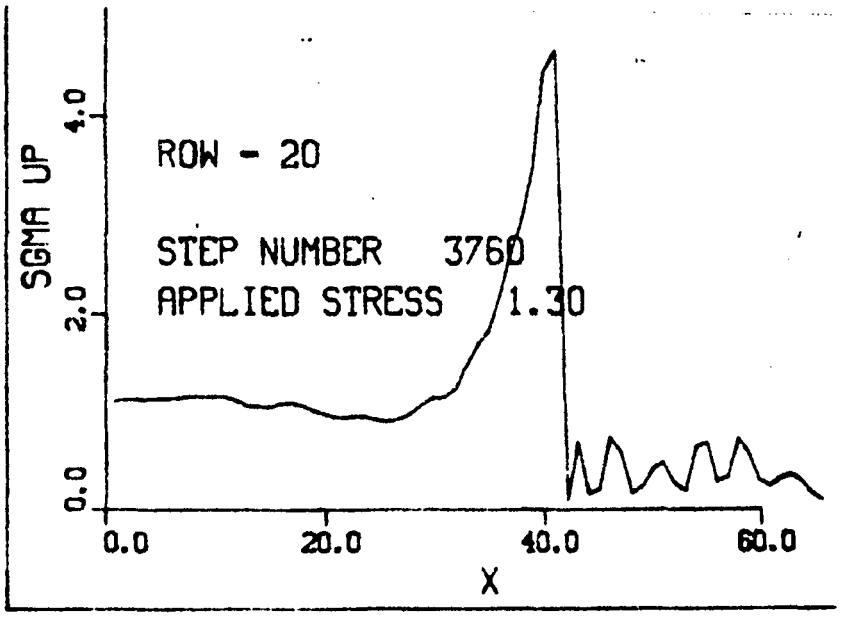

FIG. 3-128

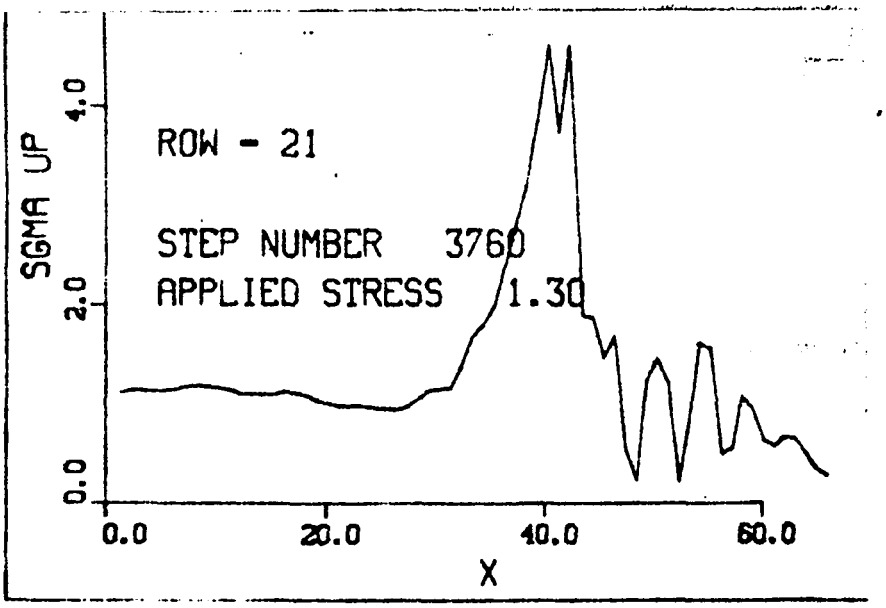

FIG. 3-129

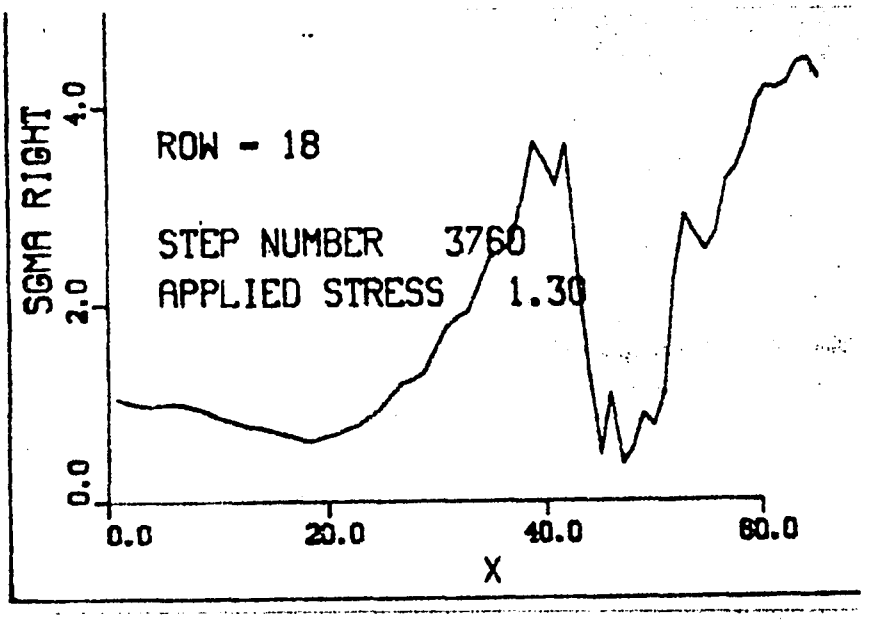

FIG. 3-130

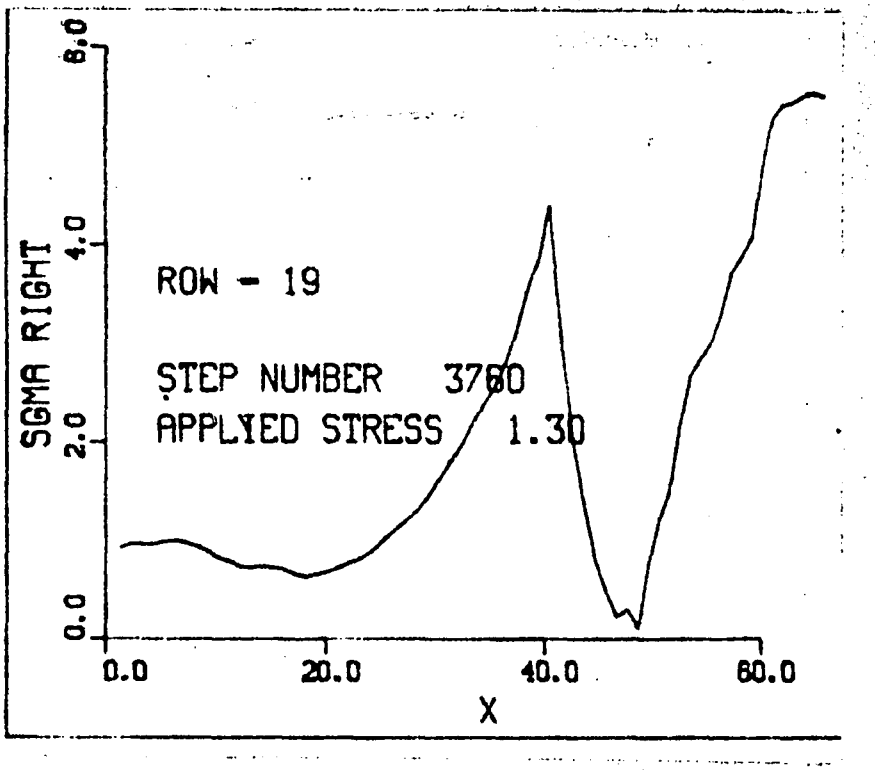

FIG. 3-131

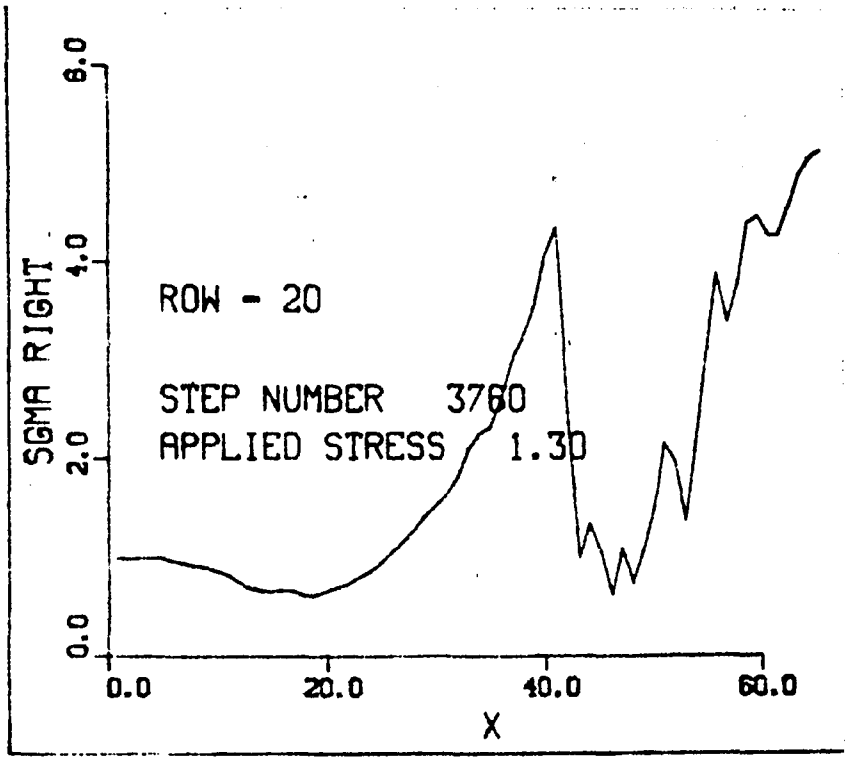

FIG. 3-132

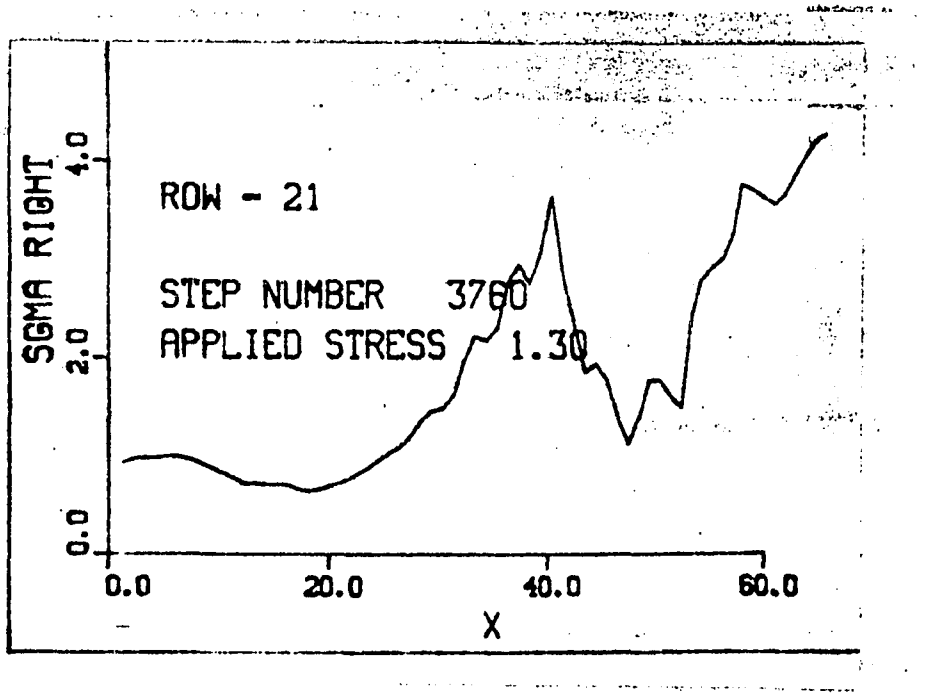

FIG. 3-133

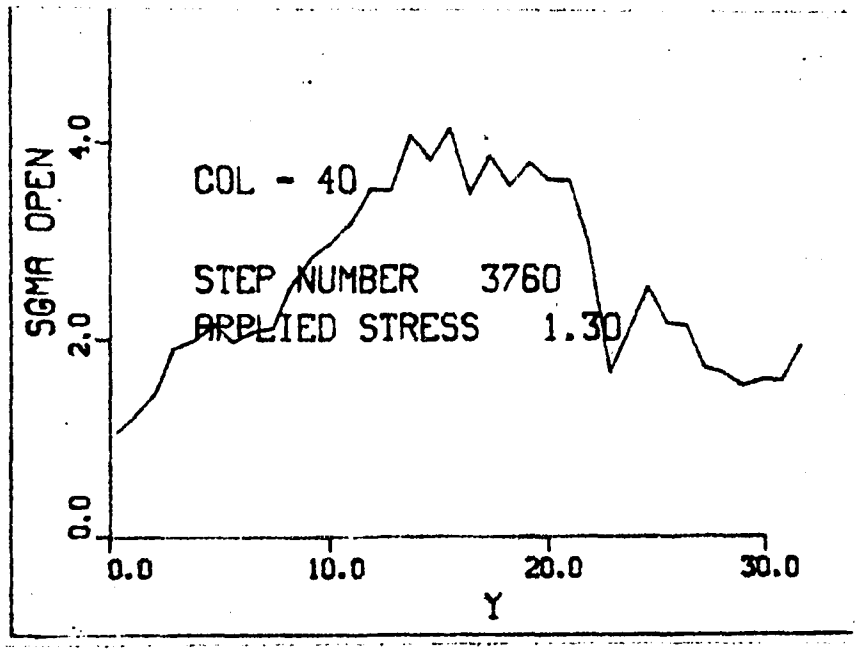

FIG. 3-134

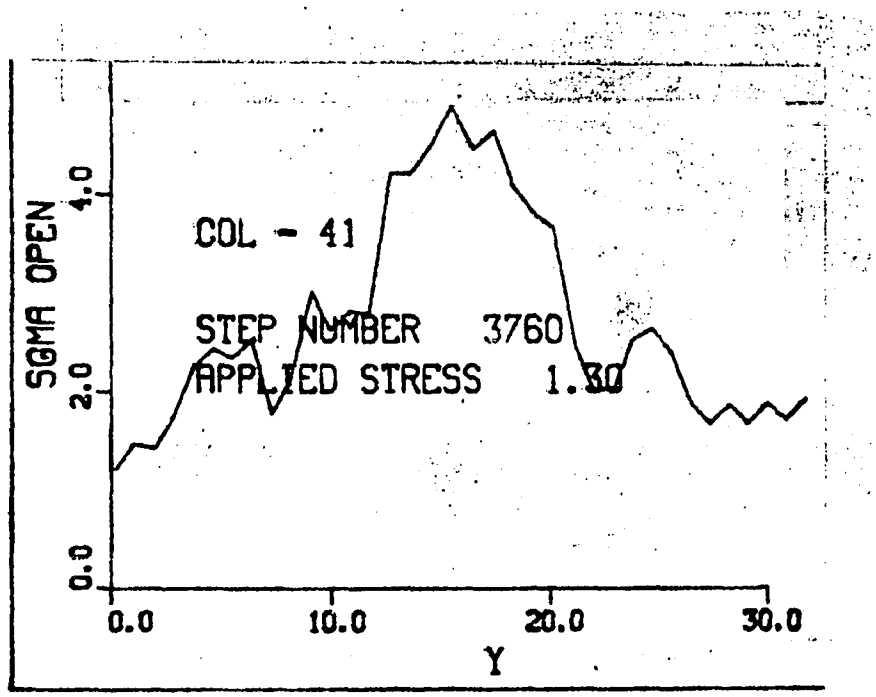

FIG. 3-135

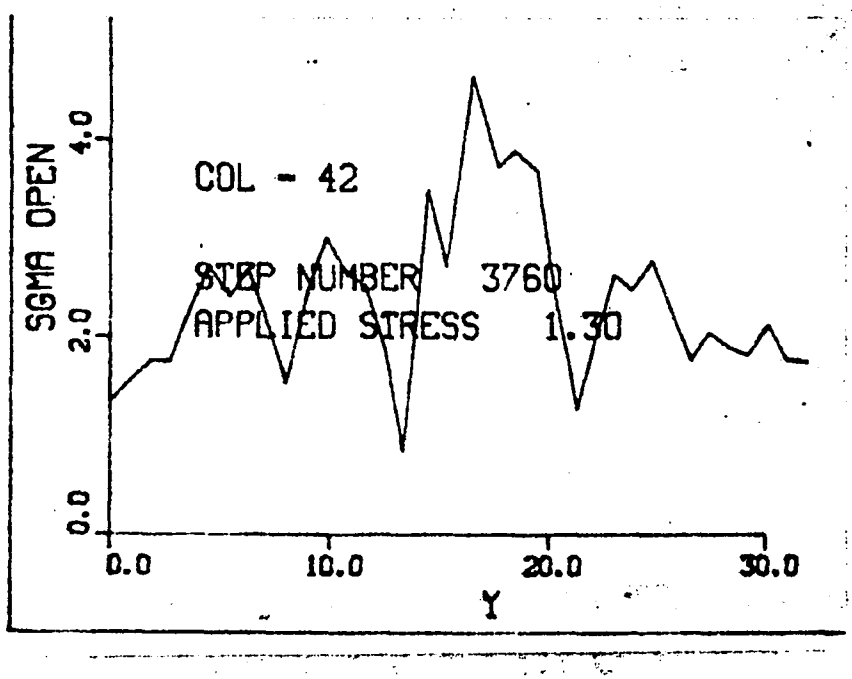

FIG. 3-136

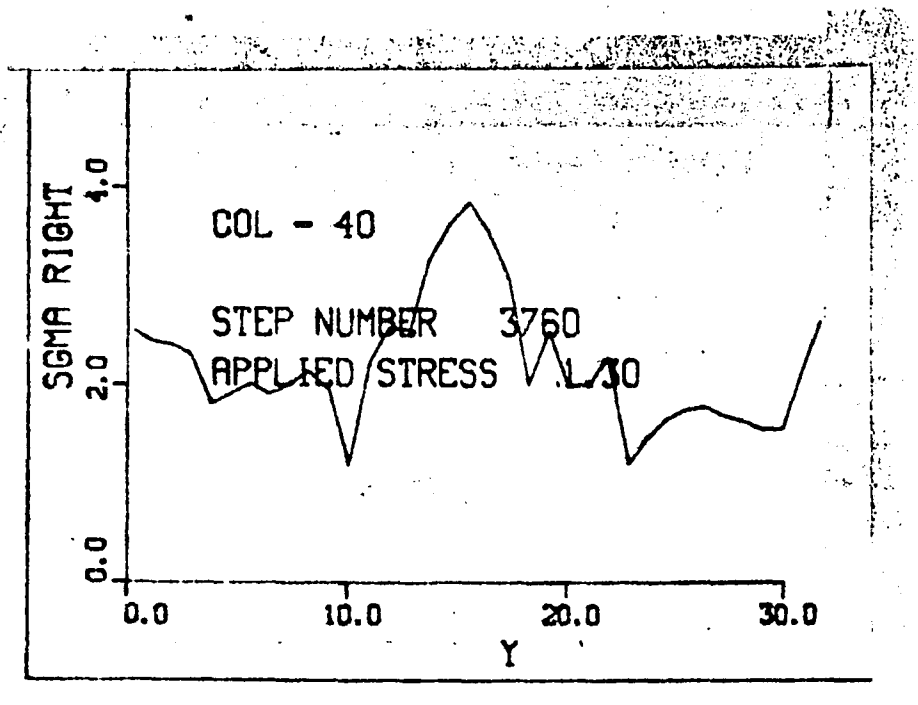

FIG. 3-137

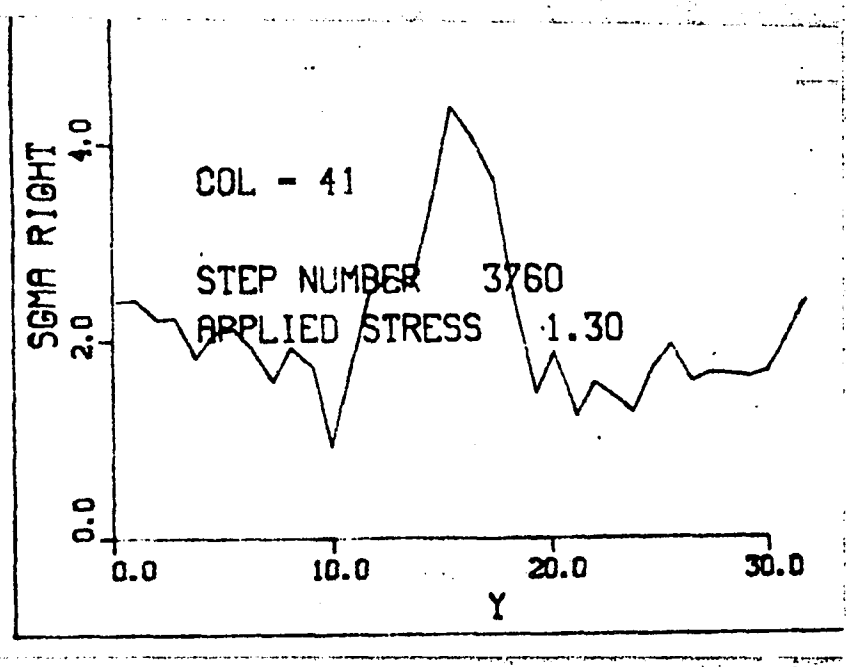

FIG. 3-138

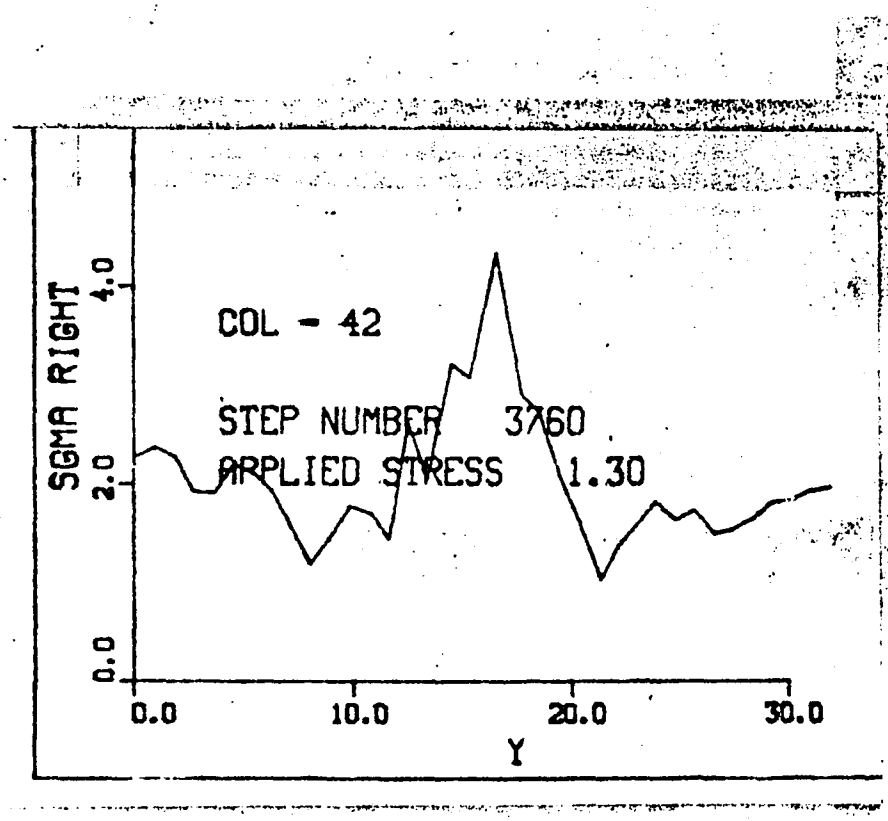

FIG. 3-139

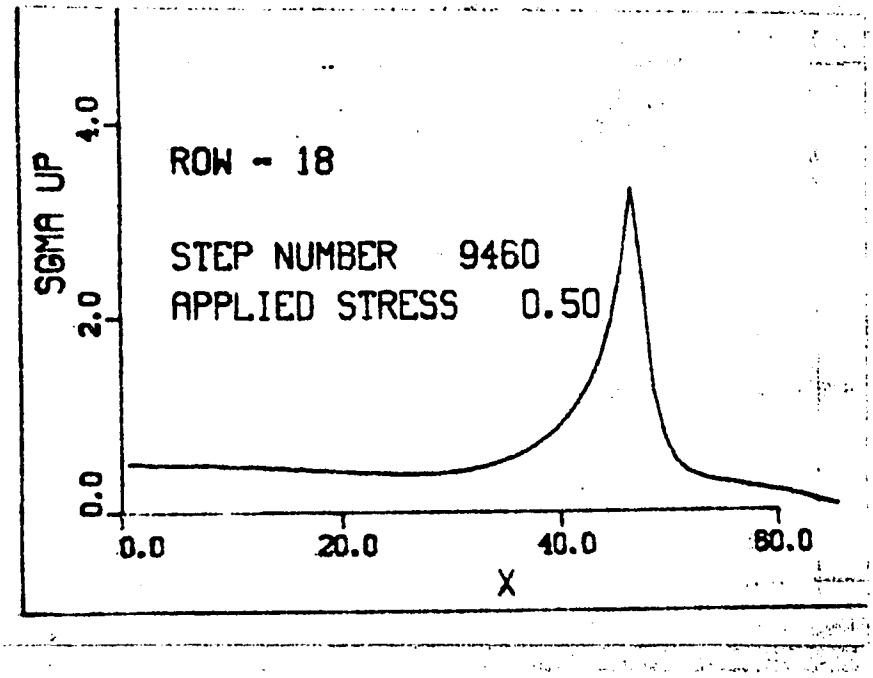

FIG. 3-140

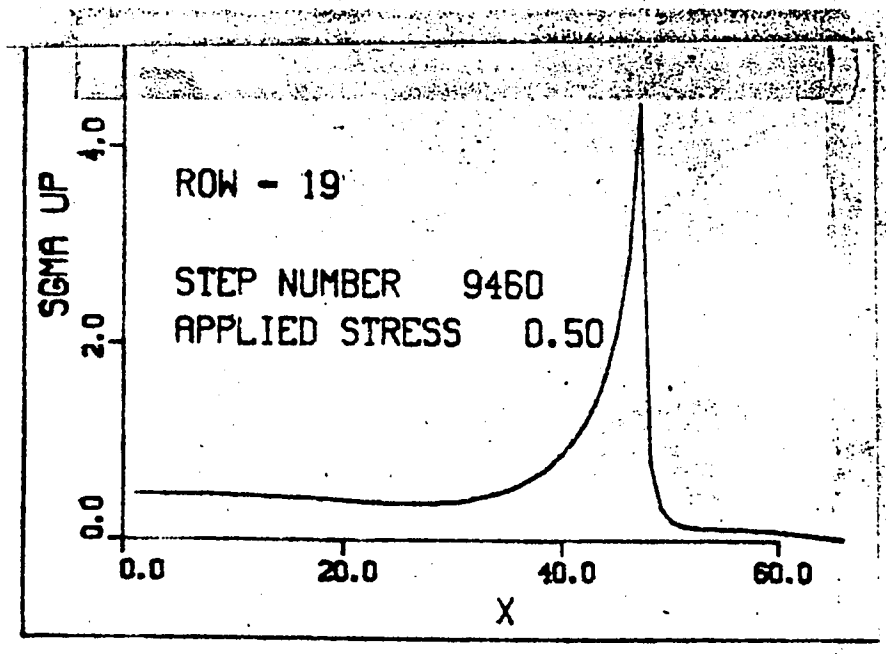

FIG. 3-141

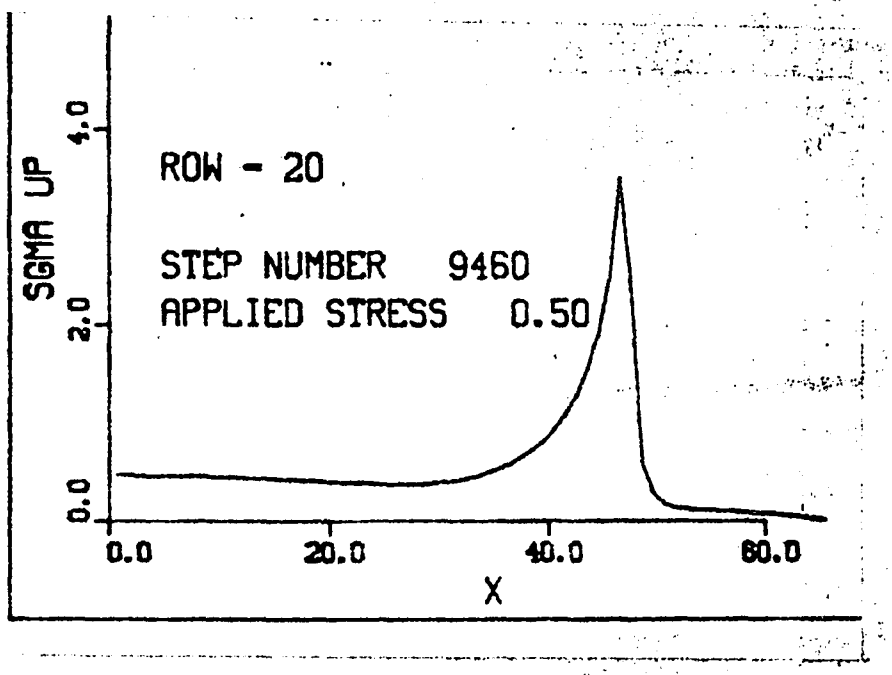

FIG. 3-142

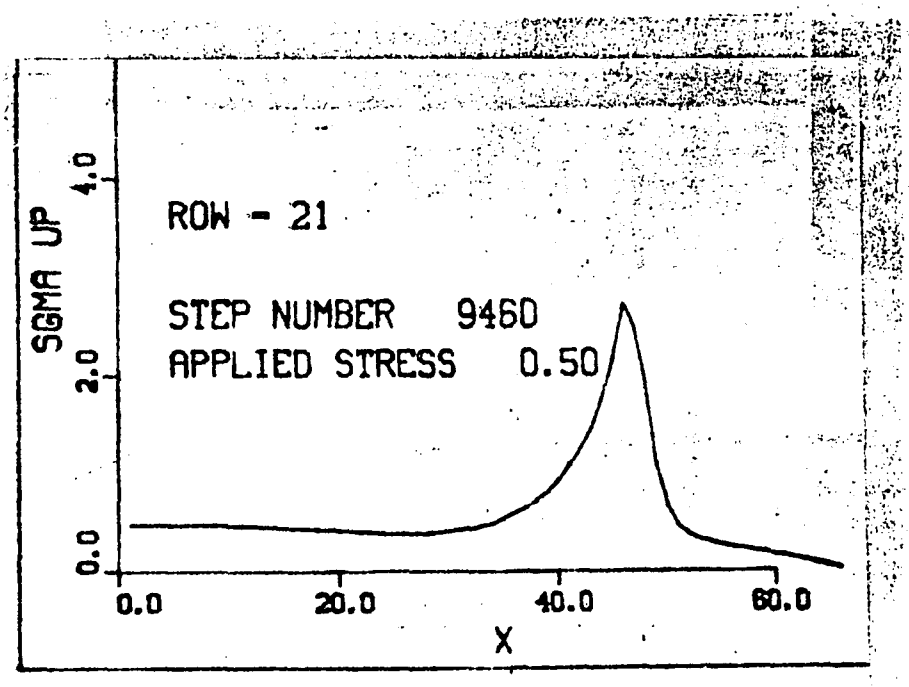

FIG. 3-143

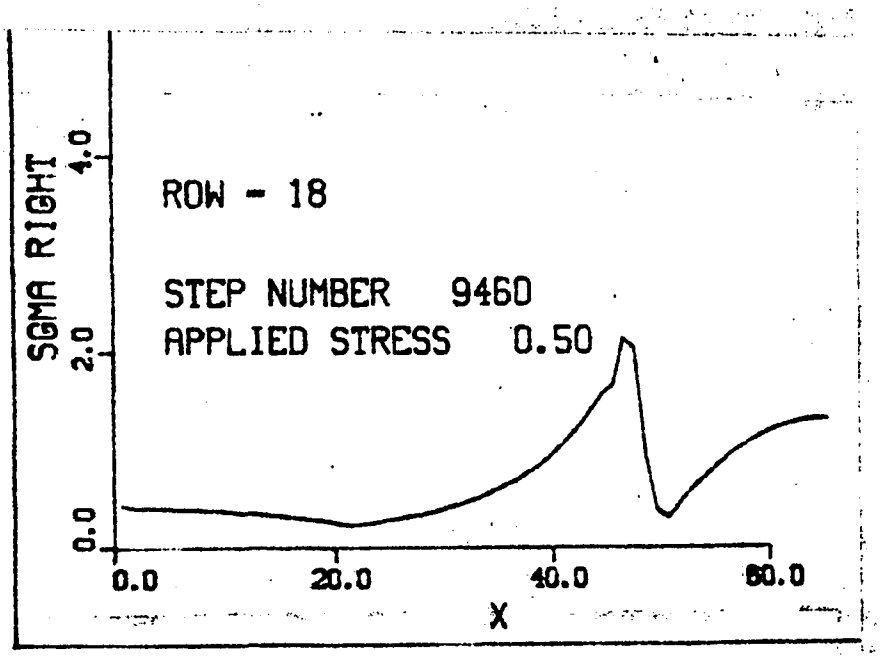

FIG. 3-144

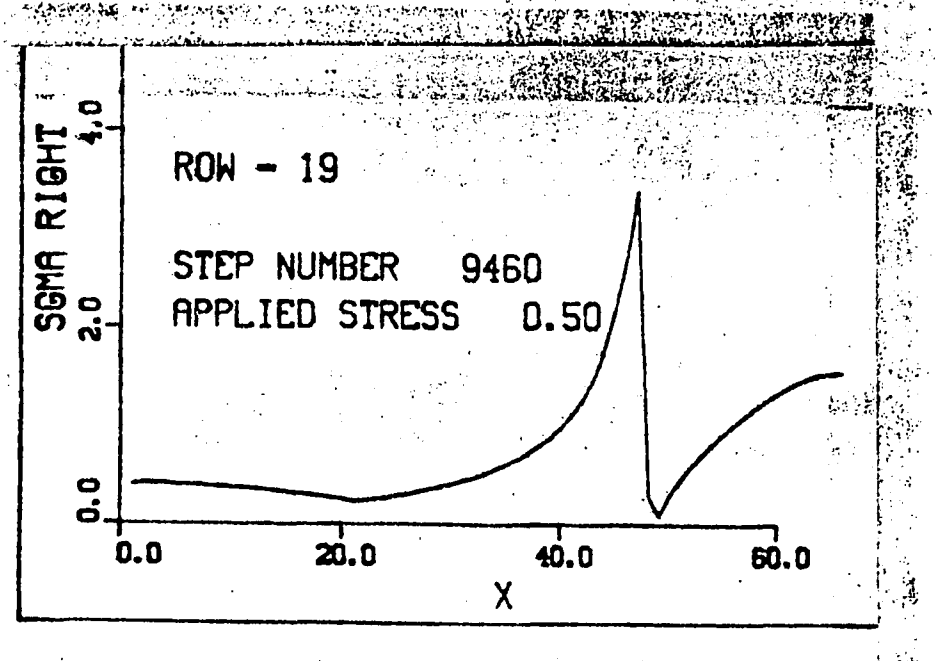

FIG. 3-145

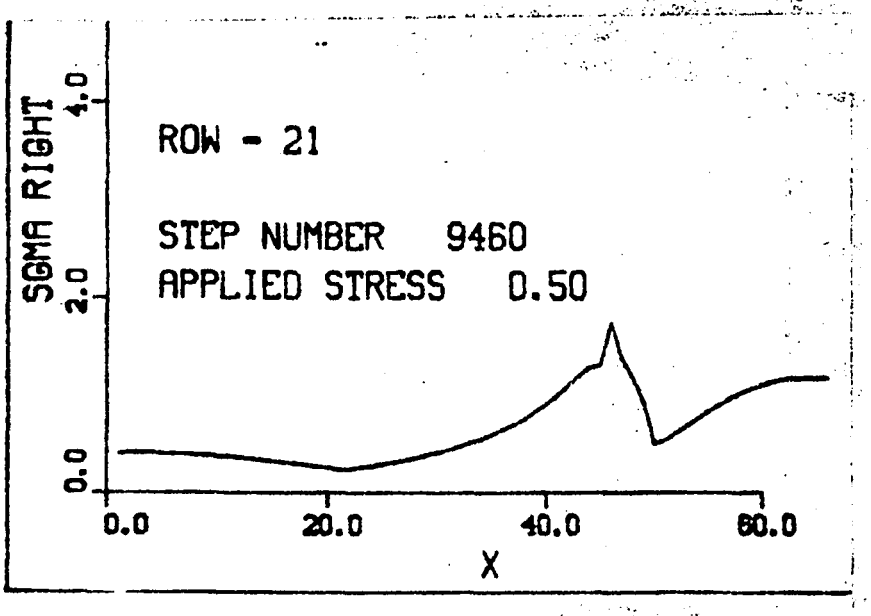

FIG. 3-146

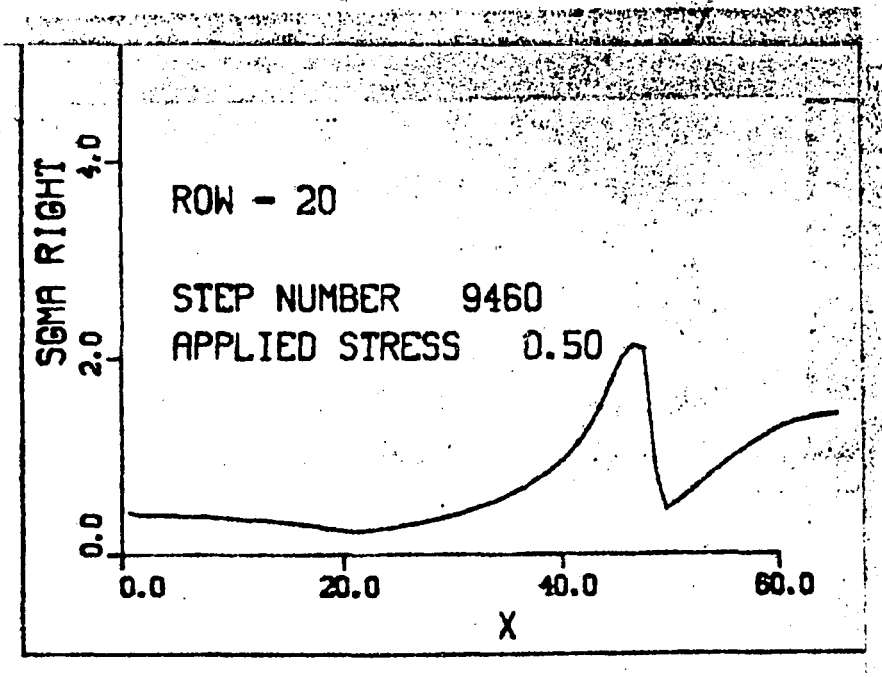

FIG. 3-147

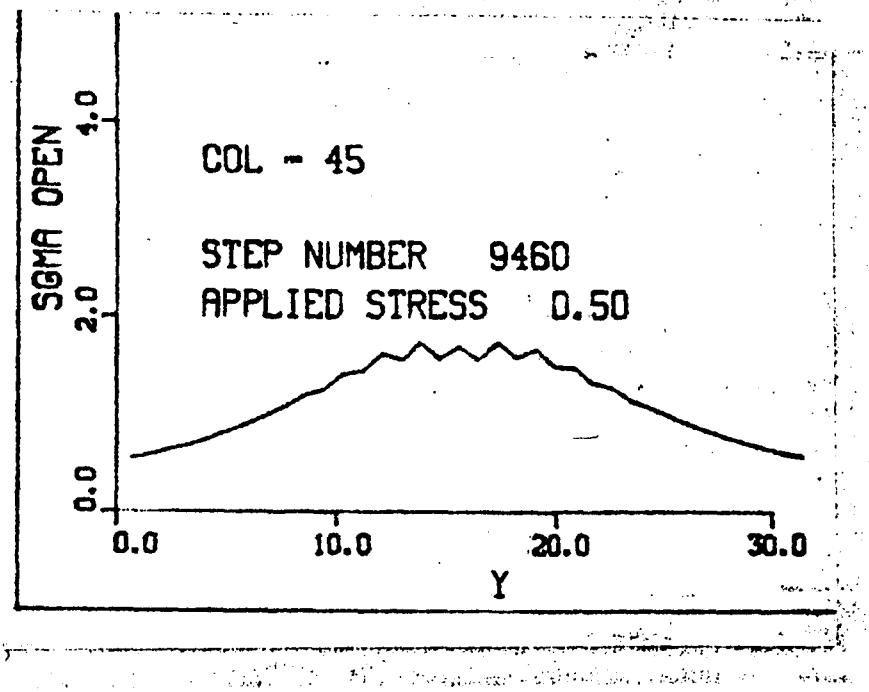

FIG. 3-148

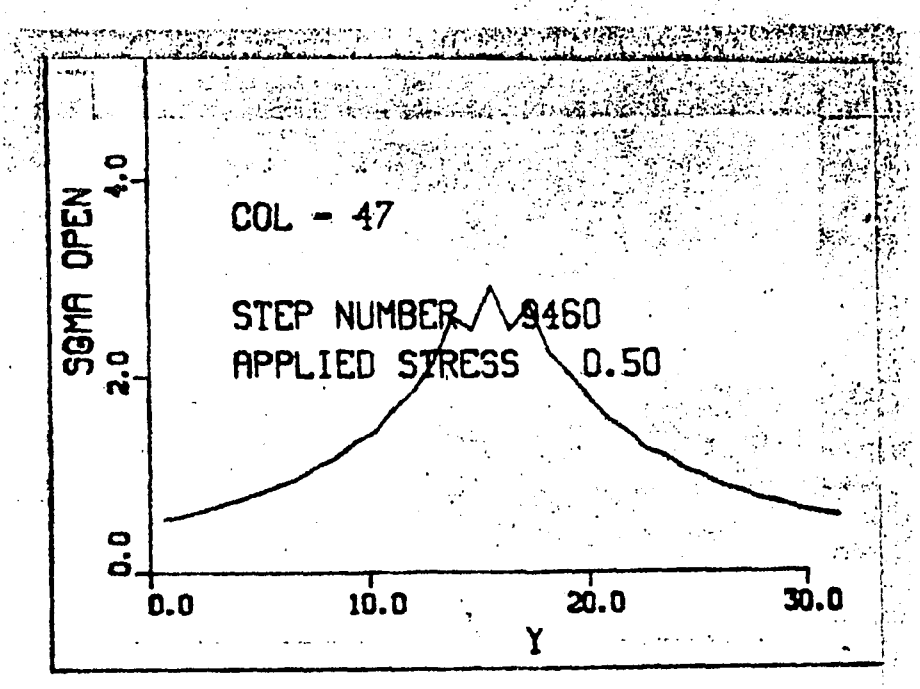

FIG. 3-149

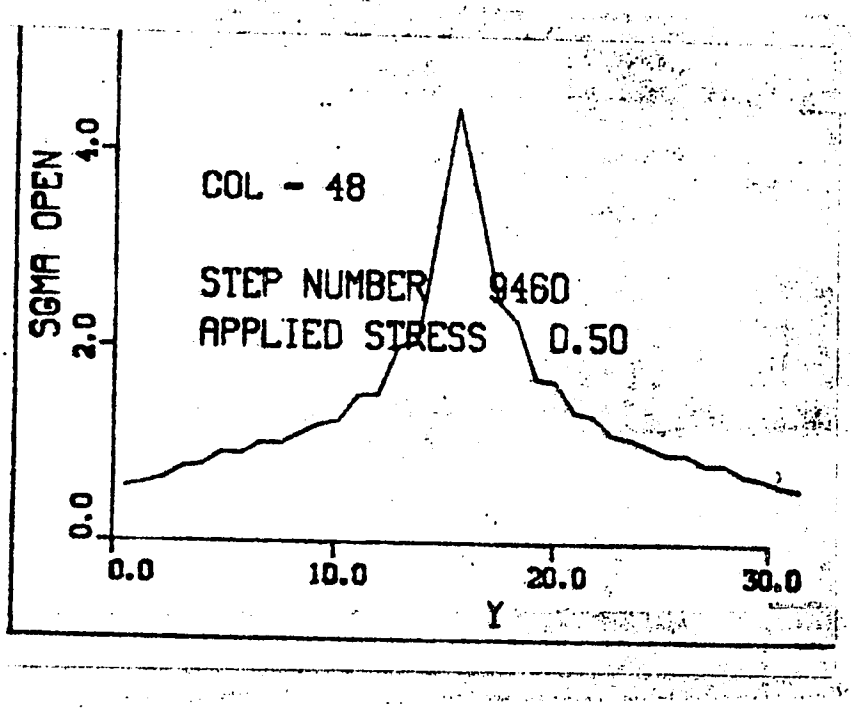

FIG. 3-150

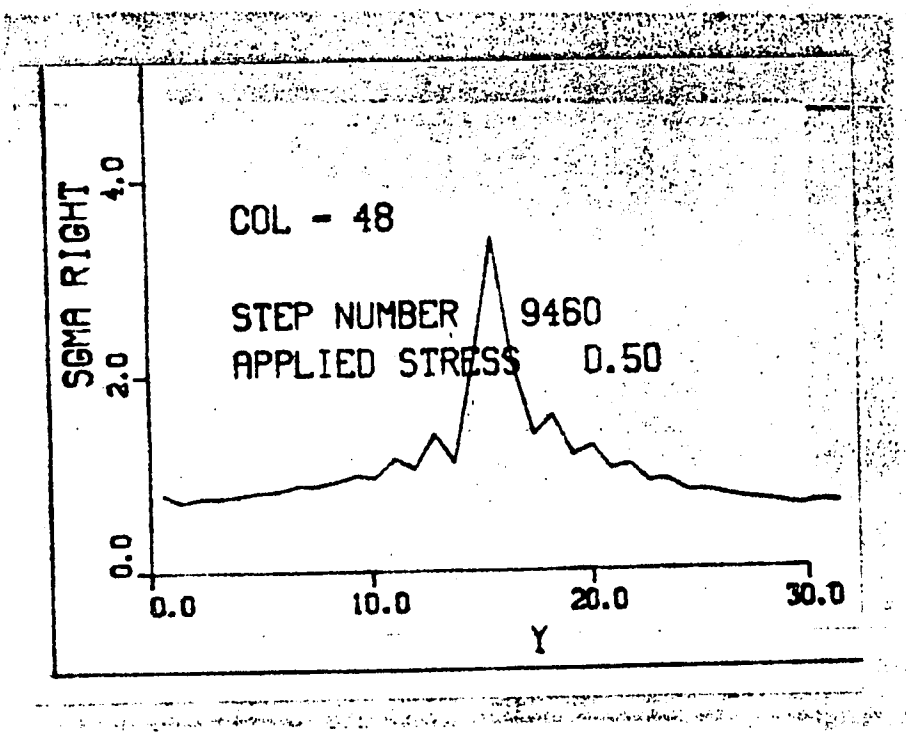

FIG. 3-151

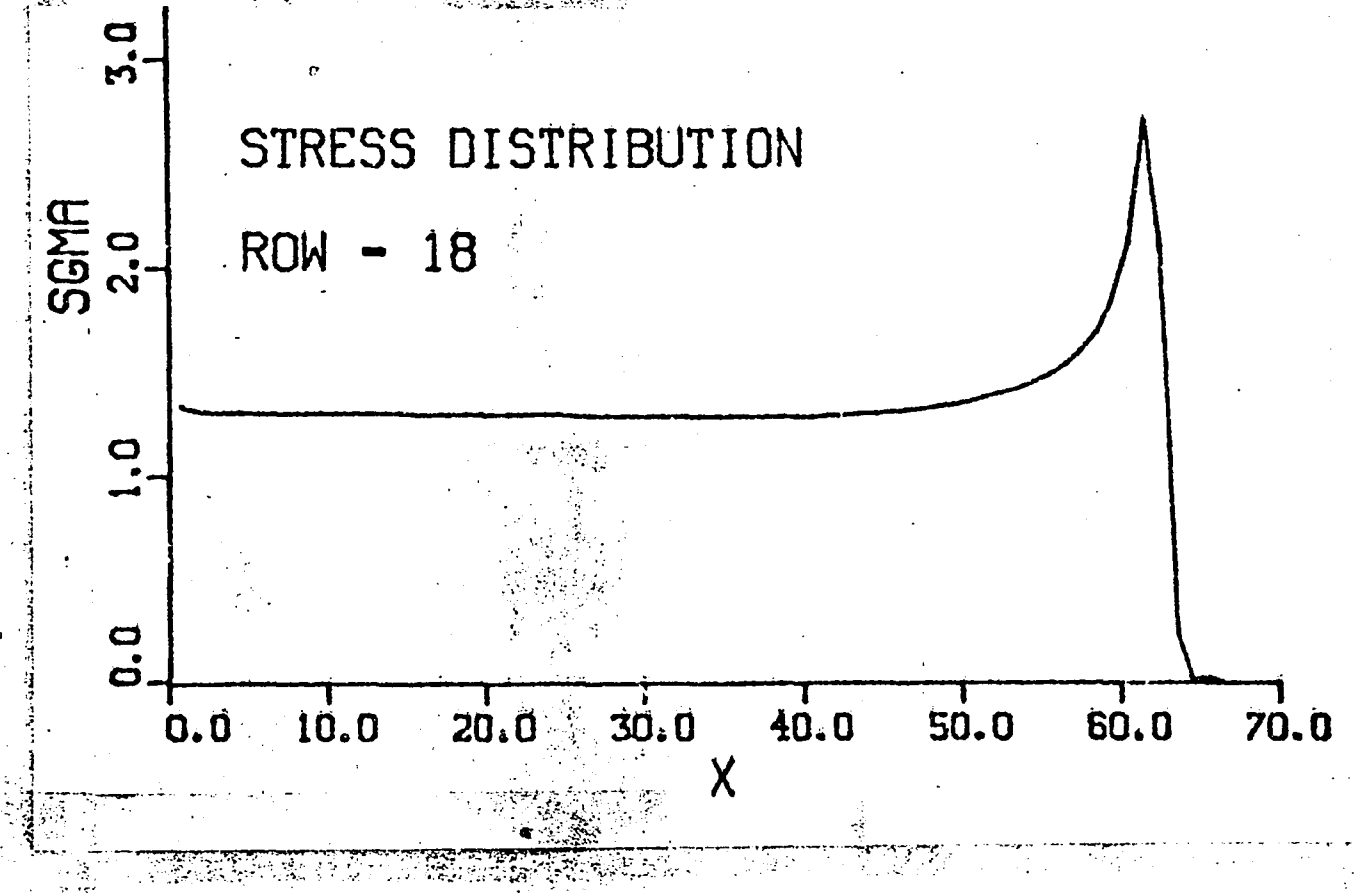
STRESS DISTRIBUTION
ROW - 18
SGMA
3.0
2.0
1.0
0.0
0.0
10.0
20.0
30.0
40.0
50.0
60.0
70.0
X

FIG. 3-152

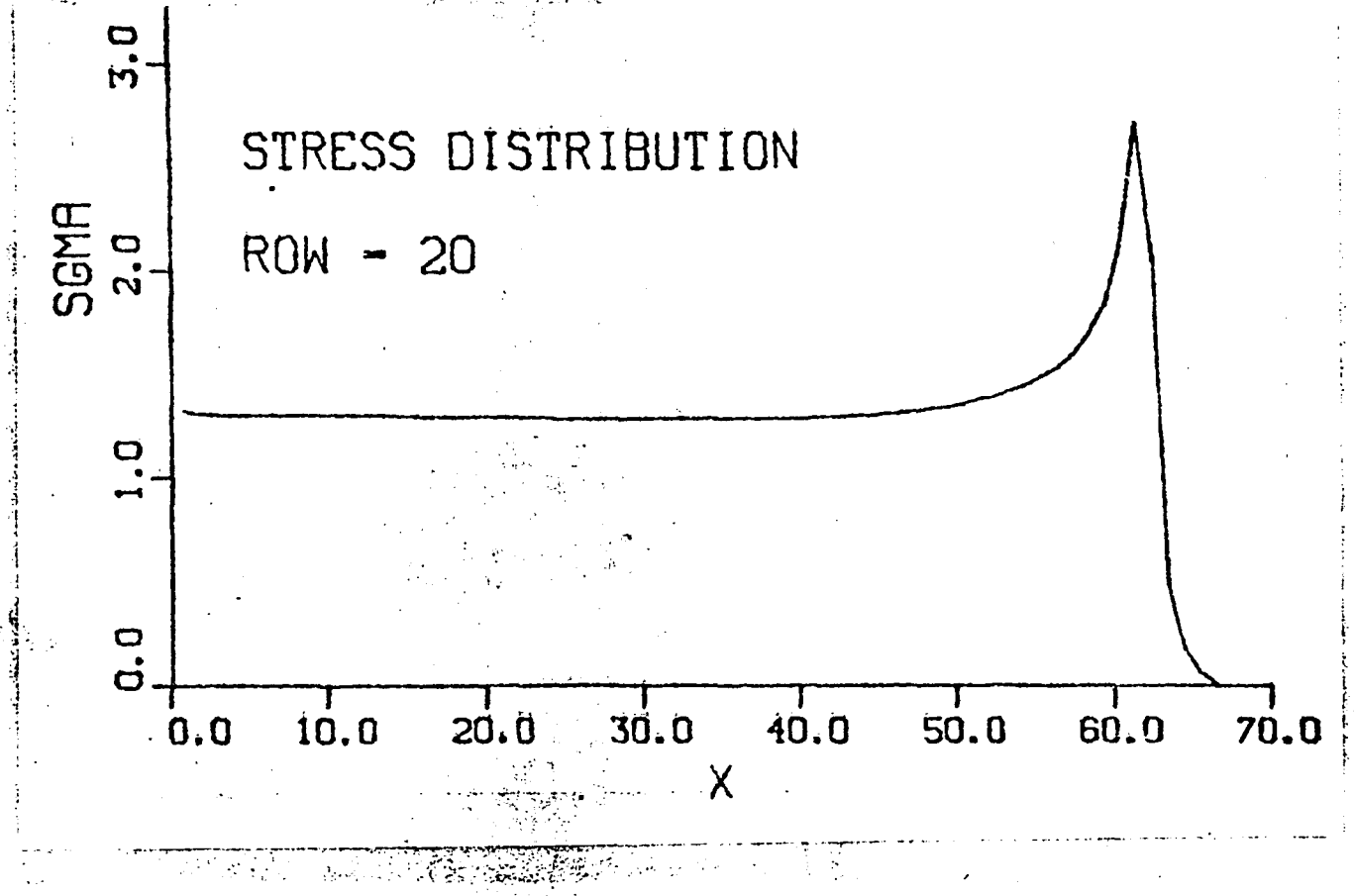
STRESS DISTRIBUTION
ROW - 20
SGMA
3.0
2.0
1.0
0.0
0.0
10.0
20.0
30.0
40.0
50.0
60.0
70.0
X

FIG. 3-153

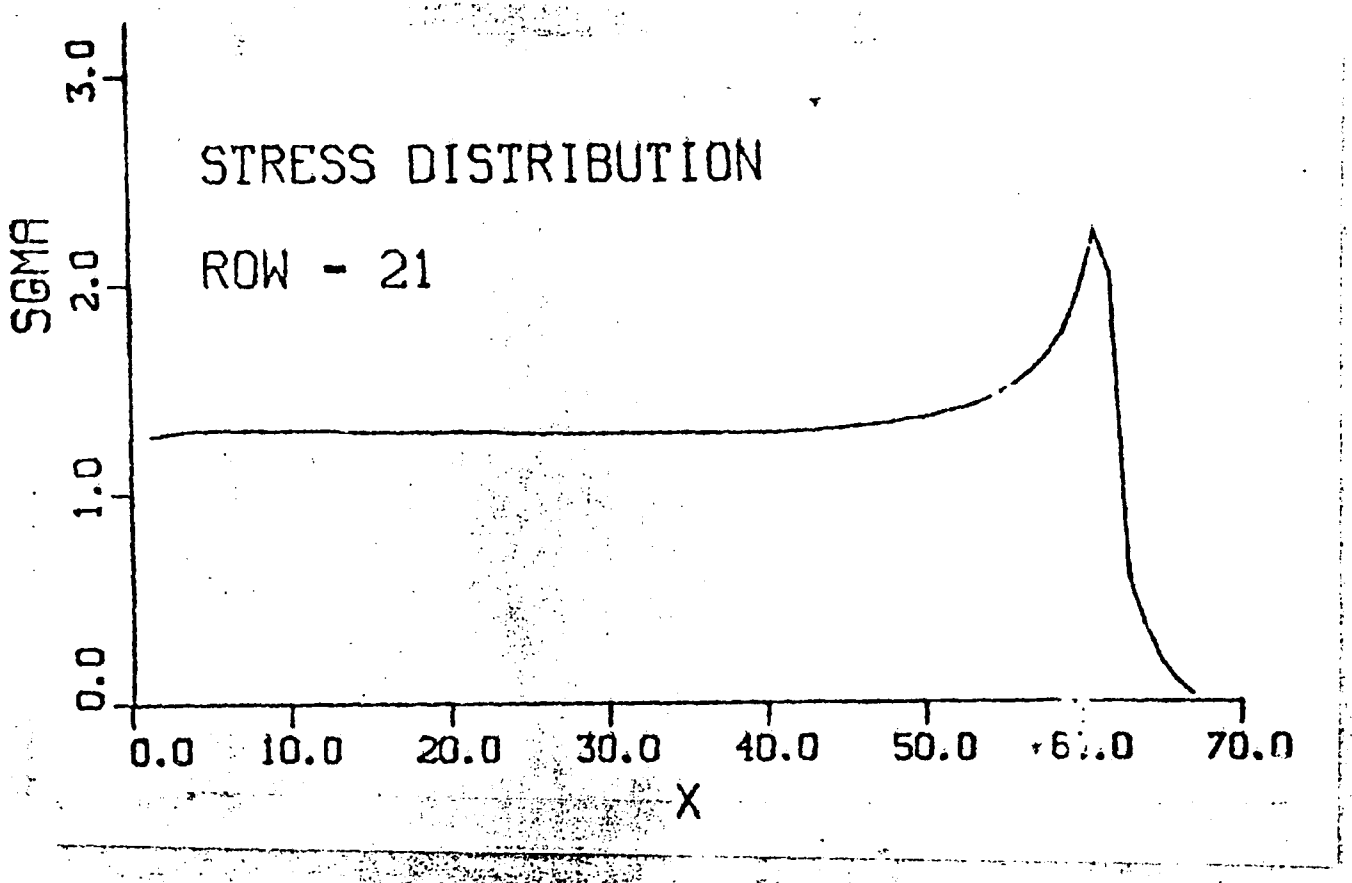
STRESS DISTRIBUTION
ROW - 21
SGMA
3.0
2.0
1.0
0.0
0.0
10.0
20.0
30.0
40.0
50.0
70.0
X

FIG. 3-154

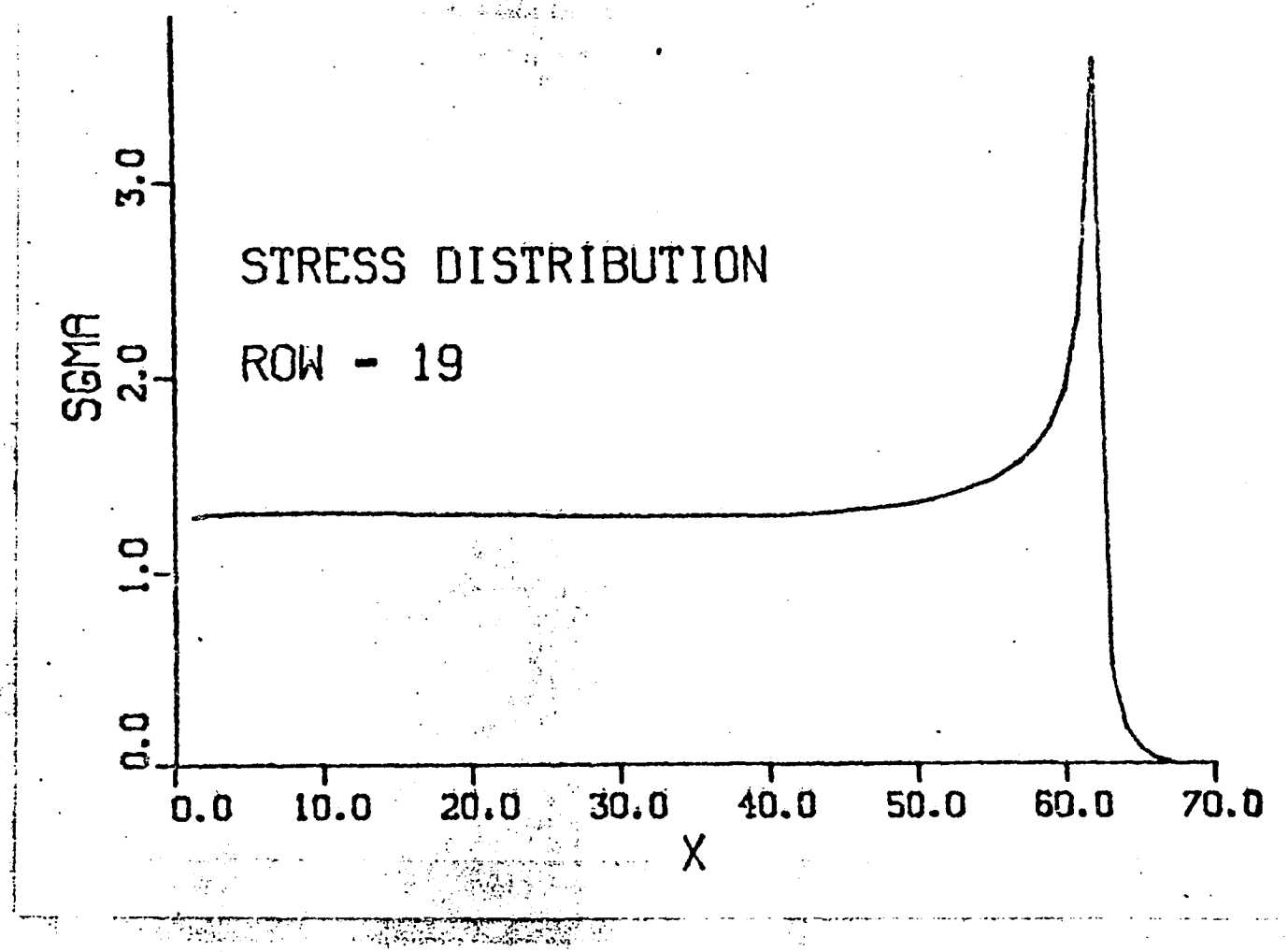
STRESS DISTRIBUTION
ROW - 19
SGMA
3.0
2.0
1.0
0.0
0.0
10.0
20.0
30.0
40.0
50.0
60.0
70.0
X

FIG. 3-155

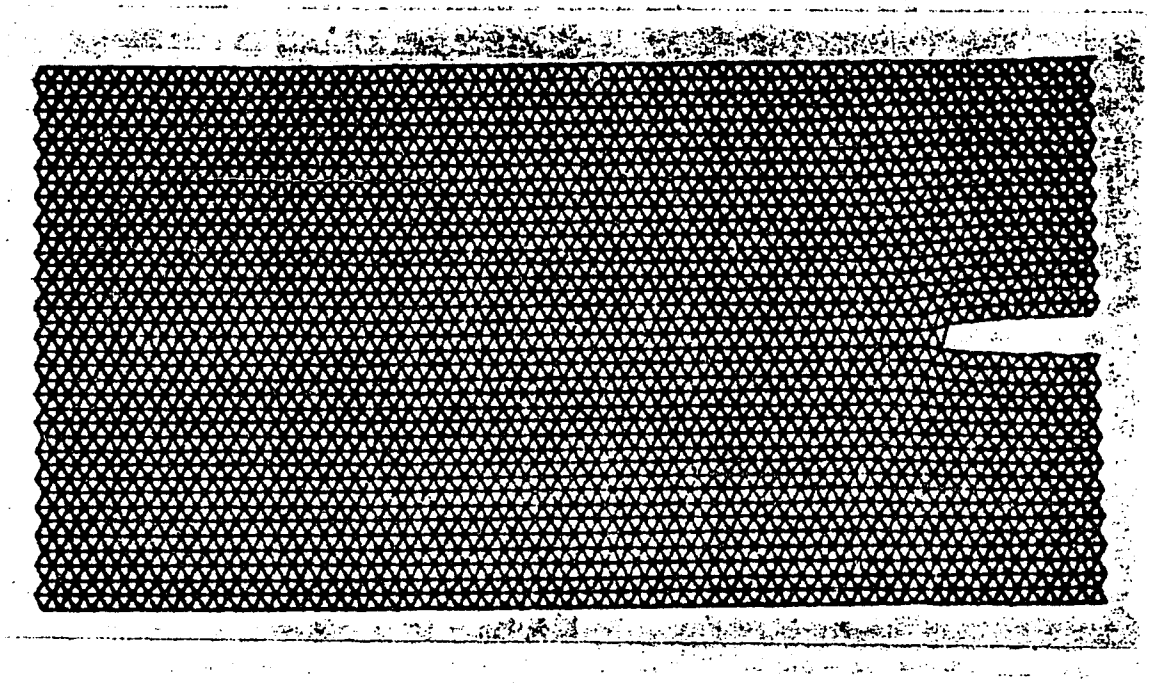

7100

FIG. 3-159

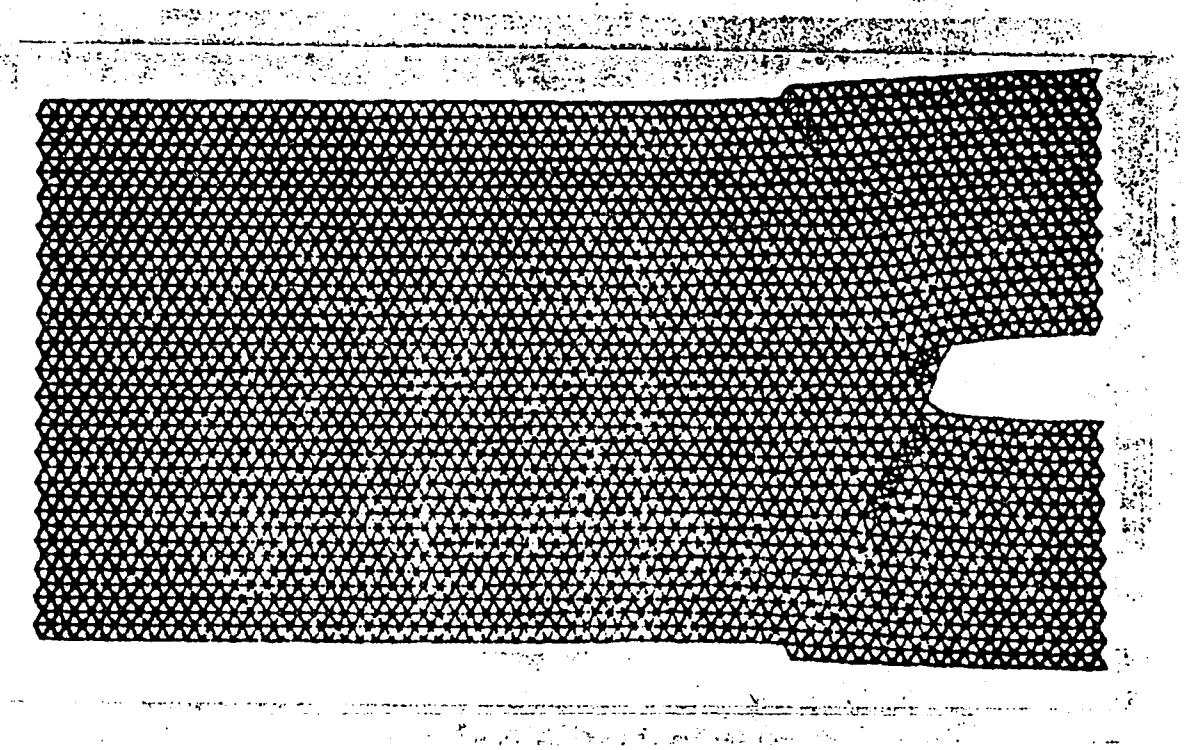

7500

FIG. 3-160

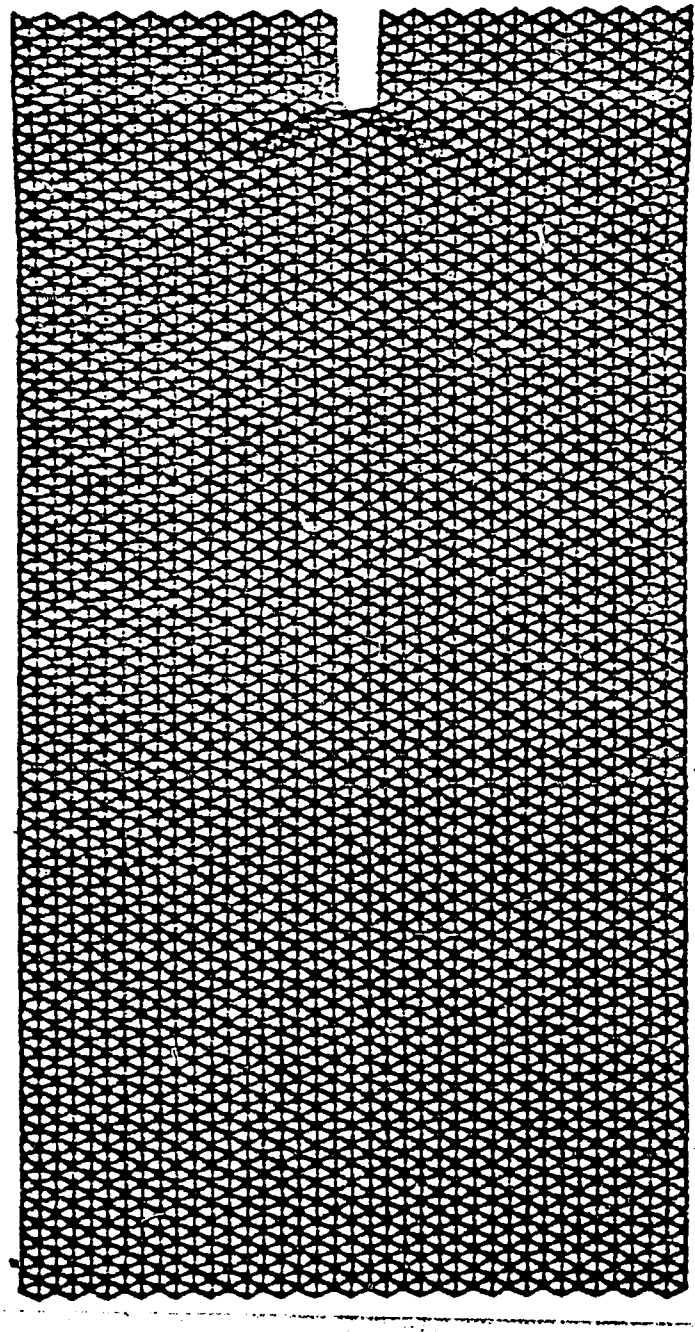

7200

FIG. 3-161

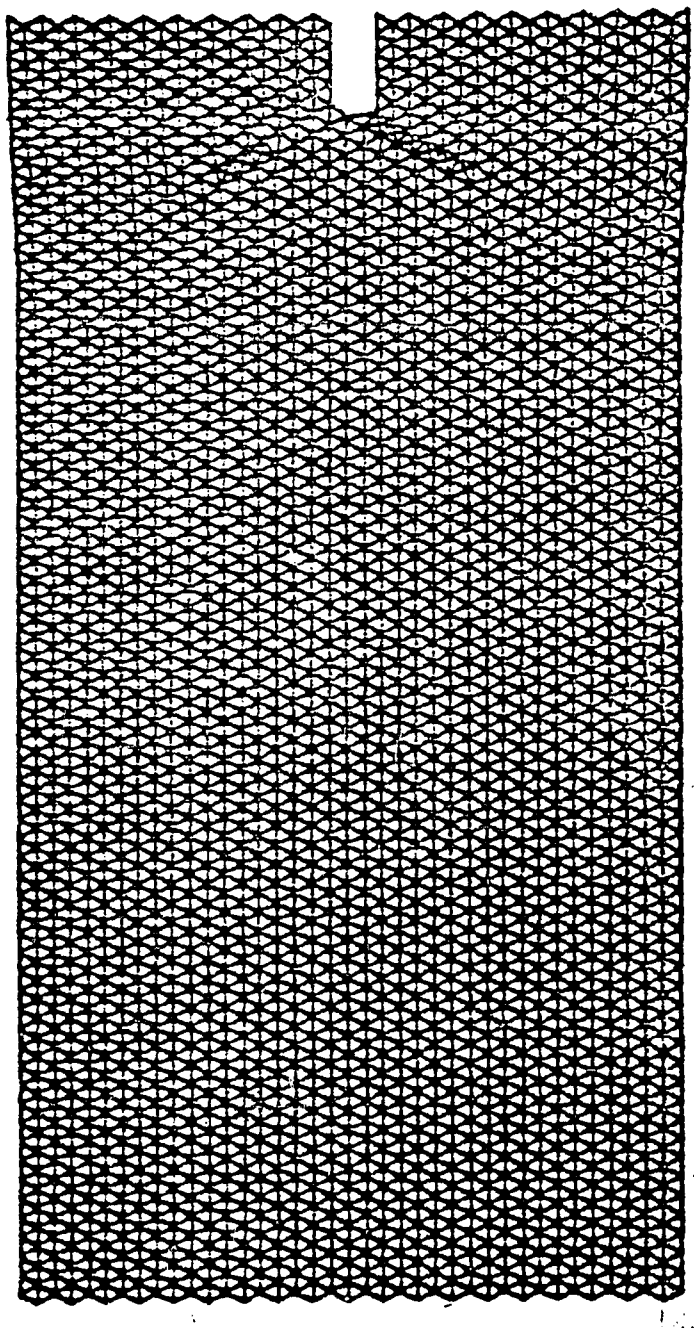

7250

FIG. 3-162

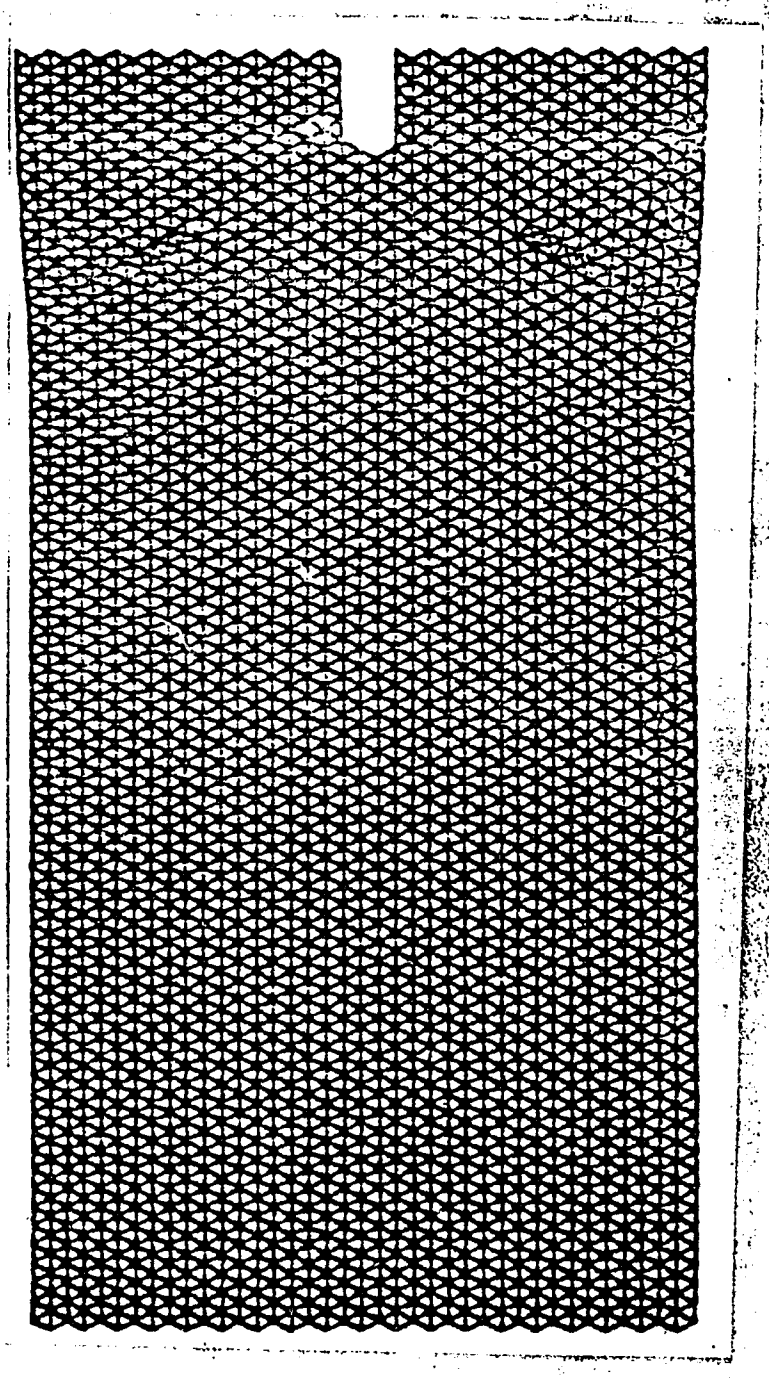

7350

FIG. 3-163

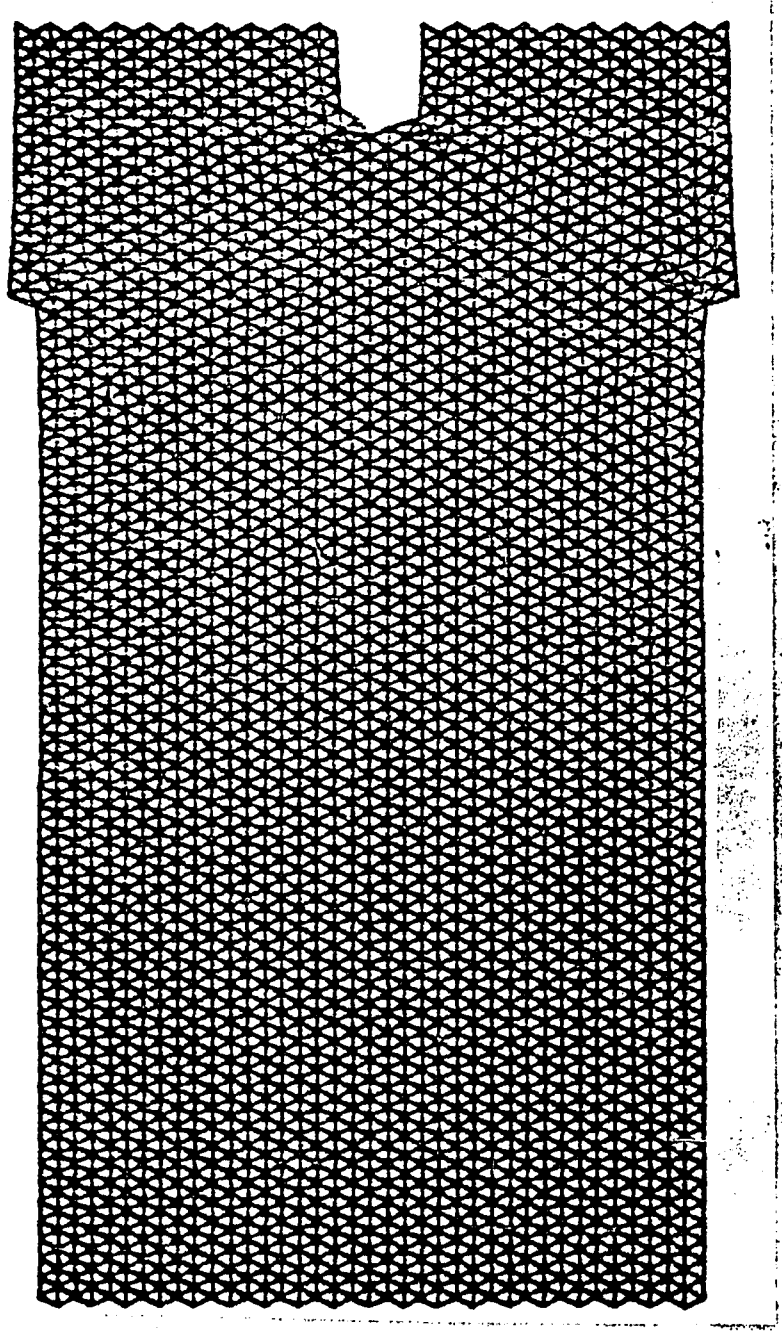

7550

FIG. 3-164

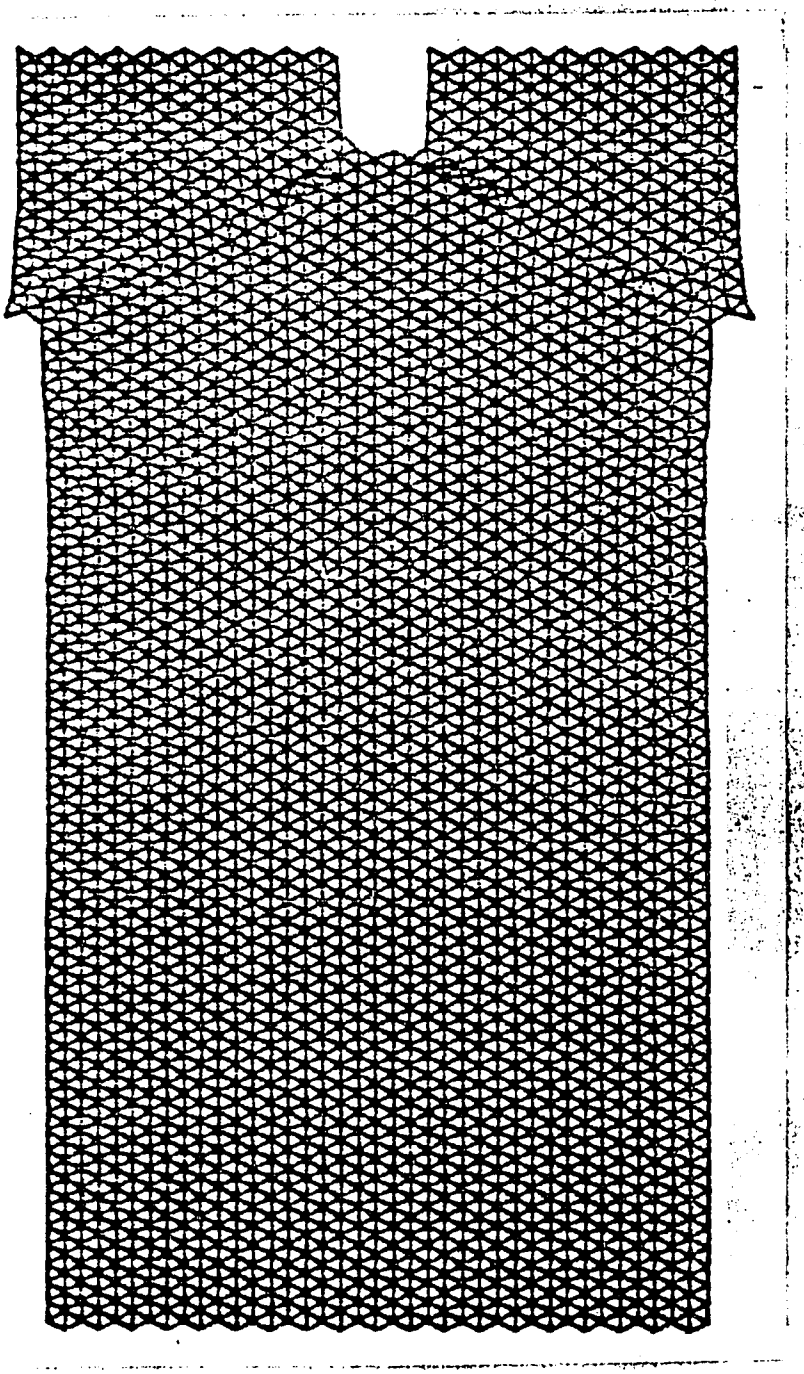

7600

FIG. 3-165

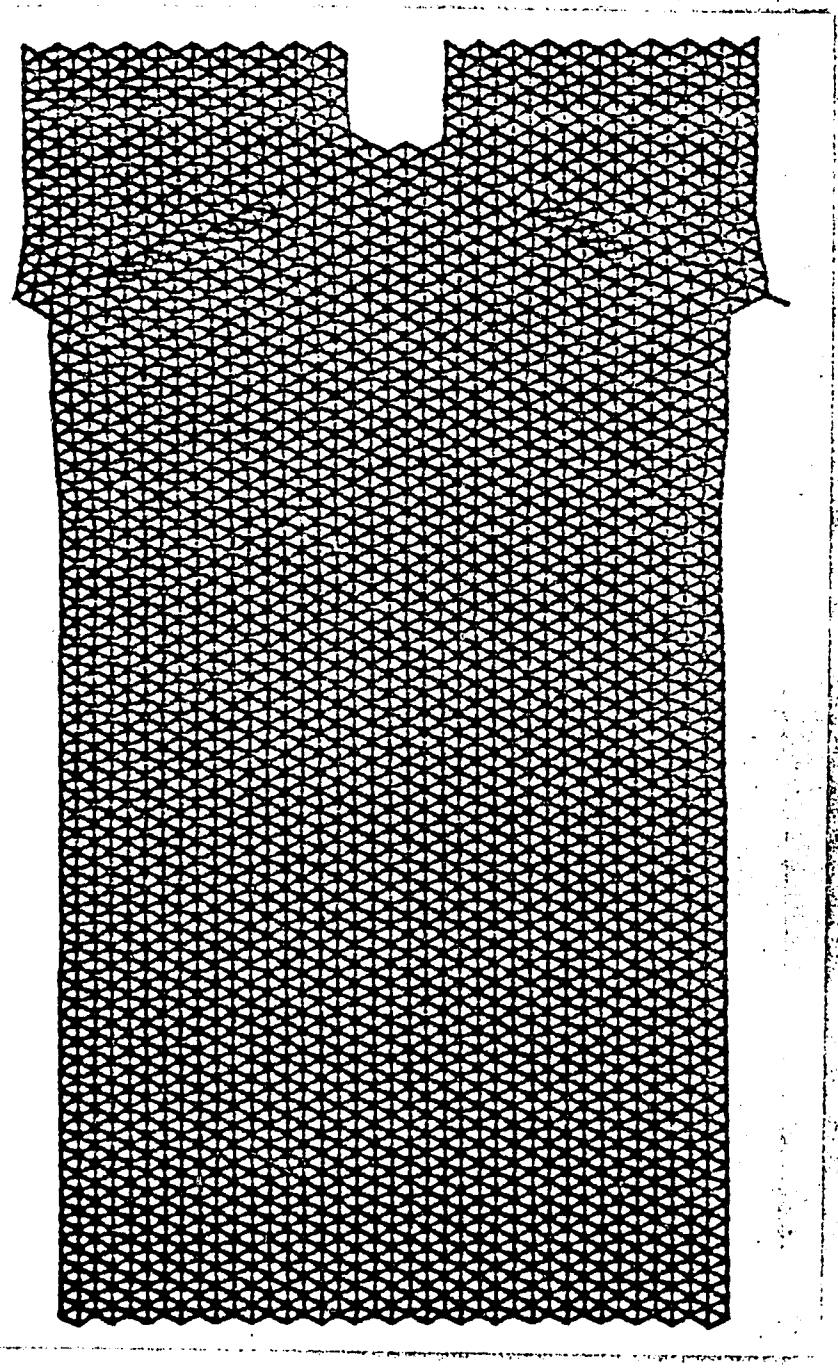

7650

FIG. 3-166

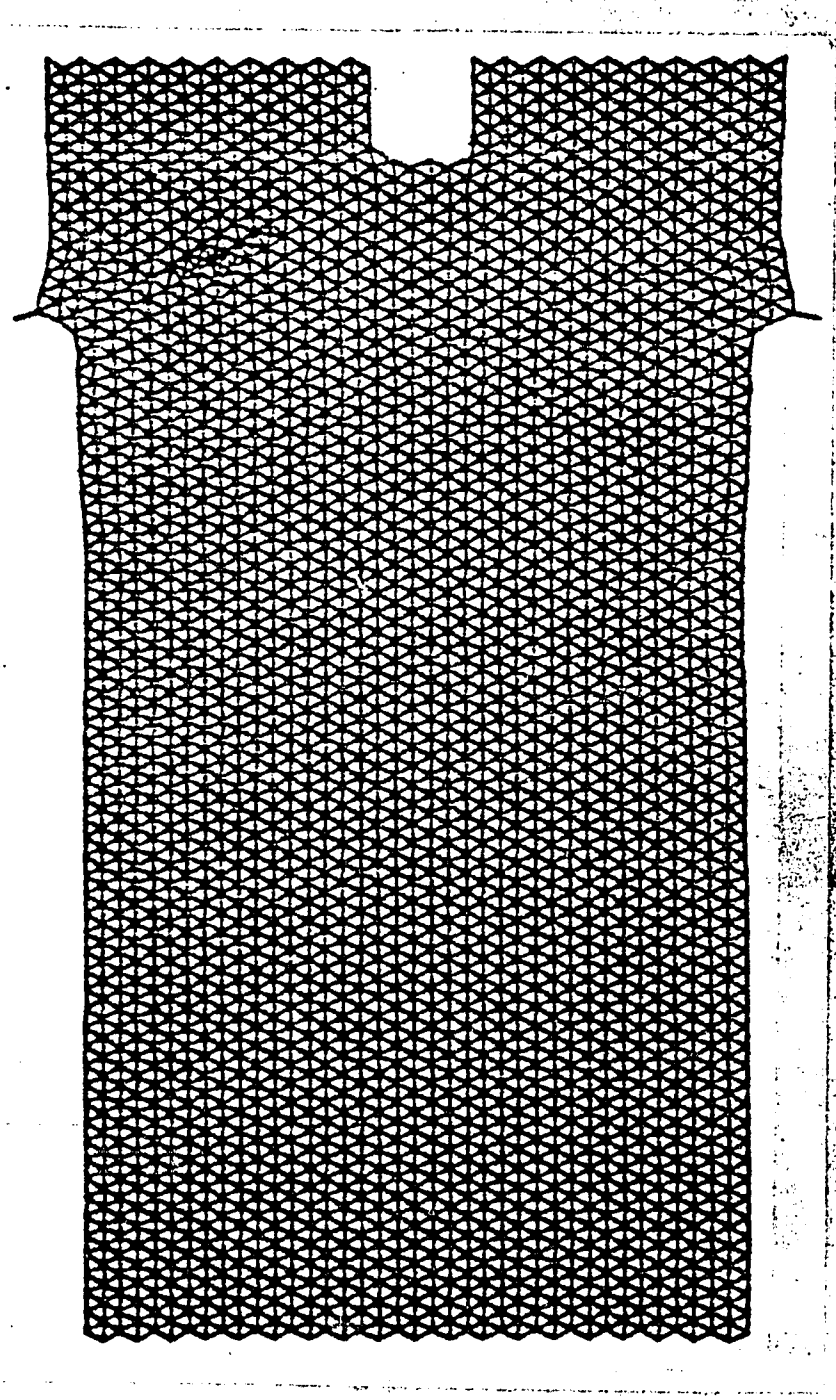

FIG. 3-167

7675

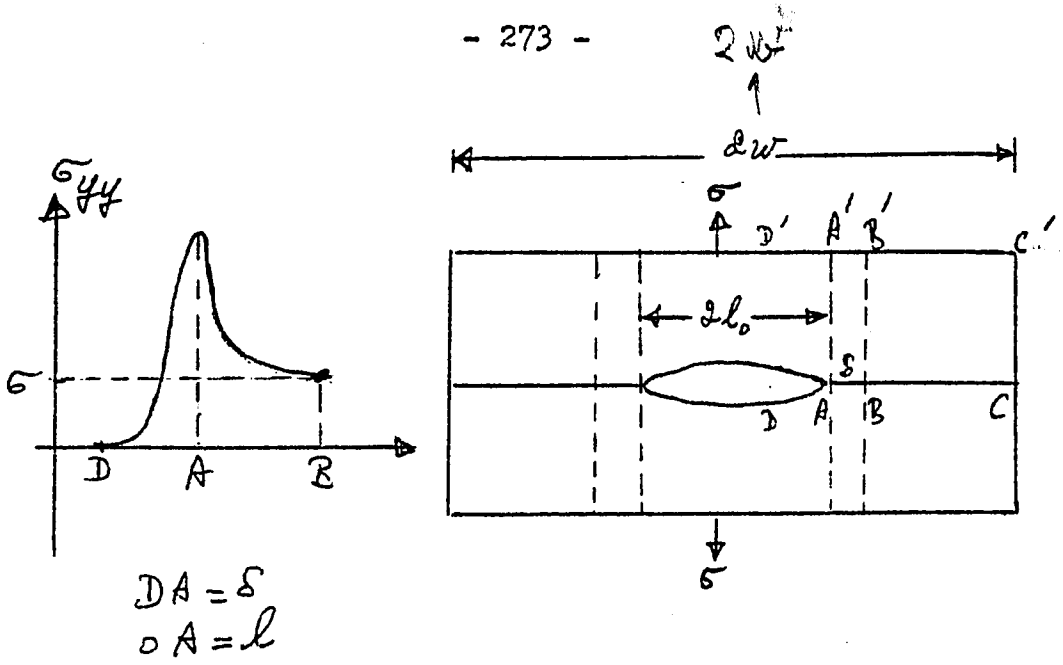

(a) (b)

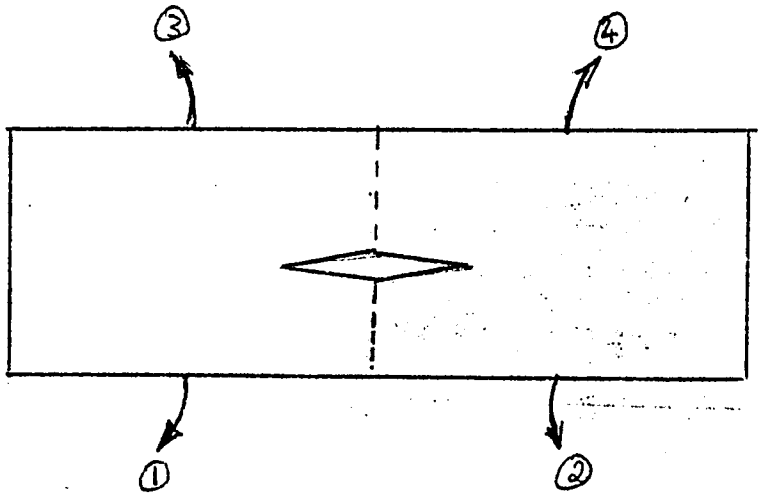

(c)

NOTE: In figure 168(c), rotations (1) & (3) are not compatible with (2) & (4) when the crack is an internal one as in (c). If the crack is on the external side of the sample(as will happen if the right side of the sample is absent) the rotations are allowable and a rigid tearing mode can occur with a finite speed.

FIG. 3-168

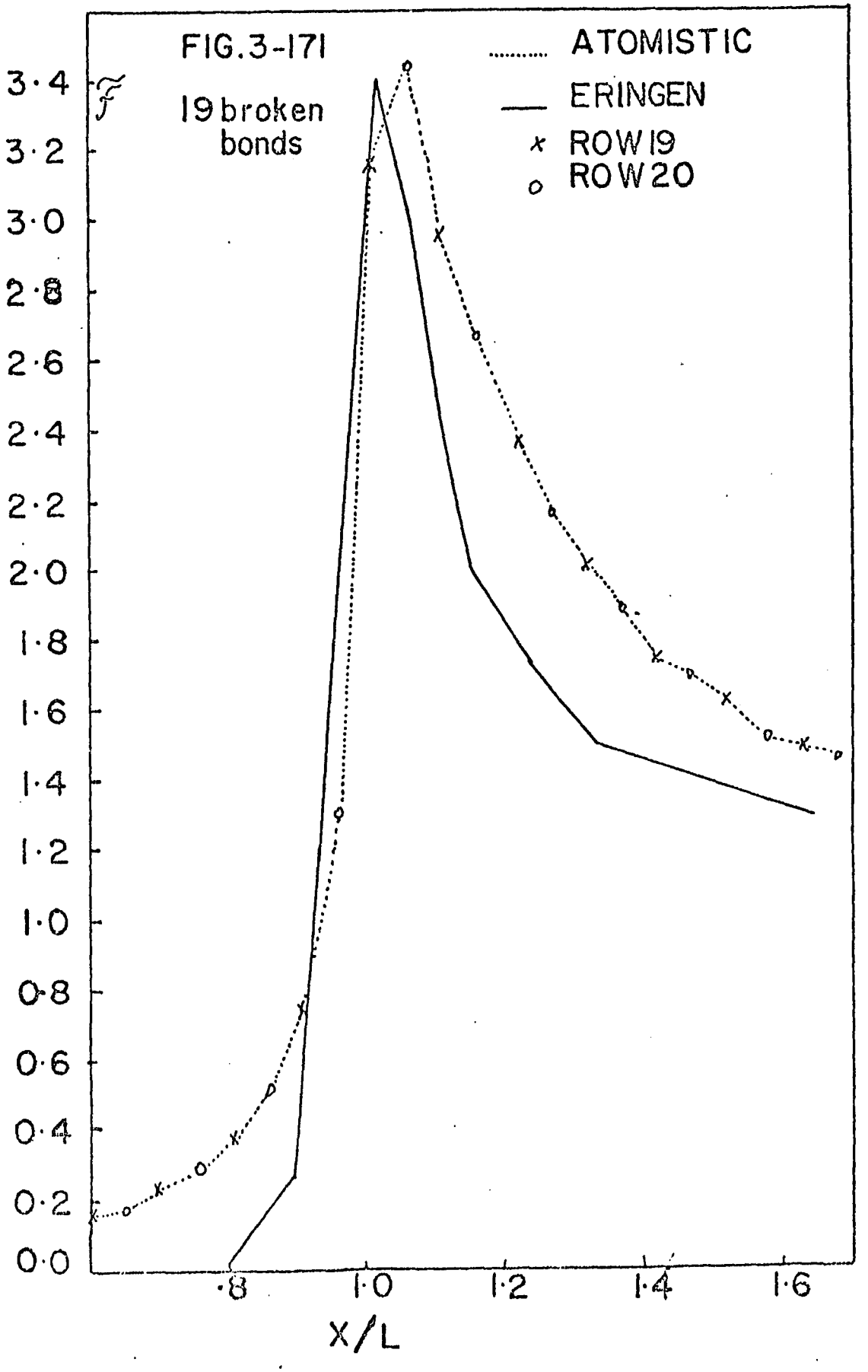
FIG. 3-171
19 broken bonds
ATOMISTIC
ERINGEN
ROW 19
ROW 20
F
3·4
3·2
3·0
2·8
2·6
2·4
2·2
2·0
1·8
1·6
1·4
1·2
1·0
0·8
0·6
0·4
0·2
0·0
·8
1·0
1·2
1·4
1·6
X/L

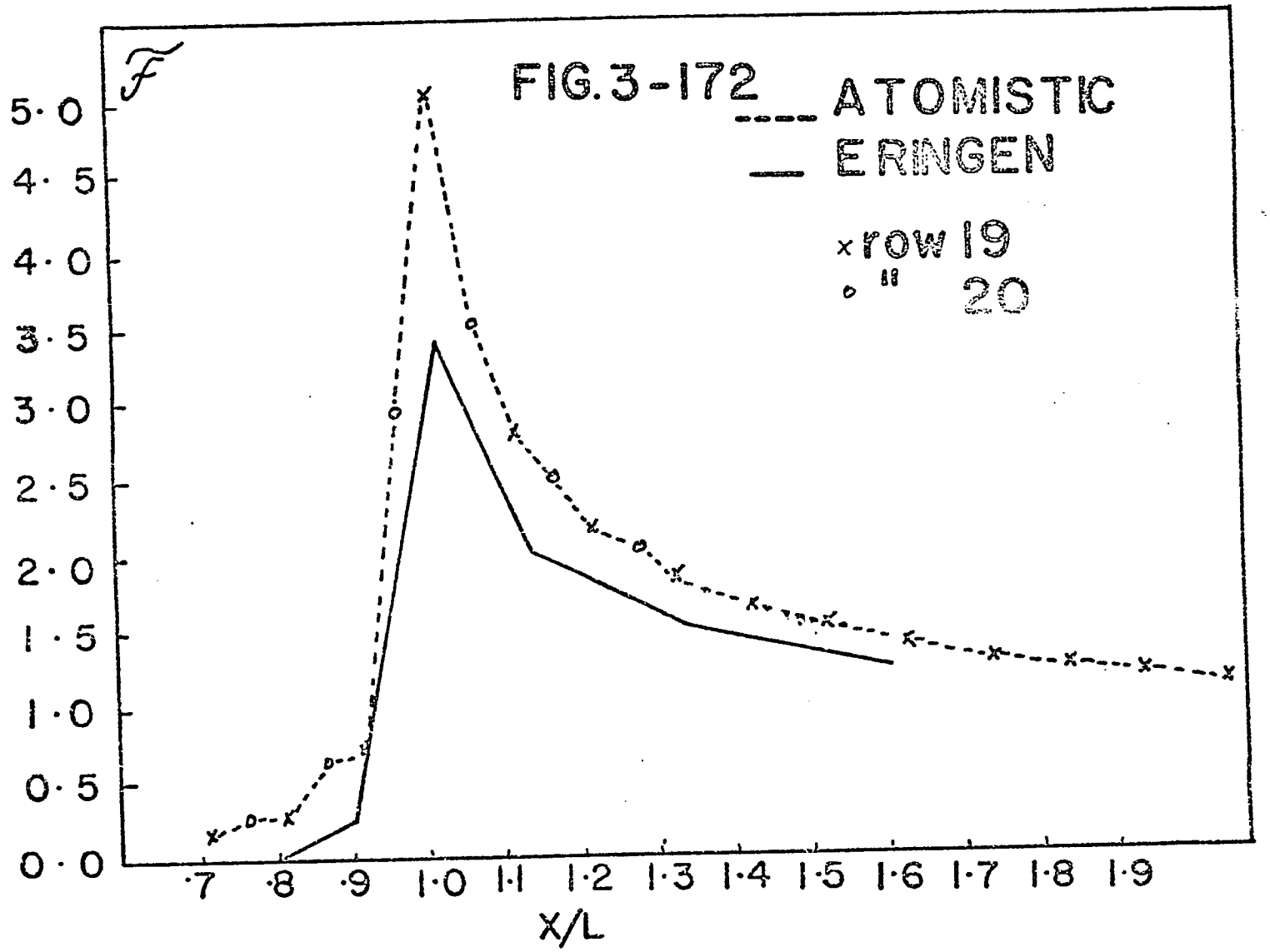
F
FIG. 3-172
ATOMISTIC
ERINGEN
x row 19
o " 20
5·0
4·5
4·0
3·5
3·0
2·5
2·0
1·5
1·0
0·5
0·0
·7
·8
·9
1·0
1·1
1·2
1·3
1·4
1·5
1·6
1·7
1·8
1·9
X/L

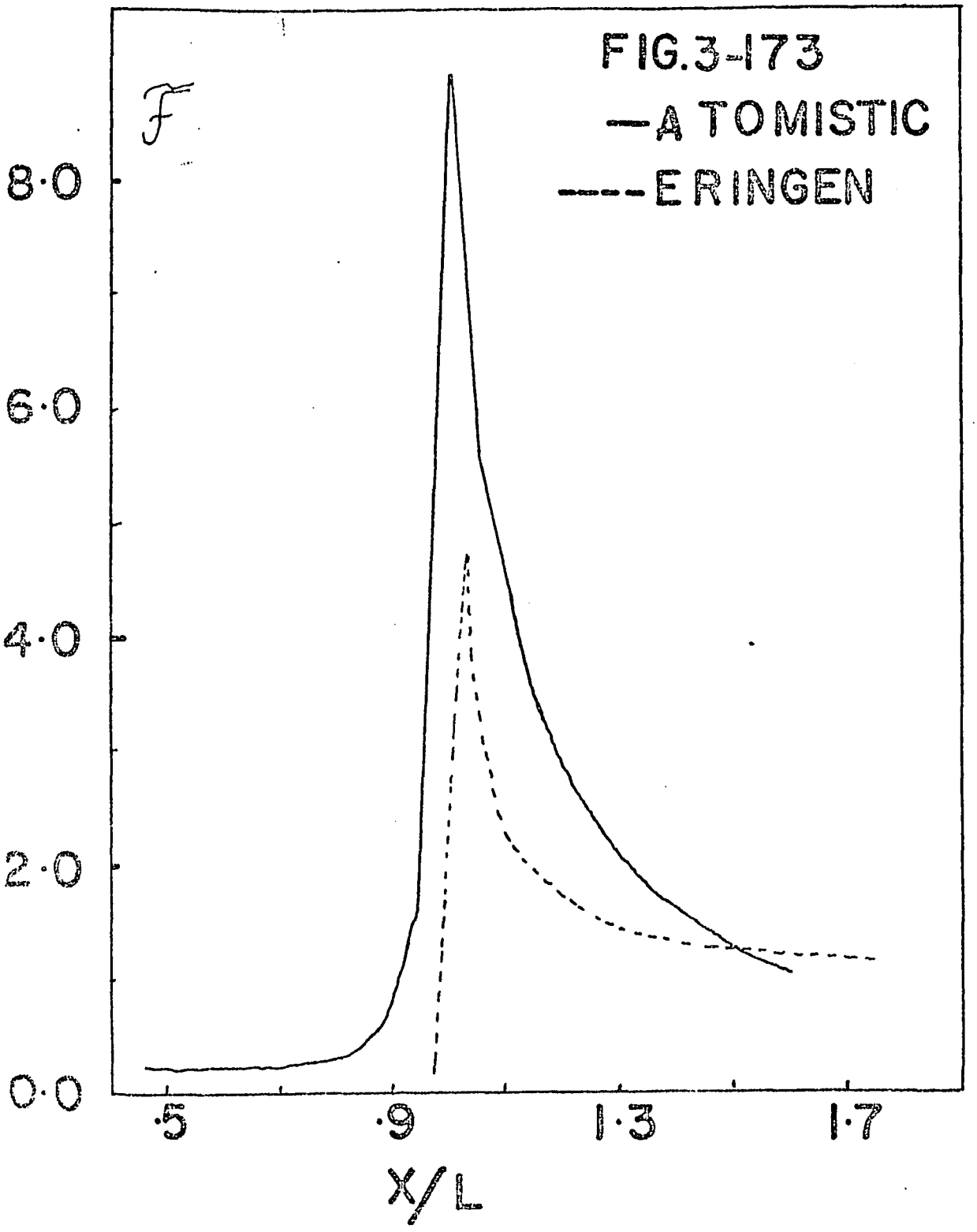
FIG.3-173
—ATOMISTIC
----ERINGEN
F
8·0
6·0
4·0
2·0
0·0
·5
·9
1·3
1·7
X/L

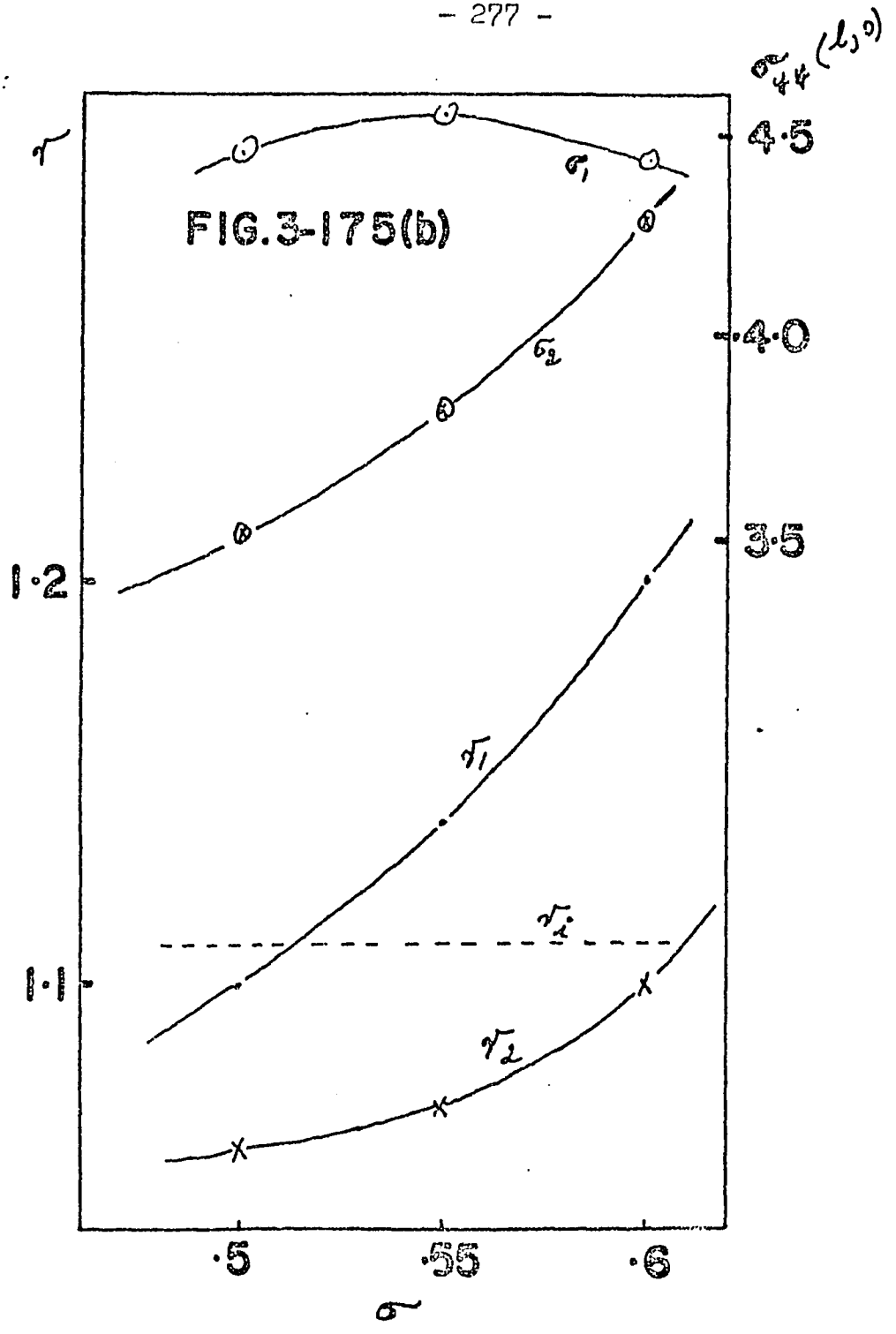
$\sigma_{44}(l,0)$
τ
4·5
4·0
3·5
1·2
1·1
σ_1
σ_2
τ_1
τ_2
τ_i
·5
·55
·6
σ

FIG.3-175(b)

APPENDIX

THE MECHANISTIC APPROACH TO THE CRACK PROBLEM

Besides the Griffith energy approach which has been introduced in chapter I there exists another approach in terms of the so-called stress intensity factor K_I (not to be confused with the stress concentration factor F). This factor K_I is defined as

$$K_I = \lim_{x \to \ell^+} \sqrt{2(x-\ell)}\ \sigma_{yy}(x,0)$$

Or equivalently it is sometimes defined by,

$$\sigma_{\alpha\beta}(r,\theta) = \frac{K_I}{\sqrt{r}} f_{\alpha\beta}(\theta)$$

K_I depends on the length of the crack and on the applied loads. It represent the intensity of the stress singularity at the tip. In such an approach, fracture is assumed to start when K_I reaches a critical value K_{Ic} which is a property of the material. This constant is taken as a fundamental constant of the material just as the surface energy γ is in the Griffith approach. The dependence of K_I on σ & ℓ is obtained by expanding different classical solutions around the tip. For the uniaxial tension case considered here

$$K_I = \sigma \sqrt{\pi \ell}$$

By considering the work done by the stress fields near the tip in expanding or closing a crack by an infinitesimal length $2(\delta l)$, Irwin (1948,1957) has been able to prove that this approach is equivalent to the Griffith one, with

$$K_c = \sqrt{2\gamma}$$

Barenblatt (1961) tried to remove the singularity by postulating a cohesive field near the tip not included in the elastic field. The postulated field has the same form as the elastic one but with a $K_{cohesive}$ of opposite sign. ($K_{cohesive}$ = a constant of the material). By requiring that the total field be finite at the tip, he arrives at

$$K - K_{cohesive} = 0 \qquad \text{at fracture .}$$

This yields the fracture criterion

$$K = K_{cohesive}$$

The origin of the cohesive fields in the Barenblatt theory is not well understood. Also a calculation of $K_{cohesive}$ from basic principles is not possible so that the theory amounts to giving a different name to the critical K of the Irwin theory.

REFERENCES

Akita, Y., and Ikeda, K. (1959). Report No.40.Transportation. Technical Research Institute Tokyo.

Ashurst, W.T., and Hoover, W.G. (1976). Phys. Rev. B, 14, 1465.

Baker, B.R. (1962). J. Appl. Mech. 29, 449.

Barenblatt, G.I. (1962), Adv. Appl. Mech. 7, 55.

Barenblatt, G.I., Salganik, R.L., and Cherepanov,G.P.(1962). Prikl. Mat. i Mek. 26, 469.

Beebe, W.M. (1966). Ph.D. Dissertation, California Institute of Technology, Pasadena.

Beeler, I.K., and Kulcinski, G.L.(1971), In Interatomic Potentials And The Simmulation Of Lattice Defects (eds. Gehlen et al), Plenum, New York.

Berry, J.P. (1960). J.Mech. Phys. Solids 8, 194, 207.

Born, M., and Huang, K. (1954). The Dynamical Theory of Crystal Lattices, Oxford U. Press, London.

Broberg, K.B. (1960). Ark. Fys. 18, 159.

Carlsson, A.J. (1963). Trans. Roy. Inst. Techno. Stokholm 205 & 207.

Craggs, J.W. (1960). J.Mech. Phys. Solids, 8, 66.

Dally, J.W. and Riley W.F.(1965). Experimental Stress Analysis. Mc Graw-Hill.

Dugdale, D.S. (1960), J.Mech. Phys. Solids 8, 100.

Eringen, A.C.,(1977) Crystal.Lattice Defects, 7, 109.

Eringen, A.C., Speziale, C.G., and Kim, B.S., (1977) J. Mech. Phys. Solids, 25, 339.

Esbjorn, P., and Jensen, E.J. (1976). J.Phys. Chem. Solids, 37, 1081.

Gehlen, P.C. (1973), Scripta Met., 7, 1115.

Gehlen, P.C., and Kanninen, M.F.,(1970) In Inelastic Behaviour Of Solids, (eds Kanninen et al) Mc Graw-Hill, New York, p. 587.

Gilman, J.J.(1959). In Fracture (eds Averback, B.L. et al), Wiley, New York, p.193.

Goodier, J.N., and Field, F.A. (1963). In Fracture Of Solids (eds Drucker et al). p. 103, Wiley, New York.

Griffith, A.A. (1920). Phil. Trans. Roy. Soc. London, Ser. A 221, 163-198.

Hahn, G.T. (1976) In Atomic Structure and Mechanical Properties of Metals Proceedings of the International School Of Physics " ENRICO FERMI" (ed gaglioti, G.), North Holland Publishing Co, Amesterdam.

Hernikoff, A. (1941). J.Appl. Mech. 8 , A-169.

Hsieh, C. & Thomson, R, (1973). J.Appl. Phys. 44, 2051.

Hull, D., and Beardmore, P.(1966). Inten. J. Fracture Mech. 2, 468.

Hull, D., Beardmore,P., and Valintine, A. (1965). Phil.Mag. 12, 1021.

Inglis, C.E.(1913) Trans. Instn. Naval Archit. 55, 219.

Kanninen, M.F. & Gehlen, P.C.(1971). Int. J. Fract. Mech. 7, 471.

Kanninen, M.F. & Gehlen, P.C. (1972). In Interatomic Potentials and Simulation Of Lattice Defects (eds. P.C. Gehlen et al.), Plenum,New York, p.713.

Kelly, A., Tyson, W.R., and Cottrell (1967), Phil. Mag., 15, 567.

Lawn, B.R., and Wilshaw, T.R.(1975) Fracture Of Brittle Solids , Camb. U. Press, Cambridge.

Liebowitz, H. (1968), (ed) Fracture Vol. 2, Academic Press, New York.

Mott, N.F. (1948). Engineering 165, 16.

Paskin, A., and Rahman, A. (1966), Phys. Rev. Letters 16, 300.

Paskin, A., and Dienes, G.J.(1972), 43, 1605.

Paskin, A., Gohar, A., and Dienes, G.J. (1977) J. Phys. C: Solid State Phys., 10 L 563, & (1978) J.Phys. C: Solid State Phys., 11, L 857.

Rice, J.R. & Thomson, R. (1974), Phil. Mag. 29, 73.

Rolfe, S., and Barsom, J. (1977) Fracture & Fatigue Control In Structures, Prentice Hall,Inc.,Engelwood Cliffs,New Jersey.

Sanders, J.L.(1960). J.Appl. Mech. 27, 352.

Schand, E.B. (1959). J. Am. Ceram Soc. 42 , 474.

Schand, E.B. (1961). J. Am. Ceram Soc. 44 , 71 & 451.

Sneddon, I.N. (1951), Fourier Transforms, Mc Graw-Hill, New York.

Sneddon, I.N., and Lowengrub, M. (1969), Crack Problems In The Classical Theory Of Elasticity, New York.

Schardin, H. (1959) In Fracture (eds. B.L. Averbach, D.K. Felbeck, G.T. Hahn & D.A.Thomas), Wiley, New York, p.297.

Schardin, H., and Struth, W. (1938). Glastech. Ber. 16, 219.

Thomson, R., Hsieh, C. & Rana, V. (1971), J.Appl. Phys. 42 , 3154.

Van Elst, H.C. (1964). Trans. AIME 230, 460.

Weiner, J.H., and Pear, M. (1975), J.Appl. Phy

Westergaard, H.M. (1939). J.Appl. Mech., 6(2), A-49.

Yoffe, E.H. (1951). Phil. Mag. 42, 739.